Glucagon-like peptide-1 influences proliferation within the spinal cord; an effect via cerebrospinal fluid contacting neurons?

Marilyn Heather May Clark

Submitted in accordance with the requirements for the degree of

Doctor of Philosophy

The University of Leeds

School of Mechanical Engineering

September 2023

The candidate confirms that the work submitted is her own, and that appropriate credit has been given where reference has been made to the work of others.

Acknowledgements

I would first like to thank my supervisor Jim Deuchars for his endless ideas and enthusiasm, and also for taking me on as a student even though I knew almost nothing about neuroscience when starting this project. It has been inspiring to work with someone who still remains unendingly curious and passionate about scientific discovery, even after many years of research. My thanks also to Sue Deuchars for your support and guidance throughout, and for just generally being an absolute powerhouse of an individual. Wishing you both only the best adventures in your retirement!

To everyone who has been in the Deuchars lab over the years I send my thanks. Predominantly to Emily and Jill, who taught me everything I know, and my flocks of students (Charlotte, Sebastian, Joe, Nathan, Katie, and Ella in particular) without whom I probably would have got more work done but had a much less enjoyable time while doing it. Additional thanks to my morale boosters within the extended lab: Andreea, Mark, Emma, and Varinder. Thank you for the Ephys therapy room sessions and for all your help and guidance, it wouldn't have been the same without you.

To everyone back home (Abigail, Brianne, Stacey, Chris, Jamie, and Andy in particular), thank you for believing in me when I didn't and for convincing me not to quit the many, many times I wanted to. Special thanks to Lewis, who has endured more than his fair share of my PhD journey and stuck with me through it, let's hope I can pay some of it back throughout your academic expedition!

Lastly, thanks to Mum and Roxy the dog for always making sure I have a lunch time walk break while writing up and reminding me that the outside world still exists.

Abstract

The influence of glucagon-like peptide-1 (GLP-1) on CNS functions, such as neurogenesis, neuroprotection, and anti-neuroinflammation, prompted investigation into its role in spinal neurogenesis. Ependymal cells (ECs) in the vicinity of the central canal, possess neural stem cell-like characteristics and rapidly proliferate after injury. While GLP-1R mRNA is distributed across spinal cord neurons and glia, its specific expression within the ependymal layer is yet to be resolved. Of particular interest are the cerebrospinal fluid contacting neurons (CSFcNs), which express GLP-1R mRNA, making them the focus of our study.

Immunohistochemistry revealed that approximately 80% of CSFcNs express GLP-1Rs, uniformly distributed throughout the spinal cord. Moreover, a significant number of CSFcNs in the thoracic region receive direct contacts from GLP-1 producing neurons, indicating their integration into the broader spinal GLP-1 network. Calcium imaging in spinal cord slices demonstrated that liraglutide, a GLP-1R agonist, elicited concentration-dependent increases in calcium spiking event frequency and decreases in amplitude. Prolonged liraglutide exposure resulted in a complete reduction of spiking activity in some CSFcNs, which recovered following extended washing with aCSF.

The effects of GLP-1R agonists on spinal cord cell proliferation were examined in *ex vivo* acute slices, organotypic spinal cord slice cultures (OSCSCs), and *in vivo* healthy mouse models. GLP-1R agonist application elicited higher levels of proliferation compared to control within the ependymal cell layer, in both acute slices and OSCSCs. This effect was enhanced when OSCSCs were cultured on liraglutide-infused hydrogels. Intriguingly, intraperitoneal injections of liraglutide *in vivo* revealed fewer labelled proliferating cells than control, particularly within the ependymal cell layer and the white matter.

In summary, this study uncovers functional GLP-1Rs in CSFcNs, influencing calcium dynamics and potentially shaping neurogenesis within the spinal cord's ependymal cell layer. These findings illuminate an intricate interplay between GLP-1 and the spinal cord network, offering promising avenues for therapeutic interventions in spinal cord injuries and degenerative conditions.

TABLE OF CONTENTS

List of figures

List of tables

Abbreviations

aCSF – artificial cerebrospinal fluid

ANOVA – analysis of variance

BrdU – 5-bromo-2’-deoxyuridine

Ca^{2+} - calcium ion

CC – central canal

CD24 – cluster of differentiation 24

CNS – central nervous system

CSF – cerebrospinal fluid

CSFcN – cerebrospinal fluid contacting neuron

DAPI – 4’, 6-diamidino-2-phenylindole

DCX - doublecortin

EC – ependymal cell

EdU – 5-ethynyl-2’-deoxyuridine

FoxJ1 – Forkhead-box J1

GABA – γ-amino butyric acid

$GABA_AR$ – GABA A receptor

GAD – glutamic acid decarboxylase

GAD65/67 – glutamic acid decarboxylase 65/67

GFAP – glial fibrillary acid protein

GFP – green fluorescent protein

GLP-1 – glucagon-like peptide-1

GLP-1R – glucagon-like peptide-1 receptor

GM – grey matter

HuC/D – neuron specific RNA binding protein

Iba1 – ionized calcium binding adaptor molecule-1

IML – intermediolateral cell column

IP – intraperitoneal

NeuN – neuronal nuclei

NSC - neural stem cell

OPC – oligodendrocyte progenitor cell

OSCSC – organotypic spinal cord slice culture

PBS – phosphate-buffered saline

PBST – phosphate-buffered saline with 0.1% triton

PFA – paraformaldehyde

PKD2L1 – polycystic kidney disease 2-like 1

PSA-NCAM - polysialylated neural cell adhesion molecule

SCI - spinal cord injury

SEM - standard error of the mean

Sox2 - sex determining region box 2

SPN - sympathetic preganglionic neuron

SVZ - subventricular zone

WM - white matter

Chapter 1 – General Introduction

1.1 CELL PROLIFERATION AND NEUROGENESIS IN THE SPINAL CORD

1.1.1 Neurogenesis in the central nervous system

Neurogenesis is the process by which new central nervous system (CNS) cells are created and is most active during embryonic development. A neurogenic niche is an area that contains a collection of cells and factors that influence CNS growth and development beyond the embryonic stage and into adulthood. A correlating factor between the neurogenic niches in the CNS is that they are highly vascularised and, in most cases, in direct contact with the CSF which both provide a wealth and complexity of signalling molecules (Lehtinen et al., 2011; Lehtinen and Walsh, 2011; Falcão et al., 2012; Stolp and Molnár, 2015).

The cells in these environments are often a mix of glial and neuronal cells that work together to provide a supportive environment for neural progenitor cells (NPCs) and neural stem cells (NSCs) to either stay quiescent or to proliferate (Bjornsson et al., 2015). NPCs and NSCs can be difficult to strictly define and while there are some well-known neurogenic niches in the CNS, such as the subventricular zone (SVZ) of the lateral ventricles and the dentate gyrus of the hippocampus (Alvarez-Buylla and García-Verdugo, 2002), it is often challenging to reliably identify the particular cell, or cells, within the population that are responsible for the stem cell like activity.

NSCs are broadly defined as cells that are capable of self-renewing to sustain their population and that can generate progeny who develop into mature cells along multiple lineages including neurons, astrocytes, and oligodendrocytes. NPCs are more limited in their differentiation, usually only replicating along their neuronal or glial sub type and have limited self-renewal capacity. There are two patterns of division for NSCs, either symmetric or asymmetric. Symmetric division results in the formation of two identical NSCs or two NPCs, whereas asymmetric division produces one replicate NSC and a progenitor daughter cell which is restricted to the neuronal lineage (Bjornsson et al., 2015).

1.1.2 The ependymal cell layer as a neurogenic niche

Within lamina X of the spinal cord exists a layer of ependymal cells that line the CSF filled central canal (CC) and form an interface between the CSF and the spinal cord parenchyma. The ependymal layer consists of a heterogenous population of cells (**Error! Reference source not found.**), the most common of which are the ependymal cells themselves, and medullo-spinal cerebrospinal fluid contacting cells (CSFcNs – covered in detail in section 1.2).

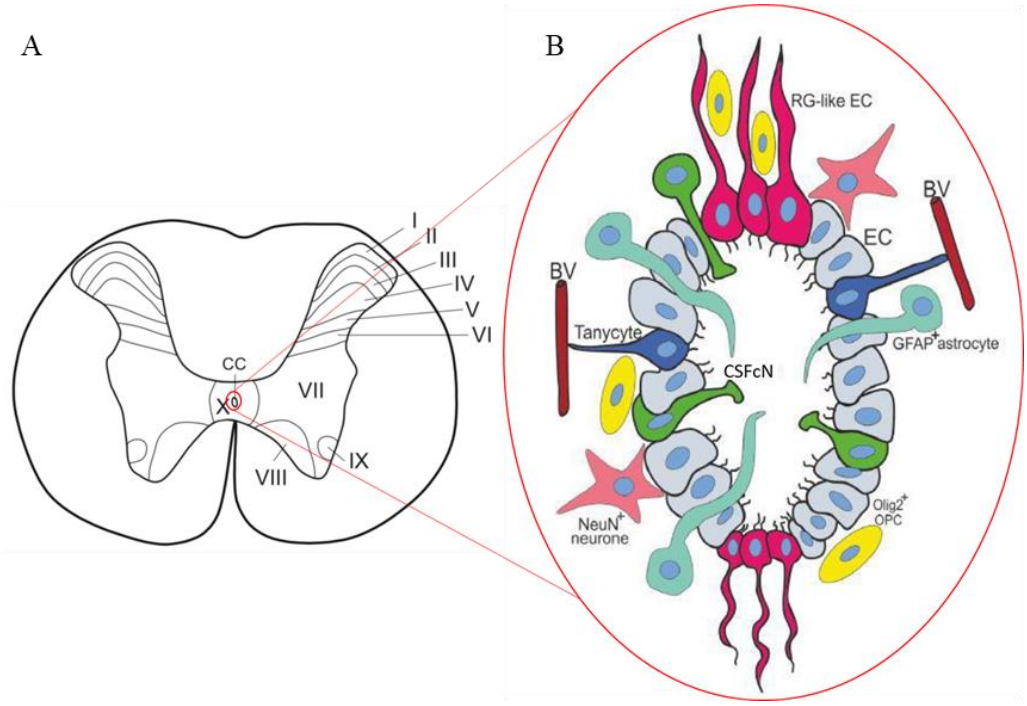

Figure 1.1. Schematic depictions of the spinal cord and central canal area.
A: Schematic depicting a coronal cross section of lower thoracic mammalian spinal cord with the 10 layers of grey matter defined as Rexed laminae. The butterfly shaped grey matter can be seen to be completely enveloped by white matter. The central canal (cc) can be seen in the middle of the lamina X. **B:** Schematic depicting the cells within the ependymal layer of the central canal of the spinal cord. Ependymal cells (EC) are interspersed by other cell types, including cerebrospinal fluid contacting neurons (CSFcNs). Abbreviations: RG-like EC, radial glia like

ependymal cells; BV, blood vessel; GFAP, glial fibrillary protein; NeuN, neuronal nuclei; OPC, oligodendrocyte progenitor cell. Image adapted from New, 2019.

The ependymal cells (ECs) provide structural support and largely resemble the choroid plexus epithelial cells in their morphology, being cuboidal and connected to their neighbours via tight junctions to form a single layer similar to the blood cerebrospinal fluid barrier (BCSFB) (Bruni, 1998; Moore, 2016). ECs are multiciliated and the continuous coordinated beating of their cilia is thought to direct the flow of CSF (Kumar et al., 2021). They contain large round nuclei and exist mainly in a single layer in the majority of the mammalian spinal cord, although can be multi-layered in lumbar and sacral regions, and are slightly more elongated in shape along the dorsal and ventral poles (Bruni and Reddy, 1987). ECs are typically multiciliated, although some biciliated or monociliated ECs can be observed through electron microscopy, indicative of a heterogenous population (Alfaro-Cervello et al., 2012).

Several other cell types have been described within this layer, including GFAP+ cells typically observed in the dorsal aspect of the CC which extend processes towards the pial mater, cells with a radial glial like morphology typically found at the dorsal and ventral poles of the CC frequently referred to as a radial EC, and others with a tanycyte morphology found in the lateral aspects of the CC that extend basal processes to wrap around blood vessels (Bruni, 1998; Marichal et al., 2012; Meletis et al., 2008; Moore, 2016; Moreno-Manzano, 2020).

1.1.2.1 The ependymal layer as a source of quiescent NSCs.

During mammalian embryonic development, ECs are derived from transcription factor homeobox protein Nkx6.1 positive neural progenitors in the ventral progenitor domain of the neural tube, and it is widely thought that they retain some of these stem cell properties in the adult spinal cord (Fu et al., 2003; Spassky et al., 2005). Immunohistochemical studies in many species have revealed that these cells express many biomarkers indicative of stem cell activity such as Nestin (Frisén et al., 1995; Barnabé-Heider and Frisén, 2008), an intermediate filament protein which is involved in the development, remodelling and structural organisation of cells and is

expressed by many undifferentiated progenitor cells in the CNS (Bernal and Arranz, 2018). SRY-box transcription factor 2 (Sox2) is another commonly used marker for the identification of neural stem and progenitor cells in the CNS and is widely expressed in the ECs in the spinal cord (Hamilton et al., 2009). Sox2 is one of the key transcriptional regulators involved in the management of pluripotency and directs early neural differentiation. CD133 is expressed on the surface of ECs (Meletis et al., 2008; Li, 2013), where it is thought to suppress differentiation aiding in the maintenance of stem cell properties, and is widely used in flow cytometry to sort adult NSCs taken from the brain (Coskun et al., 2008; Pfenninger et al., 2011).

Under normal physiological conditions ECs mainly proliferate slowly and symmetrically, as can be seen through their positive expression of proliferative marker Ki67, and staining for EdU and BrdU, in order to maintain their cell population numbers (Johansson et al., 1999; Meletis et al., 2008; Frederico et al., 2022). These cells do not appear to produce any non-ependymal progeny nor migrate any distance away from the ependymal layer as evidenced by BrdU labelled ECs being commonly found in pairs within the ependymal layer (Johansson et al., 1999; Hamilton et al., 2009). The proliferation rate of these cells is higher in young mice and rats, compared to older animals, indicating that they are involved in the growth of the spinal cord, these newly generated cells also stay within the area surrounding the central canal (Horner et al., 2000; Alfaro-Cervello et al., 2012).

1.1.2.2 Ependymal cell response to SCI

Many studies, both *in vivo* using transgenic rodent models and *in vitro* using organotypic slice or cell culture techniques, have shown that following spinal cord injury (SCI) the properties of ECs change; proliferation increases, ECs migrate towards the site of injury, and multilineage differentiation occurs. (Johansson et al., 1999; Attar et al., 2005; Mothe and Tator, 2005; Meletis et al., 2008; Lacroix et al., 2014; Stenudd et al., 2022; Frederico et al., 2022). *In vitro* neurosphere culture experiments using ependymal cells cultivated from rodents that had undergone SCI produced 5 to 10 times more neurospheres compared with cells from uninjured animals, indicating that SCI stimulates the regenerative abilities of ECs (X. Li et al., 2016; Moreno-Manzano et al., 2009; Moreno-Manzano, 2020).

Johansson et al labelled ECs using DiI, a fluorescent tracer that is retained in the lipid bilayers of the cell and found that ECs proliferate rapidly after SCI, tending towards asymmetrical division. Then one cell stays in the ependymal layer and the other daughter cell migrates towards the site of injury and displays non-differentiated stem cell characteristics (Johansson et al., 1999). The progeny of ECs observed *in vivo* appears to be different from the multilineage differentiation capabilities seen in neurosphere cultures, and seems to be limited along glial lineages with no neuronal differentiation observed in studies so far (Mothe and Tator, 2005; Stenudd et al., 2022).

ECs have been shown to contribute to oligodendrocyte populations and comprise the majority of newly proliferated astrocytes after SCI, predominantly composing the glial scar border surrounding the injury site (Barnabé-Heider et al., 2010; Sabelström et al., 2013; Stenudd et al., 2015; Cusimano et al., 2018; Llorens-Bobadilla et al., 2020). Sabelström et al found that selectively blocking EC proliferation, through the use of FoxJ1-CreER mice and deletion of Ras genes, significantly decreased the number of EdU labelled ECs and reduced the density of the glial scar causing an increase in overall cavity size and worsening functional recovery (Sabelström et al., 2013).

Other cell populations, such as astrocytes and oligodendrocytes, within the parenchyma of the spinal cord have also been identified as having progenitor characteristics, however differentiation of these cells is restricted to glial lineage only and are limited to two passages *in vitro* (Nakayama, 1976; Yamamoto et al., 2001). The ability to self-renew, as well as generate progeny along many cell lineages are key criteria in the definition of neural stem cells, and therefore it can be reasonably assumed that a subpopulation of ECs are responsible for the main stem cell behaviour within the neurogenic niche of the spinal cord.

1.2 CEREBROSPINAL FLUID CONTACTING NEURONS AND THEIR FUNCTIONS IN THE SPINAL CORD

1.2.1 The cerebrospinal fluid system in the CNS

The cerebrospinal fluid (CSF) represents the primary extracellular fluid within the central nervous system (CNS) and occupies the ventricles of the brain, the subarachnoid space, and the central canal (CC) of the spinal cord. Ependymal cells line the ventricles and CC, providing a separation between the internal brain parenchyma and the CSF. Additionally, the pia mater covers the external surface of the brain, preventing the CSF from leaking out (Brown et al., 2004). The CSF serves several crucial functions in the CNS, including acting as a shock absorber between the brain and the skull, providing buoyancy that reduces the weight of the brain by more than 60% (Segal, 1993), and clearing waste metabolites and toxins. Furthermore, the flow of CSF delivers essential ions, nutrients, and signaling molecules to cells throughout the brain and spinal cord (Brown et al., 2004).

1.2.1.1 Creation and circulation

CSF is synthesised within the choroid plexus (CP); a highly vascularised, branched series of structures consisting of numerous villi projecting into the ventricles of the brain composed of fenestrated capillaries surrounded by a layer of cuboidal epithelial cells (Figure 1.2). Tight junctions between the epithelial cells prevent the free movement of water, ions, and other small molecules into the CSF, forming the blood-CSF barrier. The synthesis of CSF occurs in two main steps, firstly a filtered form of plasma diffuses from fenestrated capillaries into the choroid interstitial space, orchestrated by a pressure gradient between blood in the capillaries and the interstitial fluid. This fluid is then actively transported through epithelial cells lining the CP into the ventricular lumen, a mechanism aided by the unidirectional transport of bicarbonate, sodium, and chloride ions from the basolateral to the apical membrane resulting in an osmotic gradient (Brown et al., 2004; Sakka et al., 2011). A series of ion channels, ion exchangers, and co-transporters exist on both the apical and basolateral sides of the epithelial monolayer mediating the concentration and flow of ions into and out of the CSF to maintain homeostasis (Brown et al., 2004).

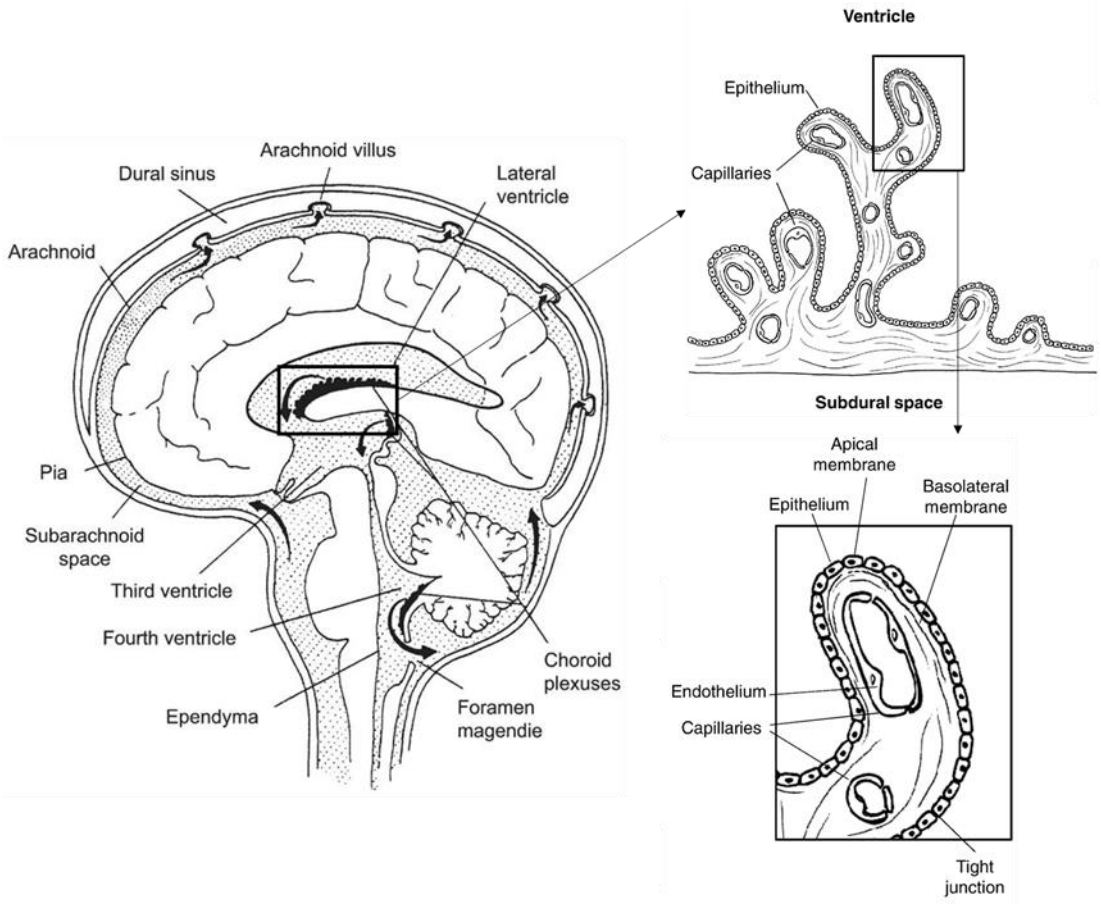

Figure 1.2: Areas of the brain involved in creation and circulation of CSF.
The CSF (represented by black dots) is produced within the choroid plexus (CP), from which it flows through the brain ventricles (direction represented by black arrows) to the central canal of the spinal cord and into the subarachnoid space at various locations. The CP (both insets) is a branched structure with villi projecting into the ventricles of the brain, and contains capillaries covered by a layer of epithelium. Figure adapted from Brown et al., 2004 and Orešković and Klarica, 2010.

CSF flows rapidly rostrocaudally from the CP within the lateral ventricles, through the third ventricle and then fourth ventricle into the central canal of the spinal cord. CSF enters the subarachnoid space through openings in the foramen magendie and the filum terminale at the caudal end of the spinal cord, a fibrous ligament connecting the spinal cord to the coccyx, which possesses openings that allow the flow of CSF from the central canal into the subarachnoid space (Nakayama, 1976). Once inside the subarachnoid space there is also a slower flow in the rostral direction

(Brown et al., 2004; Veening and Barendregt, 2010). The movement of CSF is influenced by primarily by its continual production and absorption, but is also thought to be augmented by the concerted action of cilia on ventricular ependymal cells, respiratory and cardiac rhythms, and the differences in hydrostatic pressure between the CSF and venous system (du Boulay, 1966; Orešković and Klarica, 2010). CSF is drained into the venous system through the arachnoid villi, protrusions of arachnoid mater through the dura mater and then into the lumen of a venous sinus, within the brain and spinal cord (Telano and Baker, 2022). CSF can also drain into the lymphatic system through cranial and spinal nerves within the subarachnoid space (Khasawneh et al., 2018; Laterra et al., 1999).

1.2.1.2 Composition

CSF has a complex composition; mostly composed of water (99%) with the remaining 1% being abundant in proteins, ions, neurotransmitters, and other small molecules critical to the function of physiological processes within the brain and spinal cord (Khasawneh et al., 2018). Numerous neuromodulators, neurotransmitters and neuropeptides can be found within the CSF at measurable levels (Table 1.1), albeit in levels much lower than would be measurable at synapse junctions directly after neurotransmitter release; typically in the mM range for ACh and glutamate (Scimemi and Beato, 2009). However, some neurotransmitters, such as glutamate measured at a concentration of ~2.17 μM, may be present in high enough concentrations capable of activating some high-affinity receptors such as the N-methyl-D-aspartate (NMDA) receptor with an EC50 of ~2 μM (Clements and Westbrook, 1991), but not lower affinity α-amino-3-hydroxy-5-methyl-4-isoxazolepropionic acid (AMPA) receptors which likely require synaptic input with an EC50 of ~ 500μM (Jonas and Sakmann, 1992). As such, the CSF has been proposed to be a vessel of sorts for neuromodulators involved in low level, long range, volume transmission (VT) throughout the brain and spinal cord (Bjorefeldt et al., 2018).

Table 1.1: Examples of neurotransmitters and neuropeptides present in human CSF.

	Concentration (μM)	Reference
GABA	0.087	(Perry et al., 1982)
Glutamate	2.17	(Demartini et al., 2020)
Glycine	12.5	(Palmer et al., 1994)
Acetylcholine	0.07	(Welch et al., 1976)
Dopamine	9×10^{-5}	(Goldstein et al., 2012)
Somatostatin	3×10^{-5}	(Patel et al., 1977)
VIP	3.7×10^{-5}	(Andersen et al., 1984)
Neuropeptide Y	7.6×10^{-5}	(Soleimani et al., 2014)
GLP-1	6.5×10^{-6}	(Christensen et al., 2015)

1.2.1.3 Non-synaptic transmission through the CSF

The concept of volume transmission (VT) was first conceived in the 1980's as new immunohistochemical techniques identified various areas of the brain where neurotransmitter receptor location and density did not match the location of terminals that released the required neurotransmitter. This transmitter-receptor mismatch heavily implied that the receptor was receiving input from a location other than classical synaptic networks (Agnati et al., 1986; Veening et al., 2012). VT is now a well-established concept in the central nervous system (Fuxe et al., 2010; Trueta and De-Miguel, 2012), and represents a major contributor to the non-synaptic transmission of signals via the extracellular fluid and CSF (Taber and Hurley, 2014).

VT can occur over long or short distances; short distance VT can occur though spillover of neurotransmitters from a presynaptic cleft acting on postsynaptic targets on the intended cell or neighbouring cells, such as astrocytes, and largely occurs by diffusion through extracellular fluid (Veening et al., 2012). Long distance VT occurs when compounds are released into the CSF from either the brain or spinal cord to act on downstream targets (Fuxe et al., 2010; Veening et al., 2012; Fuxe et al., 2013; Taber and Hurley, 2014). The discussion of the effects of neurotransmitters in CSF has largely revolved around the setting and maintenance of mood states and extending the duration of behavioral effects (Sewards and Sewards, 2003; Fuxe et al., 2010; Veening et al., 2012).

Neurotransmitters within the CSF are also thought to be capable of setting a level of neuronal excitation (Bjorefeldt et al., 2018). Two studies by Bjorefeldt et al investigated the difference in neuronal excitability in hippocampal CA1 pyramidal neurons (Bjorefeldt et al., 2015), and two subtypes of cortical GABAergic neurons (Bjorefeldt et al., 2016), in patch clamp recordings of rat brain using either human CSF obtained by lumbar puncture or artificial CSF which was closely matched in composition but lacking the complex mixture of endogenous neurotransmitters. In both studies, the human CSF caused a strong increase in neuronal excitability, increasing spontaneous firing rate and increasing responsiveness to excitatory input. These effects were reduced when molecules less than 8 kDa (GABA, as an example is 0.1 kDa) were removed by dialysis indicating the importance of endogenous neurotransmitters in setting neuronal excitation thresholds (Bjorefeldt et al., 2015, 2016, 2018).

1.2.1.4 Where do neuromodulators in the CSF come from?

The presence of neuromodulators within the CSF prompts the question of where these compounds come from. The release of neuromodulators into the CSF has been linked primarily to cells with dendritic varicosities in contact with the CSF that lack postsynaptic targets (Vizi et al., 2010), however the exact cells that release neurotransmitters directly into the CSF remains largely unknown. A cell type that has been heavily implicated in volume transmission and CSF monitoring is the cerebrospinal fluid contacting neuron (CSFcN), present in lower vertebrates, birds, and mammals, including humans (Zhang et al., 2003; Vígh et al., 2004; Veening and Barendregt, 2010).

In the literature, CSFcN is a non-specific term widely used to refer to any neuron that contacts the CSF, and these neurons are abundant within many areas of the brain including the fourth ventricle, hippocampus, dorsal raphe nucleus, and lateral superior olive nucleus (Zhang et al., 2003; Veening and Barendregt, 2010). A common feature of these neurons is that they extend dendritic processes into the CSF that terminate in a ciliated bulb-like ending loaded with vesicles and mitochondria. Notably, this end-bulb operates independently of any synaptic contact (Zhang et al., 2003; Vígh et al., 2004). These neurons possess vesicles containing numerous

neuromodulators, such as GABA, somatostatin, acetylcholine, and serotonin, and exhibit continuous and phasic spontaneous activity indicative of an ability to release a multitude of compounds into the CSF (Vigh and Vigh-Teichmann, 1998; Vígh et al., 2004).

1.2.2 Characteristics of medullo-spinal CSFcNs

Medullo-spinal CSFcNs are a specific population of CSFcNs existing within the CC area of the caudal brainstem and spinal cord and are the main focus of the work included in this thesis. Similar to CSFcNs within the ventricles of the brain, these cells extend a dendritic-like process towards the lumen of the CC where it contacts the CSF forming a ciliated, vesicle dense, end-bulb (Vigh et al., 1983; Alfaro-Cervello et al., 2012). These cells were first described in 1921 by Kolmer and 1922 by Agduhr, and were found to be highly conserved amongst all vertebrates studied so far (Kolmer, 1921; Agduhr, 1922; Vígh et al., 2004). Due to the unique morphology and localisation it was assumed that these cells were mechanosensory or chemosensory neurons strategically positioned to monitor the CSF (Vigh-Teichmann and Vigh, 1989; Djenoune et al., 2014). However, despite the length of time since these cells were first identified, it is only recently that some evidence of their function and connectivity within the brainstem and spinal cord, primarily of lower vertebrates, has been elucidated.

Medullo-spinal CSFcNs will be referred to only as CSFcNs from this point onwards, in line with typical nomenclature.

1.2.2.1 Distribution and localisation

CSFcNs are present within the CC along the entire length of the spinal cord from the caudal area of the fourth ventricle to the filum terminale (Vígh et al., 2004). Immunohistochemical studies of the mouse spinal cord have revealed that CSFcNs are most numerous in the thoracic and lumbar regions, with the density of cells decreasing from caudal to rostral regions (Orts-Del'Immagine et al., 2014; Daniel, 2015). CSFcN position around the CC also varies along the rostrocaudal axis; within the spinal cord, CSFcNs exist around both the dorso-ventral and lateral axes but

appear to exist predominantly in lateral positions within the brainstem (Orts-Del'Immagine et al., 2014, 2017).

1.2.2.2 Phenotypic expression characteristics

Arguably the most widely used identifiable characteristic of the medullo-spinal CSFcN is their expression of polycystic kidney disease 2-like 1 (PKD2L1). Within many vertebrate species including lamprey (Jalalvand et al., 2016), zebrafish (Djenoune et al., 2017), mouse (Huang et al., 2006), and macaque (Djenoune et al., 2014), CSFcNs are the only cell type in the CNS that express PKD2L1, making it a useful biomarker for these cells (Huang et al., 2006; Sternberg et al., 2018). Within the mouse, high levels of PKD2L1 have been found throughout the soma, dendritic process, and endbulb of the CSFcNs but the axonal processes bears little to no expression (Orts-Del'Immagine et al., 2014). PKD2L1 is a calcium regulated non-selective cation channel belonging to the family of transient receptor potential (TRP) channels, which have critical sensory roles enabling cells to detect changes in their environment, such as variances in osmolarity and pH in the CSF in the case of PKD2L1 (Venkatachalam and Montell, 2007). TRP channels are chemo-, thermo-, or mechanosensitive dependent on channel subtype (Jalalvand et al., 2018; Sternberg et al., 2018).

CSFcNs express a variety of GABAergic markers, and are primarily GABAergic neurons in the rodent spinal cord (Barber et al., 1982; Fidelin et al., 2015). Immunohistochemical studies have shown immunoreactivity for γ-aminobutyric acid (GABA), vesicular GABA transporter (VGAT), and both subtypes of the glutamate decarboxylase enzyme (GAD65/67) present in the soma, endbulb, and both the dendritic and axonal processes (McLaughlin et al., 1975; Barber et al., 1982; Djenoune et al., 2014; Orts-Del'Immagine et al., 2014; Gotts et al., 2016; Johnson et al., 2023). Furthermore, CSFcNs express functionally active GABA receptors; including both $GABA_A$ and $GABA_B$ subtypes (Margeta-Mitrovic et al., 1999; Kullmann et al., 2005; Jurčić et al., 2019), indicating a potential for autoreceptor mediated regulation of GABA release mediated by $GABA_B$ receptors predominantly located on the soma and dendrite (Jurčić et al., 2019).

1.2.2.3 Morphology

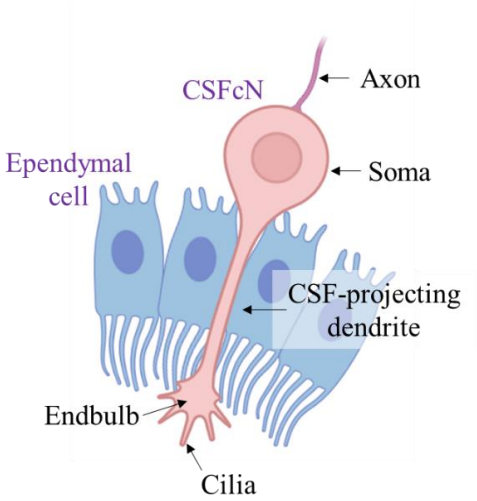

Figure 1.3: Morphological characteristics of cerebrospinal fluid contacting neurons. CSFcNs exist within the central canal of the spinal cord, they possess a soma bearing a thin unmyelinated axon and a thicker CSF-projecting dendrite at the end of which is a cilia bearing endbulb.

Soma

The soma of the CSFcN, in most vertebrate species, is placed within the ependymal or subependymal layers surrounding the CC of the spinal cord and brainstem (Figure 1.4). The shape and size of the soma can vary between and within species but is most commonly spherical or oval in shape, with an average diameter of approximately 10 µm. CSFcNs are rod-like or fusiform and are occasionally elongated oblongs forming a border along several ependymal cells; these cells can be up to 22 µm in length and approximately 7 µm in width (Barber et al., 1982; Shimosegawa et al., 1986; Stoeckel et al., 2003). CSFcN somata are randomly distributed around the central canal and can either be solitary, or existing in groups of two or three closely apposed cells (Barber et al., 1982; Orts-Del'Immagine et al., 2014).

A smaller population, approximately 30%, of CSFcNs in mammalian species can be observed distant to the CC where they extend towards the ventral median fissure (Figure 1.5) (Petracca et al., 2016; Tonelli Gombalová et al., 2020; Jurčić et al., 2021). Similar to CC-adjacent CSFcNs, the somata of these distant non-CC CSFcNs are typically small, ~10 µm, spherical, and present a bipolar morphology, although the infrequent multipolar cell can be observed using PKD2L1 immunohistochemistry in PKD2L1-eGFP transgenic mice (Jurčić et al., 2021). The presence of both bipolar and multipolar CSFcNs has also been observed in rabbit, cat, and monkey through the use of electron microscopy (Leonhardt, 1976; Lamotte, 1987). The bipolar

subtype of non-CC CSFcNs has been observed extending a long dorso-ventral process towards the CC, sporadically forming contacts with other non-CC CSFcNs in a chain formation. In comparison, multipolar non-CC CSFcNs typically did not extend a process towards the CC but instead preferentially contacted other CSFcNs; the axonal vs dendritic nature of these processes remains unclear (Tonelli Gombalová et al., 2020; Jurčić et al., 2021).

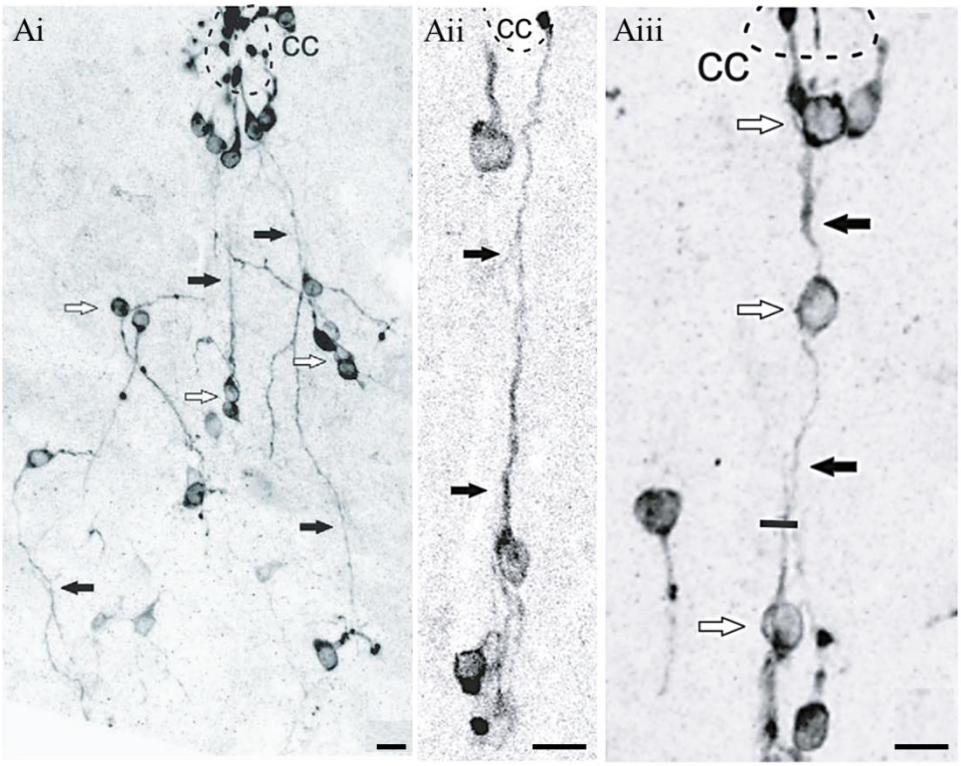

Figure 1.1.4: CSFcNs exist around the central canal, however some CSFcNs have their soma distant from the central canal and send long projections which contact the lumen or form cell chains with other CSFcNs.

Examples of PKD2L1 immunolabelled cervical spinal cord sections showing differences in CSFcN morphology. CSFcNs forming cell chains can be clearly observed in Ai and Aiii, a CSFcN with a distant soma and possessing a long process extending into the lumen can be seen in Aii. White arrows indicate PKD2L1 +ve cell bodies, Black arrows indicate PKD2L1 +ve processes. Scale bars: 50 μM. Image adapted from (Jurčić et al., 2021).

Golgi electron microscopy of the CSFcN revealed that the somata contain a dense cytoplasm with numerous round mitochondria, in contrast to the elongated mitochondria of the neighbouring ECs, and an endoplasmic reticulum with an abundance of free ribosomes (Barber et al., 1982). The nucleus of the CSFcN was

also observed to be primarily spherical, with a similar chromatin pattern to that of the ECs (Barber et al., 1982; Marichal et al., 2009). Dense granular vesicles, approximately 80 – 120 nm have been observed within the soma and CSF-projecting dendrite of the CSFcN in various mammals (Rodríguez et al., 1985).

CSF-projecting Dendrite

CSFcNs extend a thick process from their apical pole which reaches into the CSF filled lumen within the central canal. This process is assumed to be dendritic in nature due to the expression of microtubule-associated protein-2 (MAP2) (Harada et al., 2002), a protein only found within dendrites, and non-expression of neurofilament 160 (NF-160) which is only expressed in axons (Orts-Del'Immagine et al., 2014). The length of the dendrite within the mouse spinal cord was dependent on their location along the rostrocaudal axis of the spinal cord, as well as the position around the central canal. Dendrites of CSFcNs located dorsolaterally around the central canal were shorter in rostral-most sections, averaging approximately 20 μm, increasing in length in more caudal regions. The opposite was found to be true for dendrites of ventrally located CSFcNs, which are longest in more rostral locations, being approximately 32 μm in the cervical region, and becoming shorter within more caudal regions (Orts-Del'Immagine et al., 2014).

Endbulb

At the terminus of the dendrite exists the endbulb; a globular shaped protrusion existing within the CSF filled lumen, with an average diameter of 2.5 to 5 μm (Barber et al., 1982; Vigh-Teichmann and Vigh, 1989). Within the turtle, zebrafish, mouse, and rat spinal cord, CSFcNs possess long motile kinocilia as well as non-motile primary cilia thought to have a sensory function. Motile kinocilia contain microtubules arranged in 9 doublets surrounding a central pair of microtubules referred to as the 9+2 arrangement, whereas primary cilia only possess the ring of 9 microtubule pairs without the central doublet, enabling the two subtypes of cilia to be differentiated (Vigh-Teichmann and Vigh, 1989; Stoeckel et al., 2003; Orts-Del'Immagine et al., 2014; Gerstmann et al., 2022). Immunohistochemical studies

have revealed that these cilia are immunoreactive for acetylated α-tubulin (Ac-αtub) and adenylate cyclase 3 (AC3), both commonly used markers expressed in microtubule associated cilia (Orts-Del'Immagine et al., 2014; Stoeckel et al., 2003).

Axons

CSFcNs send a thin unmyelinated processes from their soma, typically on the basal or lateral surface, extending towards the ventral parenchyma and then running rostrally with a length of approximately 1800 - 4800 μm, as discovered through single cell viral labelling (Vigh et al., 1977; Nakamura et al., 2023). Varicosities, containing GAD and synaptophysin, are commonly observed along the length of these fibres indicating synaptic contacts within the parenchyma (Stoeckel et al., 2003; Jurčić et al., 2021). Double labelling experiments by Stoeckel et al, in the rat spinal cord, revealed immunoreactivity for GABA, GAD, P2X2, PSA, GAP-43; a marker for axonal outgrowth, as well as synaptic markers synaptophysin and synaptotagmin, but not dendritic marker MAP2 (Stoeckel et al., 2003). This is confirmed by Orts-Del'Immagine et al, who similarly found no expression of MAP2, but could not confirm expression of selective axonal marker NF-160 in these processes due to the high density of axons within this region (Orts-Del'Immagine et al., 2014). These results indicate that the axonal nature of this process is highly likely but has not yet been fully confirmed.

Recent immunohistochemical and single cell viral labelling studies of these fibres in the mouse have confirmed that they run dorsoventrally to the ventral median fissure and then rostrally in tracts up to the brainstem. A small number of CSFcNs, particularly at cervical and sacral levels, have projections that run bidirectionally, often forming tracts running parallel within the ventral funiculus (Jurčić et al., 2021; Nakamura et al., 2023). Tiny, unmyelinated neurite bundles, less than 150 nm in diameter, coming from the basal pole of the CSFcNs can be seen through electron microscopy and single cell viral labelling to be inserted between ependymal cells and closely apposed onto ependymal cells, most frequently along the ventral edge of the CC at cervical level (Stoeckel et al., 2003; Nakamura et al., 2023). Furthermore, several fibres from caudal CSFcNs project to the ventral median fissure when they

head rostrally, and occasionally sent branches back towards the CC terminating onto ECs and CSFcNs (Nakamura et al., 2023).

1.2.3 Functional roles of CSFcNs in spinal cord homeostasis

There is little agreement within the literature regarding the primary function of CSFcNs and, given the apparent differences in expression profiles and morphological characteristics of CSFcNs between species, there is even less agreement that these roles are conserved in all CSFcN bearing animals. However, multiple aspects of CSFcN structure and placement seem to indicate that they possess a sensory role, likely one with many differing input stimuli.

1.2.3.1 Chemosensory: changes in CSF composition

The positioning of CSFcNs around the central canal suggests a role in sensing the composition of, or responding to changes within, the CSF or interstitial fluid. As mentioned above, the main identifying characteristic of medullo-spinal CSFcNs is their expression of the non-selective cation channel PKD2L1. This channel has been implicated in the detection of sour taste caused by low pH in taste receptor cells, and has been known to be activated by even small changes in extracellular pH (Huang et al., 2006). An electrophysiological study by Huang et al found that CSFcNs significantly increased the rate of action potential firing in response to an increase in aCSF acidity from pH 7.4 to 6.9, and even more so when pH was reduced to 6.5. Orts-Del'Immagine investigated the pH sensing capabilities of CSFcNs within the mouse brainstem and found that these cells also responded robustly to alkalinisation changes from pH 7.4 to 8.8 (Orts-Del'immagine et al., 2012). It is generally accepted that in healthy conditions, CSF pH sits between 7.3 and 7.45 (Siesjö, 1972; Liao et al., 2021), and in cases of severe hypoxia or injury can be reduced to approximately pH 6.7 (Siesjö et al., 1985). It could be possible that CSFcNs respond to these changes and signal nearby cells in order to maintain, or return to, homeostatic levels. There appears to be no information in the literature regarding the pH limit of alkalinised CSF, and therefore the physiological relevance of CSFcNs sensing this is yet to be determined.

It is possible that CSFcNs respond to the presence of other neurotransmitters within the CSF. As mentioned previously, CSFcNs are responsive to application of GABA, Acetylcholine, glutamate, and glycine, all of which are present within the CSF in concentrations that may vary depending on the physiological state of the animal (See section 1.2.1.3 and Table 1.1 for further details). Many neuronal bodies and axons run near the central canal, particularly in the ventral aspect, which have been found to intermingle and form synapses with CSFcNs (Stoeckel et al., 2003; Gerstmann et al., 2022; Nakamura et al., 2023). It is possible that CSFcNs monitor and transmit information regarding the composition of the CSF to these neighbouring cells as part of the wider spinal circuitry.

1.2.3.2 Inputs to CSFcNs – direct appositions

Electron microscopy investigations of CSFcNs using mouse and rat spinal cord have indicated that CSFcNs receive many axosomatic appositions implicating them as being integrated into a functional network of sensory cells (Barber et al., 1982; Vigh et al., 1983; Orts-Del'Immagine et al., 2014). The origins of many of these appositions remains largely undiscovered, although some information is known regarding the nature of these terminals. In this section, only inputs onto rodent CSFcNs will be discussed unless specified otherwise.

Electron microscopy studies have found that presynaptic terminals onto CSFcNs contain many small, clear synaptic vesicles within the active site, as well as both small and large granular vesicles, located more peripherally (Barber et al., 1982). Classical neurotransmitters, such as GABA, acetylcholine, glycine and glutamate, are most commonly stored within small, clear vesicles whereas large, dense core vesicles (LDCVs) are used to store peptides and larger transmitters (Liu et al., 1994). Monoamines, such as serotonin, dopamine, and norepinephrine are primarily stored within smaller dense core vesicles, although they have also been found within both small clear vesicles and LDCVs (Thureson-Klein, 1983; Liu et al., 1994).

Excitatory glutamatergic and inhibitory glycinergic inputs onto CSFcNs have been observed in the lamprey and mouse spinal cords, and have been shown to be functionally active through electrophysiological studies although it was not determined where these neurotransmitters come from (Marichal et al., 2009; Orts-

Del'immagine et al., 2012; Jurčić et al., 2019). Terminals expressing glutamatergic markers VGLUT1 and VGLUT2 are located adjacent to the CC, and could be a source of glutamatergic input, they are thought to originate from glutamatergic interneurons that modulate motor output within the spinal cord (Kaneko et al., 2002). Neurons immunopositive for glycine, GABA and ACh are known to exist within various areas of the spinal cord including lamina X where it is possible that they innervate CSFcNs (Spike et al., 1993; Bradaïa and Trouslard, 2002; Gotts et al., 2016).

GABAergic inputs onto CSFcNs are well documented and are proposed to be from other GABA and GAD containing cells nearby within the spinal cord (McLaughlin et al., 1975; Barber et al., 1982; Orts-Del'immagine et al., 2012). Electrophysiological studies have shown that CSFcNs respond to application of GABA, an effect blocked by the pre-application of $GABA_A$ receptor blocker gabazine, indicating that these receptors are functional although the cells providing the presynaptic inputs were not elucidated (Orts-Del'immagine et al., 2012). It is possible that a number of these GABAergic inputs come from CSFcNs themselves existing more caudally with the spinal cord. Fibres from CSFcNs run rostrocaudal throughout the length of the spinal cord and up to the brainstem - a study by Nakamura et al used single cell tracing of an AAV-Syn-mCherry-injected cleared spinal cord, to reveal that the majority of CSFcN processes in all areas of the cord travelled firstly ventrally, towards the ventral funiculus, and then rostrally. Additionally, some fibres from these rostrally projecting bundles returned to the central canal where they terminated in the subependymal region and made functional GABAergic connections with more rostral CSFcNs (Gerstmann et al., 2022; Nakamura et al., 2023).

1.2.4 Are CSFcNs contributing towards the quiescence of ependymal layer stem cells?

GABA is known to play a crucial role in setting the inhibitory tone in the neurogenic niches of the CNS, such as the dentate gyrus and subventricular zones (Ming and Song, 2011). The inhibitory tone in these niches is essential for regulation of the balance between the proliferation and differentiation of neural stem or progenitor

cells (NSC/NPCs), ensuring that pathogenic proliferation does not occur or that the population of NSCs is not depleted.

GABA exerts its inhibitory effects through binding to GABA receptors, of which there are two types: fast responding ionotropic $GABA_A$ receptors and slow responding metabotropic $GABA_B$ receptors. Activation of $GABA_A$ receptors increases the permeability of the cell to Cl^- ions which can either result in hyperpolarisation, causing an increase in firing threshold and resulting in neuronal inhibition, or in cases with high concentrations of intracellular Cl^- ions, can result in depolarisation, neuronal excitation, and the influx of Ca^{2+} ions (Olsen and DeLorey, 1999; Olsen and Sieghart, 2008). $GABA_B$ receptor activation is slow and always inhibitory (Bettler et al., 2004; Olsen and DeLorey, 1999). These G protein coupled receptors are indirectly coupled to K+ ion channels and upon activation can significantly decrease Ca^{2+} influx, block neurotransmitter release, and inhibit the production of cAMP (Olsen and DeLorey, 1999; Bettler et al., 2004; Frangaj and Fan, 2018).

1.2.4.1 GABA modulates proliferation in neurogenic niches of the brain

The effects of GABA on proliferation within CNS neurogenic niches can be observed in the subventricular zone (SVZ) of the hippocampus. The lumen of the SVZ is lined with a population of neuroblasts, identified by expression of neuronal plasticity marker PSA-NCAM, interspersed with GFAP positive progenitor cells, which act as stem cells for this area (Doetsch et al., 1999). Doetsch et al infused mice with an antimitotic drug over 6 days, resulting in the complete elimination of all PSA-NCAM positive neuroblasts within the SVZ. They found that up to four days after this injury, there were no neuroblasts present within the SVZ, however 10 days post injury there was once again a fully connected network of PSA-NCAM positive neuroblasts (Doetsch et al., 1999). Treatment with BrdU revealed that the GFAP+ cells rapidly proliferated in the absence of SVZ neuroblasts, indicating that local signalling released from these neuroblasts regulated progenitor cell proliferation.

Liu et al performed electrophysiological recordings on cells within the SVZ and found that these GFAP+ progenitor cells hyperpolarised in response to bath

application of GABA, which was reduced by co-application of $GABA_A$ receptor antagonist bicuculine. They proposed that non-synaptic transmission of GABA from neuroblasts limits the proliferation of GFAP+ progenitors, and that removal of the neuroblasts results in extensive proliferation as seen in the study by Doetsch (Doetsch et al., 1999; Liu et al., 2005). Furthermore, treatment with the $GABA_A$ receptor antagonist bicuculine *in vivo* resulted in a 6-fold increase in the number of NSCs within the SVZ, indicating that GABA maintains the quiescent state of NSCs and removal of this encourages entry into the cell cycle (Daynac et al., 2013).

However, the effects of GABA of NSCs are not always straightforward. Tozuka et al found that, in acute hippocampal slices, GABAergic input to neuronal progenitor cells in the hippocampus results in depolarisation, an increase in intracellular calcium and the promotion of neuronal differentiation (Tozuka et al., 2005). GABAergic signalling has also been implicated in the migratory response of neuronal precursor cells in the SVZ of juvenile and adult mice; increasing ambient GABA levels resulted in a slowing of precursor migration speed, whereas the application of $GABA_A$ receptor antagonists increased migration rate (Bolteus and Bordey, 2004).

1.2.4.2 Effects of GABA on spinal cell proliferation

In vivo experiments in mice where the levels of GABA were increased through administration of vigabatrin resulted in fewer proliferating cells within the ependymal cell layer, whereas deactivation of the central benzodiazepine (CBR) binding site of the $GABA_A$ receptor through treatment with flumazenil resulted in an increase in cell proliferation (New et al., 2023). These results indicate that the ambient levels of GABA within the spinal cord are directly inversely correlated with proliferation, suggesting the presence of tonic inhibition of quiescent stem cells within the ependymal layer.

In acute spinal cord slices prepared from young rats, ECs consistently depolarise in response to GABA application resulting in an increase in intracellular calcium levels similar to that observed in the NSCs of the SVZ (Tozuka et al., 2005; Corns et al., 2013). This is thought to be mediated mainly by $GABA_A$ receptors, as the effect was reduced with co-administration of bicuculine and was not affected by application of

$GABA_B$ receptor agonist baclofen (Corns et al., 2013). This indicates that ECs possess active and functional GABA receptors and are capable of responding to local GABA levels.

Electrophysiological studies show that bath application of GABA to acute spinal cord slices results in either a depolarisation or hyperpolarisation response on CSFcNs, which is dependent on their subtype, indicating the presence of functionally active receptors (Corns, 2012; Riondel et al., 2022). CSFcNs are known to be immunoreactive for both GAD and VGAT indicating that they are capable of both synthesising and releasing GABA into the CSF and local environment (Stoeckel et al., 2003). Given the proposed ability to both uptake and release GABA it could be possible that CSFcNs release GABA into the environment in an autoregulated manner, allowing for careful balancing of endogenous levels and modulation of inhibitory tone within the ependymal layer. This suggests that CSFcNs could exhibit some control in the regulation of EC behaviour similar to how neuroblasts regulate NSC quiescence in the SVZ (Daynac et al., 2013). However, the role of these cells as potential moderators of proliferative activity within the adult spinal neurogenic niche remains largely unexplored in the literature.

1.3 GLUCAGON-LIKE PEPTIDE-1 (GLP-1) AND CNS EFFECTS

1.3.1 Overview of GLP-1

Glucagon-like peptide-1 (GLP-1) is an neuropeptide released both peripherally, mainly by intestinal endocrine L-cells (Mojsov et al., 1986), and centrally through preproglucagon (PPG) neurons within the olfactory bulb and the caudal medulla of the brainstem (Larsen et al., 1997; Drucker, 1998; Merchenthaler et al., 1999). GLP-1 systems have been found in many vertebrate species including lamprey (Graham et al., 2020; Irwin et al., 1999) and chicken (Hiramatsu, 2020; Kolodziejski et al., 2018), and have similar distributions within the brains of mice (Llewellyn-Smith et al., 2011), rats (Merchenthaler et al., 1999), macaques (Vrang and Grove, 2011), and humans (Zheng et al., 2015).

GLP-1 synthesis involves a series of molecular events originating from the proglucagon gene (Figure 1.7). Firstly, the proglucagon gene is transcribed into mRNA which then undergoes post-transcriptional modification resulting in the formation of preproglucagon, a precursor molecule, which is then translated into the proglucagon protein (Mineo et al., 1995; Vrang and Larsen, 2010). In pancreatic α-cells, proglucagon undergoes processing by prohormone convertase 2, resulting in the cleavage of the proteins and the production of glucagon alongside other peptides (Figure 1.7). In intestinal L-cells and PPG neurons in the CNS, prohormone convertase 1/3 facilitates the cleavage of proglucagon to generate the inert full length 36 amino acid length GLP-1. This is subsequently processed into the biologically active truncated GLP-1 (7-36) ubiquitously referred to in the literature simply as GLP-1 (Drucker, 1998; Holst, 2007; Vrang and Larsen, 2010; McLean et al., 2020).

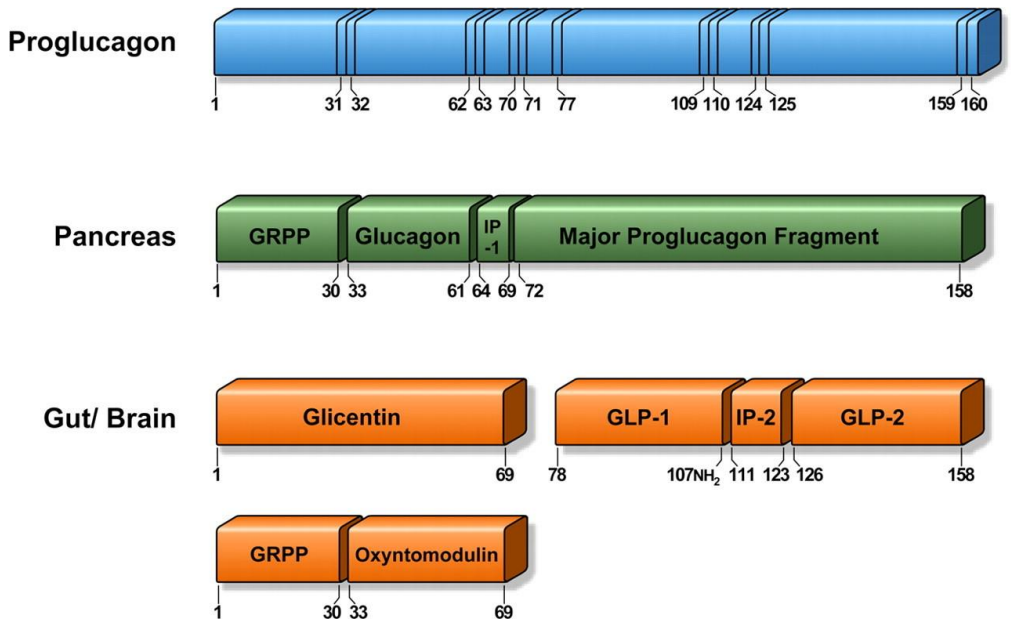

Figure 1.5: Proglucagon undergoes differential posttranslational processing in cells of the pancreas, gut and brain.

The proglucagon protein is processed within the pancreas to generate the glicentin-related pancreatic polypeptide (GRPP), Glucagon, intervening peptide-1 (IP-1), and the major proglucagon fragment. In the gut and brain proglucagon is cleaved to form glicentin, glucagon-like peptides 1 and 2 (GLP-1/2) and intervening peptide-2 (IP-2). Glicentin can be further fragmented to produce GRRP and oxyntomodulin. Amino acid positions within the 160-amino acid proglucagon sequence are numbered and typical cleavage sites are indicated by vertical lines. Image taken from Holst, 2007.

GLP-1 is thought to play many roles in the body, one of the most well-known and essential functions of GLP-1 is its peripheral effect as an incretin hormone (Baggio and Drucker, 2007). Incretin hormones are released by the gut in response to the intake of food and subsequent increase in blood glucose levels to potentiate a larger release of insulin than that produced by hyperglycaemia alone (Mcintyre et al., 1964). GLP-1 is also known to simultaneously inhibit the release of glucagon from α-cells in the pancreas (Orskov et al., 1988), and improve the uptake and utilisation of glucose in peripheral tissues such as muscles (Alcántara et al., 1997; Luque et al., 2002).

These potent effects on insulin secretion and glucose management have resulted in much interest in the use of GLP-1 as a treatment of diabetes (Knudsen, 2019; Prasad-Reddy and Isaacs, 2015). However, as GLP-1 itself is an endogenous neuropeptide it is rapidly degraded by dipeptidyl peptidase-4 (DPP-4, also known as CD26), a ubiquitous proteolytic enzyme found membrane bound on many cell types and solubilised circulating in blood plasma and cerebrospinal fluid (Boonacker and Van Noorden, 2003; Chiazza et al., 2018; Király et al., 2018). GLP-1 therefore is functionally active for only a few minutes post release, making it unsuitable for prolonged therapeutic use (Baggio and Drucker, 2007).

Several longer lasting analogues have been developed to increase the active time, two analogues in particular have undergone extensive investigation, are FDA approved, and are of interest in this work: exendin-4 and liraglutide (Collins and Costello, 2022; Knudsen, 2019; Prasad-Reddy and Isaacs, 2015; Trujillo et al., 2021). Exendin-4 was the first mimetic used clinically, a 39 amino acid long peptide derived from the saliva of the Gila monster, with a half-life of approximately 30 minutes to two hours depending on method of administration (Parkes et al., 2001). Liraglutide has a significantly longer half-life of 11-15 hours when given subcutaneously, which allows for once-daily administration. This extended half-life is mainly due to the addition of a long chain palmitoyl group on the lysine(26) residue increasing the hydrophobicity of the molecule and therefore increasing albumin binding and slowing absorption into the bloodstream (Bech et al., 2018; Knudsen, 2019).

1.3.1.1 Physiological roles of central GLP-1 signalling

GLP-1 also acts centrally, exerting many effects within the CNS, through the GLP-1 released by neurons within the brainstem (Trapp and Cork, 2015; Vrang and Larsen, 2010). While the physiological relevance and mechanisms behind many central effects of GLP-1 are still being discovered, the main roles of GLP-1 seems to be associated with feeding and stress responses (Holt and Trapp, 2016; Brierley et al., 2021; Holt and Rinaman, 2022; Trapp and Brierley, 2022). Administering GLP-1R agonists centrally or activating PPG neurons through chemo/optogenetic means to elevate GLP-1 levels in rodents reduces food intake and an increase in satiety. This effect is blocked by co-administration of the GLP-1R antagonist, exendin (9-39) (Müller et al., 2019; Holt et al., 2019; Brierley et al., 2021; Chen et al., 2021). This effect has also been observed in human studies, leading to GLP-1R agonists being investigated for treatment of obesity (Crane and McGowan, 2016; Trapp and Brierley, 2022).

PPG neurons become activated under both psychogenic stress, such as that caused by restraint (Maniscalco et al., 2015; Terrill et al., 2019; Holt et al., 2019; Holt and Rinaman, 2022), and interoceptive stress, mimicked experimentally by injection of a toxic substance (Rinaman, 1999a, 1999b; Holt and Rinaman, 2022). Activation of PPG neurons results in increased thermogenesis and activation of the sympathetic nervous system (Beiroa et al., 2014; González-García et al., 2019; Yamamoto et al., 2002), and increased heart rate particularly when longer lasting analogues such as liraglutide are delivered direct to the CNS (Lorenz et al., 2017; Smits et al., 2017; Holt et al., 2020).

The GLP-1 system has also been implicated as having roles in memory and neuroprotection, and has been explored particularly in the cases of neurodegenerative diseases such as Parkinson’s and Alzheimer’s disease, or in the case of stroke (Salcedo et al., 2012; Hansen et al., 2015; Batista et al., 2019; Erbil et al., 2019; Hölscher, 2022). This will be discussed in depth later in this chapter.

1.3.2 GLP-1R localisation within the CNS

GLP-1Rs are widely expressed in many areas of the CNS from the olfactory bulb down to the sacral spinal cord, and are involved in many sympathetic and autonomic function pathways (Llewellyn-Smith et al., 2015, 2011; Merchenthaler et al., 1999; Richards et al., 2014; Cork et al., 2015; McLean et al., 2020; Brierley et al., 2021).

1.3.2.1 In the brain

In the brain the distribution of GLP-1R expressing cells been thoroughly mapped through the use of in-situ hybridisation (Wei and Mojsov, 1995; Bullock et al., 1996; Alvarez et al., 1996; Lein et al., 2007; Merchenthaler et al., 1999; Jensen et al., 2018), radiolabelled GLP-1 binding assays (Göke et al., 1995), GLP-1R antibodies (Heppner et al., 2015; Jensen et al., 2018; Farkas et al., 2021), and transgenic mouse lines expressing fluorescent reporters in neurons that express GLP-1Rs (Richards et al., 2014; Cork et al., 2015).

While no one method is perfect (McLean et al., 2020; Pyke and Knudsen, 2013), it is largely in agreement that a high number of GLP-1R expressing neurons are present in areas involved in the control of energy balance, regulation of feeding, and stress response, such as the paraventricular and arcuate hypothalamic nuclei, the amygdala, and regions of the brainstem including the dorsal motor nucleus of the vagus and the nucleus of the solitary tract (Merchenthaler et al., 1999; Heppner et al., 2015; Cork et al., 2015). Additionally, several neurons within the dentate gyrus of the hippocampus also express GLP-1Rs (Farkas et al., 2021; Hsu et al., 2015), although the direct inputs to these cells have not been fully identified and it is thought that they may be activated through GLP-1 in the CSF (Hsu et al., 2015).

1.3.2.2 In the spinal cord

Less thorough characterisation has been done in the spinal cord, and even fewer agreements on GLP-1R distribution in this area have been reached. Llewellyn-Smith et al used transgenic mice expressing glucagon promoter-driven yellow fluorescent protein (PPG-YFP) to investigate the distribution of PPG neuron axons in the spinal

cord, axons were found largely in the lateral funiculus, ventral white commissure and the ventral median fissure (Llewellyn-Smith et al., 2015). A dense network of YFP fluorescent axons were also found to travel rostrocaudally and mediolaterally through lamina X of the spinal cord, with a rostrocaudal tract running through the dorsal section close to the central canal (Llewellyn-Smith et al., 2015). Retrograde fluorogold labelling from the thoracic (T9) spinal cord indicated that these projections have their origin in the NTS, therefore confirming the innervation of the spinal cord by axons of descending PPG neurons (Llewellyn-Smith et al., 2015). Furthering this work, Holt et al selectively ablated PPG neurons in the NTS and found that this caused a significant reduction in the levels of GLP-1 present in the spinal cord, demonstrating that brainstem PPG neurons are the primary source of spinal GLP-1 (Holt et al., 2019).

The presence of PPG neuron axons in lamina X indicates that there are likely to be innervation targets nearby (Figure 1.8). Merchenthaler et al used riboprobes to investigate the distribution of GLP-1R mRNA in the spinal cord and discovered the highest distribution of GLP-1R mRNA within lamina X of the spinal cord, as well as lower amounts throughout lamina V-IX (Merchenthaler et al., 1999).

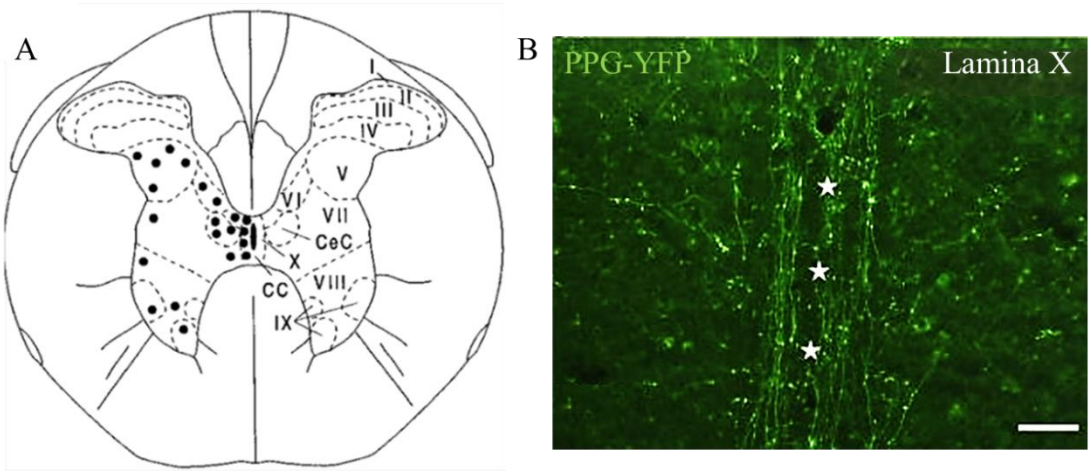

Figure 1.6: Localisation of GLP-1Rs in the mouse spinal cord and evidence of possible innervation by GLP-1 expressing neurons.

A. Data from a thoracic section of spinal cord using in-situ hybridisation, GLP-1R localisation can be seen through lamina V-X with dense expression particularly in lamina X. Image obtained from Merchenthaler et al, 1998.

B. A longitudinal section of lumbar-sacral spinal cord from a PPG-YFP transgenic mouse, dense PPG tracts (stars) can be seen running rostrocaudally along the extent of the dorsal lamina X, adjacent to the central canal. Scale bar: 100 μm. Adapted from Llewellyn-Smith et al, 2015.

1.3.2.3 Which CNS cells express the GLP-1R?

There is also a large degree of debate over the cell types within the CNS that express GLP-1Rs, particularly with respect to its expression in neuronal or glial cells. A summary of the relevant literature can be found in Table 1..

Table 1.2: A summary of the literature regarding GLP-1R expression on specifically neuronal cells, glial cells, or both cell types within the spinal cord.

Cell type(s)	Species and age	Method used	Reference
Neuron only	Mouse pups	Single cell RNA sequencing, all spinal cord regions	(Rosenberg et al., 2018)
	Adult rat	Immunofluorescence, region not specified (GLP-1R, not specified, Santa Cruz)	(Han et al., 2020)
		In-situ hybridisation, all spinal cord regions.	(Merchenthaler et al., 1999)
Neurons and glia	Adult mice	Immunofluorescence, thoracic region (GLP-1R, ab218532; Abcam)	(Qian et al., 2022)
	Adult mice, Neonatal rat	RT-PCR on rat microglial cultures Immunofluorescence, thoracic region (GLP-1R, antibody not specified)	(C.-H. Lee et al., 2018)
	Adult rats	Immunofluorescence, thoracolumbar region (GLP-1R, not specified, Santa Cruz)	(Chen et al., 2017)
Microglia only	Rat pups	RT-PCR of dorsal horn cultures Immunofluorescence, lumbar region (GLP-1R, Ab119287, Abcam)	(Gong et al., 2014)

While it is largely in agreement that some types of neurons express GLP-1Rs, the presence of this receptor on glial cells in physiological versus injury conditions is under some debate. Rosenberg et al performed single-cell RNA sequencing of all cells within the postnatal mouse spinal cord and found that only CSFcNs contained GLP-1R RNA (Rosenberg et al., 2018). Cork et al, using a transgenic GLP-1R fluorescent mouse model, found no overlap between cells expressing the GLP-1R and astrocyte marker GFAP in the brain, indicating that astrocytes are unlikely to express this receptor in detectable quantities (Cork et al., 2015).

Gong et al also found no colocalisation with GFAP using immunofluorescence methods, in both the physiological state and after peripheral nerve injury, but did identify specific upregulation of GLP-1Rs on OX42 positive microglial cells in the dorsal horn after peripheral injury (Gong et al., 2014). In direct contrast to this, Lee et al performed immunofluorescence on naïve mouse spinal cord and found GLP-1R expression on both GFAP positive astrocytes and IBA1 positive microglia, which were then significantly downregulated in both spinal cord models of experimental autoimmune encephalomyelitis and culture models treated with lipopolysaccharide (LPS) to induce microglial activation (C.-H. Lee et al., 2018).

It is likely that conflicting reports of GLP-1R expression on various cell types within the CNS are dependent on the different animal models and methods used to identify these receptors, and the different conditions they are studied in (Pyke and Knudsen, 2013). However, this conflict of opinion has not prevented the investigations into the treatment of various neurological and neurodegenerative conditions using GLP-1R agonists.

1.3.3 Therapeutic actions of GLP-1R agonists within the CNS

Neurodegenerative disease and injury to the CNS are major health challenges worldwide, and there is a pressing need for effective therapeutic strategies to combat these conditions. GLP-1R agonists have been shown in many studies to exert neuroprotective and regenerative effects within the CNS and therefore represent an attractive target for therapeutic intervention. The neuroprotective and growth factor like properties of GLP-1 have been studied extensively using cell cultures of

astrocytes (Bao et al., 2015), microglia (Gong et al., 2014; C.-H. Lee et al., 2018) and neurons (Li et al., 2009; An et al., 2015; Cai et al., 2017), wild-type and transgenic animal models of neurodegenerative disease (Li et al., 2012; Ma et al., 2015; Bassil et al., 2017) and in clinical trials involving human subjects (Jaiswal et al., 2015; Athauda et al., 2017; Gejl et al., 2017).

Within the literature, the neuroprotective effects of liraglutide are thought to be due to its anti-oxidative effects, role in reducing apoptosis and encouraging autophagy, and promotion of neurogenesis and neural differentiation. For comprehensive reviews on this subject please refer to Erbil et al., 2019, and Zhang et al., 2021.

1.3.3.1 Reducing inflammation and oxidative damage

Glucagon-like peptide 1 (GLP-1) analogues have been shown to have neuroprotective effects, which include reducing inflammation and oxidative damage caused by disease or injury within the CNS. Chronic inflammation and increased amounts of reactive oxygen species (ROS) can be found in neurodegenerative diseases such as Parkinson's or Alzheimer's disease, and are also complicating issues in the acute to chronic stages of traumatic CNS injury.

Parthsarathy and Hölscher induced chronic inflammation within the mouse brain through irradiation with x-rays and then treated a subgroup with daily intraperitoneal injections of liraglutide for 30 days. After 30 days, irradiated animals that had been treated with liraglutide had 50% and 61% fewer activated microglia and astrocytes respectively within the cortex when compared with irradiated animals without treatment. Irradiated animals treated with liraglutide also showed significantly reduced levels of inflammatory cytokines Tumour Necrosis Factor-α (TNF-α), Interleukin-6 (IL-6), Interleukin-1beta (IL-β), and Interleukin-12p70 when compared with irradiated saline mice, but not when compared with non-irradiated control mice indicating a return of inflammation to baseline levels (Parthsarathy and Hölscher, 2013).

Li et al investigated the antioxidative potential of exendin-4 in rats that had undergone contusion injury of the spinal cord and then were immediately given a large (10 μg) intraperitoneal injection of exendin-4. Twenty four hours after injury,

they found a significant lower levels of malondialdehyde (MDA), a lipid peroxidation by-product used as an indicator of cellular oxidation (Cheng et al., 2011) when compared with a group that had undergone SCI without treatment with exendin-4. In other studies, there was a significantly higher level of glutathione (GSH), a tripeptide that plays an essential role in maintaining homeostasis within the cellular redox environment and defending cells from harmful reactive oxygen species (Circu and Yee Aw, 2008) with exendin4 treatment compared to the control group,. This demonstrates that some of the neuroprotective effects of GLP-1R agonists are likely due to an anti-oxidative function (Li et al., 2015).

1.3.3.2 Reducing apoptosis and encouraging autophagy

Spinal cord injury and neurodegenerative diseases can lead to the activation of apoptotic and autophagic pathways, which contributes to the loss of neurons and glial cells in the spinal cord. Autophagy and apoptosis are two distinctive cellular processes that contribute to maintaining cellular homeostasis and regulating cell death (Oyinbo, 2011; Fan and Zong, 2013; Li et al., 2016). Autophagy involves the degradation of damaged or dysfunctional cellular components such as organelles and proteins through the lysosomal pathway, whereas apoptosis is a programmed cell death process triggered by various stimuli, including DNA damage and oxidative stress (Oyinbo, 2011; Fan and Zong, 2013). The relationship between autophagy and apoptosis is complex and context dependent (Fan and Zong, 2013). Autophagy may act as a pro-survival mechanism, preventing apoptosis by eliminating damaged cellular components and promoting cell survival (Oyinbo, 2011; Fan and Zong, 2013). However, excessive or prolonged activation of autophagy can result in cell death and facilitate apoptosis activation (Oyinbo, 2011; Fan and Zong, 2013).

In one of many studies (Perry et al., 2002; Salcedo et al., 2012; Chien et al., 2015; Zhu et al., 2016), Chen et al used a compression model of SCI in rats to investigate the role of subcutaneously administered liraglutide in suppressing apoptosis and encouraging autophagy to promote increased cell survival. They found that rats treated with liraglutide daily for 28 days showed significant improvement in locomotor recovery, smaller necrotic cavities, and lower extents of motor neuron loss compared with an untreated SCI group. Investigating this further, they observed

higher levels of apoptotic markers, caspase-3 and Bax, upregulation of the anti-apoptotic protein, Bcl-2, and a lower number of apoptotic cells as deduced by TUNEL staining in the liraglutide treated SCI group. Co-treatment with 3-MA, an autophagy inhibitor, or knockdown of the GLP-1R ameliorated the beneficial effects of liraglutide resulting in no significant difference in protein expressions or behaviour to the untreated SCI rats (Chen et al., 2017). These results indicate a role for GLP-1R agonists in promoting functional recovery after SCI through promotion of autophagy and cell survival over apoptosis and cell loss.

1.3.3.3 Promoting neurogenesis and neuroplasticity

The CNS exhibits limited regenerative capacity in response to injury or disease. This, coupled with the significant loss of neuronal and glial cells that often accompanies such conditions, often translates to poor outcomes for patients. To improve patient outcomes, it is important to encourage the survival of these cells and facilitate the growth and development of new neurons and their associated pathways. Achieving these goals may lead to enhanced recovery and improved functional outcomes in many cases of SCI or neurodegenerative disease.

In a study conducted by Yang et al, the impact of daily intraperitoneal administration GLP-1R agonist semaglutide on a rat model of stroke was investigated. The study demonstrated that after a 7-day treatment period, the size of the infarction was smaller, chronic inflammation was mitigated, and there was a significant improvement in motor activity and neurological impairments compared to stroke animals without treatment. Furthermore, a significant higher level of neurogenesis within the hippocampus were observed, as evidenced by the upregulation of neurogenesis-related biomarkers such as nestin, doublecortin, stromal cell-derived factor 1- α (SDF-1α), and its receptor CXCR4 (Yang et al., 2019).

When given to naïve rats, twice daily intraperitoneal injections of exendin-4 were found to have twice the number of BrdU positive cells within the SVZ after 7 days of treatment, compared with rats treated with saline. In addition, the number of newly proliferated cells that expressed Dcx was higher by 1.7-fold compared to control animals, indicating that exendin-4 treatment stimulated neurogenesis in the SVZ (Bertilsson et al., 2008). Similar higher numbers of newly proliferated cells co-

expressing early neuronal markers were observed in the dentate gyrus of adult mice when peripherally treated with GLP-1R agonists (Hamilton et al., 2011; McGovern et al., 2012; Yang et al., 2019).

The effects of GLP-1 and analogues on neurogenesis in the ependymal layer after traumatic spinal cord injury have not yet been discussed in the literature, but evidence exists to support a role in neuroprotection, cell proliferation and neuronal differentiation within other neurogenic niches of the CNS.

1.3.4 GLP-1R mediated exocytosis

1.3.4.1 Molecular signalling pathways

Exocytosis is a highly regulated process that allows cells to release a wide array of molecules, including hormones and neurotransmitters, to the extracellular environment. The exocytotic process is tightly controlled by a series of molecular events that involve the docking, priming, and fusion of secretory vesicles with the plasma membrane (Sudhof, 2004). Upon binding to GLP-1, or its analogues, the GLP-1R activates a complex intracellular signalling cascade that results in the modulation of several cellular processes, including exocytosis (Figure 1.7).

The modulation of exocytotic activity within the GLP-1R works through the $G\alpha_s$ subunit which begins with the adenylate cyclase mediated increase in cAMP levels (Drucker et al., 1987; Baggio and Drucker, 2007). The rise in cAMP levels activates protein kinase A (PKA), PKA phosphorylates proteins involved in increasing the activity of voltage-dependant calcium channels (VDCCs) of neurons, which are critical for Ca^{2+} influx during exocytosis (Sang et al., 2016). PKA also phosphorylates several target proteins involved in exocytotic processes such as synapsin I, a protein involved in vesicle docking and priming, leading to the mobilisation of vesicles from the reserve pool into a primed position (Yu et al., 2021), and Munc18, a protein that plays a key role a role in the assembly of SNARE complexes and regulating membrane fusion (Toonen and Verhage, 2007).

Furthermore, calcium levels are also regulated by the activity of phospholipase C (PLC) and inositol trisphosphate receptors (IP3Rs) (Dolphin, 1998). GLP-1 receptor activation stimulates PLC activity, through activation of the exchange protein

activated by cAMP (Epac) pathway, leading to the production of inositol trisphosphate (IP3) and diacylglycerol (DAG) (Baggio and Drucker, 2007). IP3 acts as a second messenger and binds to IP3Rs on the endoplasmic reticulum (ER), resulting in the release of Ca^{2+} from the ER stores. Increased calcium levels can also result in calcium induced calcium release (CICR) by stimulation of ryanodine receptors (RyR) on the ER, resulting in further calcium release and higher intracellular calcium levels (Morris and Malbon, 1999; Tomas et al., 2020). The increase in intracellular Ca^{2+} levels can then trigger vesicle fusion with the plasma membrane, the duration of which can be increased by increasing cAMP levels leading to sustained release of contents (Sudhof, 2004; Silva et al., 2021). Moreover, DAG generated by PLC activation can activate protein kinase C (PKC), which has been implicated in regulating vesicle docking and priming events (Hilfiker and Augustine, 1999).

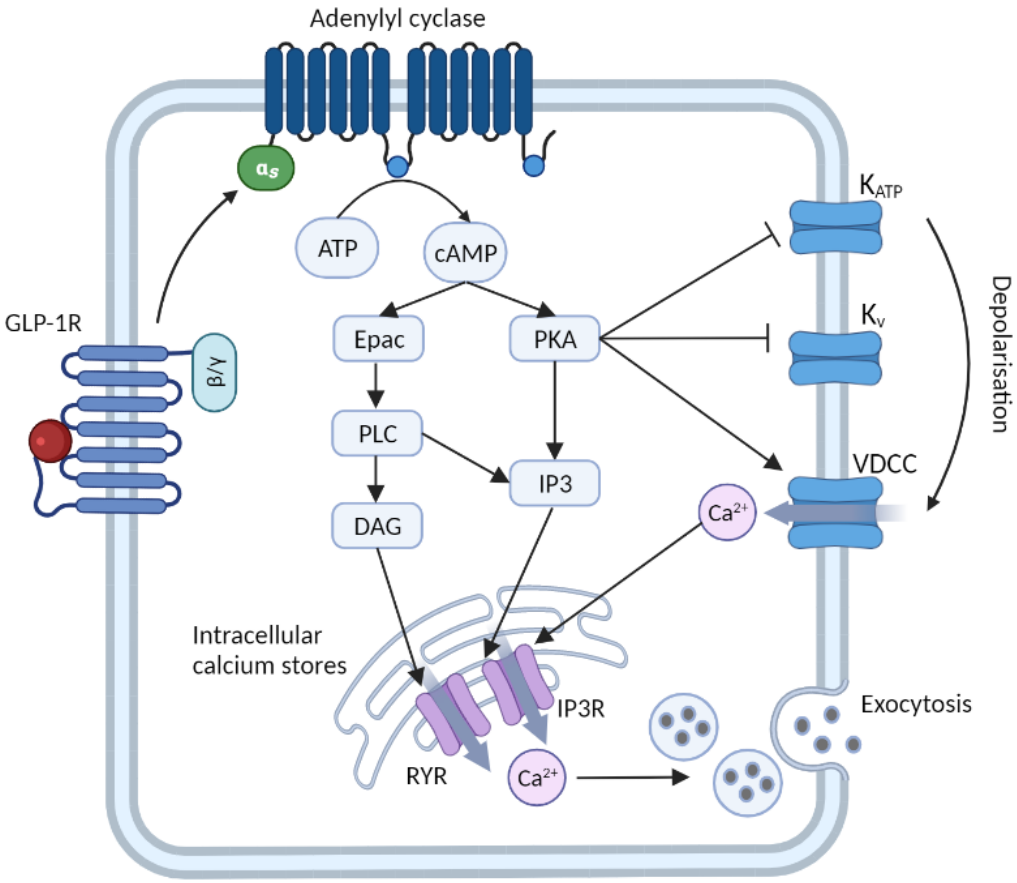

Figure 1.7: Overview of the main signalling pathways of GLP-1R resulting in exocytosis.

GLP-1 binds to the receptor which activates adenylyl cyclase and increases cAMP(Green et al., 2004). Protein kinase A (PKA) and exchange protein directly activated by cAMP (Epac) pathways are subsequently activated. PKA causes inhibition of ATP sensitive potassium channels (K_{ATP}) as well as rectifying potassium channels (K_V), this in combination with activation of voltage dependent calcium channels (VDCC) results in depolarisation, propagation of action potential, and influx of calcium. Calcium influx, and products produced through PKA and Epac pathways act on ryanodine receptors (RYR) and iono-cyotol-3-phosphate receptors (IP3R) resulting in release of calcium from intracellular endoplasmic reticulum stores, further increasing intracellular calcium and resulting in fusion of vesicles and exocytosis. Abbreviations: DAG, diacylglycerol; PLC, phospholipase-C. Figure created with Biorender.com.

1.3.4.2 GLP-1R mediated exocytotic effects: insights from experimental studies

The exocytotic effects of GLP-1 on pancreatic β cells is well studied as a mechanism behind insulin release (Drucker et al., 1987; Green et al., 2004; Graham et al., 2020), but several studies have also shown evidence that a similar mechanism occurs in neurons.

Rebosio et al investigated the exocytotic effects of GLP-1R stimulation using a model of purified synaptosomes from mouse hippocampal neurons, that possessed the GLP-1R, in combination with radioactively labelled [^{3}H]GABA and [^{3}H]D-aspartate. These synaptosomes were plated in a quasi-monolayer and continuously superfused with a physiologically appropriate solution in order to prevent the accumulation of neurotransmitters and reduce the possibility of indirect secondary effects. Application of exendin-4 (Ex-4) resulted in a 30% increase in [^{3}H]GABA release and a 37% increase in [^{3}H]D-aspartate, when compared with spontaneous release, in response to depolarisation induced by KCl. These effects were completely blocked by addition of GLP-1R antagonist exendin-(9-39) or by the adenylate cyclase inhibitor 2',5'-dideoxyadenosine, which displayed no effect when given alone (Rebosio et al., 2018). These results indicate that GLP-1R agonists display a potentiating effect on the depolarisation induced release of neurotransmitters from CNS neurons.

Further supporting this idea, a study by González-Santana investigated the potentiating effects of GLP-1R stimulation in adrenal medulla chromaffin cells. They found that incubation of these cells with exendin-4 for 24 hours resulted in the increased biosynthesis of adrenal catecholamines (CA), hormones released by chromaffin cells in response to stress (Paravati et al., 2023). Next, they used single-cell amperometry to measure the release of CA when cells were depolarized in the presence of Ex-4 for 20 minutes. They found that cells treated with Ex-4 increased the secretion of CA by 75%, but did not increase the frequency of release events, indicating that Ex-4 treatment increases the size of the vesicles primed for secretion. This was found to be mediated through the PKA pathway as incubation with H-89, a blocker of PKA activity, abolished the response to Ex-4 (González-Santana et al., 2021).

While no studies have investigated the exocytotic potentiating effects of GLP-1R modulation within cells of the spinal cord, it can perhaps be reasoned that a similar response would occur. It is possible that activation of the GLP-1R on CSFcNs within the ependymal layer could either induce, or potentiate, the release of neurotransmitters into the CSF or surrounding extracellular fluid in order to exert wider effects within the spinal cord circuitry. However, this purely remains speculative at this point and further work is needed to fully understand whether there is a link between these two systems.

1.4 HYPOTHESIS AND AIMS

The GLP-1 system within the literature has been linked to multiple functions within the CNS, including that of neurogenesis and neuroprotection. Activation of GLP-1Rs on neurons is associated with stimulating cell proliferation, enhancing neuronal survival, and mitigating neuroinflammation in a range of animal models associated with injury and disease. Investigations into the effects of these analogues have focused on well-known neurogenic niches of the brain, including the subventricular zone (SVZ) and the dentate gyrus of the hippocampus, but little is known regarding the influence of GLP-1R agonists on proliferation within the EC layer.

CSFcNs are enigmatic cells that exist within the EC layer surrounding the central canal of the spinal cord. These cells have been implicated in many aspects of spinal function, and are thought to play a role in sensing and responding to changes in the composition of the CSF. Closely neighbouring these cells are the ECs that exhibit properties akin to neural stem cells. They undergo self-renewal to maintain the cell population and display rapid proliferation when injured (Meletis et al., 2008; Moreno-Manzano, 2020). CSFcNs have been hypothesised to influence the quiescence of cells within this niche through the release of GABA, similar to the behaviour observed within the neuroblasts of the SVZ, and therefore represent an intriguing target for modulation by GLP-1R agonists.

While mRNA encoding the GLP-1 receptor (GLP-1R) has been identified in various neuronal and glial cells distributed across the spinal cord (Merchenthaler et al., 1999; Russ et al., 2021), little information exists concerning the precise cellular expression of this receptor within the EC layer vicinity.

Work performed in this thesis will be the first to investigate the presence of GLP-1 receptors within the cells of the spinal cord, with a particular focus on cells within the ependymal layer, focusing on CSFcNs. The presence of active GLP-1Rs will be investigated through the use of immunohistochemical techniques, and their functionality and sensitivity will be evaluated through the use of calcium imaging experiments.

Finally, the effects of GLP-1R agonists on neurogenesis and viability of the cells within the spinal cord will be investigated through the use of *ex vivo* models, such as

acute slice and organotypic spinal cord slice culture experiments, as well as *in vivo* intraperitoneal injections. This investigation aims to broaden the understanding of the potential therapeutic applications of GLP-1R agonists in the treatment of spinal cord injury and neurodegenerative conditions.

The aims of this study are:

1. To investigate the expression of GLP-1Rs by CSFcNs, and to determine the extent of innervation of these cells by GLP-1 neurons.
2. To determine the effects of bath application of GLP-1R agonists on intracellular calcium levels within CSFcNs.
3. To determine the potential therapeutic applications of GLP-1R agonists in the treatment of spinal cord injury by assessing their effects on proliferation in short- and long-term *ex vivo* injury models.
4. To investigate the effects of systemic application of GLP-1R agonists on proliferation and differentiation of cells within healthy *in vivo* mouse models.

Chapter 2 – General Methods

2.1 ANIMALS

All experiments were carried out in accordance with the UK Animals (Scientific Procedures) Act 1988 and the ethical standard as set out by the University of Leeds Ethical Review Committee. All mice were housed in standard conditions with a 12-hour light-dark cycle and ad-libitum access to food and water. Throughout all experiments, every effort was made to follow the 3Rs (replacement, reduction and refinement) to minimise the number of animals used and ensure welfare.

Seven strains of juvenile to adult mice (2.5 – 9 weeks) were used in these experiments. C57BL/6 wild type mice, PKD2L1-cre mice, PKD2L1-GCaMP6f mice, and VGAT-GCaMP6f mice were bred and maintained in house at the University of Leeds. Tissue from GLP1R-GCaMP3, GLP1R-RFP and PPG-YFP mice was kindly gifted by Professor Stefan Trapp and Dr Marie Holt from University College London (Reimann et al., 2008; Llewellyn-Smith et al., 2011; Richards et al., 2014; Cork et al., 2015).

The number of sections and mice used, as well as their strains and ages at time of experiments, are listed in tables within the individual methods sections for each chapter.

2.1.1 PKD2L1-Cre

PKD2L1-Cre mice (BL/6.129X1/SVJ(F1)<tm1(cre), MGI:6451758, Ye et al., 2016) were gifted by Sue C. Kinnamon (University of Colorado, USA) and maintained in lab. PKD2L1 is expressed by CSFcNs in the spinal cord (Djenoune et al., 2014), and the introduction of the IRES-Cre transgene immediately after the PKD2L1 stop codon allows for the selective targeting of this gene when crossed with a floxed mouse line or virus, enabling the visualisation of CSFcNs in the PKD2L1xGCaMP6f mouse line as discussed below.

2.1.2 PKD2L1-GCaMP6f

PKD2L1-GCaMP6f mice were used to visualise and record activity in CSFcNs, particularly for use in calcium imaging experiments. To generate PKD2L1-GCaMP6f mice, PKD2L1-Cre (BL/6.129X1SVJ(F1)<tm1(cre), MGI:6451758) were crossed in-house with GCaMP6f.flox (B6J.CgGt(ROSA) 26Sor<tm95.1 (CAGGCaMP6f), Jax stock 028865) mice.

2.1.3 VGAT-GCaMP6f

To generate VGAT-GCaMP6f mice, VGAT.Cre (B6J.129S6(FVB)-Slc32a1<tm2(cre), Jax stock 028862) mice were crossed in-house with GCaMP6f.flox (B6J.CgGt(ROSA)26Sor<tm95.1 (CAGGCaMP6f), Jax stock 028865) mice. Both mouse lines were originally from Jackson Laboratory (Maine, USA) and maintained in house.

2.1.4 Animals used in each experimental chapter

The number of sections and mice used, as well as their strains and ages at time of experiments, are listed in tables below.

Table 2.1: Numbers of animals, sections per animal, and details of region, strain and age used in experiments for Chapter 3.

Experiment reference	Animals (N)	Sections per animal (n)	Region	Strain	Age (days)
3.3.1 Figure 3.2 (Transverse)	3	5	Cervical	PKD2L1-GCaMP6f	18 - 112
		5	Thoracic		
		5	Lumbar		
		5	Sacral		
3.3.1 Figure 3.2 (Horizontal)	3	2	Cervical	PKD2L1-GCaMP6f	30 - 63
3.3.1 Figure 3.3	3	8	Thoracic	PKD2L1-GCaMP6f	45 - 63
3.3.1 Figure 3.4	3	8	Thoracic	PKD2L1-GCaMP6f	45 - 63
3.3.2 **Figure 3.5** Figure 3.5 Figure 3.6	6	5	Cervical	PKD2L1-GCaMP6f	18 - 132
		5	Thoracic		
		5	Lumbar		
		5	Sacral		
	2	5	Cervical	GLP1R-GCaMP3	90 - 160
		5	Thoracic		
		5	Lumbar		
		5	Sacral		
3.3.2 Figure 3.7	3	5	Thoracic	VGAT-GCaMP6f	75 - 112
3.3.2 Figure 3.8	2	5	Thoracic	C57BL/6	60 - 65
3.3.3 Figure 3.9	2	2	Brainstem	PPG-YFP	90 - 125
3.3.3 Figure 3.10 Figure 3.11	2	4	Cervical		
		4	Thoracic		
		4	Lumbar		
		4	Sacral		

Table 2.2: Numbers of animals, sections per animal, and details of age used in experiments for Chapter 4.

Several experiments used slices obtained from the same mouse to reduce the maximum number of animals used for this research, and therefore the total number of mice used across all experiments is 19.

Experiment reference	Animals (N)	CSFcNs (total)	Age (days)
4.2.1 Figure 4.1	19	120	18 - 72
4.2.1 Figure 4.2	3	14	23 - 27
4.2.1 Figure 4.3	4	16	18 - 52
4.2.2 Figure 4.4	4	15	18 - 32
4.2.2 Figure 4.5	6	43	18 - 72
4.2.2 Figure 4.6 Figure 4.7 Figure 4.8	1 nM: 4 10 nM: 4 100 nM: 4 1 μM: 6	32 26 43 43	18 - 72
4.2.2 Figure 4.9	4	21	24 - 46
4.2.3 Figure 4.10	4	25	22 - 52

Table 2.3: Numbers of animals, sections per animal, and details of region, strain and age used in experiments for Chapter 5.

Experiment reference	Animals (N)		Sections per animal (n)		Region	Strain	Age (days)
	Control	Test	Control	Test			
5.2.1 Figure 5.1	4	4 (10 nM) 4 (100 nM) 4 (1 μM)	3	3 (10 nM) 4 (100 nM) 3 (1 μM)	Thoraco-lumbar	PKD2L1-cre	23 – 30
5.2.2 Figure 5.2	6	6 (1 μM) 6 (10 μM)	5	7 (1 μM) 4 (10 μM)			28 - 56
5.2.2 Figure 5.3	6	6 (1 μM) 6 (10 μM)	5	3 (1 μM) 3 (10 μM)			29 - 63
Error! Reference source not found. Figure 5.4	4	4 (1 μM) 4 (10 μM)	3	3 (1 μM) 3 (10 μM)			29 - 52
5.2.3 Figure 5.8	4	4 per gel	3	3			31 - 58
5.2.3 Figure 5.6							
5.2.3 Figure 5.7							
5.2.4 Figure 5.8	5 each	5 (ex-4) 5 (lira)	5	5	Lumbar	C57BL/6	63 - 70
5.2.4 Figure 5.9							
5.2.4 Figure 5.10							
5.2.4 Figure 5.11	5 each	5 (ex-4) 5 (lira)	3	3	Hippocampus		

2.2 IMMUNOHISTOCHEMISTRY

2.2.1 Introduction

Immunohistochemistry (IHC) enables the visualisation of cells or proteins of interest by utilising the principle that primary antibodies will bind specifically to an antigen of interest, which can then be visualised through the addition of a fluorophore that binds to the primary antibody (Figure 2.1).

To generate a primary antibody, an antigen of interest can be used to immunise a host animal, such as a rabbit. Subsequently, the animal produces antibodies to the antigen, which can be extracted, purified, and utilised in biological research. Antibodies raised in this manner are typically polyclonal, meaning that they recognise and bind to multiple different epitopes within the protein. Monoclonal antibodies, on the other hand, which bind to a single epitope, can also be generated against a protein of interest using cell lines (Lu et al., 2020). A secondary antibody, raised against the species in which the primary antibody is raised, is then used for the detection of the primary antibody. This secondary antibody is labelled with a fluorescent tag for visualisation purposes.

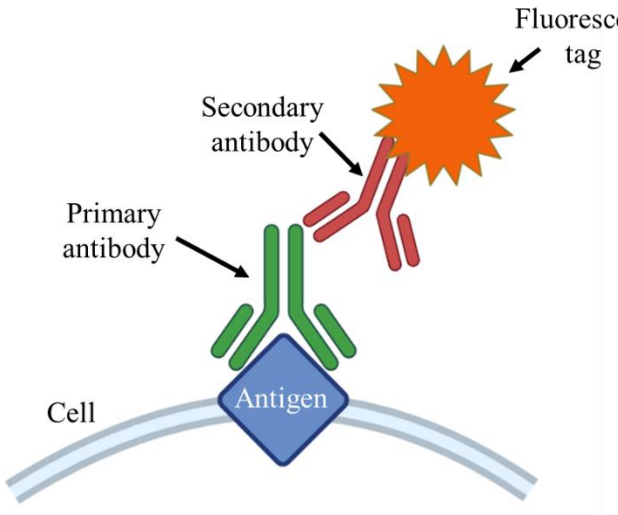

Figure 2.1: Indirect immunohistochemical labelling schematic.
This method utilises a primary antibody raised against an antigen of interest, and a secondary antibody with a fluorescent tag which binds to the primary antibody to enable visualisation.

2.2.2 Tissue preparation for IHC

Animals were terminally anaesthetised with an intraperitoneal injection of sodium pentobarbital (60 mg/kg, Euthatal, Merial Animal Health, Dublin). The absence of pedal and corneal withdrawal reflexes confirmed adequate depth of anaesthesia. The chest cavity was opened at the xiphoid process using blunt-ended scissors, followed by perforation of the diaphragm and cuts along the lateral edges of the chest wall up to the clavicle. Care was taken to avoid damaging the liver and compromising the perfusion quality. A cannula was inserted into the left ventricle of the heart, and an opening was made in the right atrium to allow transcardial perfusion. First, 50 ml of 0.1M phosphate buffer (PB) was perfused to clear the blood, followed by perfusion with 200 ml of 4% paraformaldehyde (PFA) in 0.1M PB to fix the tissue.

Following fixation, an incision was made along the midline of the back, allowing the removal of soft tissues to expose the vertebrae. The spinal cord and brain were carefully extracted using coarse forceps and small spring scissors (World Precision Instruments, catalogue # 654558). The harvested tissue was post-fixed overnight in 4% PFA at 4ºC. After postfixation, the meninges were removed using fine forceps under a dissection microscope. The spinal cords and brains were then stored in 0.1M phosphate-buffered saline (PBS) supplemented with 0.1% sodium azide at 4ºC until further use.

For the coronal sectioning of the thoracolumbar region, the spinal cord tissue was cut into sections approximately 0.5 cm long using a scalpel blade and glued to the plate of a vibrating microtome (Leica VT100S, Microsystems). The bath was filled with 0.1M PB to prevent the tissue drying out, and the tissue was serially sectioned at 40 µm with an amplitude of 0.4 mm/s and a vibrating frequency of 80 Hz. The sections were gently picked up using a paintbrush and transferred to a 24-well plate containing phosphate-buffered saline (PBS) for subsequent fluorescent labelling of cellular markers and/or EdU.

2.2.3 IHC on fixed tissue

Optimisation experiments were carried out to determine the permeabilisation solution and concentrations for each antibody used.

Sections were washed 3 x 10 minutes in 0.1 M PBS prior to incubation with primary antibody solutions to ensure removal of all PFA. Primary antibody incubations were performed for 24 hours at 4^{o}C in 0.1% Triton X-100 (PBST) as a permeabilisation agent for the cell membrane, and with 5% donkey serum as a non-specific binding blocker.

Sections were then washed 3 times with PBS (10 minutes) before addition of the appropriate Alexa Fluor conjugated secondary antibody (1:1000 in PBS, Thermofisher) at RT for 2h, slices were protected from light during this step to avoid photobleaching of the fluorophore. These were then washed twice with PBS (10 minutes) before mounting on microscope slides and allowed to air dry. Sections were covered using Vectashield with DAPI mounting media (VectorLabs, cat no. H-1800) and a glass coverslip was added and sealed using nail varnish.

Primary and secondary antibodies used can be seen in Table 2.4 and Table 2.5 respectively.

Table 2.4: All primary antibodies used on fixed tissue sections

Cell / structure type	*Antibody*	*Host*	*Dilution*	*Source / Cat. #*
GCaMP6f expressing cells	GFP	Chicken	1:1000	Abcam / ab13970
GCaMP3 expressing cells				
YFP expressing cells				
CSFcNs	PKD2L1	Rabbit	1:500	Proteintech / 13117-2-AP
Oligodendrocytes	Pan-QKI	Mouse	1:100	Neuromab / 73-168
Microglia	Iba1	Rabbit	1:1000	Thermofisher / PA5-27436
Astrocytes	S100β	Rabbit	1:1000	Abcam / ab41548
Neurons	HuC/D	Rabbit	1:1000	Proteintech / 13032-1-AP
Ependymal cells	Sox2	Rabbit	1:1000	Millipore / AB5603
GLP-1R expressing cells	GLP-1R	Mouse	1:500	DSHB / Mab7F38
Synaptic vesicles	SV2	Mouse	1:100	DSHB / SV2
	Synaptophysin	Rabbit	1:1000	Abcam / ab14692

Table 2.5: All secondary antibodies and fluorophores used for the visualisation of primary antibodies.

Antibody	*Host*	*Antigen*	*Dilution*	*Source*
Alexa Fluor 488	Goat	Chicken	1:1000 v	Invitrogen / A-11039
	Donkey	Rabbit	1:1000	Invitrogen / A-32794
Alexa Fluor 555	Donkey	Rabbit	1:1000	Invitrogen / A-31572
		Mouse	1:1000	Invitrogen / A-31570
Biotinylated azide	Donkey	Rabbit	1:500	Invitrogen / A-16027
		Mouse	1:500	Invitrogen / A-16021
Streptavidin-HRP		Biotin	1:1000	Invitrogen / N-100

2.2.4 Immunofluorescence with the GLP-1R antibody

Due to the relatively weak expression of the GLP-1 receptor in cells, additional enhancement of the signal was required.

Sections were washed 3 x 10 minutes in 0.1 M PBS prior to incubation with primary antibody solutions to ensure removal of all PFA. A peroxidase quenching step, to reduce autofluorescence and background staining, was performed using 3% hydrogen peroxide in PBS for 30 minutes at RT, and sections were again washed 3 x 10 minutes in PBS. Primary antibody incubations were performed for 24 hours at 4^{o}C in 0.1% Triton X-100 (PBST) as a permeabilisation agent for the cell membrane, and with 5% donkey serum as a non-specific binding blocker.

Following this, sections were washed 3 x 10 minutes with PBS and incubated in a solution containing a biotinylated secondary antibody (donkey-anti-mouse for GLP-1R, Invitrogen) at RT for 2 hours. Sections were then washed 3 x 10 minutes in PBS before being incubated with Streptavidin-HRP (Invitrogen) in PBS at RT for 2 hours, after which sections were again washed 3 x 10 minutes in PBS.

3,3'-Diaminobenzidine (DAB)

DAB staining is a widely used methods for visualisation of IHC due to its increased sensitivity over traditional fluorescent methods and the permanence of the staining. The reaction between the DAB substrate and HRP produces an insoluble brown precipitate at the site of antigen-antibody binding allowing localisation of these sites.

Following the steps detailed above, sections were incubated with DAB working solution (DAB substrate kit, Vector labs) for 2 – 10 minutes at RT. The reaction progress was monitored for formation of the brown precipitate through use of a light microscope, and reaction was stopped by washing sections three times with distilled water. After this, sections were mounted on gelatinised slides, dehydrated using a series of alcohol concentrations (0 – 100 % ethanol in dH_2O), and DPX non-aqueous mounting media (Sigma-Aldrich) was added before a coverslip was placed on top and sealed with nail varnish.

Tyramide signal amplification (TSA)

TSA is similar to DAB staining as it enhances weak IHC signals much more than standard secondary fluorophores while maintaining a high signal definition and localisation. However, DAB staining can be complex to use when performing double labelling IHC experiments, whereas TSA is perfectly suitable for use alongside standard IHC protocols.

Following the steps detailed above, sections were incubated with TSA working solution (DAB substrate kit, Vector labs) for 2 – 10 minutes at RT. The reaction was monitored periodically through by use of a fluorescent microscope, and the reaction was stopped by washing sections 3 x 10 minutes with PBS. Sections were mounted onto a glass slide with Vectashield with DAPI (VectorLabs, cat no. H-1800) and sealed with nail varnish.

In double labelling experiments, the standard IHC protocol was performed prior to TSA incubation.

2.2.5 Controls for IHC

To determine the specificity of the primary antibodies, multiple sources were consulted, including previous literature, manufacturer's data sheets and websites, and previously conducted tests for specificity were reviewed. The Allen Brain Atlas (http://www.brain-map.org/) was utilized as a reference to confirm the consistency of staining with their data.

To validate the absence of cross-reactivity and non-specific binding, omission controls were performed. All IHC experiments contained a control set of fixed slices (2 to 4 slices) that were incubated in the appropriate secondary antibody, without first having been incubated in the primary antibody, to identify non-specific staining of the secondary antibody and determine levels of background staining. In the case of double labelling experiments, either the primary antibody or the EdU staining was omitted from the procedure, and the absence of any undesired cross-reactivity was confirmed (data not shown).

Where the immunolabelling was dependent on a transgenic reporter mouse model, the relevant literature for the mouse model was checked for any known expression issues before co-staining was performed using the primary antibody for the antigen and the relevant primary for the fluorophore within the model. For example, co-staining with the primary PKD2L1 antibody and an anti-GFP antibody was performed for verification of the PKD2L1-GCaMP6f mouse model.

2.3 5-ETHYNYL-2-DEOXYURIDINE (EDU) TREATMENT AND DETECTION

2.3.1 Introduction

EdU (5-ethynyl-2'-deoxyuridine) has emerged as a widely adopted method for assessing cell proliferation in the CNS (Salic and Mitchison, 2008). As a nucleoside analogue of thymidine, EdU becomes incorporated into DNA during the s phase of mitosis. Its detection relies on a click chemistry reaction wherein EdU's alkyne terminal group reacts with a fluorescent-azide (or a biotinylated-azide) in the presence of copper (Figure 2.2). EdU offers distinct advantages over other DNA synthesis detection assays, such as BrdU (5-bromo-2'-deoxyuridine), which necessitates DNA denaturation for BrdU detection. In contrast, the small size of the azide molecule allows easy penetration into tissues, enabling access to EdU incorporated into DNA without damaging the sample through denaturation. Consequently, EdU offers a more convenient and efficient approach for studying DNA synthesis and cell proliferation (Salic and Mitchison, 2008).

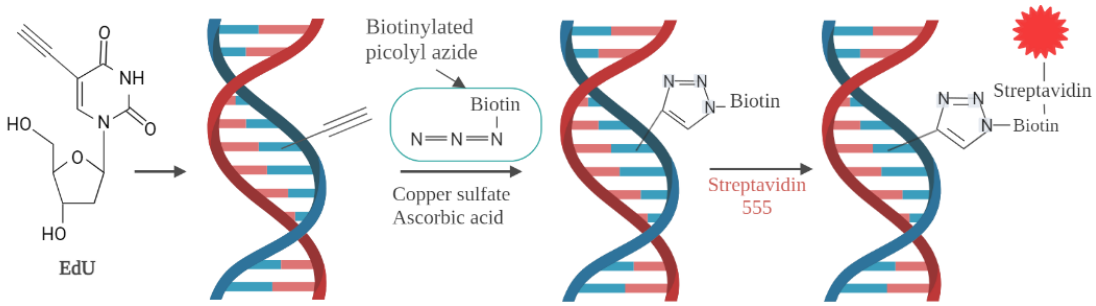

Figure 2.2: EdU labelling schematic.

EdU is incorporated into the DNA during S-phase of mitosis, this is visualised using a click chemistry reaction with biotinylated azide and streptavidin-555.

2.3.2 EdU detection in acute slices, organotypic spinal cord slices cultures, and fixed sections

All tissue undergoing EdU detection was treated in the same manner, with the exception that organotypic spinal cord slice cultures (OSCSCs) were not placed on plate shakers during the incubation steps due to their fragile nature.

The EdU detection reactions and incubation steps were conducted at room temperature. The sections were permeabilized using 0.2% PBST for 20 minutes, followed by two washes with 0.1 M Tris buffer for 10 minutes each. A solution was prepared by combining distilled water (320 µl), 2 M Tris (25 µl, pH 8.5), 5 mM Cu(II)SO4 (50 µl), and 1 mM biotinylated azide (5 µl), which was then added to each well. Subsequently, 0.5 M ascorbic acid (100 µl) was individually added to initiate the click chemistry reaction. After 15 minutes, this solution was removed and the sections were washed twice with 0.1 M Tris buffer for 10 minutes each, followed by an additional wash with PBS for 10 minutes. Next, the sections were incubated with Streptavidin 488 (1:1000) for 2 hours to facilitate visualization. Subsequently, they were washed three times with PBS for 10 minutes each. The slides were then mounted, allowed to dry, covered using Vectashield with DAPI (VectorLabs, cat no. H-1800), coverslipped, and sealed with nail varnish.

For double staining reactions involving EdU and a primary antibody, the primary antibody reaction was conducted following the initial EdU reaction step, after the final PBS wash but before the incubation with Streptavidin-488. The fluorophores for both the primary antibody and the EdU reaction were added simultaneously in the subsequent step.

2.4 ACUTE SLICE PREPARATION

2.4.1 Introduction

Acute spinal cord slices are regularly used in electrophysiological and calcium imaging techniques as these preparations preserve cellular functionality and allow the study of these cells within relatively intact local networks and cytoarchitecture. In order to obtain acute slices, the spinal cord must first be extracted from the spinal column.

Hydraulic extrusion of the spinal cord offers a significantly faster alternative to the traditional laminectomy method of spinal cord isolation, which involves extraction of the spinal cord through individually breaking the spinal vertebrae. A laminectomy must be performed delicately and swiftly in order to reduce the damage sustained by the tissue throughout the extraction process and subsequent deoxygenation, and as such is a technically difficult and time-consuming process. In contrast, hydraulic extrusion allows for rapid removal of the spinal cord while reducing the length of time required for the overall procedure and provides samples of similar overall histological quality when compared with those obtained through laminectomy (Kennedy et al., 2013; Richner et al., 2017).

2.4.2 Hydraulic extrusion and slice preparation

Mice were terminally anaesthetised with an intraperitoneal injection of sodium pentobarbital (60 mg/kg, Euthatal, Merial Animal Health, Dublin). The absence of pedal and corneal withdrawal reflexes confirmed adequate depth of anaesthesia. Mice were then rapidly decapitated using a large pair of surgical scissors. Opening of the spinal canal at the cervical region is ideal for this procedure as the spinal canal is widest at this region allowing for easy exit of the spinal cord later in the procedure. Following decapitation, a clean coronal cut was made directly through the lower lumbar portion of the spinal column, approximately at the level of the iliac crest to expose the caudal spinal cord. Particular care was taken not to damage the vertebral bone during any incisions. If the spinal cord was not visible, the column was washed with ice-cold continuously oxygenated (95% oxygen / 5% carbon dioxide, BOC) high sucrose aCSF (composition in Table 2.6) to remove any excess blood.

A 20 mL syringe was filled with ice-cold high sucrose aCSF and placed so that the tip fully surrounded the lumbar spinal canal, this was held in one hand while the other firmly but delicately gripped the spinal column. The plunger of the syringe was pushed, releasing a small amount (2-5 mL) of aCSF down the spinal column and ejecting the spinal cord into a dish containing oxygenating ice-cold high sucrose aCSF. After ejection, the full spinal cord was embedded in 3% (w/v) low melting point agar gel (Sigma-Aldrich). This agar gel was made up with aCSF to ensure correct osmolarity and prevent further osmotic shock damage to cells and was kept at 36^{o}C prior to embedding. After setting, the section of block containing the thoracolumbar spinal cord was cut using a fresh scalpel blade, extracted from the excess agar, glued to a chuck adjacent to an agar support block and submerged in continuously oxygenated ice-cold high sucrose aCSF.

The spinal cord was then sliced into 350 μm thick sections along the coronal plane using a vibrating microtome (Campden Instruments, Integraslice 7550 PSDS) with a stainless-steel blade.

2.4.3 Artificial cerebrospinal fluid compositions

Table 2.6: Compositions of high sucrose and standard artificial cerebrospinal fluid (aCSF).

Compound	High sucrose aCSF	Standard aCSF
	Concentration (mM)	
Sucrose	217	-
Sodium chloride (NaCl)	-	124
Glucose	10	10
Sodium bicarbonate ($NaHCO_3$)	26	26
Sodium phosphate monohydrate (NaH_2PO_4)	2.5	2.5
Potassium chloride (KCl)	3	3
Magnesium sulphate heptahydrate ($MgSO_4$)	2	2
Calcium chloride ($CaCl_2$)	1	2

Note: pH of aCSF was 7.4-7.5 after oxygenation, osmolarity was ~300 mOsm L^{-1}.

2.5.1 Set up and recording

Ca^{2+} imaging recordings were performed using a fluorescence microscope (BX50WI, Olympus), equipped with a Zylos sCMOS camera (Andor). Two lenses were used during these experiments: a 10x lens (Ach 10x/0.25w) for centering the slice, and a 60x lens (LUMPianFI/IP 60x/0.90w) for recordings. GCaMP6f fluorescence was excited at 470 nm using a pE excitation system (CoolLED, Andover), and images were acquired at 22.5 frames per second using the open source ImageJ plugin, MicroManager (Edelstein et al., 2010).

350 μm thick spinal cord slices were prepared as detailed in general methods (section 2.4) and compositions of standard aCSF can be found in section 2.4.3. Slices were rested and equilibrated in an incubation chamber containing room temperature, continuously oxygenated standard aCSF (Composition in Table 2.6) for 1 hour before recordings began.

Spinal cord slices were placed into a recording chamber and a small electrophysiology harp with tightly stretched threads was placed on top of the slice, with care to avoid disturbing the central canal area, to prevent the movement of the slice during recordings. A conical flask containing 400 mL of standard aCSF acted as the reservoir for recirculating aCSF during experiments and was continuously oxygenated (95% O_2: 5% CO_2) before perfusing the slice and returning to the reservoir. Perfusion was driven by a peristaltic pump (Gilson, Minipuls3) at a rate of 5 ml per minute.

2.5.1.1 Drug administration

The experimental set up remained consistent for drug administration experiments with the exception that smaller reservoirs of 100 mL standard aCSF containing the required concentration of drug were used when required. All drugs were bath applied and before switching the inlet tubing between reservoirs the pump was stopped to reduce the formation of bubbles and potential slice disturbances and restarted when submerged in aCSF.

In all experiments, a 3-minute recording of the slice during perfusion of standard aCSF was taken to characterise the spontaneous activity of each cell prior to drug administration. In general, 3-minute recordings were taken continuously during initial drug application and recirculation, reintroduction of standard aCSF, and where appropriate, after a further 5-minute recirculation with aCSF to evaluate a return to baseline spontaneous activity.

Timelines for individual experiments are shown within the figures and drugs used are listed in Table 2.7.

Table 2.7: Drugs used in experiments for this chapter.

Common name	Function	Concentration	Supplier / cat no.
GLP-1 (7-37)	GLP-1R agonist	1 μM	Novo Nordisk / 5374
Liraglutide	Long-lasting GLP-1R agonist	1 nM – 1 μM	Novo Nordisk / 6517
Exendin-(9-39)	GLP-1R antagonist	1 μM (Göke et al., 1993)	Novo Nordisk / 2081
Acetylcholine	Acetylcholine receptor agonist	10 mM (Corns et al., 2015)	Sigma / A6625
GABA	GABA receptor agonist	100 μM (Corns, 2012)	Sigma / A2129

2.5.2 Data processing and analysis

Initial processing: Raw calcium imaging data files were exported from MicroManager in the form of TIFF files and processed using Suite2p software (Pachitariu et al., 2017). Image registration of the files in batches of 200 single images allows for correction of any movement in the x- and y- planes, and any images with excessive z- plane movement were not used as consistent cells could not be identified. Region of interest (ROI) detection, based on principal component analysis of correlating pixels, was performed through the Suite2p graphical user

interface and quality control of detected ROIs was done manually; any ROIs that did not visibly appear to be cells were discarded. Activity extractions were also performed using Suite2p and involved removal of the background signal from each ROI detected and normalizing data (ΔF/F) to prevent data contamination by background noise and improve the comparison of spiking traces obtained from different slices. Suite2p then generates multiple files including ROI maps and fluorescent trace data.

Further analysis: Extracted trace files were imported into Graph Pad prism 6 where amplitudes of each peak were detected using the area under curve analysis function. Parameters were set that allowed detection of peaks that were greater than 30% of the maximum peak height, and the number of peaks counted were divided by the length of the recording (in seconds) to give the frequency of spiking per recording.

All calcium imaging traces are presented as the change in fluorescence relative to resting fluorescence (ΔF/F) against time (seconds).

2.5.2.1 Statistical analysis

For all calcium imaging experiments, statistical analysis was performed using Graph Pad Prism 6; a one-way ANOVA was performed to test for significance between groups and post-hoc analysis was performed using an appropriate multiple comparison test to determine differences between groups. Data were considered significant where $p < 0.05$ (represented on figures as *). As the majority of these data are not normally distributed, it is presented as median ± IQR where appropriate and unless otherwise specified.

2.6 ACUTE SLICE EXPERIMENTS

The preparation of acute slices in this experiment follows the procedure for slice preparation for calcium imaging experiments, as fully detailed in Chapter 2: General methods (section 2.4).

2.6.1 Incubation of slices with EdU and GLP-1R modulators

Cut slices were distributed between holding chambers containing 1ml of standard artificial cerebrospinal fluid (aCSF), EdU (1 mM), and either GLP-1R agonist liraglutide or antagonist exendin-(9-39) at 10 nM, 100 nM, or 1 µM concentrations. Holding chambers were placed into a water bath at 36 – 37ºC and continuously oxygenated using 95% oxygen: 5% carbon dioxide gas for 5 hours (**Error! Reference source not found.**). Compositions of aCSF and SaCSF can be found in Chapter 2: General methods (section 2.4.4).

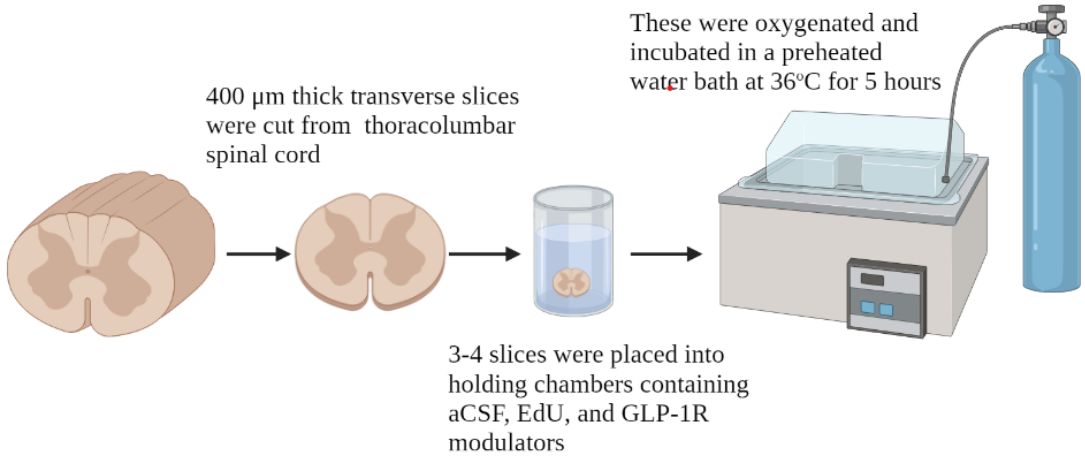

Figure 2.3: Schematic representation of acute slice experimental conditions.
The thoracolumbar spinal cord is isolated from the vertebral column and 400 µm thick coronal sections are cut. These sections are placed within slice holding chambers containing EdU (1 mM) and the appropriate concentration of GLP-1R modulator, and then incubated in a prewarmed 36ºC water bath for 5 hours with continuous oxygenation.

2.6.1.1 Acute slice fixing and re-sectioning

After incubation was complete, slices were submerged in 4% PFA in 0.1M PB overnight at 4^{o}C for fixation, before being embedded in 10% (w/v) gelatin (Sigma-Aldrich, porcine skin) in distilled water. Once the gel had partially solidified, blocks containing sections were cut out and further fixed using a 4% PFA: 0.1% glutaraldehyde mixture overnight at 4^{o}C. These were then re-sectioned into 40 μm sections using a vibratome (Leica VT 1000S, Microsystems) and collected in a 24-well plate containing PBS. All sections underwent EdU detection for assessment of proliferation as detailed in Chapter 2: General methods (section 2.3).

2.7 ORGANOTYPIC SPINAL CORD SLICE CULTURES

2.7.1 Introduction

OSCSCs have emerged as valuable tools in studying cellular proliferation and networks of cells in a controlled *in vitro* environment. This approach involves the maintenance and manipulation of spinal cord tissue slices that retain the cellular organization and functional characteristics of the original tissue. One of the key advantages of organotypic spinal cord slice cultures is the ability to investigate cellular proliferation and the dynamic interactions between different cell types in a simplified yet physiologically relevant context. This method allows the observation and manipulation of cellular processes, such as neurogenesis and gliogenesis, within a controlled experimental setting. In addition to providing a window into cellular proliferation and network dynamics, organotypic slice cultures offer practical benefits. They offer a cost-effective alternative to *in vivo* studies, reducing the need for live animals and allowing for more precise experimental control. Furthermore, the culturing conditions can be tailored to mimic specific pathological or experimental conditions, enabling the investigation of disease mechanisms and the testing of potential therapeutic interventions.

2.7.2 Culture conditions

2.7.2.1 Standard culture conditions

All equipment used in the preparation and plating of OSCSCs was autoclaved prior to use or treated with 70% ethanol to ensure sterility.

OSCSCs were prepared according to the method described in section 2.4.2 above, except after cutting, sections were transferred via sterile pipette to a petri dish containing ice-cold Dulbecco's modified eagles medium (DMEM, Gibco, Thermofisher) under a laminar flow hood. Slices were then placed on top of Millicell organotypic culture inserts (Millipore, 0.4 μm, 30 mm diameter) within a 6-well plate containing 1 ml of pre-warmed neurobasal A culture medium (Invitrogen), 1 % L-glutamine (Sigma-Aldrich), 1 % penicillin / streptomycin (Sigma-Aldrich) and 10 % foetal bovine serum (FBS, Sigma-Aldrich). Approximately 3 – 5 slices were plated per insert making sure that each slice had enough space to spread during the course of the experiments (10 days maximum). These plates were then transferred to an incubator where they were maintained at 37ºC, with 100% humidity and 4% supplemental carbon dioxide.

After 24 hours, the culture medium was replaced with FBS free neurobasal A medium supplemented with 2% B27 neuronal supplement (Invitrogen) and 1% penicillin / streptomycin. As FBS contains a cocktail of growth factors and other biological substances, it was important to remove this to reduce any possible influence on cell proliferation after 24 hours in culture. Every 48 hours after this, 500 μl of culture medium was removed and replaced with fresh medium to renew nutrients and remove any waste, while maintaining availability of any beneficial compounds released by cells within the OSCSC.

At the end point of each experiment, OSCSCs on their culture inserts were removed from the culture medium and fully submerged in 4% PFA in 0.1 M PB for 2 hours at room temperature before slices were lifted carefully using a paintbrush and placed within a 24 well plate containing PBS for further processing.

Specific timelines for experimental conditions such as drug and EdU addition can be found within the appropriate results sections within Chapter 5.

2.7.2.2 Exendin-4

OSCSCs were maintained in standard culture conditions for 5 days. Exendin-4 (1 μM or 10 μM), or the equivalent amount of PBS for the control group, was added directly to the culture media after 1, 2, and 4 days in culture. EdU (1mM) was also added after 4 days in culture and OSCSCs were fixed on day 5 by submerging in 4% PFA for 4 hours at room temperature. Slices were left in PBS before undergoing EdU detection, full details of this procedure can be found in Chapter 2: General methods (section 2.3.2).

2.7.2.3 Liraglutide - proliferation

OSCSCs were maintained in standard culture conditions for 10 days. Liraglutide (1 μM or 10 μM), or the equivalent amount of PBS for the control group, was added directly to the culture media in all wells after 1, 3, 5, 7 and 9 days in culture.

For slices that were representative of each time point EdU (1 mM) was added to the well 24 hours prior to fixation. For example, for slices to be counted at day 4, EdU was added only to that well, along with liraglutide, at day 3 and incubated for 24 hours before the slices were fixed in 4% PFA for 4 hours at room temperature. At least 3 slices were fixed per time point.

Slices were left in PBS before undergoing EdU detection.

2.7.2.4 Liraglutide – Propidium iodide

OSCSCs were maintained in standard culture conditions for 10 days. Liraglutide (1 μM or 10 μM), or the equivalent amount of PBS for the control group, was added directly to the culture media after 1, 3, 5, 7 and 9 days in culture. On days 2, 4, 6, 8, and 10 of culture, 5 μM Propidium iodide was added directly to the culture media of slices to be fixed at each time point, and were incubated for 30 minutes before washing 3x in prewarmed culture media and fixation in 4% PFA for 4 hours. Slices were then washed 3x in PBS before mounting for detection of PI.

2.7.3 Preparation of hydrogels

2.7.3.1 Manchester Biogels

Alpha 4, Gamma 4, and Epsilon 4 peptide-based hydrogels were supplied by Manchester Biogels. These self-assembling hydrogels are fully synthetic allowing for high reproducibility between batches and were delivered ready to use.

For use with Millicell culture inserts, the inserts were first prewetted with warmed neurobasal A medium to prevent air bubbles being trapped in the membrane pores. The hydrogels were warmed to room temperature and 100 µl of hydrogel was transferred on top of each culture insert (Millipore, 0.4 µm, 30 mm diameter) within a 6-well plate containing 1 ml of pre-warmed neurobasal A culture medium (Invitrogen), 1 % L-glutamine (Sigma-Aldrich), 1 % penicillin / streptomycin (Sigma-Aldrich) and 10 % foetal bovine serum (FBS, Sigma-Aldrich), with care taken not to introduce any bubbles. 250 µl of culture medium was placed on top of the gels to precondition the gels and then the plates were placed in the incubator for 2 hours to ensure the hydrogels were warmed through.

2.7.3.2 Glutamine-amide

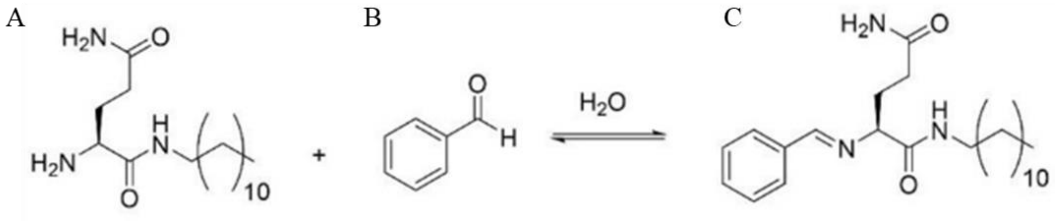

Figure 2.4: Synthetic pathway and structure of the glutamine-amide hydrogel.
A. Glutamine-amide derivative, **B**. benzaldehyde, **C**. Self-assembling glutamine-amide hydrogel.

The glutamine-amide peptide-based hydrogel was kindly gifted by Professor David Smith at the University of York. This gel is described as a supramolecular "solid-like" gel made from a low-molecular-weight gelator (LMWG), and has previously been used as a slow release delivery agent for intranasal administration of L-DOPA

(J. T. Wang et al., 2021). Full details regarding the synthesis of materials involved in the making of glutamine-amide hydrogels can be found in Hawkins et al., 2020.

This hydrogel was supplied as a powder and reconstituted under aseptic conditions. 3.5 mg of glutamine amide derivative was mixed with 1.1 µl of benzaldehyde in 1 ml of sterile water (Figure 2.4). The mixture was warmed to 60 degrees in a water bath for 2 hours with occasional stirring and sonication. Upon dissolution of all powder, the gel was allowed to cool to approximately 40 degrees before 100 µl of the gel solution was transferred on top of a culture insert (Millipore, 0.4 µm, 30 mm diameter) within a 6-well plate and placed within the incubator for 24 hours to ensure complete setting prior to use in cultures.

2.7.3.3 DBS-$CONHNH_2$

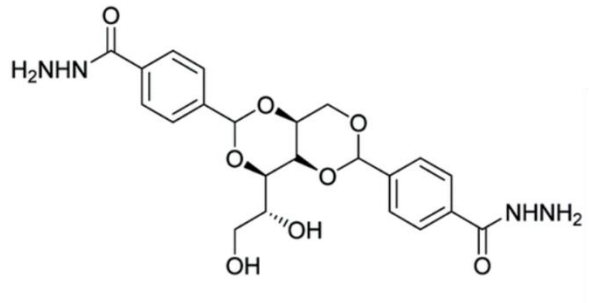

Figure 2.5: Chemical structure of the DBS-$CONHNH_2$ hydrogel

The DBS-$CONHNH_2$ peptide-based hydrogel (Figure 2.4) was kindly gifted by Professor David Smith at the University of York. Full details regarding the synthesis of materials involved in the making of DBS-$CONHNH_2$ hydrogels see Okesola and Smith, 2013.

This hydrogel was supplied as a powder as reconstituted under aseptic conditions. 3 mg of DBS-$CONHNH_2$ derivative was mixed with 1 ml sterile water. The mixture was warmed to 60 degrees in a water bath for 2 hours with occasional stirring and sonication. Upon dissolution of all powder, the gel was allowed to cool to approximately 40 degrees before 100 µl of the gel solution was transferred on top of a culture insert (Millipore, 0.4 µm, 30 mm diameter) within a 6-well plate and placed within the incubator for 24 hours to ensure complete setting prior to use in cultures.

2.7.4 Hydrogel experiments

Hydrogels, with and without liraglutide, were prepared under sterile conditions as detailed above.

100µl of each hydrogel was spread in a thin layer on top of culture inserts in a 6-well plate containing 1 ml of standard culture medium, washed twice with culture medium (30 minutes each) and equilibrated at 37°C for two hours before introduction of OSCSCs. OSCSCs were placed on top of the hydrogels, or directly on top of the culture insert for non-hydrogel controls (Figure 2.6) and maintained in standard culture conditions for 5 days. 1 µM EdU was added directly to the culture media below the insert 24 hours before fixation with 4% PFA. Slices were left in PBS before undergoing EdU detection.

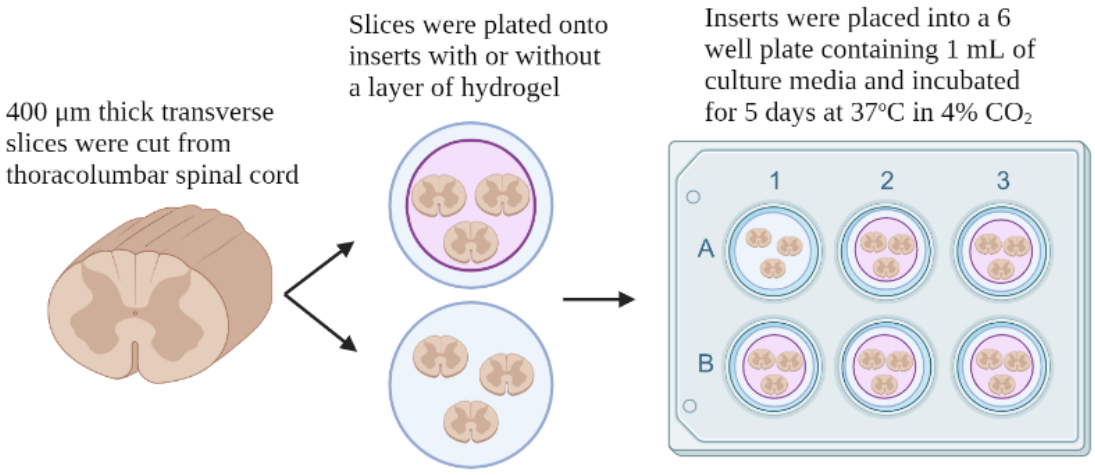

Figure 2.6: Schematic representation of conditions during organotypic slice cultures on hydrogel experiments.

The thoracolumbar spinal cord is isolated from the vertebral column and 400 µm thick coronal sections are cut. Sections are transferred onto porous cell culture inserts with or without a thin hydrogel layer and incubated at 37°C with 4% CO2 for 5 days.

Full details of anaesthesia, perfusion and dissection, cell counting, and data analysis can be found in Chapter 2: General methods. All injections were performed at approximately 5 pm every day at the start of the natural wake cycle of the mouse in order to maximise effects on proliferation (New et al., 2023).

2.8.1 Exendin-4

10 wild type mice (8 weeks old, female) were divided into control and experimental groups (N=5 each). Control groups were given intraperitoneal injections of 10 mM 5-ethynl-2-deoxyuridine (EdU, Carbosynth), 100µl in sterile saline, once every 24 hours for 4 days. Experimental groups were given 10mM EdU and Exendin-4 (10 µg/Kg, Novo Nordisk), 100µl total in sterile saline, once every 24 hours for four days.

2.8.2 Liraglutide

10 wild type mice (8 weeks old, female) were divided into control and experimental groups (N=5 each). Control groups were given intraperitoneal injections of 10 mM 5-ethynl-2-deoxyuridine (EdU, Carbosynth), 100µl in sterile saline, once every 24 hours for 4 days. Experimental groups were given 10mM EdU and liraglutide (1 µg/Kg, Novo-Nordisk) 100µl total in sterile saline, once every 24 hours for four days.

2.8.3 Image capture and data analysis

For all experiments, statistical analysis was performed using Graph Pad Prism 6; a one-way ANOVA was performed to test for significance between groups and post-hoc analysis was performed using an appropriate multiple comparison test to determine differences between groups. Data were considered significant where $p<0.05$ (represented on figures as *). Data are presented as mean ± standard deviation (SD) where appropriate and unless otherwise specified.

2.8.3.1 Measuring proliferation and differentiation

Images used for cell counting and analysis were mainly taken as z-stacks using an EVOS auto 2 fluorescent microscope at x10 magnification for the entire slice, or at x40 for central canal counts. Due to the large quantity of data in the *in vivo* experiments, and due to restrictions caused by the COVID-19 pandemic, z-stack images of spinal cord and hippocampus were taken using the Zeiss Axioscan Z.1 slide scanner at 20x magnification.

Cell counts and colocalisations were performed either manually under a Nikon Eclipse E600 fluorescent microscope or from compressed z-stacks using Fiji and collated in Microsoft Excel.

2.8.3.2 Imaging and analysis of propidium iodide experiments

Propidium iodide is a fluorescent intercalating dye that binds to the DNA of damaged cells where it becomes highly fluorescent in the spectrum of red light. This dye is membrane impermeable to intact cell membranes and as such the quantification of the degree of fluorescence can be used as an indicator of the extent of cell death within an OSCSC as detailed by protocols in previous literature (Loetscher et al., 2009; Schoeler et al., 2012).

OSCSCs from experiments described in section **Error! Reference source not found.** above were imaged using an EVOS auto 2 fluorescent microscope at x4 magnification, and images were imported into ImageJ for analysis. The red channel of these images were converted from RGB colour to digital 8-bit to allow quantification of pixel intensity. Slices with a high degree of cell death exhibited a higher degree of pixel intensity, whereas those with fewer dead cells exhibited a lower intensity. A histogram plot was generated showing the distribution of pixel intensity throughout the image (Figure 5.3). From this, the average intensity of the pixels above 50 intensity was calculated using the area under the curve for each group, with a minimum of three slices averaged per time point, per mouse.

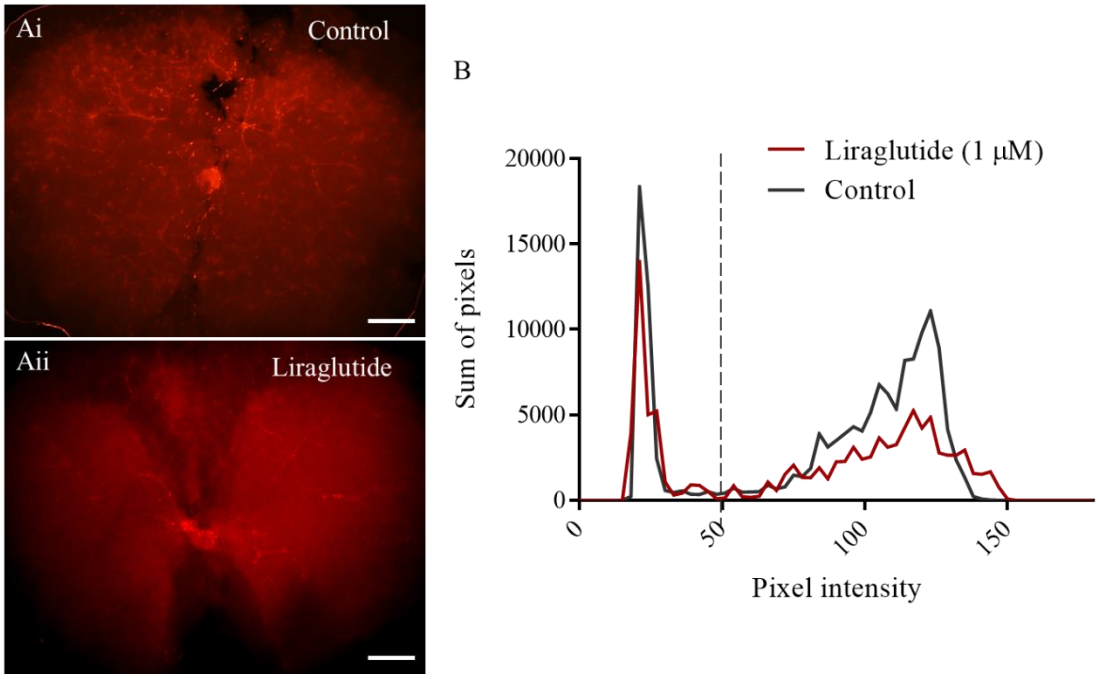

Figure 2.7: Analysis of fluorescence intensity of pixels in OSCSCs treated with propidium iodide.

A. Representative images of a control group (i) and liraglutide treated (ii) OSCSC fixed on day 4 of culture.

B. Histogram showing the distribution of pixels for the different fluorescence intensities for an OSCSC in the control group and in the 1 μM liraglutide group. Only pixels above 50 intensity (as indicated by the dashed line) were used for quantification as below this number was determined to be the result of background fluorescence.

2.9 IMAGE CAPTURE AND ANALYSIS

Images at a lower magnification were taken using an EVOS auto 2 fluorescent microscope at x10 magnification. Images of a higher magnification, where analysis was required, z-stacks were taken at x20 or x40 magnification using an upright Zeiss LSM880 Airyscan confocal microscope. Z-stacks were imported into Fiji and viewed as compressed z-stacks (Stacks > Z project at maximum intensity), or as a 3D projection in order to better view appositions (Stacks > 3D project).

Cell counts were performed manually under a Nikon Eclipse E600 fluorescent microscope, or from compressed z-stacks, and collated in Microsoft Excel.

Statistical analysis was performed using Graph Pad Prism 6; a one-way ANOVA was performed to test for significance between groups and post-hoc analysis was performed using an appropriate multiple comparison test to determine differences between groups. Data were considered significant where $p<0.05$ (represented on figures as *).

Data are presented as mean ± standard deviation (SD) where appropriate and unless otherwise specified.

Chapter 3 – Characterisation of cerebrospinal fluid contacting neurons

3.1 INTRODUCTION

This chapter will focus on using immunofluorescent labelling techniques and *in-silico* research to elucidate evidence regarding the expressions of proteins within cerebrospinal fluid contacting neurons (CSFcNs) of the murine spinal cord. Research described here will focus on two main aspects: (i) the verification of a transgenic mouse model used to identify and study CSFcNs and (ii) whether these cells express the GLP-1 receptor and receive input from GLP-1 producing neurons. These data will contribute valuable information to consider the theory that CSFcNs are neurons that can sense and respond to changes in the composition of the CSF, as well as providing additional information regarding their neural circuitry.

3.1.1 A transgenic animal model used to study CSFcNs

As discussed in Chapter 1: general introduction (section 1.2), CSFcNs are a specialised subset of neurons found within the ependymal layer surrounding the central canal of the brainstem and spinal cord. They have long been proposed to be sensory neurons responding to physical and chemical cues from the CSF (Agduhr, 1922; Kolmer, 1931). CSFcNs have also been implicated in the non-synaptic reception and transmission of signals to or from the CSF in mice and many lower vertebrates (Vígh et al., 2004; Orts-Del'Immagine et al., 2014; Bjorefeldt et al., 2018). These cells are easily identifiable due to their unique morphology and their expression of the non-selective cation channel polycystic kidney disease 2-like-1 receptor (PKD2L1), as they are the only cell type in the spinal cord to express this receptor (Huang et al., 2006; Djenoune et al., 2014).

This selective expression of PKD2L1 enables the study of these cells through transgenic mouse models, one such model is the PKD2L1-Cre mouse. In the PKD2L1-Cre mouse model, the Cre recombinase enzyme is expressed under the control of the promoter for the PKD2L1 gene, resulting in Cre expression in CSFcNs around the central canal of the spinal cord and brainstem (Huang et al., 2006). Cre recombinase is a site-specific DNA recombinase that recognises and binds to specific DNA sequences known as lox sites. When Cre recombinase binds to two loxP sites located on the same chromosome, it catalyses the recombination of the DNA

between those sites, resulting in the inversion of the intervening sequence (Kim et al., 2018). Crossing Cre transgenic mice with mouse lines that carry loxP-flanked target genes, such as fluorescent reporter proteins, allows the study of those genes specifically in the cells or tissues where the promotor is active.

Many transgenic mouse models are used experimentally throughout this thesis, full details of which can be found in Chapter 2: general methods (section 2.1), of particular relevance to this chapter is the PKD2L1-GCaMP6f transgenic mouse model. In brief, the PKD2L1-GCaMP6f mouse model was created for use in immunofluorescence and calcium imaging studies by crossing a PKD2L1-cre mouse strain with a GCaMP6f-flox strain. The GCaMP6f-flox strain is a Cre-dependent strain in which a floxed-STOP cassette is inserted upstream of the GCaMP6f (Madisen et al., 2015). When crossed with the PKD2L1-Cre strain, Cre excises the stop codon resulting in specific expression of GCaMP6f in all cells containing PKD2L1.

GCaMP6f is a genetically encoded calcium indicator protein made up of three components: a circularly permuted green fluorescent protein (cpGFP), a calcium-binding protein called calmodulin, and a calmodulin-binding peptide called M13. These three components are linked together by short flexible peptide sequences to form a single protein that is capable of detecting changes in intracellular calcium levels (Chen et al., 2013). In chapter 4 of this thesis, calcium imaging experiments will be conducted using the PKD2L1-GCaMP6f mouse strain. Therefore, it is crucial to accurately identify the cells present in the central canal that show expression of GCaMP6f and ensure localisation is restricted to CSFcNs. Since one of the components of GCaMP6f is GFP, cells that express this protein can be conveniently visualised by immunofluorescence using an antibody specific to GFP and the specificity of GCaMP6f expression can be established. In this chapter, double immunofluorescence labelling methods will be employed using anti-PKD2L1 to identify CSFcNs and anti-GFP to visualize GCaMP6f expression and colocalisation analysis conducted.

3.1.2 The glucagon-like peptide-1 receptor is expressed by cells within the spinal cord

As reviewed in Chapter 1: general introduction (1.3.4), GLP-1R agonists have been shown to exert many neuroprotective and regenerative effects within the central nervous system (Zhang and Lv, 2018), including promoting neuroplasticity and axonal growth (During et al., 2003; Han et al., 2020), and stimulating neurogenesis within the subventricular zone and dentate gyrus of adult mice (Bertilsson et al., 2008; Hamilton et al., 2011; Weina et al., 2018). In order to determine whether these effects would be similar on cells within the neurogenic niche of the spinal cord, more information must be obtained regarding the cell specific expression of the GLP-1 receptor around the CC, and the extent of integration within the GLP-1 system.

The glucagon-like peptide-1 (GLP-1) system within the spinal cord has not been extensively researched, and further information regarding the cells that exist within the spinal GLP-1 network is needed before it can be fully characterised. As discussed in Chapter 1: general introduction (1.3.3), the identity of the cells within the spinal cord that possess GLP-1 receptors is a somewhat contentious topic. The work performed in this chapter will build upon previous studies to gain a better understanding of the GLP-1R expressing cells of the spinal cord, and their connectivity into the GLP-1 spinal cord circuitry.

In a study by Merchenthaler et al., RNA in-situ hybridisation in the rat spinal cord revealed GLP-1R mRNA expression in laminae V – X. However, this investigation did not explore the specific cellular localization of the glucagon-like peptide-1 receptor (Merchenthaler et al., 1999). Building on this work, the Allen Brain Atlas, a comprehensive gene expression database obtained through RNA in-situ hybridisation in the spinal cord and brain of juvenile (4 days) and adult (56 days) mice, showed GLP-1R expression in Laminae IV – VIII, the grey matter, and the central canal area of both juvenile and adult mice (

Figure **3.1**, Ai – ii) (Lein et al., 2007). Notably, within the central canal area, cells exhibiting typical morphology and arrangement reminiscent of CSFcNs were observed, suggesting a likelihood that CSFcNs are the specific cell type in this region expressing GLP-1R RNA (

Figure **3.1**, Ai - Aii insets).

Recent advances in single cell/nucleus mRNA sequencing have provided new insights into the expression of GLP-1R in the spinal cord. Russ et al. (2021) found that low levels of GLP-1R mRNA are present in several different cell types, with the relative highest levels being expressed in sub-types of oligodendrocytes, inhibitory neurons and in CSFcNs (

Figure **3.1**, Bi – iii). This suggests a range of functions for the GLP-1R in the spinal cord, some of which may be linked to CSFcN activity.

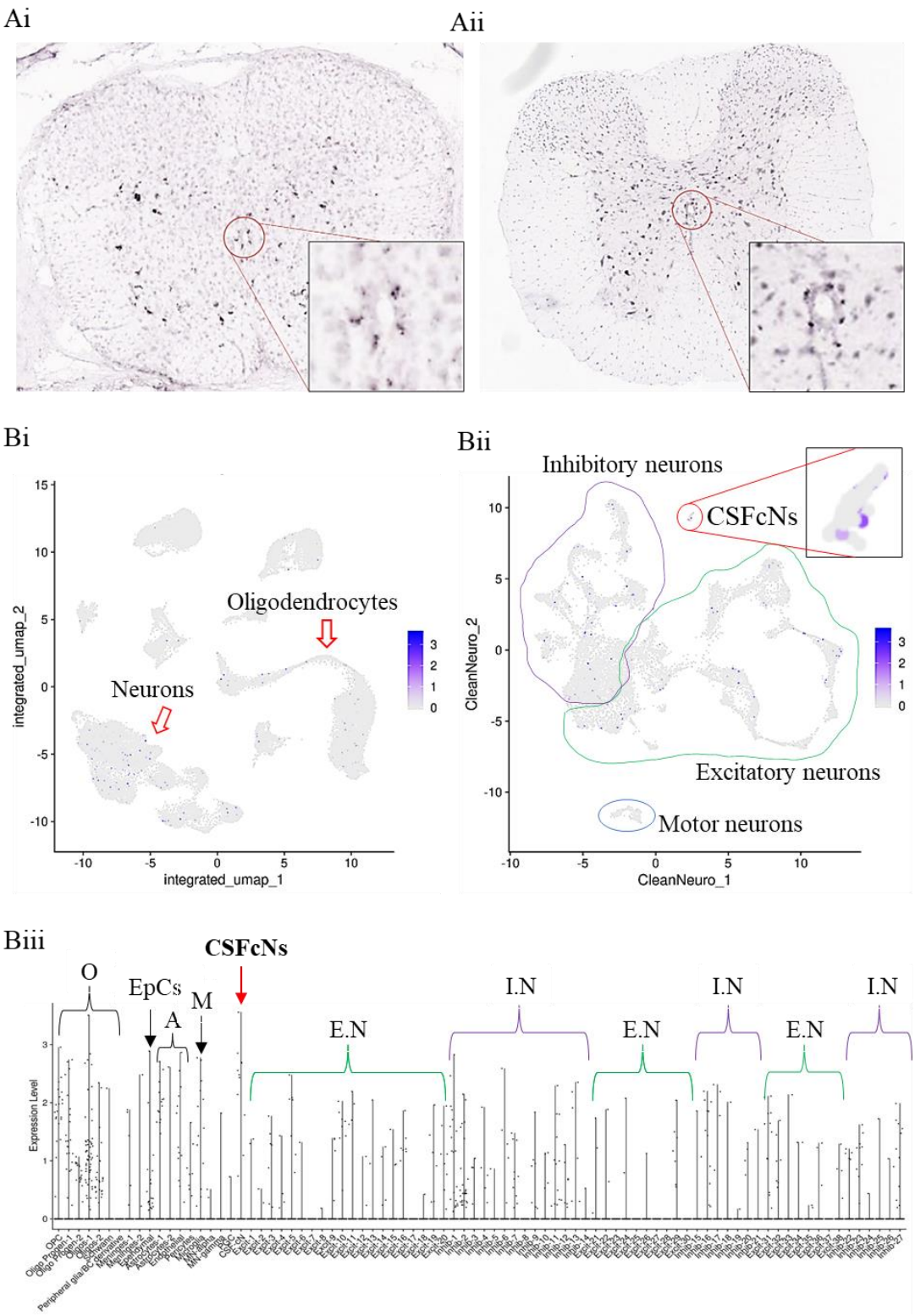

Figure 3.1: GLP-1R mRNA localisation throughout the spinal cord.

A. Localisation of the GLP-1R in postnatal (P4, i) and adult (P56, ii) mouse as determined by in-situ hybridisation. Localisation can be seen around the central canal (insets on both) in the approximate location of CSFcNs, as well as in other locations predominantly in the grey

matter. Data obtained from the Allen spinal cord atlas at mousespinal.brain-map.org (Lein et al., 2007).

B. Expression plots of GLP-1R mRNA, which can be seen predominantly in oligodendrocyte and neuronal populations (i), and more specifically in inhibitory neurons, excitatory neurons, and in CSFcNs (ii). Relative expression levels can be seen in (iii) with highest levels in oligodendrocytes (O), CSFcNs and inhibitory neurons (I.N). Lower expression can be seen in ependymal cells (ECs), astrocytes (A), microglia (M), and excitatory neurons (E.N). Data obtained from repository at seqseek.ninds.nih.gov/genes (Russ et al., 2021).

3.1.3 GLP-1 fibre tracts can be found in the spinal cord

As discussed in the general introduction of Chapter 1 (1.3.3), the innervation of GLP-1R-expressing cells by GLP-1 neurons, commonly referred to as preproglucagon (PPG) neurons (Drucker, 1998; Merchenthaler et al., 1999), in the spinal cord remains poorly understood. Llewellyn-Smith et al. investigated PPG neuron axon distribution in the spinal cord using a PPG-YFP transgenic mouse model and observed a dense network of YFP fluorescent axons in lamina X and a rostrocaudal tract near the central canal (Llewellyn-Smith et al., 2015). The origin of these projections in the NTS was confirmed through retrograde fluorogold labelling from the thoracic spinal cord, indicating descending PPG neuron axon innervation of the spinal cord (Llewellyn-Smith et al., 2015). However, the specific targets of these appositions were not fully characterised.

In this chapter, the potential innervation of CSFcNs by GLP-1 positive axons will be explored using double labelling experiments with the PPG-YFP mouse model and the extent of appositions in each region will be quantified. This research will contribute valuable information regarding the spinal GLP-1 circuitry, as well as identifying whether CSFcNs may form part of this network.

3.1.4 Hypothesis and aims

Given that PKD2L1 is known to be selectively expressed in CSFcNs of the murine spinal cord, it is hypothesised that 100% of the cells that are immunopositive for GCaMP6f in a PKD2L1-GCaMP6f transgenic mouse strain will also display

immunoreactivity for PKD2L1. Future work in this thesis will rely on the successful identification of CSFcNs in this mouse model.

Furthermore, as several studies have shown GLP-1R mRNA expression within the central canal area, and in cells that resemble CSFcNs, it is hypothesised that a number of CSFcNs express the GLP-1R and therefore may receive appositions from GLP-1 producing neurons.

This chapter uses immunofluorescence on perfusion fixed spinal cord sections from several transgenic mouse models to:

- Investigate the extent of colocalisation of GCaMP6f expression and PKD2L1-immunofluorescence in a PKD2L1-GCaMP6f mouse model to determine whether this is a suitable model for CSFcN identification and for use in the calcium imaging experiments in chapter 4 of this thesis.
- Identify whether CSFcNs express the GLP-1R and if there are any differences in expression when using a GLP-1R primary antibody on wildtype C57BL/6 mice and PKD2L1-GCaMP6f transgenic mice, or when visualising the GCaMP3 in a GLP1R-GCaMP3 transgenic mouse model along with PKD2L1-immunofluorescence.
- Determine whether CSFcNs receive appositions to their somata or processes from GLP-1 containing expressing neurons through use of the PPG-YFP mouse model, and to evaluate the extent of these appositions throughout different spinal cord regions.

3.2 RESULTS

3.2.1 Verification of PKD2L1xGCaMP6f transgenic mouse model

As PKD2L1 is an ion channel associated with plasma membrane in sour taste receptors (Huang et al., 2006), it was expected that PKD2L1 immunostaining would be mostly localised to the plasma membrane of CSFcNs as reported in zebrafish and mouse previously (Djenoune et al., 2014; Orts-Del'Immagine et al., 2014). In contrast, GCaMP6f should be present throughout the cytosol (Chen et al., 2013).

In all spinal cord sections, there was an almost 100% colocalisation between the anti-PKD2L1 and anti-GFP immunolabelling, with no significant differences in the levels of co-expression between regions (Cervical 99.7 ± 0.4%, Thoracic 99.7 ± 0.3%, Lumbar 99.5 ± 0.4%, Sacral 99.6 ± 0.6%). In this mouse model, CSFcNs were primarily localised around the central canal in all sections with a small number located between the CC and the ventral fissure area (Figure 3.2, Cii-Ciii), consistent with labelling seen in wild type mouse models (data not shown) and in the literature (Djenoune et al., 2014; Jurčić et al., 2021).

No significant differences were observed in expression patterns between the age ranges of mice used in this experiment indicating that PKD2L1 is present in all CSFcNs throughout the lifespan of the mouse (age range tested: juvenile 18 – 42 days, adult 56 – 112 days, data shown collated in Figure 3.2, D).

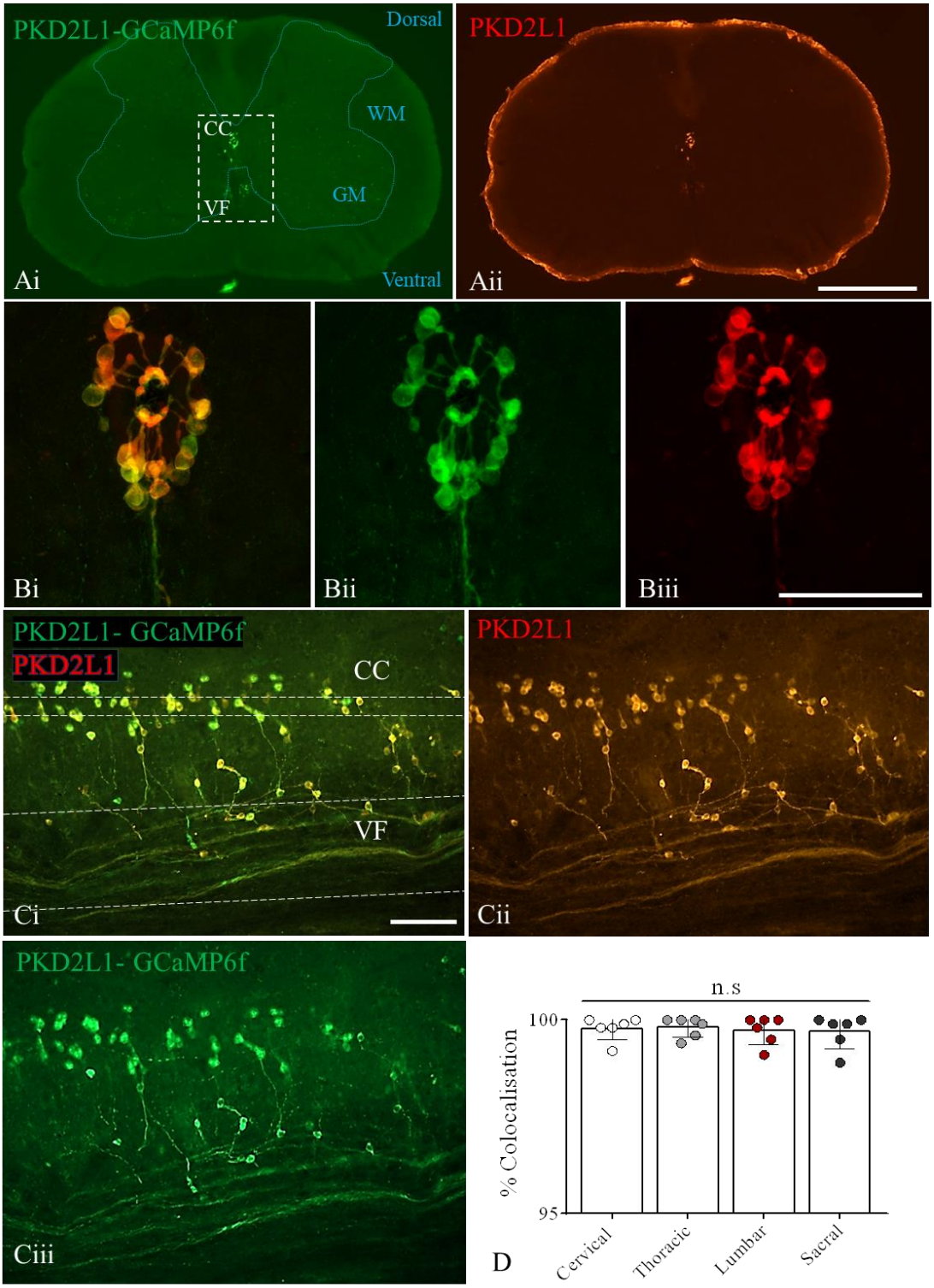

Figure 3.2: All GCaMP6f-positive CSFcNs are immunoreactive for PKD2L1.

A. Low magnification images of coronal spinal cord sections showing immunofluorescent localisation of GCamP6f and PKD2L1-IR located around the central canal (CC) in lamina X of the grey matter (GM). Several cells can be seen ventral to the ependymal layer located between the CC and the ventral fissure (VF) of the white matter (WM). Scale bar: 200 µm

B. High magnification compressed Z-stack images of merged (i), GCaMP6f (ii), and PKD2L1-IR (iii) localisation in coronal lumbar spinal cord section. Scale bar: 50 μm.
C. Horizontal sections of merged (i), GCaMP6f (ii), and PKD2L1-IR (iii) localisation. CSFcNs, and connecting processes, can be seen lining the CC or lying between the CC and the VF. Scale bar: 50 μm.
D. Bar chart showing approximately 100% colocalisation of PKD2L1-IR and GCaMP6f (enhanced with GFP) in the PKD2L1xGCaMP6f transgenic mouse model. Only coronal sections were quantified, see Table 2.1 for details regarding sections and cells counted. No significant differences were observed between regions. Statistical analysis: One-way ANOVA with Tukey's multiple comparison test.

3.2.1.1 Low levels of colocalisation between PKD2L1-GCaMP6f and oligodendrocyte cell markers can be observed outside of the central canal area.

Upon further investigation of the enhanced GCaMP6f labelling in this mouse model, several cells that could not be labelled using the PKD2L1 antibody were observed outside of the central canal area that had not been previously characterised at the time of this investigation (Figure 3.3). These cells did not possess morphological characteristics typical of CSFcNs and instead appeared to be glial cells, which was confirmed through double labelling experiments with PanQKI, an oligodendrocyte marker (4.37 ± 1.05% of PanQKI positive cells co-expressed GCaMP6f). There was no colocalisation of GCaMP6f and PanQKI-IR around the central canal area, indicating that CSFcNs do not typically express PanQKI. Neither was colocalisation observed between GCaMP6f and the astrocyte marker S100b, nor the microglial marker IBA1, either within or outside the central canal area in any sections studied (data not shown).

Since performing this analysis, some new literature had become known that confirmed the presence of low levels of PKD2L1 mRNA in a subpopulation of oligodendrocytes. Single cell/nucleus RNA sequencing performed and collated by Russ et al confirmed the presence of PKD2L1 mRNA predominantly in CSFcNs, but also in two subpopulations of oligodendrocytes refered to as oligos-1 and oligos-2 (Figure 3.3, Di – Dii). A similar pattern of PKD2L1 expression in oligodendrocytes was recently confirmed by Nakamura et al through immunostaining using an

alternative oligodendrocyte marker (Olig2) in a PKD2L1-cre x CAG-lox-CAT-lox-EGFP reporter strain (Nakamura et al., 2023).

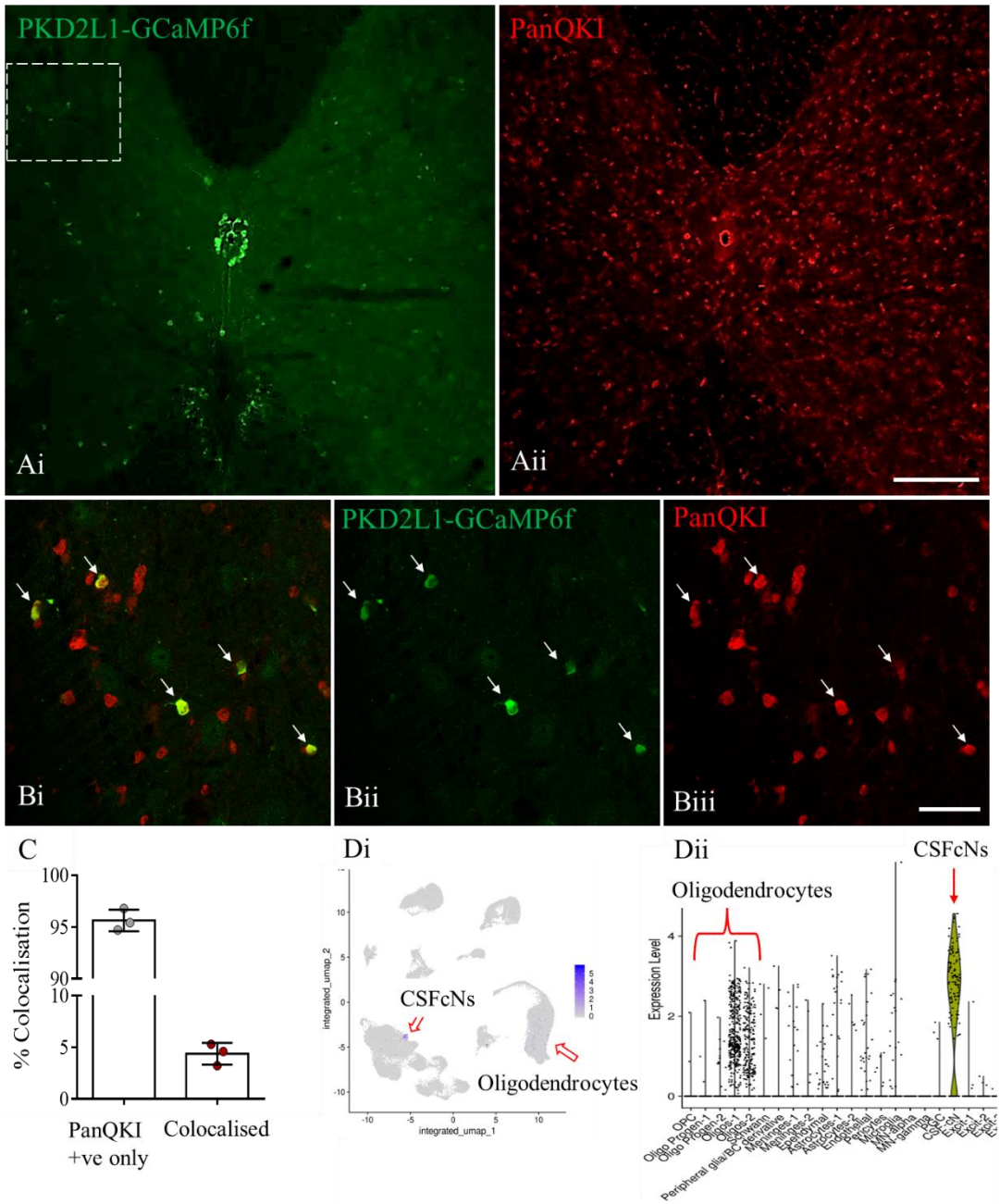

Figure 3.3: A small subset of oligodendrocytes express PKD2L1.

A. Low magnification images showing localisation of GCaMP6f (i) and PanQKI-IR (ii) in coronal sections of thoracic spinal cord. GCaMP6f localisation can be seen predominantly around the central canal area, with lower levels of localisation seen in the grey matter. PanQKI-IR can be observed both in the grey and white matter. Scale bar: 100 μm.

B. Higher magnification compressed z-stack images of merged (i), GCaMP6f (ii), and PanQKI-IR (iii), arrows indicate colocalised cells. Scale bars: 50 μm.
C. Graph showing 95.64 ± 1.05% of PanQKI-IR cells are not colocalised with GCaMP6f, compared with 4.37 ± 1.05% of PanQKI-IR cells co-expressing GCaMP6f.
D. PKD2L1 mRNA expression plots showing the presence of PKD2L1 predominantly in CSFcNs with low levels present in oligodendrocytes, specifically sub-types oligos-1 and oligos-2. Data obtained from repository at seqseek.ninds.nih.gov/genes (Russ et al., 2021).

3.2.1.2 Colocalisation between PKD2L1-GCaMP6f and Sox2 occurs mainly around the central canal

To continue characterisation of the cells within the spinal cord that display immunoreactivity for GCaMP6f, colocalisation with the SRY (sex determining region Y)-box 2 (Sox2) antibody was determined. Sox2 is commonly used as a marker for ependymal cells and is particularly important in the development of the central nervous system. Its expression is required for the maintenance of neural stem cells and the differentiation of neurons and glial cells (Alfaro-Cervello et al., 2012).

The highest intensity of Sox2 localisation was observed around the central canal area, consistent with the ependymal layer and likely indicating the ependymal cells. It was also observed that a number of CSFcNs, identified through morphology and GCaMP6f localisation, were also immunopositive for Sox2 however staining appeared less intense than in the ependymal cells (49.9 ± 11.3%, Figure 3.4, Bi – Biii and C).

As previously mentioned, most cells outside of the central canal area that express GCaMP6f were also PanQKI-IR, indicating an oligodendrocyte lineage. Further analysis revealed that a small number of GCaMP6f immunopositive cells also expressed Sox2 outside of the central canal area (1.81 ± 0.64%, Figure 3.4, C), although it was not confirmed whether these cells also expressed PanQKI. Single cell/nucleus RNA sequencing indicates that Sox2 mRNA may be somewhat ubiquitous in the spinal cord, with many different cell types expressing Sox2 mRNA including sub-populations of oligodendrocytes and astrocytes (Figure 3.4, Di - Dii) (Russ et al., 2021) , which may be responsible for the localisation pattern observed using the Sox2 antibody and colocalisation with GCaMP6f.

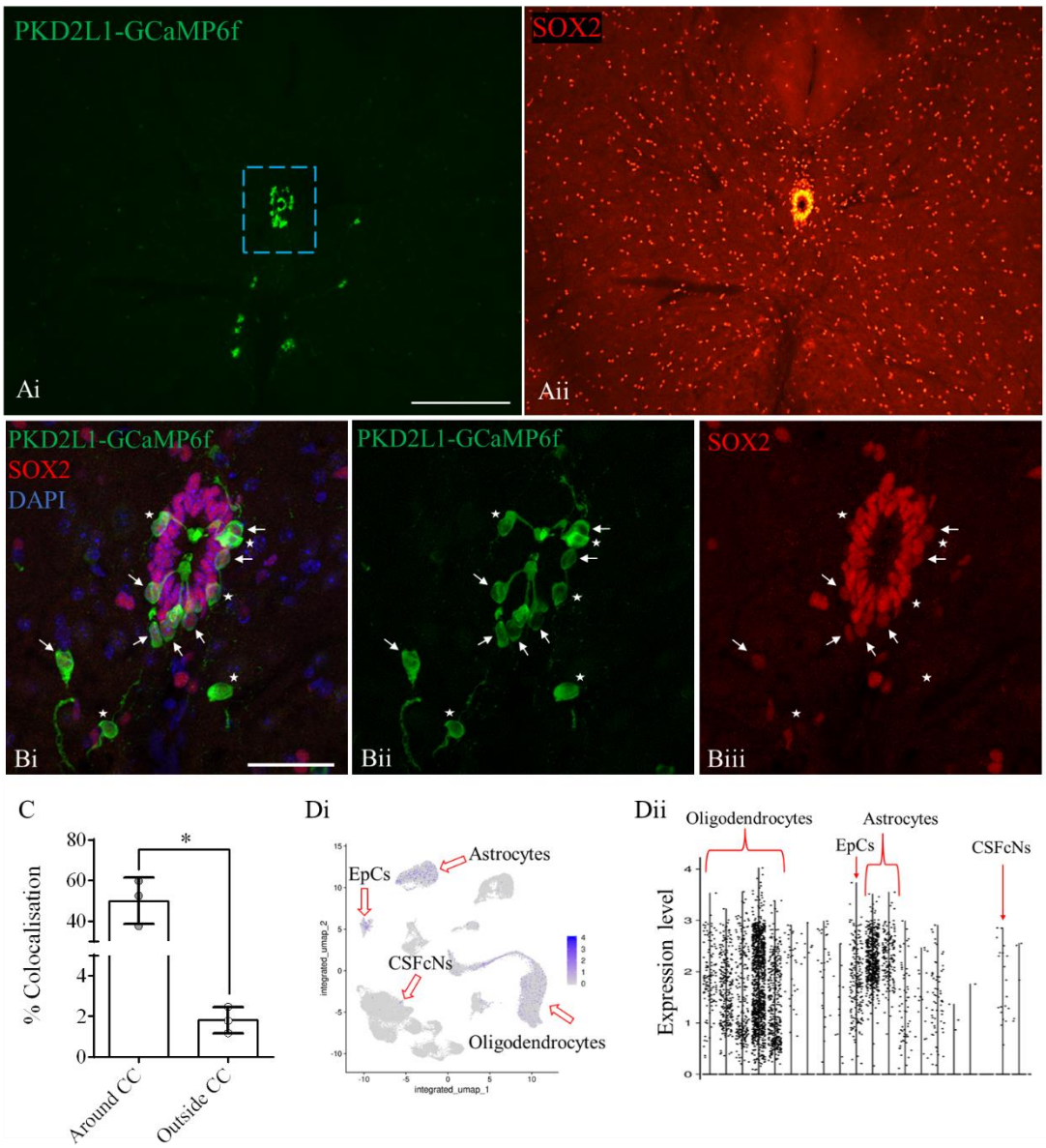

Figure 3.4: Several CSFcNs around the central canal express SOX2, although no colocalisation can be seen in those outside the central canal area.

A. Low magnification images showing localisation of GCaMP6f (i) and Sox2 (ii) in a thoracic section of spinal cord. GCaMP6f can be seen mostly surrounding the central canal with some cells observed ventral to the CC. The highest levels of Sox2 localisation can be seen surrounding the central canal, although localisation can be seen throughout the parenchyma. Scale bar: 150 μm.

B. Higher magnification compressed z-stack images of merged (i), GCaMP6f (ii), and Sox2 (iii) localisation. Arrows indicate colocalised cells, stars indicate cells that only express GCaMP6f. Scale bar: 50 μm.

C. Graph showing percentage colocalisation of GCaMP6f immunopositive cells that are also Sox2-IR in CSFcNs located dorsally and ventrally within the ependymal layer, as well as other cells outside the central canal. Statistical analysis: One-way ANOVA with Tukey's multiple comparison test, significance level $p < 0.05$ (indicated by *).

D. Expression plots of mRNA showing expression of Sox2 in many types of cells within the spinal cord including CSFcNs, astrocytes, oligodendrocytes, and ependymal cells (ECs). Data obtained from repository at seqseek.ninds.nih.gov/genes (Russ et al., 2021).

3.2.2 The majority of CSFcNs express the GLP-1R

Three different mouse strains were used in this investigation to assess any potential differences that may arise between the apparent localisation of the GLP-1R when identified using the GLP-1R primary antibody or a transgenic mouse model where GCaMP3 is expressed under the GLP-1R promoter. Details regarding the mouse strains used can be found in Chapter 2: general methods (section 2.1).

Firstly, the GLP-1R antibody was investigated independently of any other antibody using a wild type C57BL/6 mouse strain and visualised using the DAB substrate, or enhanced using tyramide signal amplification (TSA). GLP-1R immunoreactive cells were present in the grey matter and surrounding the central canal (Figure 3.5, Ai – Aii), concurrent with observations from the Allen Brain Atlas and prior literature (Merchenthaler et al., 1999; Russ et al., 2021). The cells within the central canal area shared typical morphological characteristics with CSFcNs, having a soma outside the ependymal layer and a bulbous apical projection into the lumen of the central canal, and so double labelling experiments with the GLP-1R antibody were performed using the PKD2L1-GCaMP6f transgenic mouse strain to confirm expression in this cell type. A large degree of colocalisation between the GLP-1R immunofluorescence and GCaMP6f was observed around the central canal (81.98 ± 1.55% average across all regions, Figure 3.5, Bi – Biii), indicating that most CSFcNs do indeed possess the GLP-1R. Also observed were several cells that expressed GCaMP6f but not the GLP-1R (10.08 ± 1.59% average across all regions), and cells which expressed the GLP-1R but not GCaMP6f (7.95 ± 1.59% average across all regions).

As additional confirmation, double labelling experiments were also performed with the PKD2L1 primary antibody and a GLP1R-GCaMP3 transgenic mouse strain (Figure 3.5, Ci – iii). Comparable results were seen as with the GLP-1R antibody; most cells within the central canal area were immunopositive for both PKD2L1 and GCaMP3 (78.20 ± 1.21% average across all regions), some cells were PKD2L1-IR but not GCaMP3 immunopositive (11.34 ± 1.18% average across all regions), and some cells expressed GCaMP3 but not PKD2L1-IR (10.38 ± 1.09% average across all regions). No significant differences in percentage localisation over different regions of the spinal cord were observed in either model (Figure 3.5, D), nor were

any changes in localisation observed between juvenile and adult mice (data only obtained for PKD2L1-GCaMP6f mice, data not shown).

In both models, GLP-1R localisation appeared to be particularly focused on the endbulbs of CSFcNs (Figure 3.6), located extensively on the outer membrane and within the cytoplasm.

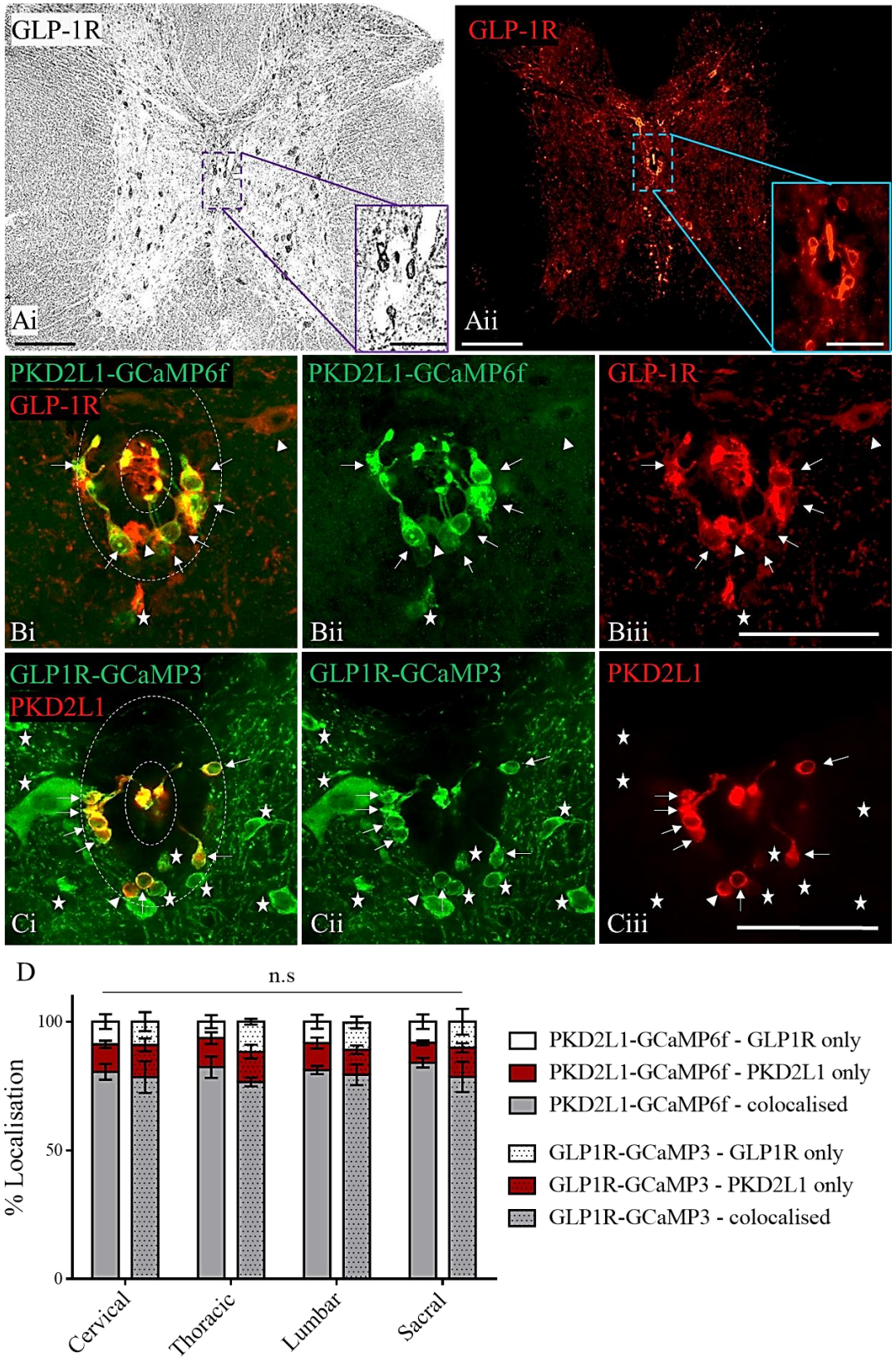
GLP-1R
Ai
GLP-1R
Aii
PKD2L1-GCaMP6f
GLP-1R
Bi
PKD2L1-GCaMP6f
Bii
GLP-1R
Biii
GLP1R-GCaMP3
PKD2L1
Ci
GLP1R-GCaMP3
Cii
PKD2L1
Ciii
D
n.s
% Localisation
100
50
0
Cervical
Thoracic
Lumbar
Sacral
PKD2L1-GCaMP6f - GLP1R only
PKD2L1-GCaMP6f - PKD2L1 only
PKD2L1-GCaMP6f - colocalised
GLP1R-GCaMP3 - GLP1R only
GLP1R-GCaMP3 - PKD2L1 only
GLP1R-GCaMP3 - colocalised

Figure 3.5: The majority of CSFcNs display immunoreactivity for the GLP-1R.

A. Representative images of GLP-1R primary antibody staining on wild-type mouse thoracic spinal cord, (i) enhanced through DAB, (ii) enhanced with TSA. Localisation of GLP-1R-IR can be seen around the central canal (insets) in cells with the morphology of CSFcNs, faint immunolabelling can also be seen in cells of the grey matter and ventral median fissure. Scale bars: main images: 100 μm, insets: 50 μm.

B. Images showing immunolabelling of GLP-1R enhanced using TSA. Compressed z-stack images of merged (i), GCaMP6f (ii), and GLP-1R antibody (iii) localisation in a PKD2L1-GCaMP6f mouse showing high degrees of colocalisation between GCaMP6f and GLP-1R-IR in CSFcNs. Scale bar: 50 μm.

C. Compressed z-stack images of merged (i), GCaMP3 (ii), and PKD2L1-IR (iii) localisation in a GLP1R-GCaMP3 mouse showing prominent levels of colocalisation in CSFcNs, as well as GLP-1R localisation in cells outside the central canal. Scale bar: 50 μm. Arrows indicate double-labelled cells, arrowheads indicate cells only expressing GLP-1R, stars indicate cells only expressing PKD2L1.

D. Graph showing quantification of percentage immunolabelling over the cervical, thoracic, lumbar, and sacral regions in both PKD2L1-GCaMP6f (clear bars) and GLP1R-GCaMP3 (dotted bars) models. There were no significant differences between either model in the percentage of cells that expressed PKD2L1, GLP-1R, or both. Neither were differences observed across regions studied. Statistical analysis: RM two-way ANOVA with Tukey's multiple comparison test.

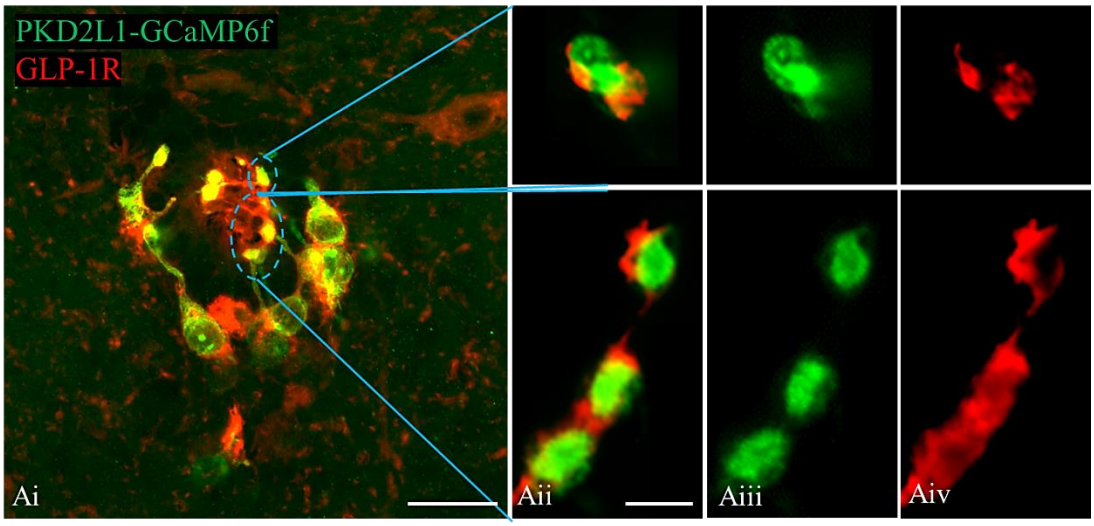

Figure 3.6: The GLP-1R is highly expressed on the endbulbs of CSFcNs.

A. Compressed z-stack image of GCaMP6f and GLP-1R-IR within the central canal. Higher magnification images of merged (ii), GCaMP6f (iii), and GLP-1R-IR (vi) shows a high intensity of labelling around the endbulbs. Scale bars: (i) 50 μm, (ii) 5 μm.

3.2.2.1 Many GLP-1R positive cells also express VGAT

The GABAergic nature of CSFcNs has been discussed extensively in the literature previously (Vigh-Teichmann and Vigh, 1989; Orts-Del'immagine et al., 2012; Fidelin et al., 2015). Previous work in the Deuchars lab has shown that VGAT is present in all CSFcNs throughout the lifespan of the mouse (age range tested: juvenile 18 – 42 days, adult 56 – 112 days) and across all regions of the spinal cord (Johnson et al., 2023). A VGATxGCaMP6f mouse strain was used in this investigation, for details see Chapter 2: General methods (section 2.1.3).

The relationship between GABAergic cells and expression of the GLP-1R however is less well defined. Using the VGAT-GCaMP6f mouse model and anti-GLP1R it was found that, around the central canal area, significantly more cells co-expressed both GCaMP6f and the GLP-1R (83.47 ± 5.74%, $p < 0.05$) than expressed only GCaMP6f (12.17 ± 1.70%), whilst the remaining cells only expressed the GLP-1R (4.37 ± 4.19%) (Figure 3.7). This is largely in agreement with the extent of localisation of the GLP-1R on CSFcNs seen using the GLP1R-GCaMP3 mouse line and antibody mentioned in the previous section, as would be expected. Outside of the central canal area, most cells that expressed either GCaMP6f or the GLP-1R were found in the grey matter, with the significant majority of the cells expressing the GLP-1R also being GCaMP6f positive (63.37 ± 2.95%, $p < 0.05$; Figure 3.7 B and Cii). The remaining GLP-1R positive cells were not investigated using this model.

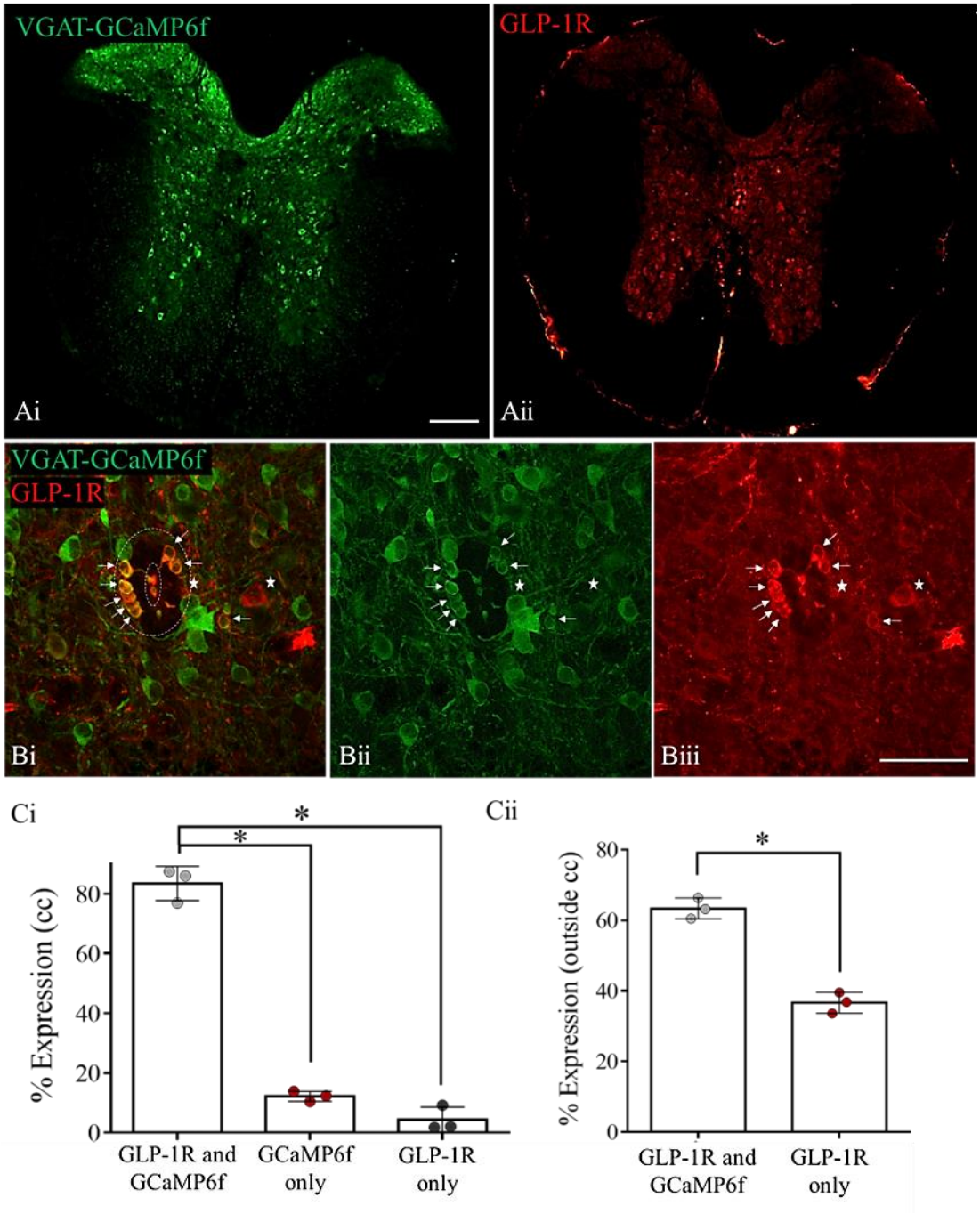

Figure 3.7: GCaMP6f under the VGAT promotor can be seen localised to most cells that also express GLP-1R immunoreactivity.

A. Low magnification images of GCaMP6f (i) and GLP-1R (ii) in a VGAT-GCaMP6f mouse model. Localisation of VGAT can be seen throughout the grey matter indicative of widespread GABAergic neurons, a large amount of GLP-1R localisation can also be seen throughout the grey matter in a similar pattern. Scale bar: 100 μm.

B. Compressed z-stack images of merged (i), GCaMP6f (ii), and GLP-1R (iii) showing extensive colocalisation in cells with morphological characteristics of CSFcNs surrounding

the central canal. Arrows indicate double labelled cells; stars indicate cells only expressing GLP-1R.

C. Graph showing percentage localisation of markers within the central canal (CC). Statistical analysis: One-way ANOVA with Tukey's multiple comparison test, significance level $p < 0.05$ (indicated by *).

D. Graph showing percentage localisation of markers outside of the central canal. Statistical analysis: Unpaired t-test, significance level $p < 0.05$ (indicated by *).

3.2.2.2 GLP-1R positive CSFcNs also express proteins in the end-bulb that are consistent with release from vesicles

SV2 is a large, transmembrane glycoprotein specific to vesicles that undergo calcium mediated exocytosis in neural and endocrine cells (Ciruelas et al., 2019). Several studies using SV2 knockout mice have indicated that loss of SV2 does not alter the frequency of spontaneous neurotransmitter release independent of action-potentials, nor does it reduce the number of vesicles synthesised or retained at presynaptic membranes (Ciruelas et al., 2019). Instead, SV2 appears to have a role in priming vesicles for calcium-dependent fusion and exocytosis, along with cofactor synaptotagmin (Schivell et al., 1996; Custer et al., 2006; Chang and Südhof, 2009).

Synaptophysin is the most abundant integral membrane protein within the presynaptic synaptic vesicle, and has roles in formation of the synapse, synaptic plasticity, and both exocytosis and endocytosis (Rehm et al., 1986; Janz et al., 1999; Tarsa and Goda, 2002; Xie et al., 2017). Synaptophysin, potentially through complex formation with synaptobrevin, is also implicated in the vesicle recycling pathway; knockout of synaptophysin in a mouse model resulted in a significant depletion in synaptic vesicles, as well as a slower retrieval rate of synaptic vesicles after sustained neuronal activity (Kwon and Chapman, 2011; White and Stowell, 2021).

Double labelling experiments using anti-GLP1R, to identify CSFcNs, and either anti-synaptophysin or anti-SV2 were performed to identify the expression of these proteins within CSFcNs. Both SV2-IR and synaptophysin-IR were detected in punctate structures apposed to the soma, and to a lesser extent the processes of GLP-1R positive CSFcNs (Figure 3.8), suggesting that CSFcNs receive synaptic contacts

onto their cell bodies and are incorporated into functional neuronal circuits. SV2 and synaptophysin are also extensively expressed within the end bulbs indicating a potential capability to release compounds into the CSF.

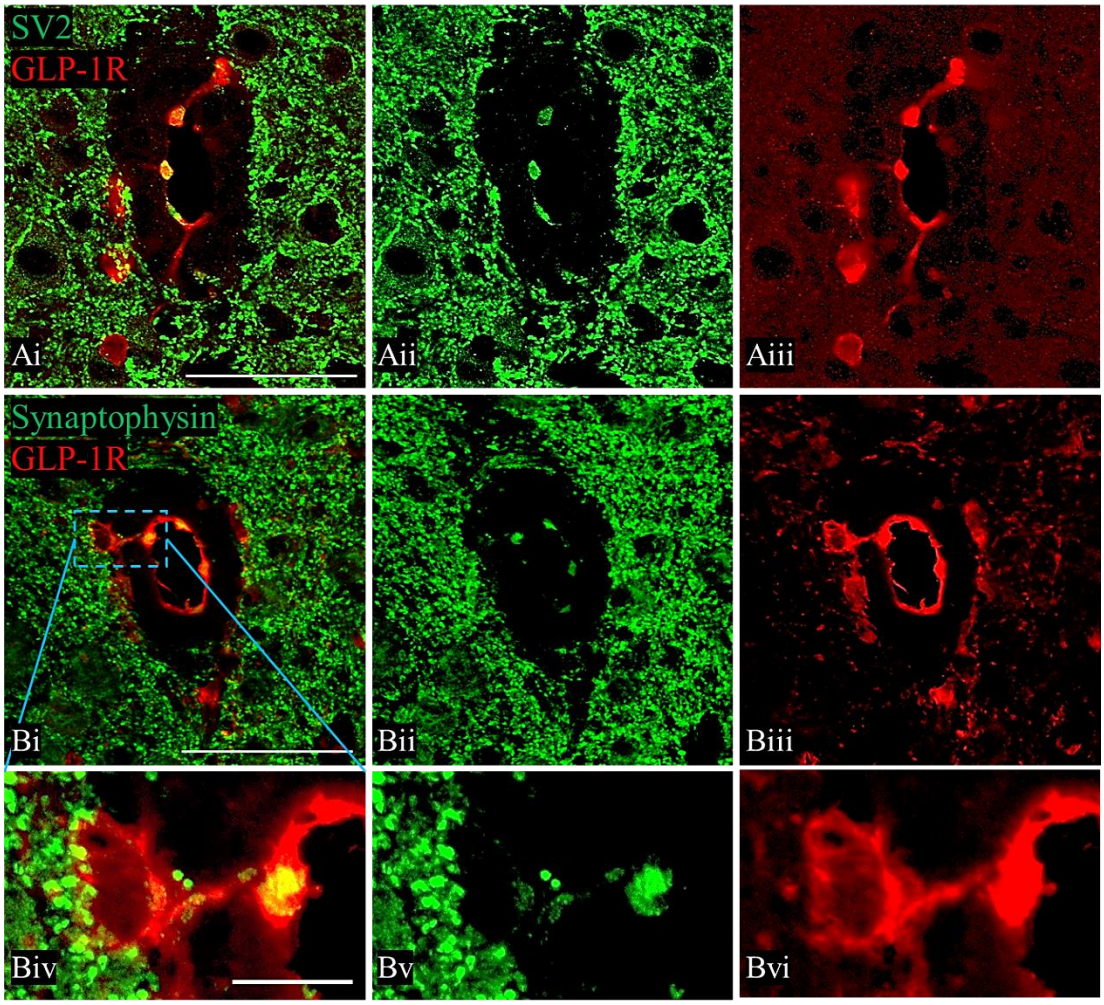

Figure 3.8: CSFcNs express SV2 and synaptophysin, particularly in the end bulbs.

A. Images of merged (i), SV2-IR (ii), and GLP-1R- IR (iii) localisation within the central canal. Punctate SV2 staining can be observed around the soma and extensively within the endbulbs of GLP-1R positive cells assumed to be CSFcNs. Scale bars: 50 μm.

B. Images of merged (i), synaptophysin (ii), and GLP-1R (iii) localisation within the central canal. Punctate synaptophysin staining can be observed around the soma and extensively within the endbulbs of GLP-1R positive cells assumed to be CSFcNs. Scale bars: 50 μm. A higher magnification image revealing low levels of synaptophysin on the cell dendrite as well as soma (iv). Scale bars: 10 μm.

3.2.3 CSFcNs have close appositions to their somata and processes originating from GLP-1 producing cells

As mentioned in the introduction, GLP-1 is produced by PPG neurons in the brainstem (Merchenthaler et al., 1999; Llewellyn-Smith et al., 2011), and as such a PPG-YFP transgenic mouse strain, where YFP is expressed under the glucagon promoter, can be used to assess whether CSFcNs receive direct input from GLP-1 producing neurons. These PPG neurons can be found in the caudal brainstem region arranged bilaterally in two large clusters within the nucleus of the solitary tract (NTS) and the intermediate reticular nucleus (IRN). A small number of PPG neurons can also be seen along the midline ventral to the central canal within the raphe obscurus (Figure 3.9). This localisation pattern matches that seen in the literature (Jin et al., 1988; Merchenthaler et al., 1999; Llewellyn-Smith et al., 2011, 2013), and the presence of YFP not only in the cell bodies but also in the dendrites and axons makes this a suitable model for use in this investigation.

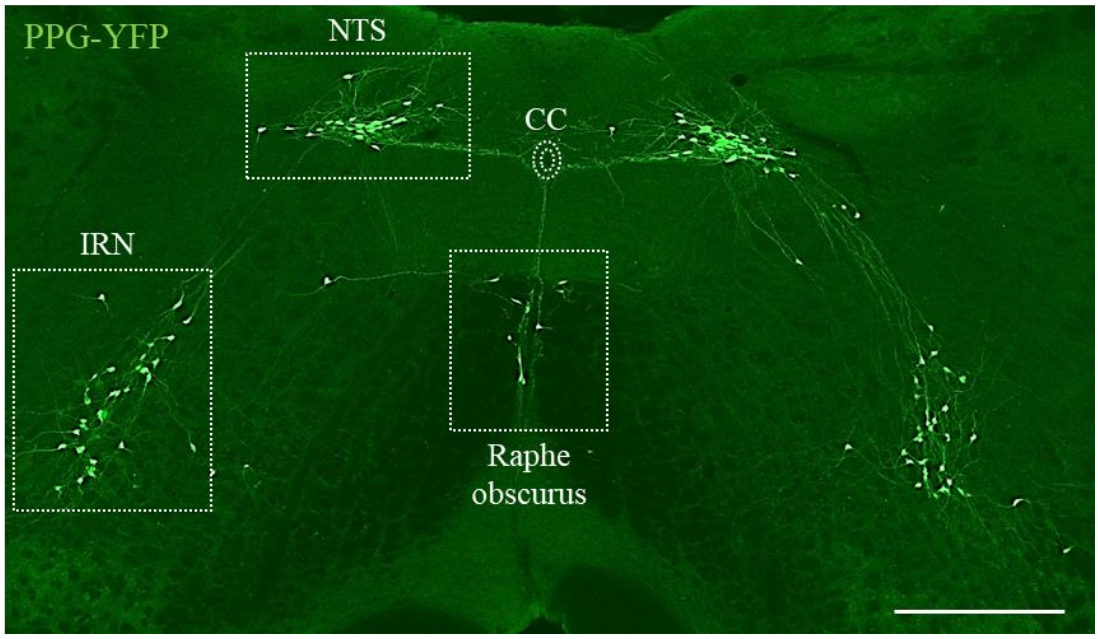

Figure 3.9: PPG-YFP transgenic mouse strain labels GLP-1 neurons in the caudal brainstem.

Numerous perikarya and projections can be observed within the nucleus of the solitary tract (NTS), intermediate reticular nucleus (IRN) and the *raphe obscurus*. Projections can also be observed both bilateral and ventral to the central canal (CC). Scale bar: 500 μm.

To assess the extent of innervation from GLP-1 neurons within the spinal cord, double labelling experiments were performed with anti-PKD2L1 and anti-GFP to visualise PPG-YFP. Examination of sections from all regions in the spinal cord revealed that every region had some extent of innervation from PPG-YFP fibres, but the thoracic region contained substantially more fibres than any other region (Figure 3.10, Figure 3.11)

Quantification of the appositions from GLP-1 neurons onto CSFcN cell bodies indicated that individual cell innervation was also region dependent. Appositions onto cell bodies were significantly higher in the thoracic region (3.51 ± 1.23 appositions per CSFcN), when compared with cervical ($p = 0.001$, 0.06 ± 0.09 appositions per CSFcN), lumbar ($p = 0.001$, 0.67 ± 0.42 appositions per CSFcN), or sacral ($p = 0.001$, 0.63 ± 0.55 appositions per CSFcN) regions. The majority of CSFcNs within the cervical, lumbar, and sacral regions did not receive any appositions, and no CSFcNs at any region received more than 9 close appositions (Figure 3.10, Figure 3.11).

Comparable results were found when quantifying close appositions onto the first 10 μm of processes coming from CSFcNs, with PKD2L1 positive processes in the thoracic (4.51 ± 1.25 appositions per CSFcN process) region receiving significantly more appositions from GLP-1 neurons than those in cervical ($p = 0.001$, 0.63 ± 0.32 appositions per CSFcN process), lumbar ($p = 0.001$, 0.53 ± 0.26 appositions per CSFcN process), or sacral ($p = 0.001$, 0.43 ± 0.19 appositions per CSFcN process) regions. Again, the majority of CSFcNs received no appositions to their processes from GLP-1 neurons within the cervical, lumbar, and sacral regions, and no processes at any region received more than 12 close appositions at any region (Figure 3 10, Figure 3 11). The occasional processes from a GLP-1 neuron could be observed forming close appositions on processes from more than one CSFcN, indicating a potential link between these cells (Figure 3 10, Ai).

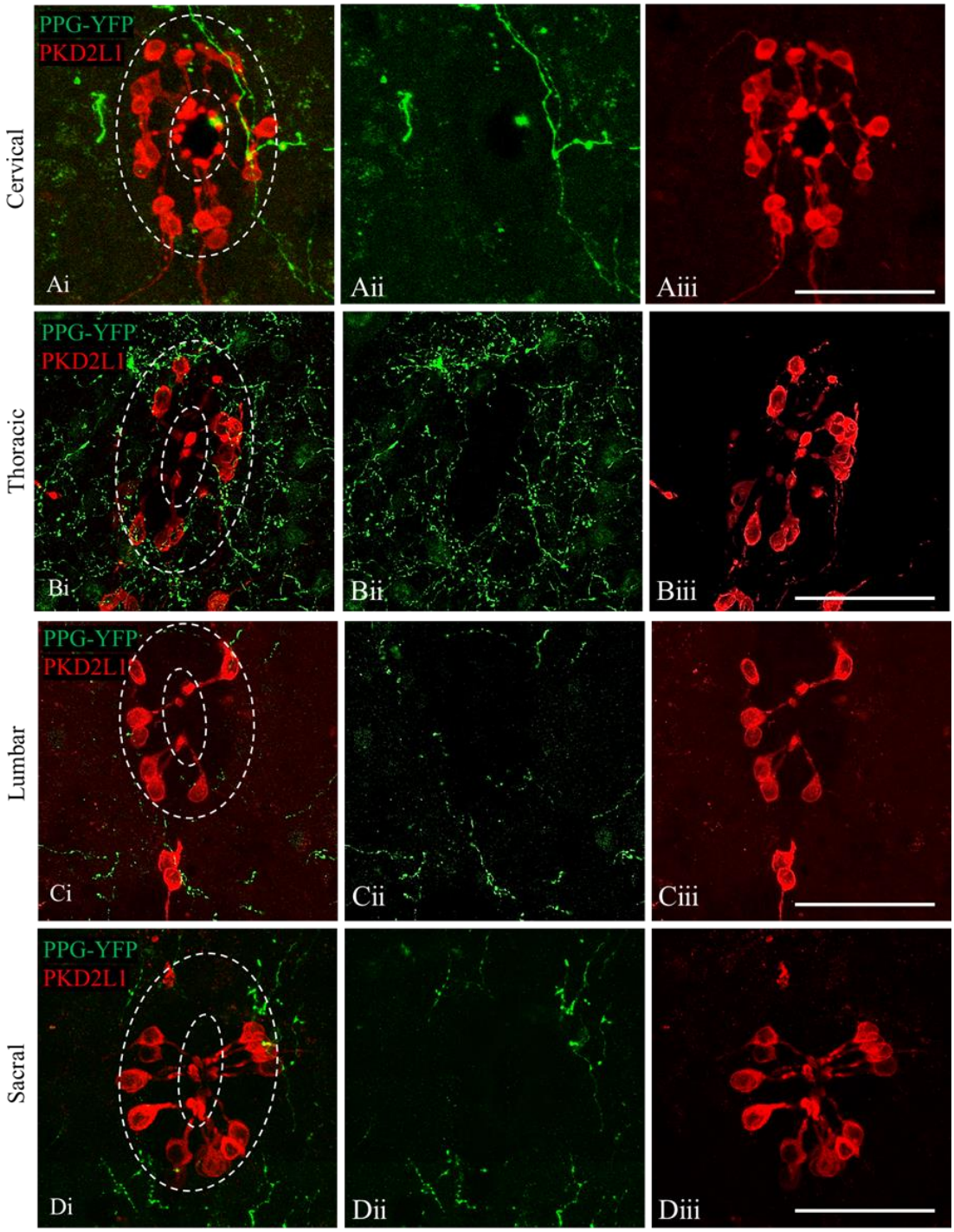

Figure 3.10: The thoracic region of the spinal cord contains substantially more PPG axons than other regions.

Compressed z-stack representative images of merged (i), PPG-YFP (ii), and PKD2L1 (iii) immunofluorescence in cervical (**A**), thoracic (**B**), lumbar (**C**), and sacral (**D**) spinal cord. PPG-YFP axons reach all regions of the spinal cord with the highest extent of innervation by PPG-YFP fibres appearing to be in the thoracic region, where they form many close appositions with PKD2L1 positive CSFcNs. Scale bars: 50 μm.

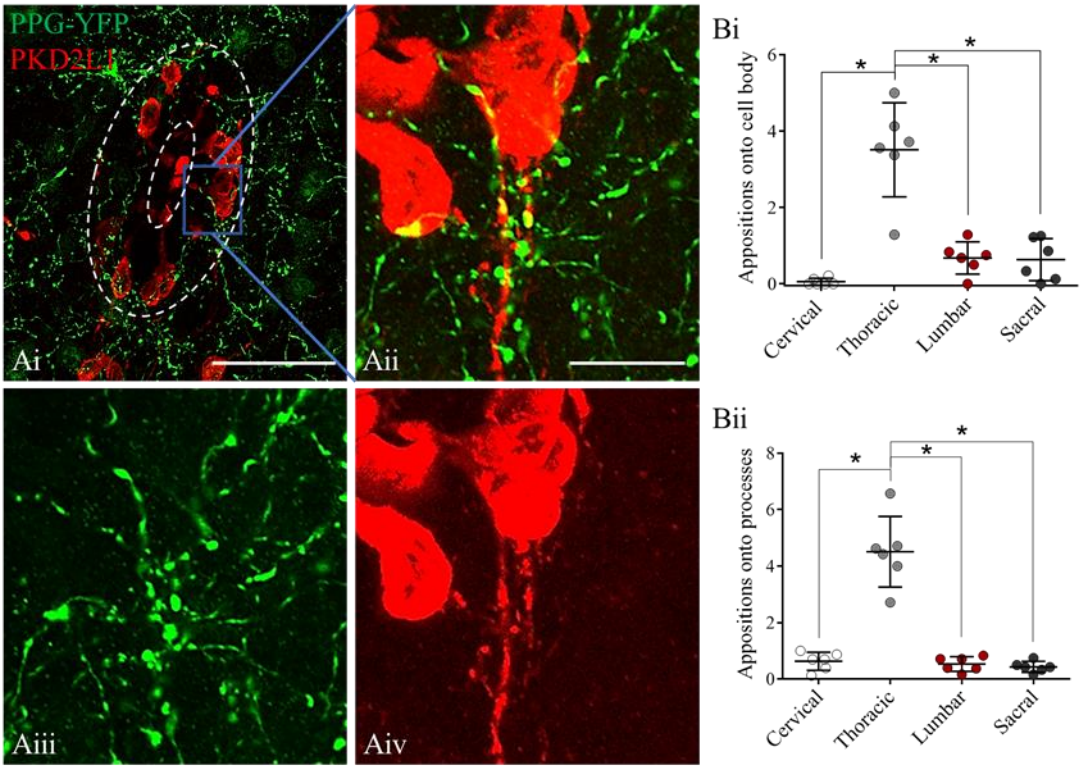

Figure 3.11: CSFcNs in the thoracic region receive significantly more appositions to their processes and cell bodies from GLP-1 neurons.

A. Compressed z-stack representative images of PPG-YFP appositions within the thoracic central canal region (i), and high magnification images of merged (ii), YFP (iii), and PKD2L1 (iv) showing extensive appositions onto both CSFcN perikarya and processes. Scale bars: (i) 50 μm, (ii) 10 μm.

B. Graphs of quantification of PPG-YFP appositions on CSFcN perikarya (i) and the first 10μm of PKD2L1 positive processes (ii). A significantly higher number of appositions can be seen in the thoracic regions of both instances. Statistical analysis: One-way ANOVA with Tukey's multiple comparison test, significance level $p < 0.05$ (indicated by *).

3.3 DISCUSSION

Within this chapter three main topics are addressed: the use of PKD2L1-dependant expression of GCaMP6f as a proxy-marker for CSFcNs, the presence of GLP-1Rs on CSFcNs within the central canal of the spinal cord, and the presence of GLP-1 positive appositions on CSFcN soma and projections.

Firstly, double labelling experiments using anti-PKD2L1 and anti-GFP to identify GCaMP6f expressing cells were conducted, and colocalisation analysis revealed almost 100% colocalisation between PKD2L1 and GCaMP6f. CSFcNs were primarily located around the central canal area, with a small number of PKD2L1 positive cells located between the CC and the ventral fissure area as previously noted in the literature (Jurčić et al., 2021). Further investigation of GCaMP6f expression revealed the presence of glial cells outside the central canal area, which did not express PKD2L1 but expressed PanQKI, an oligodendrocyte marker.

Furthermore, several GCaMP6f positive CSFcNs around the central canal displayed faint immunoreactivity for Sox2, and a small number of GCaMP6f positive cells outside of the central canal also colocalised with Sox2, but these were not confirmed to be CSFcNs or PanQKI positive cells. Single cell/nucleus RNA sequencing revealed the presence of PKD2L1 mRNA in two subpopulations of oligodendrocytes, and Sox2 mRNA in many different cell types, including CSFcNs, sub-populations of oligodendrocytes, and astrocytes (Lein et al., 2007; Russ et al., 2021).

Next, the study aimed to investigate the expression of the GLP-1R protein in different mouse strains using GLP-1R primary antibody on wild type or PKD2L1-GCaMP6f mouse tissue, and a transgenic mouse model expressing GCaMP3 under the GLP-1R promoter. Results showed that GLP-1R positive cells were present predominantly within the grey matter and surrounding the central canal. Approximately 80% of GLP-1R immunopositive cells around the central canal also expressed PKD2L1, identifying them as CSFcNs, and interestingly a small population of CSFcNs could not be identified as being immunoreactive for the GLP-1R. No significant differences were observed in percentage localisation when using different mouse models, between juvenile and adult mice, or between different regions of the spinal cord.

Additionally, within the VGAT-GCaMP6f transgenic mouse model there was approximately 63% colocalisation between cells within the spinal cord that were immunopositive for GCaMP6f and GLP-1R, indicating that a large percentage of cells possessing the GLP-1R are GABAergic. CSFcNs that were immunopositive for GLP-1R were also found to be immunoreactive for VGAT, SV2, and synaptophysin, indicting a potential role in releasing compounds into the CSF and integration into the circuitry of the spinal cord.

Lastly, this study investigated the extent of innervation of CSFcNs by GLP-1 producing neurons using a PPG-YFP transgenic mouse model. The PPG neurons were found bilaterally in the nucleus of the solitary tract and the intermediate reticular nucleus in the caudal brainstem, with a small number in the raphe obscurus, consistent with previous studies (Hisadome et al., 2010; Llewellyn-Smith et al., 2011; Trapp and Cork, 2015). The study found that every region of the spinal cord had some extent of innervation from PPG-YFP fibres, with the thoracic region containing substantially more fibres than any other region. The innervation of individual CSFcNs was region-dependent, with the thoracic region having significantly higher numbers of appositions from GLP-1 neurons onto both their soma and projections, compared to the cervical, lumbar, and sacral regions. The majority of CSFcNs in the cervical, lumbar, and sacral regions did not receive any appositions from GLP-1 neurons, however the occasional processes from a GLP-1 neuron could be observed forming close appositions on processes from more than one CSFcN.

3.3.1 PKD2L1-GCaMP6f as a suitable model for use in calcium imaging experiments

Research in this chapter has determined that all CSFcNs that can be identified through the PKD2L1 primary antibody are also identified through the enhancement of GCaMP6f in the transgenic mouse model, thus determining that this model is indeed suitable for use for the immunohistochemical identification of CSFcNs and in calcium imaging experiments in the following chapter. With regard to the small number of PanQKI positive oligodendrocytes that also express GCaMP6f in the grey matter, as these cells predominantly exist outside of the central canal, and do not

display spontaneous calcium activity, it is unlikely that they will interfere with these experiments.

3.3.1.1 Localisation of PKD2L1 in a subset of oligodendrocytes

Within the PKD2L1-GCaMP6f mouse model, a small number of GCaMPf labelled cells could be observed outside of the central canal where they were seen to colocalise with the oligodendrocyte marker, PanQKI. It could be possible that the localisation of PKD2L1 in oligodendrocytes is an artifact of the mouse model used; the model used here was a gift from Sue Kinnamon, University of Colorado, and is originally described in a paper by Ye, et al. This model has since then been used to characterise CSFcNs in several studies, none of which noted localisation of PKD2L1 in any other cells within the spinal cord (Gerstmann et al., 2022; Riondel et al., 2022).

The model used in this experiment has a different origin than that used by Nakamura et al, who also noticed similar localisation patterns in oligodendrocytes when PKD2L1-cre was crossed with a CAG-lox-CAT-lox-EGFP reporter line (Nakamura et al., 2022), validating the results in this chapter. However, further complicating this discussion is that other studies using the same mouse line as Nakamura et al did not report any expression outside of CSFcNs (Huang et al., 2006; Orts-Del'immagine et al., 2012; Orts-Del'Immagine et al., 2014, 2016; Jurčić et al., 2021).

It is more likely that this is a case of genuine expression of PKD2L1 in a subset of oligodendrocytes, perhaps due to a shared neural progenitor as it is known that a subtype of CSFcNs originate from the same temporal and spatial location as oligodendrocytes early in development (Djenoune et al., 2014; Petracca et al., 2016). This may be in line with mRNA expression data from Russ et al, and also in-situ hybridisation (ISH) studies from Allen brain atlas, which confirms the presence of PKD2L1 mRNA in some oligodendrocytes (Lein et al., 2007; Russ et al., 2021). This indicates that it is unlikely to be an artifact of the mouse model.

3.3.1.2 Localisation of Sox2 in a subset of CSFcNs; are they quiescent stem cells?

The localisation of Sox2, a transcription factor commonly used as a marker for neural stem cells (Ellis et al., 2004), in approximately half of CSFcNs investigated in this study raises the question of whether some CSFcNs have quiescent neural stem cell (NSC) properties.

Petracca et al found Sox2 expression in CSFcNs in postnatal (P0) mice through colocalisation of the antibody and PKD2L1 (Petracca et al., 2016), and a study by Wang et al has identified Sox2 in cultures of PKD2L1 positive cells *in vitro* (S. Wang et al., 2021). In the latter study, PKD2L1 positive cells were sorted by fluorescence activated cell sorting (FACS) and cultured in a medium enriched with fibroblast and epidermal growth factors. The resulting neurospheres were found to express Sox2, Nestin, GFAP, and proliferative marker Ki67, and displayed the ability to differentiate into neurons, astrocytes, and oligodendrocytes (S. Wang et al., 2021).While it is possible that this could be due to CSFcNs possessing latent stem cell like properties, it is also possible that cell sorting was not entirely accurate and some contamination from other cells within the ependymal layer occurred. While it is possible that CSFcNs may revert to an earlier stage of development, potentially one with NSC-like properties, when stimulated by the appropriate growth factors *in vitro*, it is extremely unlikely that this would occur *in vivo* in a mammalian model. CSFcNs are not known to express Nestin or GFAP mRNA *in vivo* (Rosenberg et al., 2018; Russ et al., 2021), nor have they been found to proliferate postnatally (Marichal et al., 2009; Corns et al., 2015).

A recent, comprehensive review by Mercurio et al proposes that not all Sox2 expression is solely related to possession of NSC properties in differentiated neurons and glial cells (Mercurio et al., 2019b). While CSFcNs are not mentioned within this review it may still give some insight about the potential non-NSC function of this factor in CSFcNs; studies using Sox2 knock-out mice have shown that Bergmann glia cells in the cerebellum and Müller glia cells in the retina do not form in a typically linear ordered array, but instead are displaced from their typical locations in a disordered fashion indicating that Sox2 may have an effect on cell migration and spatial positioning (Bachleda et al., 2016; Cerrato et al., 2018). Sox2 also appears to be implicated in the correct development and organisation of neuronal projections;

deletion of Sox2 in post-mitotic neurons from three different thalamic nuclei shows that neuronal projections from these area to their target areas in the visual or auditory cortex are reduced, absent, or entirely disorganized occasionally being misrouted to incorrect areas (Mercurio et al., 2019a). It is entirely possible that Sox2 localisation within postnatal CSFcNs is related to the establishment of correct spatial positioning around the central canal, and the integration of their processes into neural networks instead of being a marker for potential stem cell activity.

3.3.2 CSFcNs and the GLP-1 system in the spinal cord

As discussed in the introduction (section 1.3.3) the specific cell types that express the GLP-1R in the spinal cord has been debated, with astrocytes, microglia, and some types of neurons discussed as likely candidates (Gong et al., 2014; Llewellyn-Smith et al., 2015; C.-H. Lee et al., 2018; Rosenberg et al., 2018). The data in this study demonstrates that approximately 80% of CSFcNs possess the GLP-1R, regardless of method used to investigate, which is particularly highly expressed in the endbulbs contacting the CSF. This finding is in agreement with the literature observing GLP-1R mRNA in cells surrounding the central canal (Merchenthaler et al., 1999; Lein et al., 2007; Russ et al., 2021). This investigation also confirms the innervation of the spinal cord by PPG neurons (Llewellyn-Smith et al., 2015), and found that is significantly higher in thoracic regions compared with cervical, lumbar, and sacral regions. Direct apposition of PPG-YFP fibres onto CSFcN soma and processes is also highest in thoracic regions, with limited appositions being seen in other regions.

3.3.2.1 CSFcNs may be capable of sensing and responding to GLP-1 in the CSF

Throughout all regions of the spinal cord, the extent of colocalisation of GLP-1R and PKD2L1 remains consistent. Immunolabeling can be observed most intensely on the cell bodies and on the endbulbs within the central canal lumen. Rather unexpectedly, appositions from GLP-1 producing neurons were found to be highly region-dependent with a significantly higher extent of innervation being observed within the thoracic region compared with limited innervation in other regions. This potentially

indicates a functional diversity in the roles of GLP-1R positive CSFcNs within different regions of the spinal cord. CSFcNs in the thoracic region may be more extensively integrated into circuitry within the spinal cord, responding to GLP-1 release onto their soma, whereas CSFcNs in cervical, lumbar, and sacral regions may have a more prominent role in sensing GLP-1 levels within the CSF.

Cells that express the GLP-1R but do not receive close appositions from PPG neurons are known in the central nervous system; neurons in the ventral hippocampal formation (HPFv), an area associated with learning and memory and implicated in control of food intake regulation, being one example (Cork et al., 2015; Hsu et al., 2015; Jensen et al., 2018). A study by Hsu et al found that GLP-1R positive neurons in the adult rat HPFv responded to direct ICV infusion of GLP-1R agonist exendin-4 by reducing food intake, whereas blocking HPFv GLP-1Rs increased food intake indicating that the receptors are functional (Hsu et al., 2015). Immunohistochemical investigation into endogenous sources of the GLP-1 ligand revealed no GLP-1 positive axons within the HPFv, in agreement with past reports (Jin et al., 1988; Llewellyn-Smith et al., 2011).

However, Hsu et al did find GLP-1 positive axons contacting ependyma at various rostrally located ventricular sites such as the third ventricle, lateral ventricle, and the subfornical organ. Injection of the retrograde tracer Fluorogold into the lateral ventricle resulted in expression of Fluorogold within approximately a third of NTS GLP-1 neurons, confirming that they have access to the CSF and therefore could potentially release GLP-1 into the CSF to act on HPFv neurons (Hsu et al., 2015). The presence of active GLP-1 was also found in the serum and CSF of fasted rats, in agreement with a previous study (Heile et al., 2009), further indicating that this may be a mechanism underlying the presence of GLP-1 in the CSF (Hsu et al., 2015). This contributes evidence that cells exist which may respond to non-synaptic transmission of GLP-1 through close proximity to the CSF, as well as evidence that active GLP-1 circulates in the CSF, a mechanism which may similarly be exploited by CSFcNs.

The presence of active GLP-1 in the spinal cord is further confirmed through an experiment by Holt et al where selective bilateral ablation of NTS PPG neurons through use of a cre dependent diphtheria toxin subunit A (DTA) dramatically

reduced the total amount of GLP-1 present in the spinal cord compared with injection with a control virus (Holt et al., 2019). As whole spinal cords were homogenised for use during this study it is difficult to say exactly which region of cord contained the most GLP-1, or indeed if the main source was from direct PPG innervation or from the CSF, however when measured against blood, GLP-1 levels in the spinal cord were approximately 30 times higher indicating that blood within the samples was not the main source of GLP-1 (Holt et al., 2019).

How CSFcNs respond to stimulation by GLP-1 is currently unknown but will be discussed in detail in the following chapter. However, given that the majority of GLP-1R positive cells surrounding the central canal also express VGAT it is reasonable to speculate that activation of CSFcNs may induce release of GABA into the circulating CSF where it may act upon fellow CSFcNs, or neighbouring ependymal cells (Orts-Del'immagine et al., 2012; Corns et al., 2013). CSFcNs have long been proposed to release compounds into the CSF due to the presence of numerous small synaptic vesicles and large granular vesicles on their end bulbs (Vigh et al., 1977; Vígh et al., 2004; Djenoune et al., 2017). The research performed in this chapter confirms the presence of synaptic proteins SV2 and synaptophysin within the endbulbs, localisation which is consistent with literature (Conte et al., 2008; Jay and McDearmid, 2015; Wu et al., 2021). The presence of proteins that are involved in the calcium evoked release of vesicles, as well as the uptake of peptides or neuromodulators, further implicates CSFcNs as cells that sense and modulate CSF composition (Agduhr, 1922; Kolmer, 1931; Vígh et al., 2004).

3.3.2.2 An increase in innervation by PPG neurons at thoracic level may be part of a feedback loop involving CSFcNs and sympathetic preganglionic neurons

It has been shown in this investigation that the thoracic area of the spinal cord receives a significantly higher degree of innervation from brainstem PPG-YFP axons than other regions, both throughout the sections and through increased close appositions with CSFcNs. Injection of a retrograde fluorogold tracer into the T9 section of a PPG-YFP mouse spinal cord revealed that approximately half of the PPG neurons situated within the NTS and IRT extended axons to the lower thoracic region, although it is not specified whether these innervate cholinergic neurons,

CSFcNs, or both (Llewellyn-Smith et al., 2015). There was a high degree of direct innervation to ChAT positive neurons in the intermediolateral cell column (IML) and the central autonomic area (CAA) of lamina X, with lesser innervation being observed in the intercalated nucleus (IC) and a small number of motor neurons in the ventral horn, a finding replicated by work performed in the Deuchars lab (Llewellyn-Smith et al., 2015; Katherine Mortimer: Deuchars lab unpublished MRes thesis, 2022). Additionally several YFP positive cell bodies were found within the lumbosacral region, where these cells project to was not fully characterised but no spinal YFP containing neurons were observed to project rostrally to the brain nor leave the spinal cord, indicating possible involvement in spinal GLP-1 signalling (Llewellyn-Smith et al., 2015).

Several studies have shown that application of GLP-1R agonists both centrally and systemically increase heart rate (Yamamoto et al., 2002; Griffioen et al., 2011; Robinson et al., 2013; Jessen et al., 2017), a study by Holt et al shows that application of exendin-4 directly to the thoracic spinal cord increases heart rate mediated by spinal GLP-1Rs, thought to be those specifically on sympathetic preganglionic neurons (SPNs) as this effect was ameliorated through cotreatment with beta-1 receptor antagonist atenolol (Holt et al., 2020). This pathway could help to explain the significantly higher levels of apposition by PPG-YFP axons that are seen in the thoracic sections of spinal cord in this study, particularly those forming close appositions with SPNs (Llewellyn-Smith et al., 2015; Katherine Mortimer: Deuchars lab unpublished MRes thesis 2022). However, this does not necessarily explain the increase in close appositions from PPG neurons onto CSFcNs in the thoracic region compared with others.

It could be that CSFcNs form an inhibitory feedback system with ChAT positive neurons to regulate SPN activity. Although SPNs are only known to project out of the spinal cord towards the sympathetic ganglia, functional cholinergic inputs to spinal CSFcNs have been well established through immunohistochemistry using ChAT and PKD2L1 primary antibodies in rat (Corns et al., 2015), and mouse (Orts-Del'immagine et al., 2012), and CSFcNs are known to depolarise in response to acetylcholine (Corns et al., 2015). The connectivity between cholinergic neurons and CSFcNs is further demonstrated by a study using a ChAT-EGFP mouse model and AAV labelled CSFcNs which found that ChAT positive cells and neurites located

around the CC and midline received frequent appositions from inhibitory CSFcN fibres, and intermingled with subependymal CSFcN fibre bundles, indicating that these cells may be part of a circuit (Nakamura et al., 2023).

With these points considered, it may be theoretically possible that SPNs increase heart rate by responding to GLP-1 released by PPG neurons (Yamamoto et al., 2002; Holt et al., 2020), CSFcNs may also receive increased GLP-1 input either from appositions from PPG neurons, or through sensing an increase in CSF GLP-1 which results in stimulation of these neurons and a release of inhibitory neurotransmitters from CSFcNs onto SPNs which may reduce SPN activity (Barber et al., 1982; Nakamura et al., 2023). This theory would require further work to determine whether these cells form a feedback loop that is integrated into the GLP-1 network in the spinal cord.

3.3.2.3 Potential CSFcN involvement in brainstem GLP-1 pathways

The precise details of how CSFcNs fit into the GLP-1 system remain unclear, and much further work is needed to assess the full extent of the overlap between these networks of cells. However, some hypotheses can perhaps be drawn due to the similarities in brainstem locations of these two cell populations.

CSFcNs have previously been identified around the central canal within the dorsal vagal complex of the caudal brainstem (Orts-Del'immagine et al., 2012), an area encompassing the dorsal motor nucleus of the vagus nerve (DMX), the nucleus of the solitary tract (NTS), and the area postrema (AP), which forms the main integrative centre of the mammalian autonomic nervous system (Bauer et al., 2005; Ludwig et al., 2021). Although projections from CSFcNs within this area have been difficult to identify, due to the lack of PKD2L1 in CSFcNs axons (Orts-Del'Immagine et al., 2014), preliminary evidence from a study within the Deuchars lab using a PKD2L1-GCaMP6f transgenic mouse model where the GCaMP6f was enhanced using the tyramide signal amplification (TSA) method to enhance weak labelling of GCaMP6f positive fibres presumed to be from CSFcNs may give some indications. It was found that GCaMP6f positive fibres project laterally towards the dorsal motor nucleus of the vagus nerve (DMX), NTS, and ventrally towards the midline and hypoglossal nucleus (XII). DAB enhancement of PKD2L1 labelling

similarly revealed the presence of PKD2L1 positive fibres along the ventral midline, and interestingly both soma and fibres within the DMX (Charlotte Marx-Carr, unpublished Masters by Research thesis, 2021).

The presence of PPG neurons and projections within the NTS, laterally to the CC from the NTS, and along the ventral midline to the raphe obscurus very closely overlaps with these observed projections from CSFcNs. This could indicate a potential relationship whereby both types of cells sense and respond to information involved in autonomic nervous system function and are perhaps involved in the regulation of homeostasis by integrating signals from the CSF with those from other circuits (Hisadome et al., 2010; Orts-Del'immagine et al., 2012)

3.3.3 Conclusion

In this chapter, the cell types expressing GCaMP6f in the PKD2L1-GCaMP6f transgenic mouse model have been successfully identified. The almost 100% colocalisation of GCaMP6f in CSFcNs around the central canal area validates the suitability of this model for use within the next chapter of this thesis, which focuses on investigating the effects of GLP-1R agonists on calcium events within CSFcNs.

It has also been shown that the majority of CSFcNs express the GLP-1 receptor, and a substantial percentage of these cells within the thoracic region receive direct appositions from GLP-1 neurons. The localisation of GLP-1Rs on the end bulbs of CSFcNs, as well as on their somata, indicates a potential for CSFcNs to sense GLP-1 within the CSF or extracellular fluid. In addition, the presence of appositions from GLP-1 neurons implies a likelihood that CSFcNs are integrated into the wider GLP-1 network in the spinal cord, and potentially within the brainstem.

This research contributes new insights into the GLP-1 system within the spinal cord, and is the first evidence of the potential contributions of CSFcNs within this network. In the next chapter, the functionality of these receptors will be investigated using calcium imaging in acute spinal cord slices.

Chapter 4 – Modulation of CSFcN Ca^{2+} spiking activity by GLP-1R agonists

4.1 INTRODUCTION

The research presented within this chapter investigates the impact of GLP-1R modulation on the Ca^{2+} spiking activity of CSFcNs. Initially, the study characterised the spontaneous Ca^{2+} spiking of CSFcNs and their response to application of common agonists such as acetylcholine and GABA. Subsequently, the responses of CSFcNs to a series of concentrations of liraglutide, a GLP-1R agonist, was determined. Finally, co-application experiments using liraglutide with the GLP-1R antagonist exendin-(9-39) were conducted to demonstrate that the observed effects are indeed mediated by the GLP-1R.

This research contributes unique information regarding the responsiveness of CSFcNs to modulation of the GLP-1R, information which has not been previously established in the literature.

4.1.1 How do GLP-1R agonists affect neuronal activity in the CNS?

In chapter 1: general introduction (section 1.3.5), the effects of, and mechanisms behind, GLP-1R stimulation of exocytosis were introduced, however, this did not fully cover the complexity of responses observed in electrophysiological and calcium imaging studies using GLP-1R agonists. Cells expressing the GLP-1R are found in many areas of the brain, and stimulation of these receptors leads to a diverse set of responses depending on the cell, their inherent neurochemical and membrane properties, and the other neurotransmitters influencing them (Chen et al., 2021).

The effects of GLP-1R stimulation on neuronal activity have largely focused on areas of the brain that are related to feeding (Mietlicki-Baase et al., 2013; Reiner et al., 2016; Trapp and Brierley, 2022), and the results of many of these studies are summarised in Table 4.1. Largely, it can be agreed that application of GLP-1, or analogues, to the majority of GLP-1R expressing neurons in various regions of the brain results in depolarisation of the membrane potential and an increase in the spontaneous firing rate of the neuron. In a smaller number of neurons, GLP-1R stimulation elicits a hyperpolarisation, reducing the firing frequency of the neuron. In several cases, this heterogeneity in response is due to indirect network effects,

such as synaptic input from GABAergic or glutamatergic neurons that also express the GLP-1R (Oka et al., 1999; Acuna-Goycolea and van den Pol, 2004; Mietlicki-Baase et al., 2014; Secher et al., 2014; Williams et al., 2018; He et al., 2019). Various ion channels, such as non-selective cation channels (Acuna-Goycolea and van den Pol, 2004; Cork et al., 2015), voltage dependent K+ channels (Thiebaud et al., 2016; Schwartz et al., 2021), and TRPC5 channels (He et al., 2019), are likely involved in the mediation of depolarising or hyperpolarising responses to GLP-1R stimulation. The ability of GLP-1R agonists to exert both pre-and post-synaptic effects on a neuron existing within a network further adds to the complexity of the situation (Acuna-Goycolea and van den Pol, 2004; Mietlicki-Baase et al., 2014; Farkas et al., 2021).

Table 4.1: Stimulation of the GLP-1R modulates electrophysiological properties within several brain areas.

Note: all drugs are bath applied unless otherwise specified.

Brain region	Neurons	Electrophysiological effects of GLP-1R activation	GLP-1R agonist	Conc.	Reference
mNTS	PPG	No change in spontaneous activity or synaptic transmission	Exendin-4, GLP-1	100 nM	(Hisadome et al., 2010; Alhadeff and Grill, 2014)
ARC	POMC/CART	Depolarisation and increase in spontaneous firing rate, increase of EPSCs frequency	Liraglutide, GLP-1	1.5 mM 100 nM	(Secher et al., 2014; He et al., 2019)
	NPy/AgRP	Indirect hyperpolarisation via $GABA_A$ mediated neurotransmission			
	Kisspeptin expressing	Depolarisation and increase in firing rate in 60% of cells	Liraglutide	300 nM	(Heppner et al., 2017)
LH	Orexinergic	Depolarisation and increase in firing rate via postsynaptic non-specific cation channels. Presynaptic enhancement of glutamatergic and GABAergic neurotransmission.	Exendin-4	1 μM	(Acuna-Goycolea and van den Pol, 2004)
PVN	Hypocretin	Dose-dependent depolarisation and increase in spike frequency – blocked by antagonist. Enhanced frequency of mEPSCs and sEPSCs, no effect on amplitude	GLP-1 Exendin-4 Exendin-(9-39)	0.1, 1, and 10 μM	
	Paraventricular hypothalamic neurons	Heterogenous response, most neurons increased frequency, small number decreased – decrease blocked by synaptic antagonists			
		Depolarisation and decrease in membrane resistance	GLP-1	100 nM	(Cork et al., 2015)
BNST	Unidentified	Heterogenous, not subtype dependent; 42% depolarised, increasing firing; 68% hyperpolarised, decreasing firing.	GLP-1	100 nM	(Cork et al., 2015; Williams et al., 2018)

HC	Pyramidal	Heterogenous, depolarisation in four of five neurons, hyperpolarisation in one.	GLP-1	100 nM	(Cork et al., 2015)
		Increase in firing rate followed by decrease – blocked by the EAA antagonist CNQX and GLP-1R antagonist	GLP-1 (puff) Exendin-(9-39)	1 μM 100nM	(Oka et al., 1999; Gullo et al., 2017)
VTA	Dopaminergic	Increase in sEPSC, decrease in amplitude of mEPSCs	Exendin-4	1 μM	(Mietlicki-Baase et al., 2013; Wang et al., 2015)
PVT	PVT-to-NAc projecting	Hyperpolarisation and suppression of spontaneous firing, blocked by antagonist	Exendin-4 Exendin-(9-39)	10 nM 100 nM	(Ong et al., 2017)
PBN	Unidentified	Substantial increase in firing rate – antagonist did not affect basal firing rate but attenuated ex-4 response	Exendin-4 Exendin-(9-39)	1 μM 1 μM	(Richard et al., 2014)
NAc	MSNs	Increase in frequency of mEPSCs through presynaptic AMPA/kainite signalling, no direct action.	Exendin-4	1 μM	(Mietlicki-Baase et al., 2014)
OB	MCs	Concentration-dependent increase in firing ~65% cells, shortened interburst interval, decreased excitation threshold through inhibition of voltage dependent K+ channels	GLP-1 Exendin-4	100 nM and 1 μM	(Thiebaud et al., 2016; Schwartz et al., 2021)

Abbreviations used: ARC, arcuate nucleus; BNST, bed nucleus of the stria terminalis; CRH, corticotropin-releasing hormone; EPSCs, excitatory postsynaptic currents; HC, hippocampus; LH, lateral hypothalamus; MCs, mitral cells; mEPSCs, miniature excitatory postsynaptic currents; mNTS, medial subnucleus of the nucleus tractus solitaries; MSNs, medium spiny neurons; N/A, not applicable; NAc, nucleus accumbens; NPY/AgRP, Neuropeptide Y/Agouti gene related peptide; OB, olfactory bulb; PBN, parabrachial nucleus; POMC, proopiomelanocortin; PVN, paraventricular nucleus; PVT, paraventricular thalamic nucleus; VTA, ventral tegmental area; EAA, excitatory amino acid.

4.1.2 Detecting neuronal activity through Ca^{2+} imaging studies

The relationship between intracellular Ca^{2+} levels and neuronal activity, such as action potentials and synaptic transmission, has established dynamic changes in intracellular Ca^{2+} concentration as a proxy for neuronal activity (Inoue, 2021). Neurons typically maintain low levels of intracellular calcium, however, when stimulated, calcium influx can occur through various channels, including voltage-gated and ligand-gated calcium channels. This increase in Ca^{2+} concentration can trigger downstream signalling events, including activation of calcium-binding proteins like calmodulin, activation of calcium-dependent enzymes like calcium/calmodulin-dependent protein kinases (CaMKs), and modulation of ion channels and neurotransmitter release (Clapham, 2007). Measuring changes in intracellular Ca^{2+} concentration is possible through the use of calcium-sensitive fluorescent indicators, which selectively bind to calcium ions and alter their fluorescence intensity in response to changes in Ca^{2+} concentration (Chen et al., 2013).

In this chapter, the PKD2L1-GCaMP6f mouse line will be used to visualise CSFcNs, having been established as a reliable and specific identifier for these cells in the previous chapter. GCaMP6f, a genetically encoded calcium indicator, was chosen due to its improved sensitivity to small fluctuations in calcium activity, increased photostability, and enhanced signal-to-noise ratio allowing for more precise detection of Ca^{2+} spiking compared with other GCaMP variants (Chen et al., 2013). The fast response dynamics of GCaMP6f enables detection of rapid changes in Ca^{2+} activity making it ideal for studying quick neuronal processes. Further details of this model can be found in Chapter 2: general methods (section 2.1.2) and Chapter 3: Introduction (section 3.1.1).

4.1.3 Hypothesis and aims

In the previous chapter it was established that a substantial number of CSFcNs express the GLP-1 receptor, and many CSFcNs within the thoracic region receive appositions from GLP-1 producing neurons. Therefore, it is hypothesised that CSFcNs respond to GLP-1R agonists through changes in intracellular Ca^{2+} concentration.

The aims of this chapter are to:

- Characterise the spontaneous Ca^{2+} activity profile of CSFcNs and investigate whether application of specific agonists elicits changes in Ca^{2+} spiking activity.

- Investigate the effects of bath application of GLP-1 and increasing concentrations of liraglutide on the intracellular Ca^{2+} dynamics of CSFcNs.

- Examine the effects of liraglutide on CSFcNs after incubation with the GLP-1R antagonist.

4.2.1 CSFcNs exhibit spontaneous Ca^{2+} spiking activity in acute slices, and alter this activity in response to application of agonists

4.2.1.1 Spontaneous Ca^{2+} spiking in CSFcNs is not influenced by the age of the animal

Firstly, in order to determine whether Ca^{2+} spiking in CSFcNs could be reliably observed and to understand the baseline activity of these cells, the cells were imaged, and spontaneous Ca^{2+} spiking activity was characterised. Techniques used in this research are similar to those employed by Johnson et al, which confirms that these spikes are mediated by changes in intracellular Ca^{2+} (Johnson et al., 2023).

Spikes were detected using their first derivative, above a specified baseline, which enables the separation of added spikes (Figure 4.1, C). Spontaneous Ca^{2+} spiking was observed in a number of CSFcNs, the characteristics of which varied between individual CSFcNs with most displaying a variety of high and low amplitude spikes (Figure 4.1, Bi - Biv). The median frequency of Ca^{2+} spiking observed across all CSFcNs was 0.154 ± 0.090 Hz (Figure 4.1, Ei), with a median spike amplitude of 0.675 ± 0.576 ΔF/F (1774 events, n = 120 cells, N = 19 animals, Figure 4.1, Eii). These results are similar to those seen in previous work using the VGATxGCaMP6f mouse line (Johnson et al., 2023), and recorded within zebrafish CSFcNs (Sternberg et al., 2018).

The research within this chapter, and within the wider thesis, uses animals across a range of ages and therefore it is important to investigate whether the properties of CSFcNs change along with the age of the animal. The age of the animal that slices were taken from did not significantly affect the median amplitude or frequency of Ca^{2+} spiking observed within CSFcNs. CSFcNs recorded from slices obtained from juvenile mice (less than 6 weeks old at time of experiment) had a median spike rate of 0.162 ± 0.093 Hz, with a median spike amplitude of 0.681 ± 0.549 ΔF/F (Figure 4.1, Ei and Eii). Spikes recorded from CSFcNs within slices obtained from adult animals (more than 6 weeks old at time of experiment) had a similar median spike amplitude of 0.655 ± 0.658 ΔF/F, with a median spike rate of 0.132 ± 0.085 Hz (Figure 4.1, Ei and Eii). The frequency of spike rate per CSFcN in older animals appeared to be lower than that of the juvenile animals, but this was not statistically significant. Furthermore, when the median amplitudes and frequency of Ca^{2+} spiking within

individual CSFcNs were plotted against each other it was found that there was a very weak negative linear correlation between the two variables that did not differ between the ages of the animals but was significant for juvenile animals (Figure 4.1, F, <6 weeks: r = -0.2898, p = 0.006, 6+ weeks: r = -0.2812, p = 0.132).

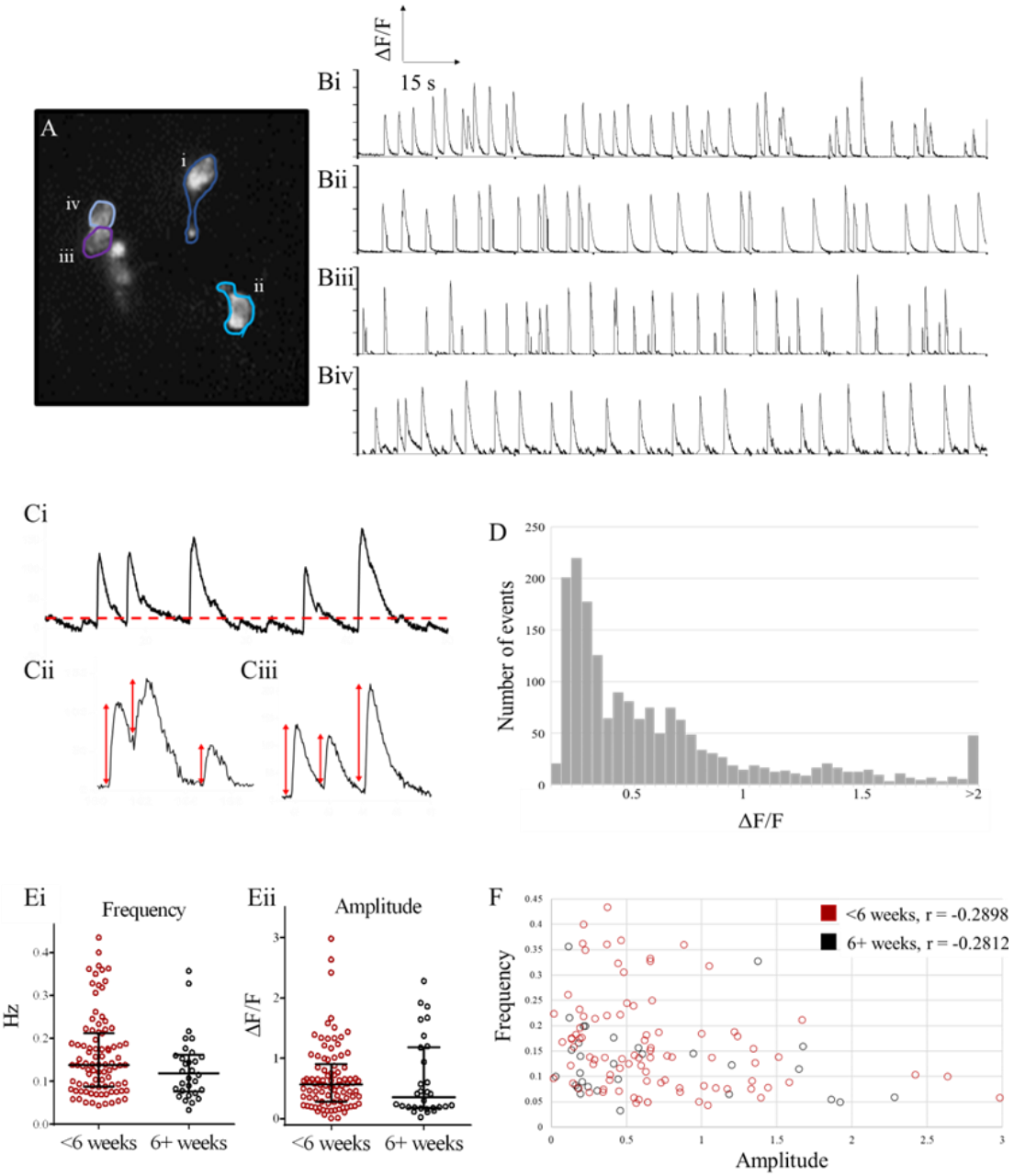

Figure 4.1: CSFcNs exhibit spontaneous Ca^{2+} spiking activity which is not significantly affected by the age of the animal.

A. Representative image of recorded CSFcNs, with (B) corresponding traces from each CSFcN.

C. Spikes were detected on the differentiated trace with an automatically detected threshold (**i**), red arrows indicate individual amplitude measurements (**ii – iii**).

D. Histogram of individual calcium event amplitudes from 1774 events over 120 CSFcNs (N = 19). Median amplitude was 0.675 ± 0.576 ΔF/F, Shapiro-Wilk normality test $p < 0.001$, indicating amplitudes are not normally distributed.

Ei. Median amplitude across 90 CSFcNs (N = 13) from juvenile mice aged 6 weeks or less was 0.681 ± 0.549 ΔF/F (median ± IQR), median amplitude across 30 CSFcNs (N = 6) from adult mice aged 6+ weeks was 0.655 ± 0.658 ΔF/F (median ± IQR). No significant difference between groups, two-tailed t-test. Shapiro-Wilk normality test $p < 0.001$, indicating amplitudes are not normally distributed for either group. **Eii.** Median frequency across 90 CSFcNs (N = 13) from juvenile mice aged 6 weeks or less was 0.162 ± 0.093 Hz (median ± IQR), median frequency across 30 CSFcNs (N = 6) from adult mice aged 6+ weeks was 0.132 ± 0.075 Hz (median ± IQR). No significant difference between groups, two-tailed t-test. Shapiro-Wilk normality test $p < 0.001$, indicating frequencies are not normally distributed for either group.

F. Correlation plot of median calcium event frequency vs median amplitude of event measured in individual CSFcNs, organised into juvenile or adult group. For <6 week group Spearman correlation, $r = -0.2898$, $p = 0.006$ and for 6+ weeks, Spearman correlation, $r = -0.2812$, $p = 0.132$, indicating a weak negative correlation between frequency and amplitude of events.

4.2.1.2 CSFcNs respond to Acetylcholine and GABA with changes in their Ca^{2+} spiking activity

Acetylcholine

After establishing the baseline spontaneous activity of CSFcNs, the possibility of influencing Ca^{2+} spiking activity through the application of acetylcholine (Ach), a common neurotransmitter in the CNS, was investigated. Using patch clamp electrophysiology Corns et al found that pressure ejection of Ach directly depolarised 100% of CSFcNs, although the extent of response varied between cells (Corns et al., 2015).

Overall, puff application of 10 mM Ach resulted in an immediate and significant increase in both the median amplitude of Ca^{2+} spikes (Figure 4.2, Bi, $p = 0.001$, spontaneous: 0.414 ± 0.351 ΔF/F versus ACh: 0.810 ± 0.599 ΔF/F), and the frequency of Ca^{2+} spiking (Figure 4.2, Bii, $p = 0.001$, spontaneous: 0.152 ± 0.091 Hz versus Ach: 0.489 ± 0.277 Hz).

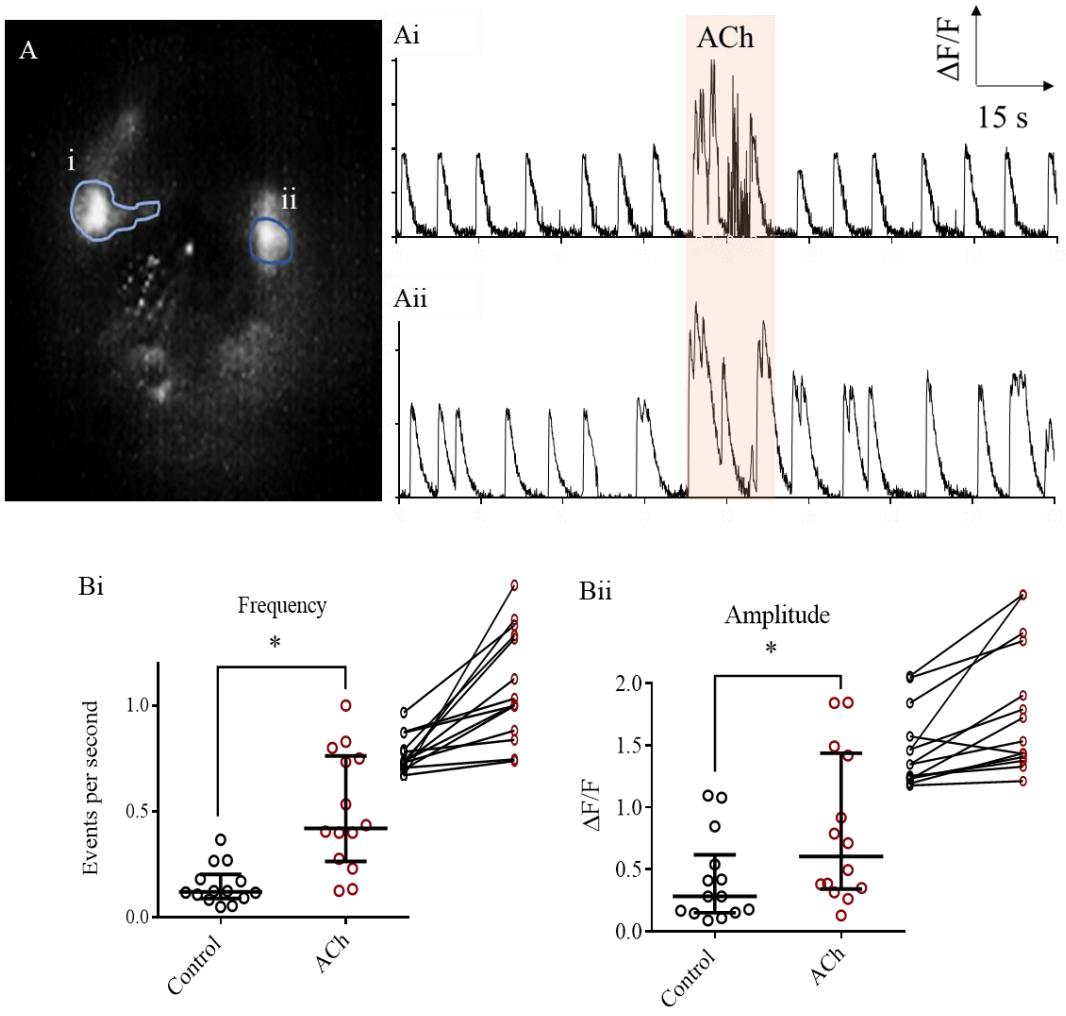

Figure 4.2: CSFcNs respond to acute application of ACh by increasing the frequency and amplitude of Ca^{2+} spiking.

A. Average projection representative image of recorded CSFcN, with corresponding traces of their Ca^{2+} spikes.

Bi. Median frequency of Ca^{2+} spikes in 14 CSFcNs (N=3) before and during 1mM ACh application, median frequency for spontaneous activity (Spon.) was 0.152 ± 0.091 Hz (median ± IQR), compared with 0.489 ± 0.277 Hz (median ± IQR), P = 0.0001 (two-sample non-parametric t-test, Wilcoxon matched-pairs). Inset shows matched responses from individual cells. **Bii**. Median amplitudes of spikes from 14 CSFcNs (N=3) before and during 1mM ACh application, median amplitude for spontaneous activity (Spon.) was 0.414 ± 0.351 ΔF/F (median ± IQR), compared with 0.810 ± 0.598 ΔF/F (median ± IQR), P = 0.0009 (two-sample non-parametric t-test, Wilcoxon matched-pairs). Inset shows matched responses from individual cells.

GABA

As mentioned in Chapter 1: general introduction (section 1.2.2), CSFcNs are predominantly GABAergic neurons that express various GABAergic markers, including GABA, VGAT, and both subtypes of GAD65/67 enzymes (Orts-Del'Immagine et al., 2014; Johnson et al., 2023). They have functional $GABA_A$ and $GABA_B$ receptors, suggesting the possibility of autoregulation through these receptors (Margeta-Mitrovic et al., 1999; Jurčić et al., 2019), and have previously been shown to respond to GABA application through either depolarisation or hyperpolarisation (Marichal et al., 2009; Corns, 2012). The effects of both immediate and prolonged GABA exposure on the Ca^{2+} spikes of CSFcNs were investigated to gain further insight into the response of these cells to this inhibitory neurotransmitter.

Notably, the response of CSFcNs to bath application of GABA appeared to correlate with the duration of exposure, with an increase in frequency of Ca^{2+} spikes from baseline particularly in approximately the first 45 seconds of drug exposure (Figure 4.3, Bi-iv and C). After this period, there was a decrease in frequency of Ca^{2+} spikes in most cells. This difference is also reflected in the significant change in frequency of Ca^{2+} spiking between these two periods (Figure 4.3, Di, Immediate GABA response: 0.201 ± 0.078 Hz vs GABA recirculation response: 0.075 ± 0.054 Hz, p = 0.001). For these reasons, although the exposure to GABA is continuous over the entirety of 3 minutes, the responses of CSFcNs have been characterised into the 'immediate' and 'recirculation' response for analytical purposes and to better reflect the changes seen in this time period (Figure 4.3, A, for timeline schematic).

Immediately upon bath application of GABA the amplitude of Ca^{2+} spikes did not significantly change (Figure 4.3, Dii, Immediate GABA response: 0.448 ± 0.341 ΔF/F vs spontaneous activity: 0.414 ± 0.335 ΔF/F, p = 0.594), however overall, the frequency of Ca^{2+} spiking significantly increased (Figure 4.3, Di, Immediate GABA response: 0.201 ± 0.078 Hz vs spontaneous activity: 0.147 ± 0.057 Hz, p = 0.026). There was however, a large degree of heterogeneity in the responses of individual CSFcNs to GABA application (Figure 4.3, Di inset) since GABA caused a decrease in frequency of Ca^{2+} spikes in approximately a third of CSFcNs and increased the frequency of Ca^{2+} spikes in the remaining CSFcNs.

During continuous exposure to GABA the frequency of these events significantly decreased when compared to the spontaneous activity levels (GABA recirculation response: 0.075 ± 0.054 Hz vs spontaneous activity: 0.148 ± 0.037 Hz, p = 0.001), but the median amplitude of

these events remained consistent (GABA recirculation response: 0.441 ± 0.315 ΔF/F vs spontaneous activity: 0.414 ± 0.335 ΔF/F, p = 0.891). After recirculation of GABA, standard aCSF was reintroduced to wash off any remaining GABA and allow a return of spontaneous activity. Upon removal of GABA, CSFcNs activity was not found to be significantly different from pre-application spontaneous activity in regard to the amplitude (Post GABA: 0.371 ± 0.328 ΔF/F, p = 0.487 vs spontaneous) or frequency (Post GABA: 0.148 ± 0.079 ΔF/F, p = 0.999 vs spontaneous) of Ca^{2+} spiking.

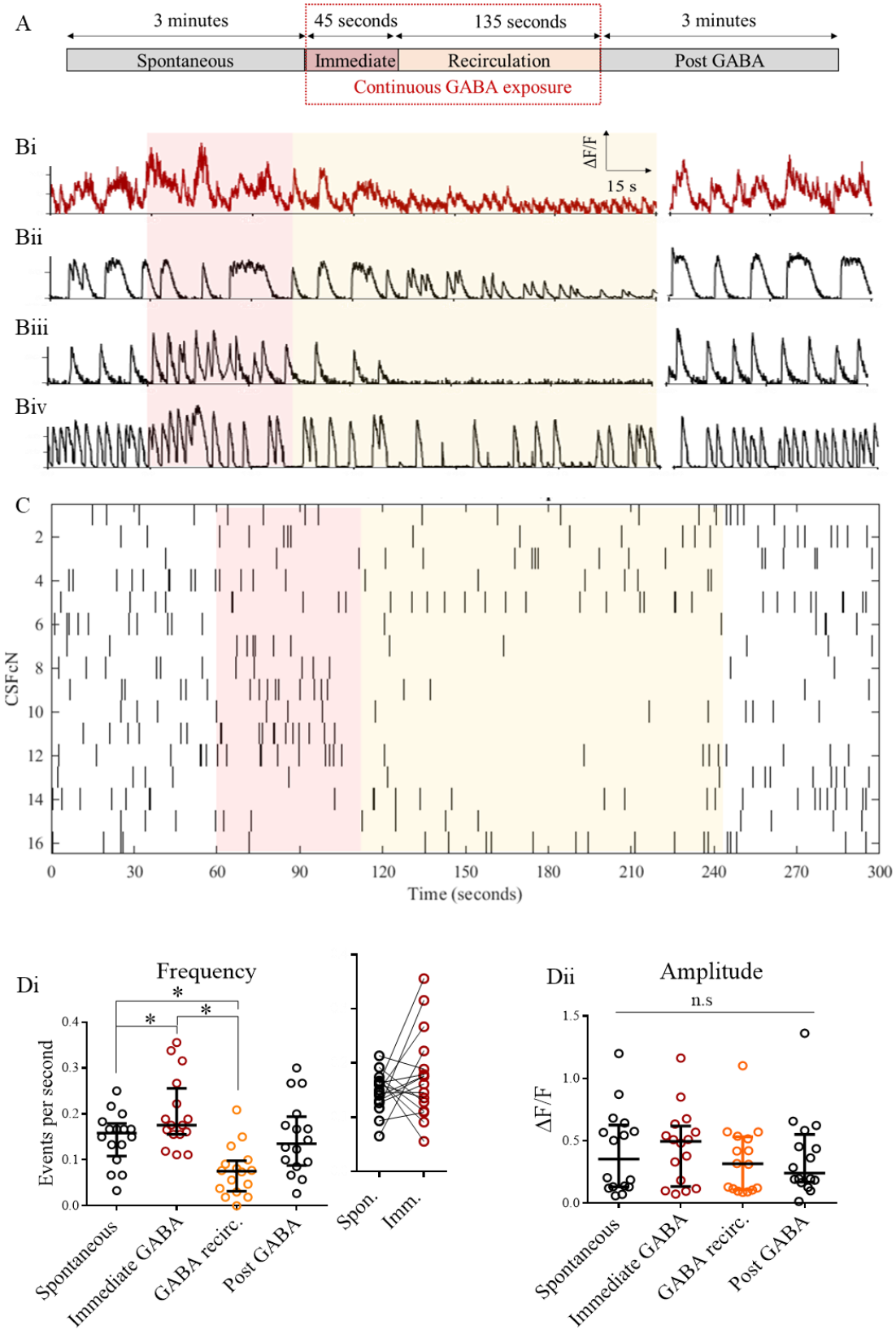
A
3 minutes
45 seconds
135 seconds
3 minutes
Spontaneous
Immediate
Recirculation
Post GABA
Continuous GABA exposure
Bi
Bii
Biii
Biv
ΔF/F
15 s
C
CSFcN
Time (seconds)
Di
Frequency
Events per second
Spontaneous
Immediate GABA
GABA recirc.
Post GABA
Spon.
Imm.
Dii
Amplitude
n.s
ΔF/F

Figure 4.3: CSFcNs respond to bath application of GABA through changes in their Ca^{2+} spiking activity

A. Schematic of experimental timeline.

Bi. Averaged trace from all CSFcNs. **Bii - iv**. Example traces from 3 CSFcNs.

C. Raster plot displaying all spikes across all 16 CSFcNs.

D. Median frequencies (**i**) and amplitudes (**ii**) of spikes from 16 CSFcNs (N=4) before, during, and after application of 100 μM GABA, shown on graph as median ± IQR with inset displaying matched responses from CSFcNs spontaneous activity to the immediate liraglutide response. Statistical analysis: One way ANOVA with Tukey's multiple comparison test against spontaneous activity, significance noted by * if $p < 0.05$.

4.2.2 CSFcNs exhibit a concentration dependent response to GLP-1R agonists through an increased frequency of low amplitude spikes

4.2.2.1 Response to GLP-1

As GLP-1 is the endogenous ligand for the GLP-1 receptor, the effect that this drug has on CSFcNs was examined. 1 μM GLP-1 was bath applied and recirculated for a total of three minutes to determine the immediate and longer-term effects of continuous exposure on CSFcN Ca^{2+} spiking activity.

Similar to the response seen during the bath application of GABA (Figure 4.3), there was a relationship between the response of CSFcNs and the duration of drug exposure. Changes in CSFcN activity were observed within approximately the first 45 seconds of exposure; the median frequency of Ca^{2+} spikes significantly increased (Figure 4.5, Cii, Spontaneous activity: 0.142 ± 0.045 Hz vs. Immediate GLP-1 response: 0.199 ± 0.089 Hz, $p = 0.007$, $n = 15$). However, this response was heterogenous, with approximately a quarter of CSFcNs decreasing their activity and approximately three quarters of CSFcNs increasing activity (Figure 4.5, Di inset). This response differs significantly from the remainder of the 3-minute exposure window (Figure 4.4, Immediate GLP-1 response: 0.199 ± 0.089 Hz vs GLP-1 recirculated response: 0.119 ± 0.043 Hz , $p = 0.011$).

During recirculation of GLP-1 the frequency of Ca^{2+} spiking was reduced compared to initial responses, but not significantly different from the baseline spontaneous activity (GLP-1 recirculated response: 0.119 ± 0.043 Hz, $p = 0.395$). However, upon returning to aCSF and washout of GLP-1, the frequency of Ca^{2+} spiking was significantly reduced compared with baseline spontaneous activity (Post GLP-1 response: 0.108 ± 0.047 Hz, $p = 0.036$), with the majority of CSFcNs exhibiting a decrease in Ca^{2+} spike frequency.

There were no significant differences seen in the amplitudes of CSFcN Ca^{2+} spikes throughout the experiments when compared with the spontaneous activity (Figure 4.5, Dii, Spontaneous activity: 0.484 ± 0.194 ΔF/F vs. Immediate GLP-1 response: 0.457 ± 0.294 ΔF/F, $p = 0.978$, GLP-1 recirculated response: 0.397 ± 0.242 ΔF/F, $p = 0.609$, and post GLP-1 response: 0.437 ± 0.193 ΔF/F, $p = 0.903$).

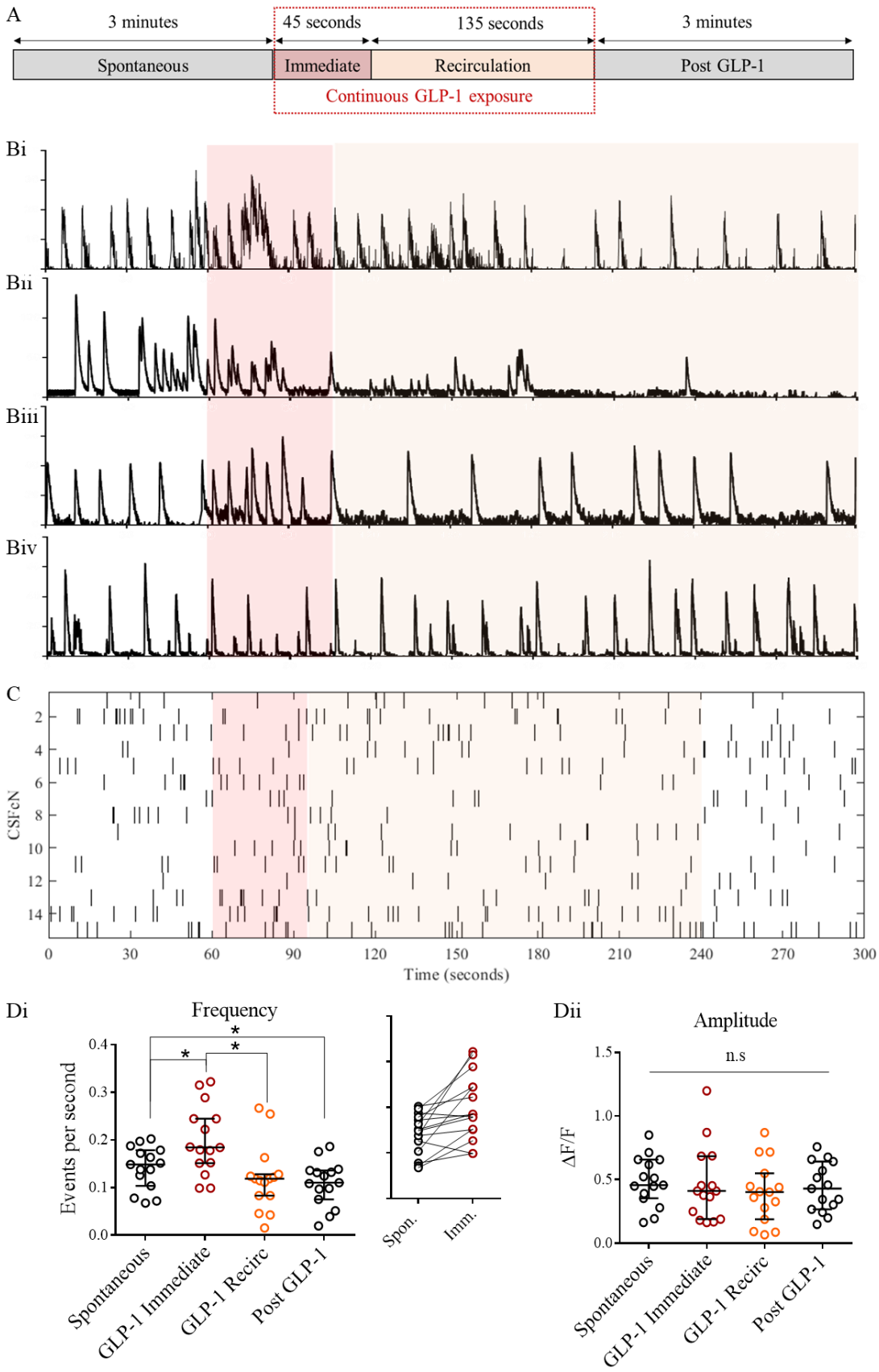
A
3 minutes
45 seconds
135 seconds
3 minutes
Spontaneous
Immediate
Recirculation
Post GLP-1
Continuous GLP-1 exposure
Bi
Bii
Biii
Biv
C
CSFeN
Time (seconds)
Di
Frequency
Events per second
Spontaneous
GLP-1 Immediate
GLP-1 Recirc
Post GLP-1
Spon.
Imm.
Dii
Amplitude
n.s
ΔF/F

Figure 4.4: CSFcNs respond to application of GLP-1 by increasing the frequency of their Ca^{2+} spiking

A. Schematic of experimental timeline.

Bi-iv. Representative traces from CSFcNs

C. Raster plot of spikes over time for all CSFcNs (n = 15, N = 4)

D. Amplitudes (**Di**) and frequencies (**Dii**) of Ca^{2+} spiking from all CSFcNs before, during, and after application of 1 μM GLP-1, shown on graph as median ± IQR. Inset showing matched responses from CSFcNs showing change in frequency of events from spontaneous activity to response induced by immediate GLP-1 application. Statistical analysis: One way ANOVA with Tukey's multiple comparison test against spontaneous activity, significance noted by * if $p < 0.05$.

4.2.2.2 CSFcNs respond to liraglutide

Liraglutide was chosen for the following experiments as it is a more potent and longer lasting analogue of GLP-1 (Knudsen, 2019) In this experiment, 1 μM liraglutide was bath applied and recirculated for a total of three minutes to determine the immediate and longer-term effects of continuous exposure on CSFcN Ca^{2+} spiking activity (Figure 4.5, A).

Over the time course of the experiment, CSFcNs exhibited a response to liraglutide similar to their response to GLP-1. Initially, within the first 45 seconds of exposure, there was a significant and rapid rise in the frequency of Ca^{2+} spikes compared to the pre-application control (Figure 4.5, Di, Spontaneous activity: 0.146 ± 0.095 Hz, Immediate liraglutide response: 0.246 ± 0.153 Hz, $p = 0.002$).

This response gradually diminished with prolonged exposure, but still remained significantly higher than the pre-application control (recirculated liraglutide response: 0.183 ± 0.125 Hz, $p = 0.001$ vs spontaneous, $p < 0.001$ vs immediate response.

Interestingly, although most CSFcNs responded through higher frequency of Ca^{2+} spikes, the responses of individual CSFcNs varied considerably with a small number of cells (approximately 15%) exhibiting fewer Ca^{2+} spikes and some remaining largely unchanged. A small proportion of CSFcNs (approximately 1 - 3% of all cells for each concentration) initially did not display any Ca^{2+} spikes but became active upon bath application of liraglutide (Figure 4.5, Cii).

Notably, following prolonged exposure and drug removal, the decline in CSFcN Ca^{2+} spikes was more pronounced than that observed with GLP-1 (Post GLP-1: 0.108 ± 0.047 Hz vs. Post liraglutide: 0.051 ± 0.072 Hz), with several CSFcNs losing all detectable Ca^{2+} spikes during this phase (this aspect is covered in sections 4.3.2.5 and 4.3.2.6).

Unlike GLP-1, liraglutide exposure significantly reduced the overall amplitude of Ca^{2+} spikes at all time points throughout the experiment when compared to the pre-application spontaneous activity (Figure 4.5, Dii, Spontaneous activity: 0.501 ± 0.492 ΔF/F vs immediate liraglutide response: 0.279 ± 0.326 ΔF/F, $p = 0.003$, recirculated liraglutide response: 0.251 ± 0.229 ΔF/F, $p = 0.002$, and post liraglutide: 0.088 ± 0.129 ΔF/F, $p = 0.001$). Examination of the distribution of amplitudes from individual CSFcN Ca^{2+} spiking revealed that upon immediate application of liraglutide there was a shift towards a higher number of lower amplitude events, unlike the pattern observed in the spontaneous control or upon recirculation of liraglutide, which may partially explain the overall lowering of amplitudes observed (Figure 4.5, E).

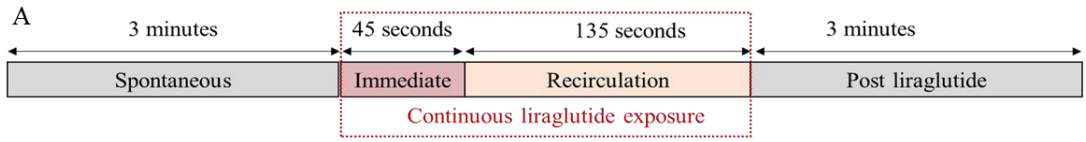
A
3 minutes
45 seconds
135 seconds
3 minutes
Spontaneous
Immediate
Recirculation
Post liraglutide
Continuous liraglutide exposure

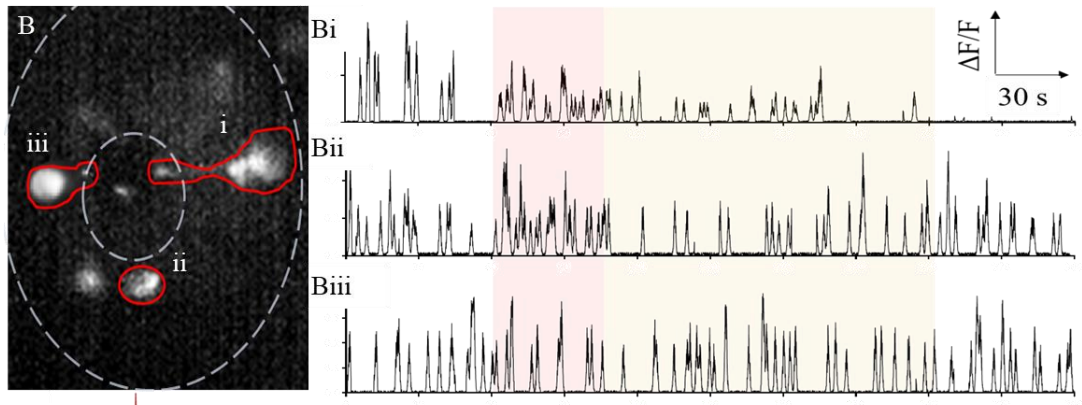
B
i
ii
iii
Bi
Bii
Biii
ΔF/F
30 s

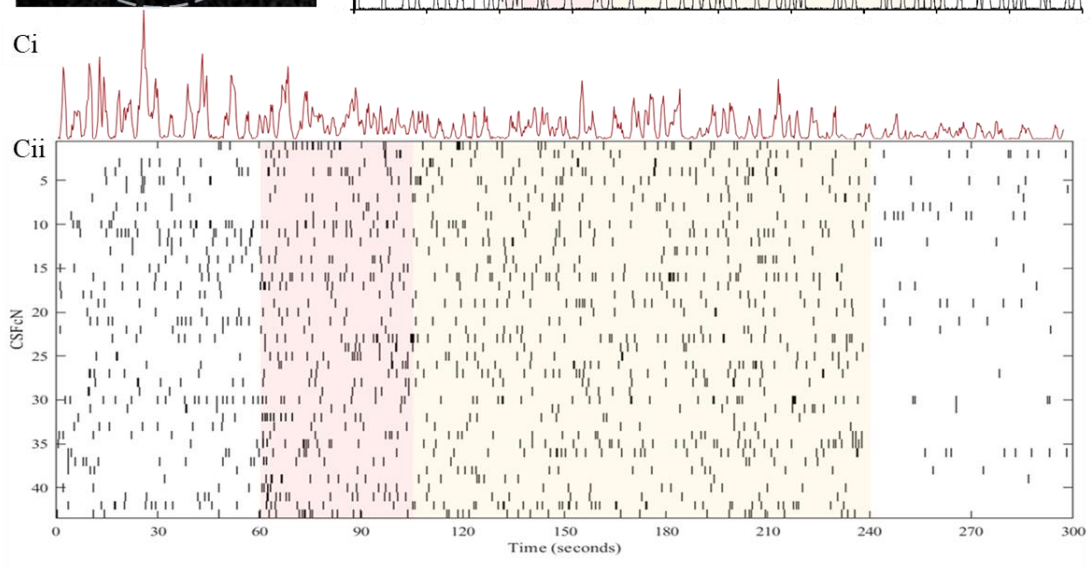
Ci
Cii
CSFeN
Time (seconds)

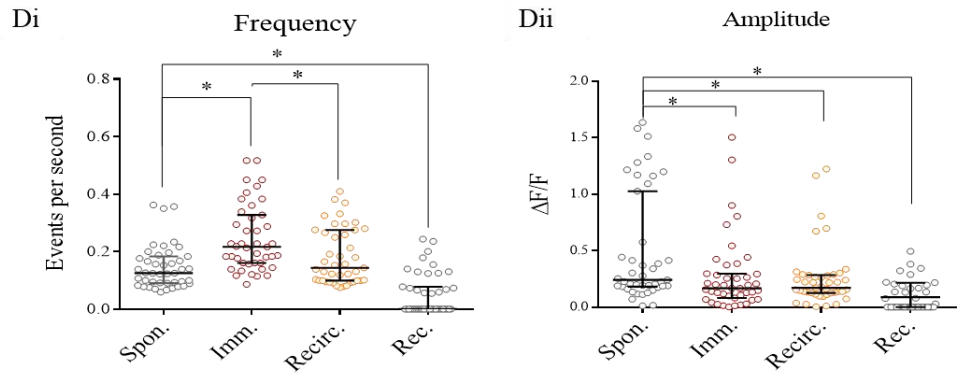
Di
Frequency
Events per second
Spon.
Imm.
Recirc.
Rec.

Dii
Amplitude
ΔF/F
Spon.
Imm.
Recirc.
Rec.

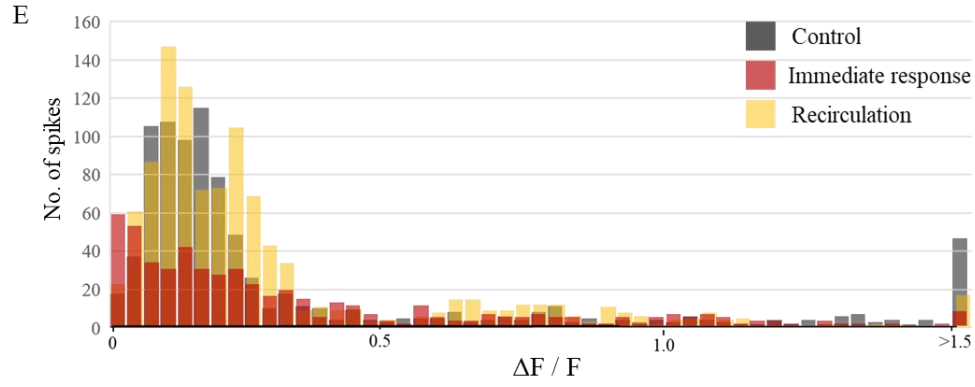
E
Control
Immediate response
Recirculation
No. of spikes
ΔF / F

Figure 4.5: CSFcNs respond to application of liraglutide through changes in their Ca^{2+} spiking activity

A. Schematic of experimental timeline.

B. Average projection representative image of CSFcN Ca^{2+} spiking activity, with corresponding traces.

Ci. Trace representing averaged Ca^{2+} spiking activity of all CSFcNs (n = 43, N = 6). **Cii**. Raster plot displaying frequency of all spikes with corresponding time points marked.

D. Frequencies (**i**) and amplitudes (**ii**) of Ca^{2+} spiking from 43 CSFcNs (N=6) before, during, and after application of 1 μM liraglutide, shown on graphs as median ± IQR. Statistical analysis: One way ANOVA with Tukey's multiple comparison test, significance noted by * if $p < 0.05$.

E. Histogram of individual spike amplitudes from all CSFcNs for spontaneous activity, during the immediate liraglutide response, and during the recirculation phase.

4.2.2.3 CSFcNs respond to liraglutide in a concentration dependent manner

To test whether this effect was concentration dependent, liraglutide was bath applied in a series of concentrations (1 nM – 1 μM) and each response was normalised to a recording of equal length of spontaneous CSFcN activity without liraglutide to account for any photobleaching effects and permit direct comparison of results.

In general, CSFcNs responded to application of liraglutide by increasing the frequency and decreasing the overall amplitude of Ca^{2+} spiking immediately (within the first 45 seconds of exposure) after application. During the recirculation phase, which is the remainder of the three-minute total exposure time, the amplitude of events remained consistent, but the frequency of events returned close to baseline spontaneous levels. After liraglutide was washed off by recirculation of standard aCSF both the median amplitude and frequency of Ca^{2+} spiking were reduced compared with the pre-application spontaneous activity control for each concentration (Figure 4.6).

The immediate effects of liraglutide on CSFcNs were not significant at 1nM and 10 nM concentrations when amplitude and frequency are compared with those of the time matched control, similar results are seen with the response to recirculation of liraglutide. However, for both concentrations there was a significant reduction in frequency and amplitude of events

after this prolonged exposure, deemed the post liraglutide phase (Median CSFcN response values and p-values for significance are detailed in Figure 4.6, Tables Ai and Bi).

At 100 nM and 1 μM concentrations of liraglutide the effects were more pronounced. Application of both concentrations significantly increased frequency and decreased median amplitudes of Ca^{2+} spikes compared with time matched controls, this decrease in amplitude remained significant at both the recirculation phase and after removal of liraglutide (Figure 4.6, Tables Ai and Bi for median CSFcN response values and p-values for significance).

For all concentrations, a number of CSFcNs at each concentration went completely silent after prolonged exposure to liraglutide, with no Ca^{2+} spiking activity detected within 3 minutes after liraglutide was removed (discussed further in sections 4.3.2.5 and 4.3.2.6).

A

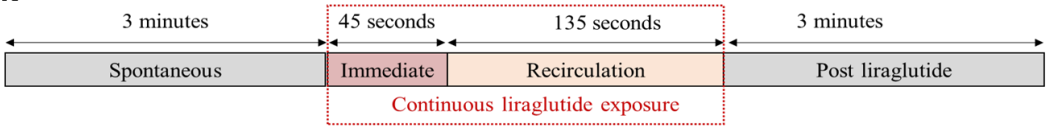

Bi

Frequency (Hz): median values ± IQR, significance and p-values (vs. control)

	Lira immediate	Lira recirculation	Post lira
Control	**0.155 ± 0.073**	**0.148 ± 0.057**	**0.149 ± 0.127**
1 nM	0.167 ± 0.084 (n.s)	0.150 ± 0.093 (n.s)	0.094 ± 0.092 * (0.022)
10 nM	0.209 ± 0.136 (n.s)	0.165 ± 0.109 (n.s)	0.092 ± 0.086 * (0.001)
100 nM	0.225 ± 0.097 * (0.001)	0.179 ± 0.092 (n.s)	0.077 ± 0.099 * (0.006)
1 µM	0.246 ± 0.153 * (0.001)	0.183 ± 0.125 (n.s)	0.051 ± 0.072 * (0.001)

Bii

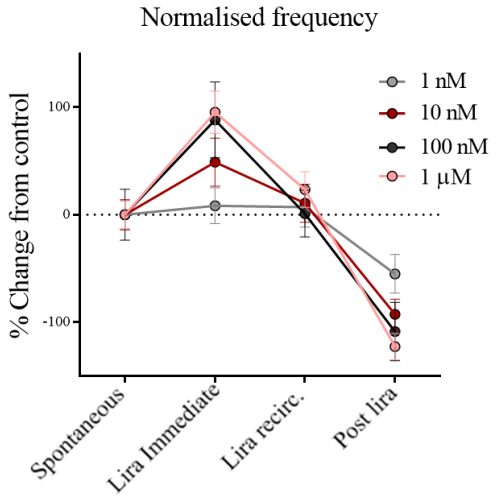

Ci

Amplitude (ΔF/F): median values ± IQR, significance and p-values (vs. control)

	Lira immediate	Lira recirculation	Post lira
Control	**0.453 ± 0.258**	**0.409 ± 0.484**	**0.388 ± 0.518**
1 nM	0.378 ± 0.276 (n.s)	0.383 ± 0.262 (n.s)	0.289 ± 0.307 * (0.007)
10 nM	0.342 ± 0.252 (n.s)	0.353 ± 0.247 (n.s)	0.248 ± 0.283 * (0.007)
100 nM	0.311 ± 0.279 * (0.007)	0.292 ± 0.254 * (0.012)	0.134 ± 0.172 * (0.001)
1 µM	0.279 ± 0.326 * (0.003)	0.251 ± 0.229 * (0.002)	0.088 ± 0.129 * (0.001)

Cii

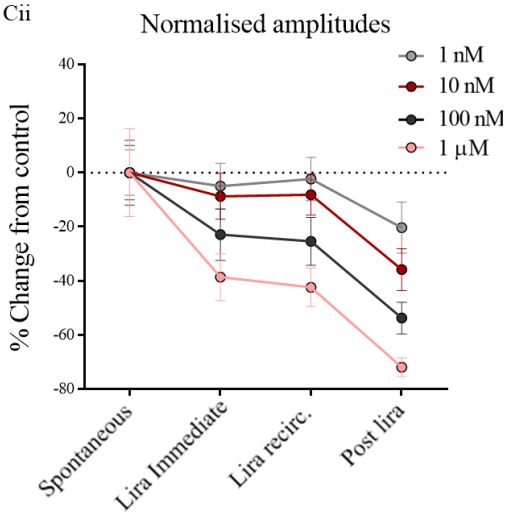

Figure 4.6: The response to liraglutide is concentration dependant

A. Schematic of experimental timeline.

Bi. Table showing the median frequency values ± IQR, significance, and p-values of Ca^{2+} spiking during immediate exposure to liraglutide, during recirculation, and post liraglutide exposure for the time matched control and all concentrations tested. 1 nM: N = 4 mice, 32 CSFcNs, 10 nM: N = 4 mice, 27 CSFcNs, 100 nM: N = 4 mice, 46 CSFcNs, 1 µM: N = 4 mice, 43 CSFcNs. Significance denoted by * with p-value given in brackets. Statistical analysis: individual one-way ANOVAs of each time point for all concentrations with Dunnett multiple comparison test vs. control. **Bii**. Normalised frequencies of CSFcNs at each time point for all concentrations used against time matched control (dashed line).

Ci. Table showing the median amplitude values ± IQR, significance, and p-values of Ca^{2+} spiking during immediate exposure to liraglutide, during recirculation, and post liraglutide exposure for the time matched control and all concentrations tested. 1 nM: N = 4 mice, 32 CSFcNs, 10 nM: N = 4 mice, 27 CSFcNs, 100 nM: N = 4 mice, 46 CSFcNs, 1 μM: N = 4 mice, 43 CSFcNs. Significance denoted by * with p-value given in brackets. Statistical analysis: individual one-way ANOVAs of each time point for all concentrations with Dunnett multiple comparison test vs. control. **Cii**. Normalised amplitudes of CSFcNs at each time point for all concentrations used against time matched control (dashed line).

4.2.2.4 Variability in individual CSFcN responses to immediate liraglutide application changes with the concentration of liraglutide

Similar to results seen previously within this chapter, the responses of individual CSFcNs varied considerably, with some increasing frequency of Ca^{2+} spiking in response to liraglutide, some decreasing frequency of Ca^{2+} spiking, and some remaining largely unchanged (Figure 4.7, Bi and Ci insets for matched individual cell responses). To better quantify the differences within the individual CSFcN responses, the percentage differences of each cell against their paired spontaneous activity were calculated. These responses were classified according to the percentage difference in Ca^{2+} spiking activity with cells exhibiting a decrease in Ca^{2+} spiking frequency (< -10% difference), no change (cells that exhibit less than ±10% change), and a robust increase (> 10% difference) in all conditions (Figure 4.7, Bii and Cii).

Increasing the concentration of liraglutide increased the percentage of cells responding with an increase in Ca^{2+} spiking frequency (1 nM: 53.1%, 10 nM: 58.7%, 100 nM: 72.1%, and 1 μM: 76.9%). Fewer cells did not appear to respond at the higher doses (1 nM: 26.3%, 10 nM: 15.2%, 100 nM: 18.6%, and 1 μM: 11.5%), while on the whole, the higher doses elicited decreased frequency of Ca^{2+} spikes in fewer cells compared to lower doses of liraglutide (1 nM: 20.6%, 10 nM: 26.1%, 100 nM: 9.3%, and 1 μM: 11.5%).

The opposite was found to be true with regards to the changes in amplitude, increasing the concentration of liraglutide resulted in more CSFcNs displaying an overall decrease in their median spike amplitudes (1 nM: 34.4%, 10 nM: 43.5%, 100 nM: 61.5%, and 1 μM: 65.1%). Again, a number of cells did not appear to respond strongly (1 nM: 50.0%, 10 nM: 43.5%, 100 nM: 26.9%, and 1 μM: 16.3%), and some increased spike amplitude (1 nM: 15.6%, 10 nM: 13.0%, 100 nM: 11.5%, and 1 μM: 18.6%).

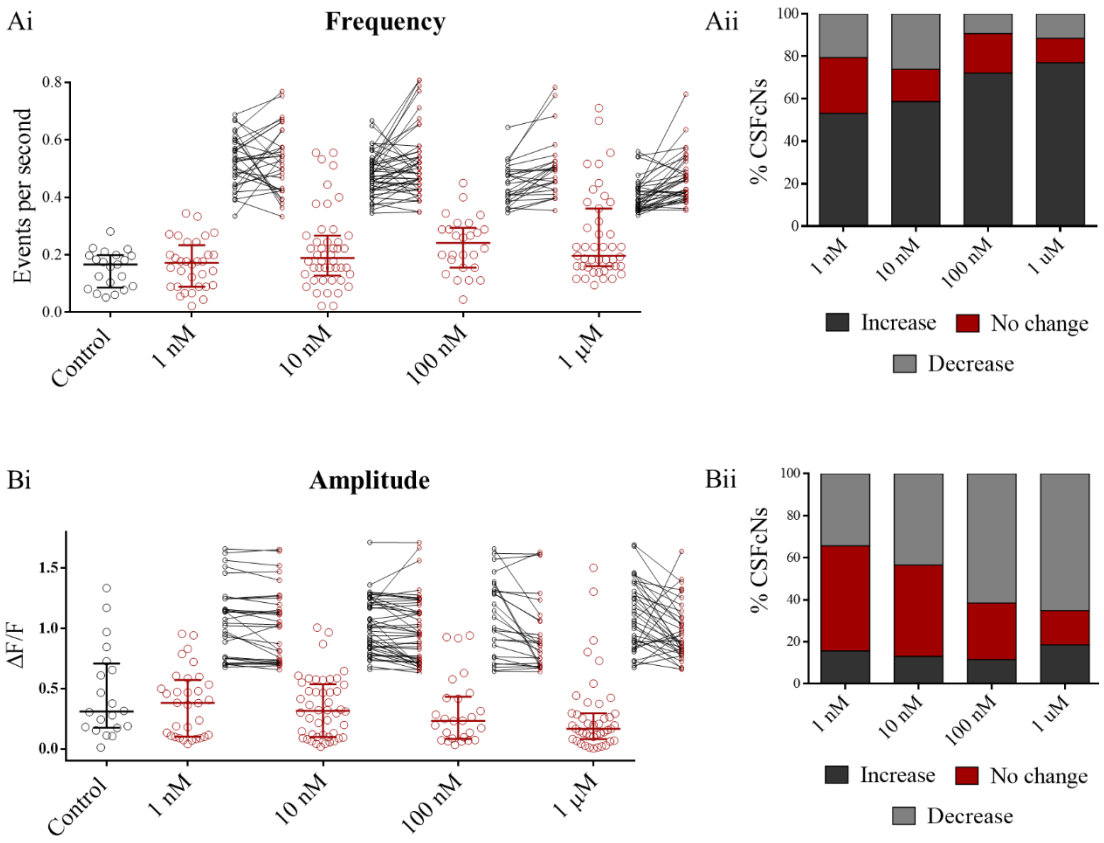

Figure 4.7: CSFcN response to immediate application of liraglutide is heterogenous

Ai. Frequencies of Ca^{2+} spiking per CSFcN upon immediate bath application of liraglutide for all concentrations, data shown as median ± IQR. Insets show matched responses from spontaneous activity (black circles) to immediate liraglutide response (red circles) for each CSFcN. **Aii**. Corresponding chart showing the percentage of CSFcNs displaying a decrease in frequency (< -10%), no change (-10% to 10%), and an increase in frequency (> 10%).

Bi. Amplitudes of spikes per CSFcN upon immediate bath application of liraglutide for all concentrations, data shown as median ± IQR. Insets show matched responses from spontaneous activity (black circles) to immediate liraglutide response (red circles) for each CSFcN. **Bii**. Corresponding chart showing the percentage of CSFcNs displaying a decrease in amplitude (< -10%), no change (-10% to 10%), and an increase in amplitude (> 10%).

4.2.2.5 CSFcN Ca^{2+} spiking activity is reduced after 3 minutes of continual exposure to liraglutide with some CSFcNs losing any detectable activity.

The responses of CSFcNs to prolonged application of liraglutide were found to be varied, with most, but not all, CSFcNs exhibiting both reduced amplitude and frequency of Ca^{2+} spiking (Figure 4.8). To gain further insight into the individual responses of CSFcNs, the percentage difference change in activity between the post-liraglutide response and the spontaneous activity for each cell was quantified as in section 4.3.2.4.

As the concentration of liraglutide increased, most CSFcNs exhibited lower frequencies of Ca^{2+} spiking in response to prolonged application (1 nM: 39.1%, 10 nM: 68.8%, 100 nM: 74.1%, and 1 μM: 88.3%), while fewer CSFcNs did not respond (1 nM: 38.9%, 10 nM: 13.3%, 100 nM: 6.7%, and 1 μM: 6.9%). The percentage responding with increased Ca^{2+} spike frequency varied considerably with the different concentrations (1 nM: 21.9%, 10 nM: 17.9%, 100 nM: 19.2%, and 1 μM: 4.7%) (Figure 4.8, Ci).

Similarly, at higher concentrations of liraglutide, a higher percentage of CSFcNs displayed smaller overall Ca^{2+} spike amplitudes (1 nM: 65.6%, 10 nM: 58.7%, 100 nM: 86.1%, and 1 μM: 88.9%), while fewer CSFcNs did not respond (1 nM: 21.9%, 10 nM: 8.7%, 100 nM: 2.4%, and 1 μM: 0.5%). Once again, the percentage responding with increased Ca^{2+} spike amplitude varied considerably with the different concentrations (1 nM: 12.5%, 10 nM: 32.6%, 100 nM: 11.5%, and 1 μM: 10.6%) (Figure 4.8, Cii).

After 3 minutes of liraglutide recirculation, many CSFcNs were observed to completely lose detectable Ca^{2+} spiking activity (1 nM: 31.3%, 10 nM: 36.9%, 100 nM: 42.3%, and 1 μM: 58.1%). This loss of activity was strongly correlated with an increasing concentration of liraglutide (Figure 4.8 D, R^2: 0.9209, $p = 0.05$).

To determine whether this silencing response was due to a change in the movement of the microscope objective along the z-axis during recordings, an average intensity projection from the first 3 minutes of the recording (Figure 4.8, Ei) was taken and compared with an average intensity projection from the last 3 minutes of the recording (Figure 4.8, Eii). In these images, the CSFcNs that display the most activity have stronger fluorescence compared with those with lesser activity. In Figure 4.8, Eii, one CSFcN is absent from the projection, corresponding to the CSFcN that has been completely silenced before the last 3 minutes of recording whereas two CSFcNs with reduced activity leading to silencing can be faintly observed. A CSFcN without any significant change in activity can be observed in both Ei and

Eii in the same location, indicating that the silencing effect is indeed due to the effects of liraglutide exposure and not movement of the lens along the z-axis. The same test was performed for all recordings taken (data not shown).

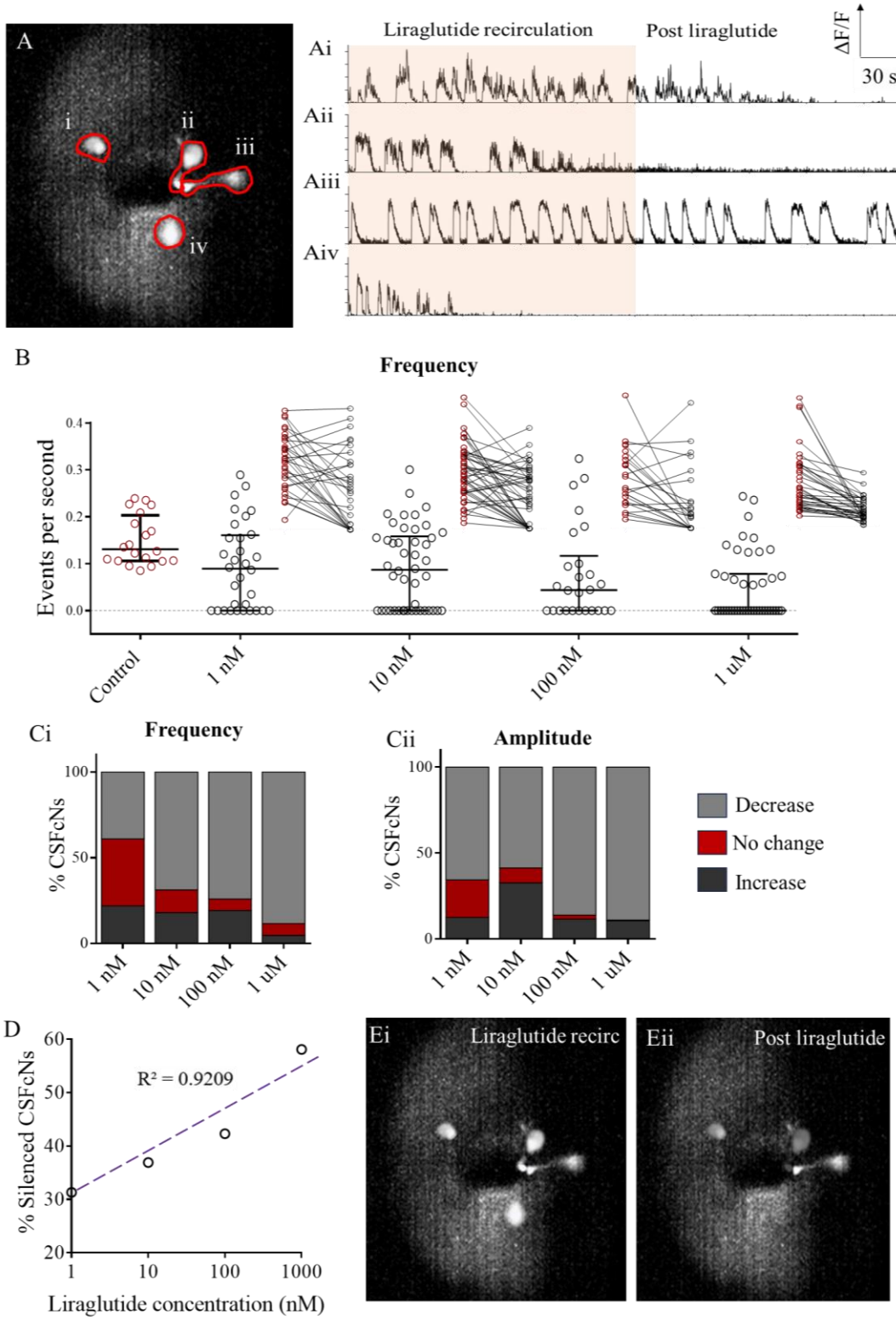

Figure 4.8: Prolonged exposure to liraglutide results in silencing of Ca^{2+} spiking activity in a subset of CSFcNs.

A. Representative traces showing changes in calcium activity after prolonged recirculation of 1 μM liraglutide.

B. Frequencies of Ca^{2+} spiking per CSFcN after 3 minutes of prolonged exposure to liraglutide, compared with time matched control (red circles). Insets show individual matched activity comparisons from spontaneous pre-application activity from each set of experiments (red circles) to post liraglutide response (black circles).
C. Corresponding chart showing the percentage of CSFcNs displaying a decrease (< -10%), no change (-10% to 10%), or an increase (> 10%) in frequency (**Ci**) or amplitude (**Cii**) of Ca^{2+} spiking.
D. Plot of the percentage of CSFcNs that lose all detectable Ca^{2+} spiking activity after prolonged liraglutide exposure. Statistical analysis: Pearson's correlation test, R^2: 0.9209, p = 0.05.
E. Average intensity projections from recordings for first 3 minutes of liraglutide exposure (**i**), and last three minutes of post-liraglutide recording (**ii**).

4.2.2.6 CSFcN Ca^{2+} spiking activity is returned to baseline spontaneous levels after 8 minutes of washing with aCSF

Since a significant number of CSFcNs became inactive after prolonged exposure to liraglutide (Figure 4.8), it was intriguing to examine whether this change was reversible. The primary focus was to determine if the spontaneous activity of CSFcNs would revert to its baseline level after a period of rest. The experimental timeline remained consistent with previous experiments, with the exception that after the 3-minute post liraglutide phase there was an additional 5 minutes of recirculating standard aCSF (Figure 4.9, A). This rest period was not recorded to reduce the potential risk of cells photobleaching to the point that Ca^{2+} spiking could not be detected. 1 μM liraglutide was used for this set of experiments as it exerts the greatest effect on CSFcNs.

After this rest period, the vast majority of CSFcNs (91.52%) had regained calcium signalling activity to the point of non-significant difference to their baseline spontaneous activity in terms of both the amplitude and frequency of Ca^{2+} spiking (Figure 4.9, Ci and Cii, Amplitude - spontaneous activity: 0.519 ± 0.607 ΔF/F vs recovery activity: 0.407 ± 0.303 ΔF/F, p = 0.626. Frequency - spontaneous activity: 0.153 ± 0.082 Hz vs recovery activity: 0.130 ± 0.064 Hz, p = 0.542). A small number of CSFcNs (9.52%) remained undetectable. It is possible that this recovery delay may be due to ongoing effects of signalling pathways downstream of the metabotropic GLP-1R, though ongoing washout cannot be excluded entirely. Further research is needed to fully evaluate whether this silencing is permanent or requires further rest time before baseline activity is restored.

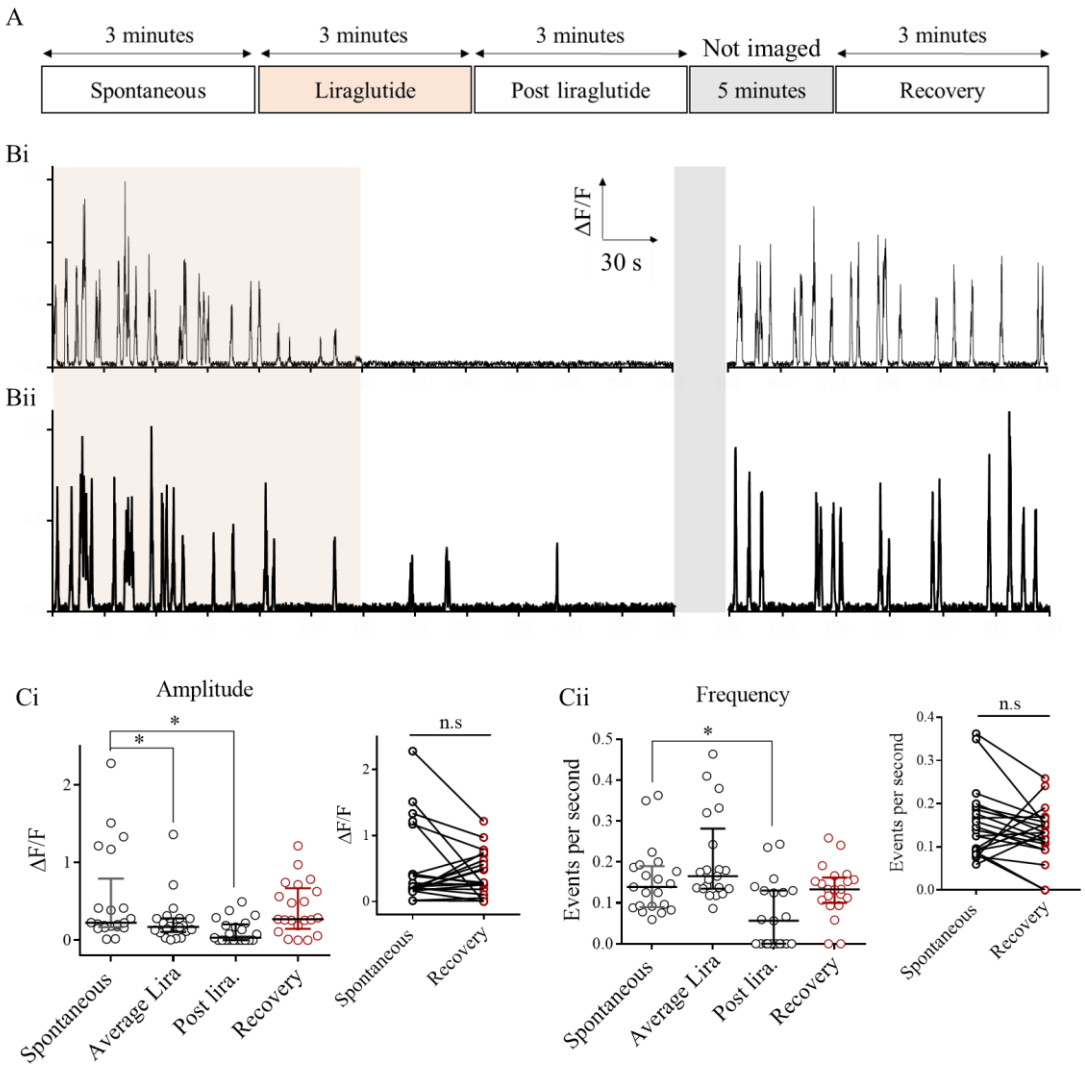

Figure 4.9: Ca^{2+} spiking activity returns in most CSFcNs after prolonged washing with aCSF

A. Schematic of experimental timeline

B. Representative traces of CSFcNs (i and ii) showing changes in Ca^{2+} spiking activity after prolonged recirculation of 1 µM liraglutide up until after recovery period.

Ci. Amplitudes from 21 CSFcNs (N=4) before during and after 1 µM liraglutide application, and during recovery phase, shown on graph as median ± IQR. Statistical analysis: One way ANOVA with Tukey's multiple comparison test, significance noted by * if $p < 0.05$. **Inset** Matched responses from individual cells showing change in amplitude of events from spontaneous activity to recovery phase after liraglutide application and a 5-minute rest.

Cii. Frequencies from 21 CSFcNs (N=4) before during and after 1 µM liraglutide application, and during recovery phase shown on graph as median ± IQR. Statistical analysis: One way ANOVA with Tukey's multiple comparison test, significance noted by * if $p < 0.05$. **Inset**. Matched responses from

individual cells showing change in frequency of events from spontaneous activity to recovery phase after liraglutide application and a 5-minute rest.

4.2.3 Changes in Ca^{2+} spiking evoked by liraglutide can be antagonised by preincubation with the antagonist exendin-(9-39)

4.2.3.1 Pre-incubation with antagonist, exendin-(9-39)

Exendin-(9-39) is a selective, competitive antagonist for the GLP-1 receptor (Schirra et al., 1998), pre-incubation with the antagonist should therefore should reduce the effect of liraglutide application on CSFcNs. Pre-incubation with exendin-(9-39) will also confirm whether the effects of liraglutide on CSFcNs are indeed due to stimulation of the GLP-1R.

No significant differences were observed in either the amplitude or frequency of Ca^{2+} spikes during application of the antagonist when compared with the baseline spontaneous activity, indicating that antagonising the GLP-1R has no effect alone (Figure 4.10, Bi and Ci Amplitude - spontaneous activity: 0.659 ± 0.677 ΔF/F vs antagonist response: 0.690 ± 0.651 ΔF/F, $p = 0.390$. Frequency - spontaneous activity: 0.146 ± 0.101 Hz vs antagonist response: 0.125 ± 0.076 Hz, $p = 0.212$).

No changes in the frequency of Ca^{2+} spiking were observed upon application of 1μM liraglutide (Figure 4.10, C, spontaneous activity: 0.146 ± 0.101 Hz vs immediate liraglutide response: 0.168 ± 0.186 Hz, $p = 0.872$), or upon recirculation (0.118 ± 0.079 Hz, $p = 0.258$), and no significant difference in amplitudes in either the immediate or recirculation response (Figure 4.10, B, spontaneous activity: 0.659 ± 0.677 ΔF/F, vs immediate response: 0.295 ± 0.786 ΔF/F, $p = 0.262$, and recirculation response: 0.437 ± 0.512 ΔF/F, $p = 0.095$). The lack of significance displays overall efficacy of the antagonist to block the GLP-1R.

There were also no significant differences upon removal of liraglutide (Figure 4.10 Bii and Cii, Amplitude – post liraglutide response: 0.412 ± 0.483 ΔF/F, $p = 0.055$, Frequency – post liraglutide response: 0.118 ± 0.110 Hz, $p = 0.743$), indicating that neither drug has a lasting effect on CSFcN activity.

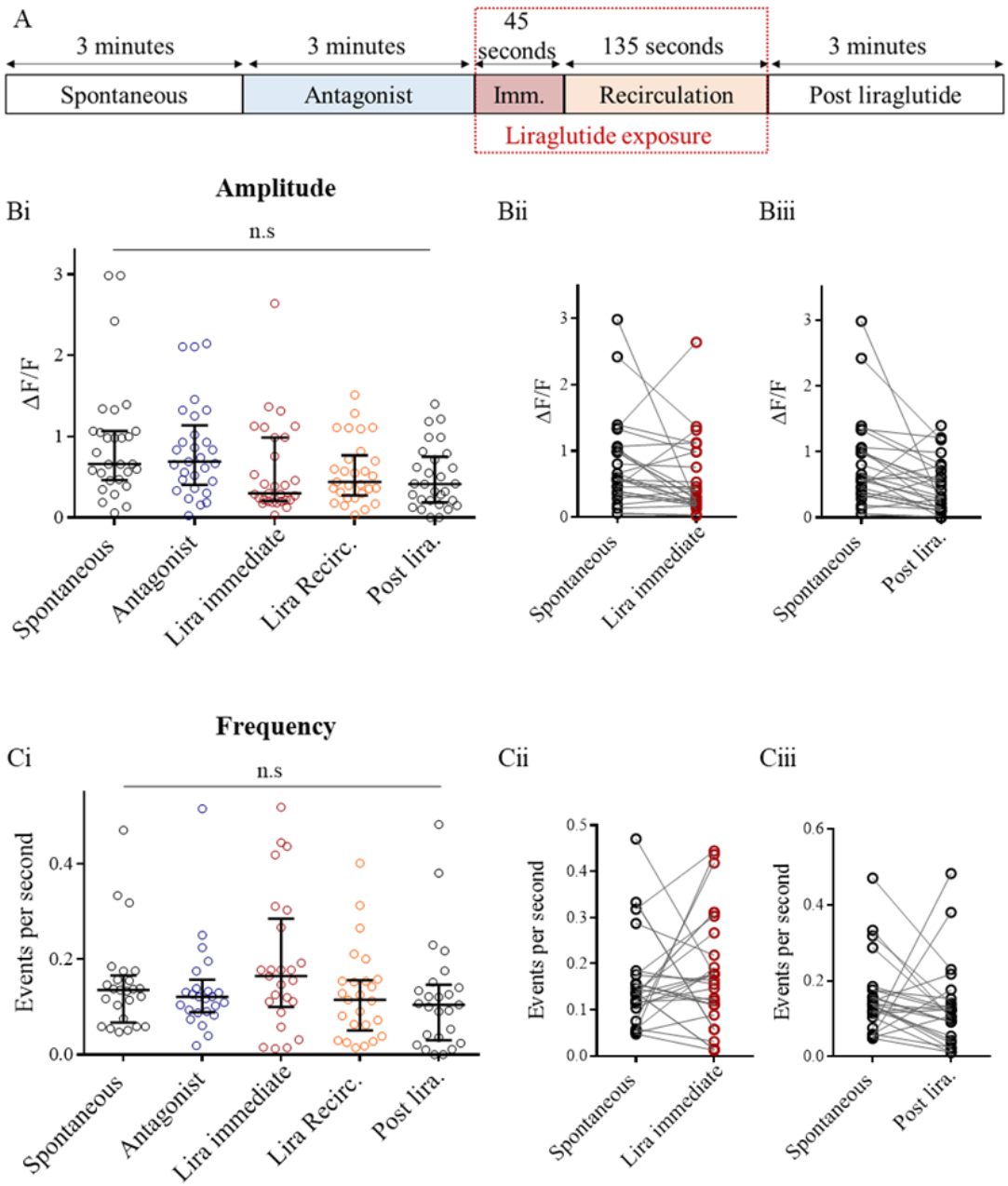

Figure 4.10: Pre-incubation of slices with a GLP-1R antagonist abolishes effects of liraglutide

A. Schematic of experimental timeline.

Bi. Amplitudes from 25 CSFcNs (N=4) before, during, and after pre-incubation with antagonist exendin-(9-39) and 1 μM liraglutide application, shown on graph as median ± IQR. Statistical analysis: One way ANOVA with Dunnett's multiple comparison test against spontaneous activity, no significance observed. **Bii**. Matched responses from individual cells showing change in amplitude of events from spontaneous activity to immediate liraglutide response. **Biii**. Matched responses showing change in amplitude of events from spontaneous activity to post liraglutide phase.

Ci. Frequencies from 25 CSFcNs (N=4) before, during, and after pre-incubation with antagonist exendin-(9-39) and 1 μM liraglutide application, shown on graph as median ± IQR. Statistical analysis: One way ANOVA with Dunnett's multiple comparison test against spontaneous activity, no significance observed. **Cii**. Matched responses from individual cells showing change in frequency of events from spontaneous activity to immediate liraglutide response. **Ciii**. Matched responses showing change in frequency of events from spontaneous activity to post liraglutide phase.

4.3 DISCUSSION

The research within this chapter investigates the spontaneous Ca^{2+} spiking activity within CSFcNs and explores alterations in this activity triggered by exposure to common neurotransmitters. Notably, this investigation offers the first evidence of the functional action of GLP-1 receptors within CSFcNs. This functional status is evidenced by the observable changes in Ca^{2+} spiking activity following the application of GLP-1 and liraglutide, a GLP-1R agonist.

Spontaneous Ca^{2+} spiking activity was observed in CSFcNs, which was not significantly affected by the age of the animal from which the slices were obtained, with the characteristics of these events varying among individual cells and most CSFcNs displaying a combination of high and low amplitude spikes. Furthermore, this research agrees with previous literature, confirming that both ACh and GABA can modulate the activity of CSFcNs (Corns et al., 2013; Johnson et al., 2023), with individual cells exhibiting diverse responses to these neurotransmitters further confirming the heterogeneity of CSFcNs as a population.

Next, the responses of CSFcNs to GLP-1 and liraglutide, at various concentrations, were examined to determine receptor functionality and sensitivity. Overall, stimulation of GLP-1R prompted an immediate increase in event frequency coupled with a decrease in overall amplitude. After extended exposure and subsequent washout, both frequency and amplitude of Ca^{2+} spiking diminished. Increasing liraglutide concentrations resulted in a greater percentage of CSFcNs displaying decreased event amplitudes and increased event frequencies and amplified the significance levels of these effects. Prolonged exposure to liraglutide also resulted in some CSFcNs losing all observable Ca^{2+} spiking activity. However, the majority of CSFcNs regained Ca^{2+} signalling activity after a rest period indicating that this inhibitory effect is reversible.

Pre-incubation experiments using the antagonist exendin-(9-39) revealed that the antagonist itself did not result in any changes in Ca^{2+} spiking activity, indicating that blocking the GLP-1 receptor does not affect the basal activity of CSFcNs. It is important to consider that this work was performed in an acute slice where descending input to CSFcNs has been severed and no endogenous CSF is present, and therefore may not fully represent an *in vivo* physiological situation. Furthermore, there were no significant changes in CSFcN Ca^{2+} spiking activity during or after the application of liraglutide. These findings imply that the

antagonist effectively blocked the effects of liraglutide, confirming that the observed effects of liraglutide on CSFcNs were indeed a result of stimulation of the GLP-1 receptor.

4.3.1 CSFcNs exhibit a variable and concentration dependent response to GLP-1R agonists

4.3.1.1 CSFcNs are a heterogenous population

In this study, regardless of which neurotransmitter was used, it is clear that CSFcNs, as a population, have a varied response to activation of different receptors. Many CSFcNs when stimulated by GLP-1 or liraglutide responded with a significant increase in the frequency of their Ca^{2+} spiking activity, while others responded with a decrease or indeed a complete reduction of activity altogether and therefore when considering the Ca^{2+} responses of CSFcNs it is important to note that CSFcNs are a heterogenous population.

Several studies have classified CSFcNs into at least two subtypes depending on their electrophysiological properties, location, and originating progenitor domains (Marichal., 2009; Corns et al., 2015; Petracca et al., 2016; Djenoune et al., 2017; Di Bella et al., 2019), and therefore it is likely that these subpopulations exhibit different Ca^{2+} responses to activation of GABAergic, cholinergic, or indeed GLP-1 receptors. It is also important to note that these subtypes are more likely to exist along a continuum of properties, instead of having definitive boundaries on what exactly a subype-1 vs subtype-2 CSFcN represents; occasionally CSFcNs were even observed to change a characteristic subtype response during the process of recording, further complicating matters (MacLean, 2016).

The variation in CSFcN responses observed within this chapter mirrors those previously observed in the literature. Cork et al found that hippocampal pyramidal cells exhibited heterogeneity in their response to GLP-1, with most cells exhibiting depolarisation and fewer exhibiting hyperpolarisation (Cork et al., 2015). Similarly, Williams et al investigated the effects of GLP-1 on neurons in the BNST, a population of neurons known to encompass three subtypes with distinct electrophysiological properties (Williams et al., 2018). They found that the cellular effects of GLP-1R modulation were both excitatory and inhibitory, but that this effect was not strongly correlated with cellular subtype, nor dorsal-ventral location of the individual cells (Williams et al., 2018). It is possible that the results seen in these studies, and those observed in CSFcNs are due to a combination of factors including the influence of

presynaptic transmission (discussed below in section 4.4.1.2), or in differences in expression of voltage gated K+ channels and Na+ channels in individual CSFcNs.

In the paper by Johnson et al, the influence of different Ca^{2+} channels on the amplitudes of spikes was investigated, which may be of some relevance here. They found that the generation of larger amplitude spikes was predominantly mediated by high voltage-activated Ca^{2+} channels and could be blocked by the application of Cd^{2+}. However, this did not completely eliminate Ca^{2+} spiking in these cells as smaller amplitude spikes remained and upon further investigation, these smaller amplitude spikes were found to be generated by T-type calcium channels. Interestingly, these different amplitude spikes were found to indicate input by different neurotransmitters, with CSFcNs responding to cholinergic input through high amplitude spikes and purinergic inputs generating smaller T-type channel dependant spikes. It is possible that the amplitude changes in CSFcNs in response to liraglutide are driven by similar recruitment of T-type calcium channels over high voltage-activated Ca^{2+} channels, favouring the generation of smaller amplitude spikes over larger amplitude spikes. This would require further investigation, suggestions for which are covered in chapter 6: general discussion (section 6.6.1).

It is also important to note the mouse model used in these experiments; the PKD2L1-GCaMP6f mouse. By using a model in which the fluorescent calcium indicator GCaMP6f is expressed in all CSFcNs, both the population of CSFcNs expressing the GLP-1R (approximately 80% as discussed in Chapter 3 of this thesis) and not expressing the GLP-1R are included in recordings. This is represented in the results by a number of CSFcNs that do not appear to show any remarkable differences in their activity when exposed to liraglutide, but still display spontaneous activity.

4.3.1.2 CSFcNs exist within a complex neuronal network

CSFcNs exist within a complex network of cells, receiving GABAergic (Barber et al., 1982; Orts-Del'immagine et al., 2012; Nakamura et al., 2023), glutamatergic (Marichal et al., 2009; Jurčić et al., 2019), and cholinergic innervation (Orts-Del'immagine et al., 2012; Corns et al., 2015), amongst others. Given that CSFcNs are not the only cells within the CNS that express the GLP-1R (Merchenthaler et al., 1999; Lein et al., 2007; Llewellyn-Smith et al., 2011, 2015; Cork et al., 2015; Russ et al., 2021), it is entirely possible that some of the responses

seen are at least partially mediated by presynaptic network effects with other cells responding to GLP-1R stimulation by releasing transmitters that modulate CSFcN activity.

The enhancement of presynaptic transmission by GLP-1R agonists has previously been observed in the literature (Acuna-Goycolea and van den Pol, 2004; Mietlicki-Baase et al., 2014; He et al., 2019). Acuna-Goycolea et al studied the effects of GLP-1 on LH hypocretin neurons and found that these neurons depolarised even when GLP-1 was delivered in the presence of TTX, indicating that this is a direct effect on hypocretin neuron GLP-1Rs. However, they also found that GLP-1 significantly increased the frequency of both EPSCs and IPSCs, effects that were abolished by the co-application of AMPA and NMDA or bicuculline receptor antagonists confirming the presynaptic influence (Acuna-Goycolea and van den Pol, 2004).

Similar results were observed in PVN neurons, except that responses to GLP-1 were more heterogenous with the majority of cells depolarising, and a smaller number hyperpolarising (Acuna-Goycolea and van den Pol, 2004; Cork et al., 2015). Interestingly, when synaptic activity was blocked through application of TTX only the excitatory effects of GLP-1 were observed (Acuna-Goycolea and van den Pol, 2004). This indicates that the heterogeneous effects of GLP-1 are partially mediated by presynaptic glutamate or GABA release onto the postsynaptic neurons from local excitatory and inhibitory neurons (Li et al., 2002; Acuna-Goycolea and van den Pol, 2004). Similar presynaptic effects were also observed in the hippocampus (Oka et al., 1999), ARC (Secher et al., 2014; He et al., 2019), BNST (Ong et al., 2017; Williams et al., 2018), and NAc (Mietlicki-Baase et al., 2014).

Given that CSFcNs are known to have both functional glutamatergic and GABAergic receptors (Marichal et al., 2009; Orts-Del'immagine et al., 2012; Corns et al., 2013; Gotts et al., 2016; Jurčić et al., 2019), and receive appositions from these neurons (Kaneko et al., 2002; Gotts et al., 2016; Nakamura et al., 2023), it is not inconceivable to think that similar mechanisms could be responsible for some of the heterogeneity observed in CSFcN response, especially when considering the presence of GLP-1Rs in other neurons within the spinal cord (See chapter 3, section 3.3.2.1, Merchenthaler et al., 1999; Russ et al., 2021).

Additionally, due to the experimental set up, the acute slices used in this investigation were chosen from the thoracolumbar regions of the spinal cord. As established in Chapter 3 (results section 3.3.3) and in previous work within the Deuchars lab (Mortimer, unpublished MRes thesis, 2022), CSFcNs receive significantly higher numbers of appositions to their somata

from PPG neurons in the thoracic region compared with the lumbar region. It is possible that the expression of the GLP-1 receptor on the somata of CSFcNs shows a similar variation, although this was not observed in immunohistochemical studies in this thesis (chapter 3, section 3.3.2). As an increased number of receptors on one cell would generate an increase in the intensity of the response upon stimulation (Marzvanyan and Alhawaj, 2023), it may be that some of the heterogeneity in response is due to the differing expression levels of the receptor on individual cells. As sections from both the thoracic and lumbar regions were used, it is difficult to decipher the region dependant effect of GLP-1R stimulation. Further work would be required in order to test this hypothesis and measure the cell specific expression of the receptor and how this correlates with activity in each spinal cord region.

4.3.2 Inactivation of CSFcNs by prolonged liraglutide exposure

Perhaps the most interesting result gained from this set of experiments is the observed silencing of a number of CSFcNs after prolonged exposure to liraglutide and stimulation of the GLP-1R. At first, it was assumed that this response was perhaps due to the movement of the camera lens along the z-axis during recording, but as determined by average intensity projections of time points throughout the experiments no movement could be perceived. Additionally, within an individual slice there could often be observed a combination of cells some of which were silenced, while some were not, indicating that this is likely to be more of a subtype or exposure limit response.

In this chapter, the effects of GABA on CSFcNs were also explored and it was found that many CSFcNs responded to bath application of GABA through a decrease in Ca^{2+} event frequency with prolonged exposure. As mentioned above (section 4.4.1.2), GLP-1 is thought to increase presynaptic transmission of GABA from local inhibitory neurons that act upon the postsynaptic neuron (Acuna-Goycolea and van den Pol, 2004; Ong et al., 2017), and therefore it is possible that some of the silencing effects of CSFcNs after prolonged exposure to liraglutide may be due to presynaptic GLP-1R stimulation that triggers GABA release from other inhibitory GABAergic neurons.

It may also be possible that this response is a form of regulation by other CSFcNs; Nakamura et al show that CSFcNs extend processes from one cell that target more rostral CSFcNs and CSFcNs are known to possess machinery related to GABA synthesis and release, such as

GAD65/67 and VGAT (Gotts et al., 2016; Djenoune et al., 2014; Fidelin et al., 2015; Johnson et al., 2023; Nakamura et al., 2023). It is possible that stimulation of the GLP-1R on CSFcNs results in the release of GABA from these cells onto neighbouring CSFcNs inhibiting any further response to continued stimulus. Further experiments involving the co-application of liraglutide with a GABA antagonist would yield further information regarding this hypothesis.

The GLP-1R is a GPCR, and as such it is possible that this silencing effect may be due to stimulation of the receptor and generating of downstream second messenger molecules which regulates further cellular activity. While GLP-1R is classically thought to couple to the $G\alpha_s$ stimulatory G-protein subunit, there is evidence that they may also pleiotropically couple with $G\alpha_i$ and α_o inhibitory subunits (Montrose-Rafizadeh et al., 1999; Hällbrink et al., 2001; Weston et al., 2014; Deganutti et al., 2022). As $G\alpha_i$ and α_o subunits both inhibit adenylyl cyclase, which reduces the production of cAMP and subsequently suppresses Ca^{2+} channel activity, reducing Ca^{2+} influx and activity within the neuron (Gao and van den Pol, 2001; Currie, 2010). Similarly, activity by the G-protein $\beta\gamma$ subunits may also contribute to the suppression of Ca^{2+} spiking activity by directly inhibiting voltage-gated Ca^{2+}channels (Herlitze et al., 1996; Ikeda, 1996; Currie, 2010).

The strength of this effect on CSFcNs was also closely correlated with the increase in liraglutide concentration and may very well represent a form of adaption or desensitisation to a stimulus as seen in many other neuronal systems (Webster, 2012; Whitmire and Stanley, 2016). If CSFcNs are indeed monitors of CSF composition or have a number of different functions depending on input (Fidelin et al., 2015; Sternberg et al., 2018; Johnson et al., 2023; Nakamura et al., 2023. Also see Chapter 1: General introduction section 1.2.3 for discussion of CSFcNs functional roles), it seems likely that they would need to adapt to prolonged exposure to one particular compound in order to maintain the ability to react to other changes.

4.3.3 Antagonism by exendin-(9-39) confirms that the effects are mediated through activation of GLP-1Rs

Within this chapter, the actions of liraglutide on CSFcNs were verified though pre-incubation of the slices with the antagonist, exendin-(9-39). Exendin-(9-39) is known to be a high

affinity, orthosteric, competitive antagonist (Schirra et al., 1998; Donnelly, 2012a; Gasbjerg et al., 2021), with similar affinity to the GLP-1R as exendin-4 and liraglutide; approximately 1 – 3 nM (Thorens et al., 1993; Montrose-Rafizadeh et al., 1997; Donnelly, 2012b; Lau et al., 2015; Knudsen, 2019). Pre-incubation of slices with exendin-(9-39) suppressed the excitatory effects of liraglutide in a number of CSFcNs. This effect was as expected, as exendin-(9-39) has been shown to selectively antagonise the effects of GLP-1R agonists in several studies (Acuna-Goycolea and van den Pol, 2004; Richard et al., 2014; Gullo et al., 2017). However, further work is required to evaluate whether this effect is due to direct antagonism of GLP-1Rs on CSFcNs or a mechanism mediated through indirect antagonism of other GLP-1R expressing cells.

However, as the drugs were not co-applied, the antagonist was assumed to have washed off during application of liraglutide. Therefore, it is unusual that the effect of liraglutide was entirely absent and not just delayed. One possible explanation for this may be that the antagonist remained present within the aCSF for longer than expected, therefore exerting competitive inhibition for the GLP-1R and preventing full binding, and subsequently full effect, of liraglutide. Further research would be needed in order to fully investigate the length of time that the antagonist exerts influence on the GLP-1R and the effects of co-application with liraglutide.

4.3.4 Conclusion

In this chapter, the changes in intracellular Ca^{2+} concentrations of CSFcNs have been characterised, along with the responses of CSFcNs to differing concentrations of GLP-1R agonists. It has been found that CSFcNs are capable of responding to stimulation of the GLP-1R through changes in their intracellular Ca^{2+} concentrations activity, effects that are blocked by pre-incubation with the antagonist. This is the first study to show that CSFcNs are capable of responding to exogenous bath application of GLP-1R agonists, however further work is needed to fully determine whether these effects are due to direct stimulation of the GLP-1R. This chapter has contributed novel evidence towards the short-term actions of liraglutide on cells within the spinal cord, which will be further explored in the subsequent chapter.

Chapter 5 - Effects of GLP-1R agonists on spinal cell proliferation *ex vivo* and *in vivo*

5.1 INTRODUCTION

5.1.1 The ependymal layer as a source of quiescent stem cells

Neurogenesis within the mammalian CNS occurs at several sites, including the dentate gyrus of the hippocampus (Abbott and Nigussie, 2020), the subventricular zone (SVZ) which borders the lateral ventricles (Alvarez-Buylla and García-Verdugo, 2002), and the ependymal layer within the central canal area of the spinal cord (Mothe and Tator, 2005). These areas commonly share direct access to the CSF which provides a wealth and complexity of signalling molecules, several of which are known to regulate the quiescence or activity of the neural stem cells that they contain (Lehtinen and Walsh, 2011; Massirer et al., 2011).

There is limited proliferation of ECs in the intact spinal cord, most of which is restricted to self-renewal and thought to be involved in the maintenance of the barrier between the CSF and the parenchyma (Jiménez et al., 2014). This has been evidenced through long-term studies where BrdU, a thymidine analogue which is incorporated into the DNA of proliferating cells, was administrated in the drinking water of mice and rats. In these studies, ependymal cells showed limited proliferation, with the majority of proliferated cells found in pairs indicative of symmetrical division and duplication (Johansson et al., 1999; Meletis et al., 2008). Although these cells remain quiescent during homeostatic conditions, they can proliferate rapidly in response to injury of the spinal cord (See Chapter 1: General introduction, section 1.1.3, Moore, 2016; Stenudd et al., 2022).

Several studies have shown that it is possible to influence ependymal cell proliferation *in vivo* in the intact spinal cord (Corns et al., 2015). New et al found that heterozygous GAD67-GFP transgenic mice had a haplodeficiency in the GAD67 gene which resulted in approximately 65-70% less GABA in the brain and spinal cord compared with wild-type mice when measured with HPLC (New et al., 2023). Compared to wild-type controls, EdU injections in GAD67-GFP mice revealed a 3.8-fold higher number in the total of proliferated cells and an 11-fold higher number of newly proliferated cells around the central canal. (New et al., 2023). To further test the effects of GABA modulation on proliferation within the CNS, animals treated with vigabatrin, a GABA transaminase inhibitor to increase GABA concentrations in the brain, had 62% fewer EdU positive cells within the ependymal layer compared to saline treated control, indicating that GABAergic signalling can modulate ependymal cell proliferation (New et al., 2023).

It is possible that latent proliferative potential exists within the spinal cord, which, under the appropriate set of conditions or pharmacological influence, could modulate regeneration. Since proliferation is not always beneficial, as seen in cases of pathological ependymal cell overgrowth leading to the formation of cancerous ependymomas, it is essential to further understand contributing factors that maintain the quiescence of proliferative cells within the CNS. Limited understanding exists regarding pharmacological factors that can influence endogenous proliferation in the spinal cord. Further knowledge in this area could lead to better therapeutic interventions for spinal cord injuries, CNS cancers, and other neurodegenerative conditions that have previously lacked adequate treatments.

5.1.2 Proliferative effects of GLP-1R agonists

The neuroprotective and proliferative effects of GLP-1R agonists have been studied thoroughly in pancreatic cells, and to a more limited degree, within the brain and spinal cord. Much of this research is covered in depth in Chapter 1: Introduction (Section 1.3.4).

Taken together, these studies indicate a potential role for GLP-1R agonists in the treatment of spinal cord injury and other neurodegenerative conditions. While the proliferative effects of GLP-1 modulators have been investigated in the hippocampus, the effects on proliferation within the spinal cord are currently unknown. This chapter will focus predominantly on the immediate and longer-term effects of GLP-1R agonists exendin-4 and liraglutide, as well as antagonist exendin-(9-39) on the proliferation of cells within the central canal area of the spinal cord using *ex vivo* techniques such as acute slices and organotypic spinal cord slice cultures (OSCSCs), as well as *in vivo* mouse models.

5.1.3 Hydrogels as drug delivery systems

Many strategies in the treatment of CNS injuries and spinal cord repair, particularly in the fields of biomaterials and tissue engineering, have focused on the use of hydrogels as deliverers of therapeutic agents (for comprehensive reviews see Macaya and Spector, 2012 and Vigata et al., 2020). Hydrogels, characterized by their three-dimensional structure and composed of hydrophilic polymers of natural, synthetic, or semi-synthetic origin, exhibit a wide range of polymer compositions. This diversity allows precise control over the

biocompatibility, biodegradability, and physical attributes of these hydrogel matrices; rendering them tunable to a specific environment, such as the soft tissue of the CNS (Bartlett et al., 2016). Additionally, the porous nature of these hydrogels enables the encapsulation of drugs, proteins, and other small molecules, endowing them with drug delivery functionality. This capacity allows hydrogels to transport pharmacological agents or growth factors directly to targeted regions, thereby aiming to enhance cell survival, proliferation, and migration, ultimately fostering efficient treatment for spinal cord injuries.

Within this chapter, a range of hydrogels of varying compositions and mechanical properties will be examined to assess their impact on cell proliferation within OSCSCs. Furthermore, the combination of these hydrogels with liraglutide will be explored to evaluate the effects of a hydrogel delivery system that enables sustained release of liraglutide on cell proliferation. The findings from this study will contribute valuable insights to the field of GLP-1-based regenerative strategies, enhancing understanding of how hydrogel properties and liraglutide delivery systems can influence cell proliferation in OSCSCs.

5.1.4 Hypothesis and aims

Given that GLP-1R agonists are known to increase the proliferation of cells within the hippocampus and have been shown to increase functional recovery in cases of spinal cord injury, it is hypothesised that administration of GLP-1R agonists will increase proliferation of cells within the central canal of the spinal cord.

The aims of this chapter are to:

- Elucidate whether there are any immediate effects of GLP-1R modulation on cell proliferation using an acute spinal cord slice model.
- Determine whether GLP-1R agonists affect the level of cell survival and proliferation within the central canal area when studied over 5 or 10 days in OSCSCs.
- Investigate the potential enhancement of cell proliferation in organotypic spinal cord slice cultures by combining liraglutide with a hydrogel delivery system.
- Investigate the changes in proliferation and differentiation of spinal cord cells in two *in vivo* mouse experiments treated with either exendin-4 or liraglutide, and compare with the effects of these drugs on proliferation within the dentate gyrus of the hippocampus.

5.2.1 Modulation of the GLP-1R affects proliferation within the central canal in short term acute spinal cord slices

In this experiment, spinal cord slices were incubated with 1 μM EdU and either GLP-1R agonist liraglutide, or GLP-1R antagonist exendin-(9-39) immediately after cutting to determine the effects of acute modulation of the GLP-1R on cell proliferation. These drugs were given at three different concentrations and slices were incubated for 5 hours in warmed aCSF (Figure 5.1).

At lower concentrations of liraglutide no significant differences could be observed in the number of EdU positive cells within the central canal (10nM liraglutide: 3.7 ± 0.5, p = 0.723 and 100nM liraglutide: 4.1 ± 0.9, p = 0.372 vs control: 3.1 ± 0.7), or the rest of the slice, when compared with controls (10nM liraglutide: 14.1 ± 0.9, p = 0.333 and 100nM liraglutide: 14.8 ± 2.1, p = 0.675 vs control: 16.3 ± 2.9).

Application of 1 μM liraglutide resulted in a significantly higher number of EdU labelled cells within the central canal (p = 0.046, 4.7 ± 0.7) when compared with the control (3.1 ± 0.7). However, no significant differences could be observed in the number of EdU labelled cells outside of the central canal area (1μM liraglutide: 15.9 ± 1.9, p = 0.996 vs control: 16.3 ± 2.9).

Application of the antagonist exendin-(9-39) did not result in any significant differences in the number of EdU labelled cells observed in either the central canal area (10nM antagonist: 3.1 ± 1.2, p = 0.999, 100nM antagonist: 2.5 ± 0.8, p = 0.821 and 1μM antagonist: 1.9 ± 0.4, p = 0.213 vs control: 3.1 ± 0.7), although this tended towards a lower number at the highest concentration. Neither were any significant differences observed in the rest of the slice when the antagonist was administered at any concentration tested (10nM antagonist: 13.3 ± 1.2, p = 0.107, 100nM antagonist: 13.5 ± 1.1, p = 0.144, and 1μM antagonist: 12.9 ± 1.1, p = 0.066 vs control: 16.3 ± 2.9).

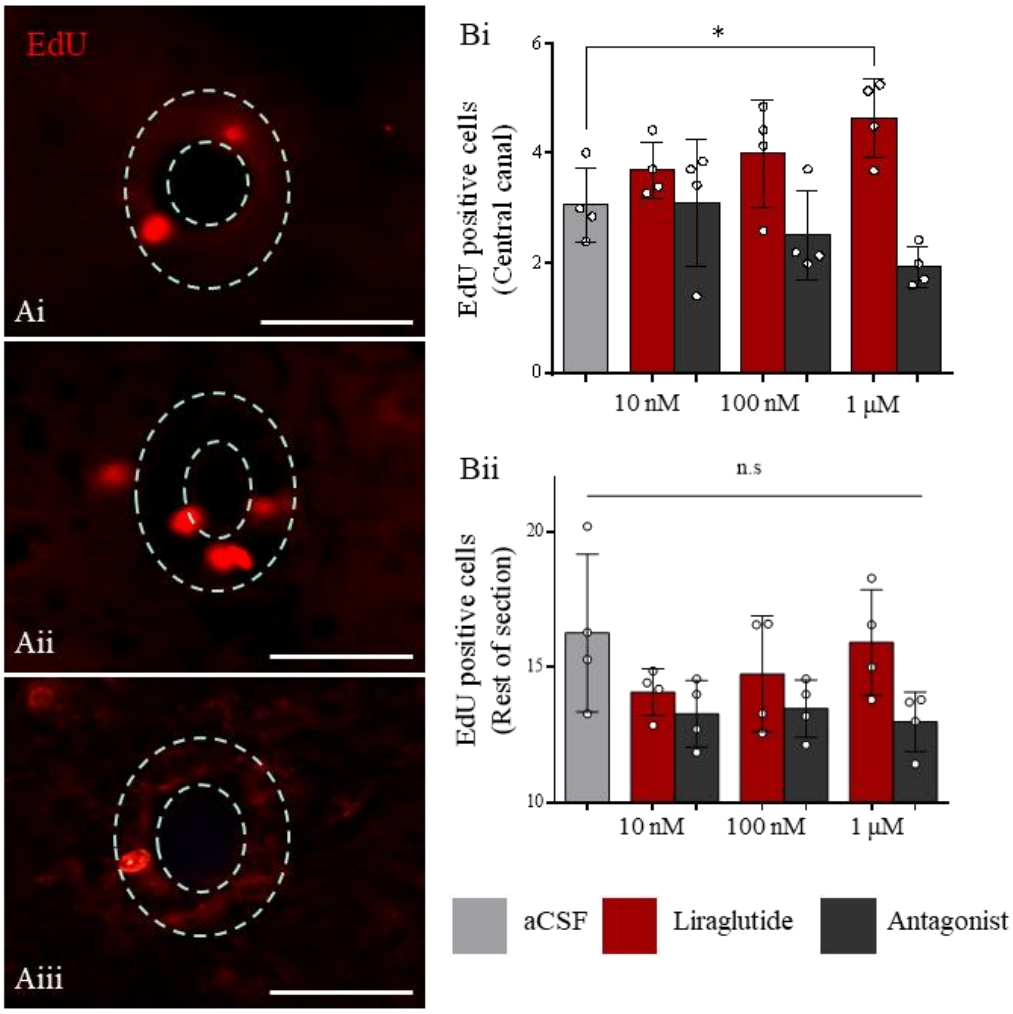

Figure 5.1: Limited differences in the number of newly proliferated cells can be observed after GLP-1R modulation in acute spinal cord slice experiments.

A. Representative images showing EdU positive cells around the central canal of control (**i**), 1 µM liraglutide (**ii**) and 1 µM exendin-(9-39) GLP-1R antagonist (**iii**) treated slices (N=4). Scale bars: 50 µm. **B**. Bar charts showing the mean number of EdU positive cells ± SD in the central canal (i) and rest of section (ii) for three different concentrations of GLP-1R agonist liraglutide and GLP-1R antagonist exendin-(9-39), compared with median aSCF only control. Sections taken from thoracolumbar region. Statistical analysis: One-way ANOVA with Dunnett's multiple comparison test against control condition, significance level $p < 0.05$ (indicated by *).

5.2.2 GLP-1R agonists influence proliferation and cell survival in long term organotypic spinal cord slice cultures

5.2.2.1 Exendin-4 application results in higher number of newly proliferated cells in the central canal in OSCSCs when administered over 5 days

To determine whether GLP-1R agonist exendin-4 would have any effect on the number of newly proliferated cells when administered over a longer period of time OSCSCs were cultured for 5 days during which they received exendin-4 three times. Exendin-4 was tested at two different concentrations, and 1 μM EdU was added to the culture media along with the final dose of exendin-4 24 hours before the slices were fixed and processed for visualisation (Figure 5.2).

After 5 days in culture the number of EdU positive cells within the central canal area was significantly higher when OSCSCs were treated with 1 μM exendin-4 (13.2 ± 4.1, $p = 0.047$) compared with OSCSCs in control conditions (7.9 ± 3.1). Somewhat surprisingly, there were no significant differences in the numbers of EdU labelled cells around the central canal of the group treated with 10 μM exendin-4 (10.7 ± 3.4, $p = 0.442$) when compared with control OSCSCs.

No significant differences in the total numbers of EdU labelled cells were observed in either group (1 μM exendin-4: 121.8 ± 24.4, $p = 0.616$ and 10 μM exendin-4: 106.2 ± 17.4, $p = 0.898$ vs control: 111.7 ± 11.3).

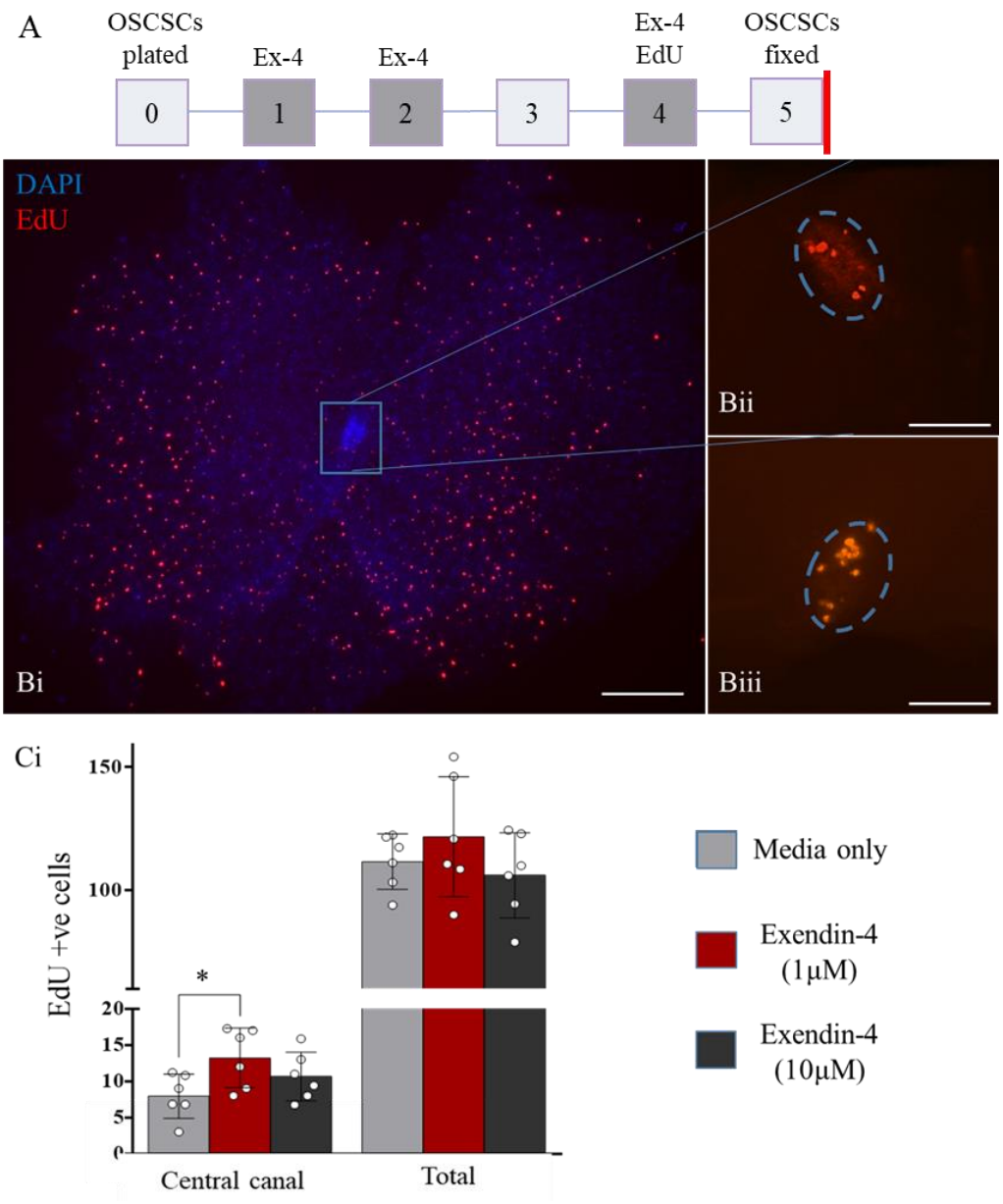

Figure 5.2: Treatment with Exendin-4 results in higher proliferation of central canal cells in 5-day organotypic spinal cord slice culture model.

A. Schematic of the experimental timeline. **B**. Representative image of entire control OSCSC (**i**), central canal of a control slice (**ii**), and central canal treated with 1 μM exendin-4 (**iii**). Scale bars: (**i**) 300 μm, (**ii**) 50 μm. **C**. Bar chart showing the mean number of EdU positive cells ± SD in the central canal (**i**) and total EdU positive cells per section (**ii**) for two different concentrations of GLP-1R agonist exendin-4, compared with media only control. Sections taken from thoracolumbar region. Statistical analysis: One-way ANOVA with Dunnett's multiple comparison test against control condition, significance level $p < 0.05$ (indicated by *).

5.2.2.2 Liraglutide application resulted in higher numbers of newly proliferated cells in the central canal in OSCSCs when administered over 10 days

Liraglutide, being a longer lasting analogue of GLP-1 than exendin-4, was expected to have more of an effect on the number of newly proliferated cells within the central canal of OSCSCs. The duration of this experiment was also increased from 5 days to 10 days to determine if the effects increased or decreased in line with chronic modulation of the GLP-1R.

Addition of liraglutide at both 1 μM and 10 μM resulted in significantly higher numbers of newly proliferated cells at 2 days (1 μM: 11.6 ± 3.1, $p = 0.004$ and 10 μM: 10.0 ± 4.6, $p = 0.022$ versus control: 4.5 ± 1.7), 6 days (1 μM: 12.5 ± 3.8, $p = 0.005$ and 10 μM: 12.6 ± 3.8, $p = 0.004$ versus control: 6.1 ± 1.5), 8 days (1 μM: 13.4 ± 1.9, $p = 0.001$ and 10 μM: 13.5 ± 3.1, $p = 0.001$ versus control: 4.8 ± 2.2), and 10 days in culture (1 μM: 12.7 ± 2.8, $p = 0.001$ and 10 μM: 11.7 ± 3.5, $p = 0.003$ versus control: 3.7 ± 1.9) (Figure 5.3).

Liraglutide at 1 μM, but not 10 μM, resulted in significantly higher numbers of newly proliferated cells at 4 days in culture when compared with controls (1 μM: 14.67 ± 3.39, $p = 0.001$ and 10 μM: 12.33 ± 3.73, $p = 0.064$ versus control: 7.22 ± 4.12).

No significant differences were observed between groups treated with liraglutide at either concentration across any time point studied, nor were there any significant differences in the numbers of EdU positive cells observed between the control groups across any time points.

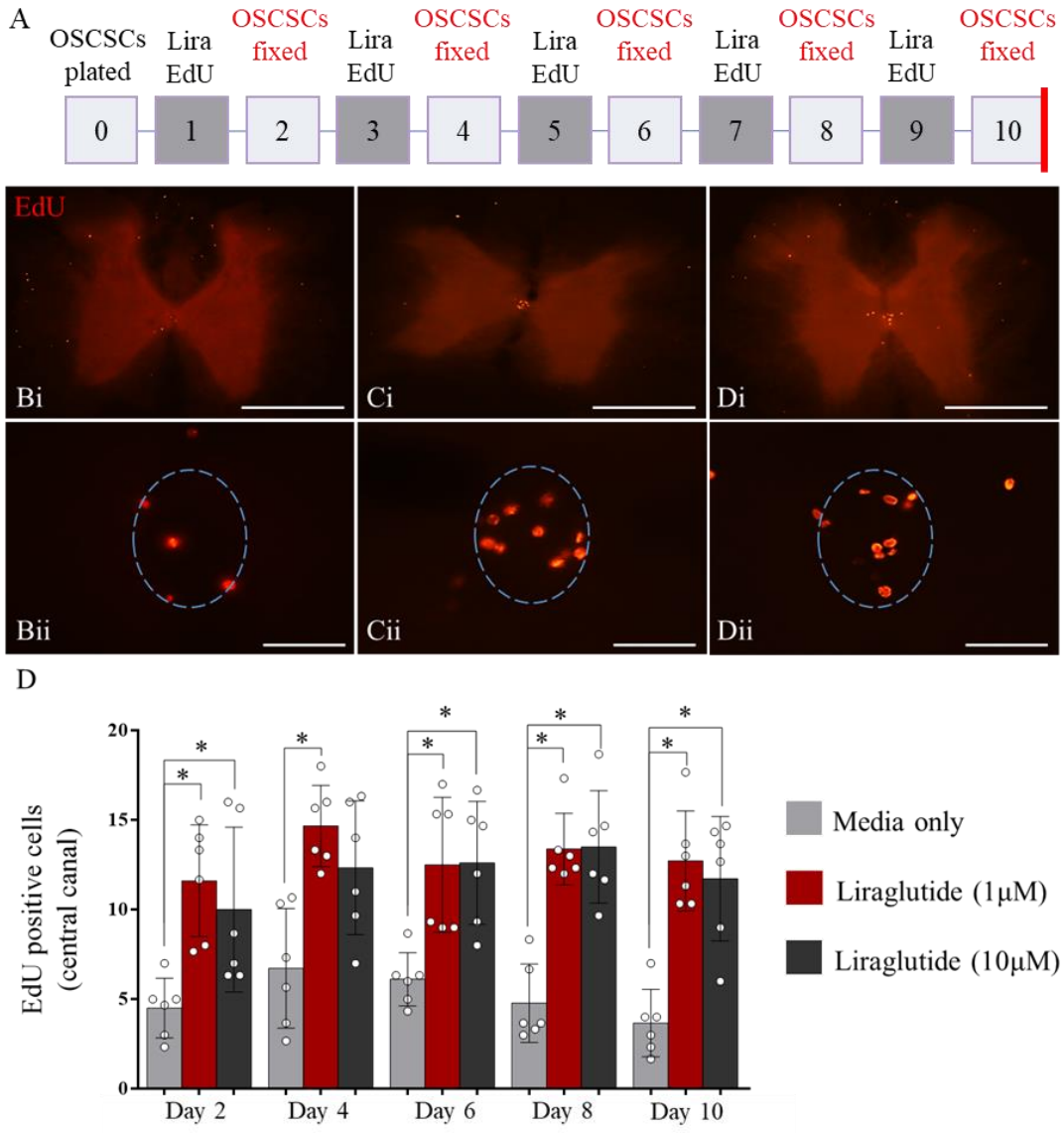

Figure 5.3: Liraglutide application resulted in higher numbers of newly proliferated cells around the central canal in organotypic spinal cord slice cultures.

A. Schematic of the experimental timeline. **B**. Representative image of entire control OSCSC (**i**), and central canal (**ii**) of control (**B**), 1 μM liraglutide (**C**), and 10 μM liraglutide (**D**). Scale bars: (**i**) 500 μm, (**ii**) 50 μm. **C**. Bar chart showing the mean number of EdU positive cells ± SD in the central canal for two different concentrations of GLP-1R agonist liraglutide, compared with media only control, at five time points throughout the experiment. Sections taken from thoracolumbar region. Statistical analysis: One-way ANOVA with Dunnett's multiple comparison test against control condition for each time point, significance level $p < 0.05$ (indicated by *).

5.2.2.3 Liraglutide attenuates cell death on day 2, and prevents a peak in cell death on day 4 of culture

As in the previous experiment, OSCSCs were treated with liraglutide on days 1, 3, 5, 7, and 9. Propidium iodide, a fluorescent DNA intercalating dye which is membrane impermeable in healthy cells, was added 1 hour before OSCSC fixation to determine the extent of cell death within the slices and to indicate whether liraglutide displays a neuroprotective effect in this model.

When OSCSCs were fixed and the fluorescence intensity of the OSCSCs analysed on days 6, 8, and 10 of culture, there were no significant differences in the average fluorescence intensity between any of the groups studied when compared with the respective media only control (Figure 5.4). On day 2 of culture, 48 hours after plating, there was significantly lower fluorescence intensity in the OSCSCs treated with 10 μM liraglutide compared with the control group ($12.8 \pm 3.2 \times 10^3$, $p = 0.037$ versus control: $7.5 \pm 1.6 \times 10^3$), indicating that there was less cell death within this group.

On day 4 of culture there was significant higher average fluorescence intensity in the control group ($18.1 \pm 2.4 \times 10^3$) when compared with the groups treated with 1 μM ($9.4 \pm 1.8 \times 10^3$, $p = 0.004$), or 10 μM ($8.6 \pm 2.7 \times 10^3$, $p = 0.001$) liraglutide.

When control group data was compared amongst itself (One-way ANOVA, Tukey's multiple comparison test between control groups, not shown on Figure 5.4) the fluorescence intensity was highest on day 4 ($18.1 \pm 2.4 \times 10^3$) and was significantly higher than on days 6 ($11.8 \pm 2.9 \times 10^3$, $p = 0.031$), 8 ($10.2 \pm 3.1 \times 10^3$, $p = 0.006$), and 10 ($8.9 \pm 1.4 \times 10^3$, $p = 0.002$), but not significantly higher than on day 2 ($12.9 \pm 3.2 \times 10^3$, $p = 0.087$). This indicates that the peak levels of cell death occur over the first 96 hours in culture, and then is reduced as the slice culture equilibrates.

No significant differences were observed when results from the 1 μM, or 10 μM liraglutide groups were compared between respective timepoints, although a trend towards an increase in fluorescence intensity on day 4 was observed for both groups.

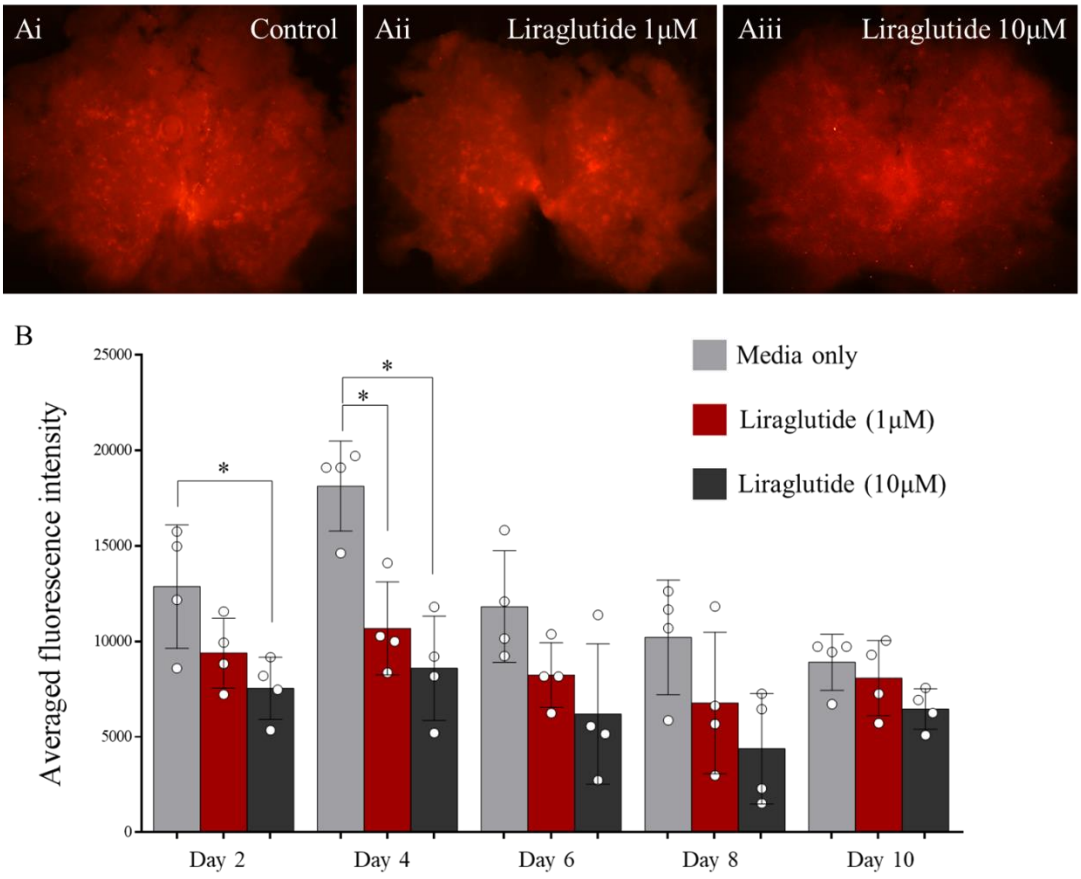

Figure 5.4: Treatment with liraglutide attenuates cell death on days 2 and 4 of culture in OSCSCs.

A. Representative images of propidium iodide staining in control OSCSC (i), OSCSC treated with 1μM liraglutide (ii), and OSCSC treated with 10μM liraglutide (iii) after 4 days of incubation.

B. Bar chart showing the mean fluorescence intensity of pixels ± SD, measured from OSCSCs treated with propidium iodide 1 hour before fixation (N=4). Two different concentrations of GLP-1R agonist liraglutide were studied and compared with media only control, at five time points throughout the experiment. Sections taken from thoracolumbar region. Statistical analysis: One-way ANOVA with Dunnett's multiple comparison test against control condition for each time point, significance level $p < 0.05$ (indicated by *).

5.2.3 Hydrogels infused with liraglutide enhance proliferation in OSCSCs

5.2.3.1 The mechanical properties of the hydrogels affect spinal cell proliferation in the central canal and grey matter, independent of liraglutide

It is generally agreed that the stiffness of the spinal cord sits somewhere between 100 – 2,000 Pa (Franze et al., 2013), and therefore a selection of hydrogels both commercially available and gifted by collaborators in York were used that span this range of stiffnesses (Table 5.1).

Table 5.1: The mechanical properties of the hydrogels used in the investigation for chapter 5.
E: Young's modulus (also known as the elastic deformation modulus). Measured in Pascals (Pa).

GEL	E / Pa	SOURCE
DBS-CONHNH2	1200	Prof. David Smith, York (K. Patterson and K. Smith, 2020)
Alpha 4	1000	Manchester Biogels
Gamma 4	500	Manchester Biogels
Epsilon 4	100	Manchester Biogels
Glutamine-amide	85	Prof. David Smith, York (J. T. Wang et al., 2021)

Hydrogels were used as a base for culturing of spinal cord slices for five days and EdU was added 24 hours before fixation to determine whether the different mechanical stiffnesses of the hydrogels affected cell proliferation. In this experiment, the control group was OSCSCs cultured without a hydrogel base.

After 5 days in culture there were no significant differences in the number of newly proliferated EdU labelled cells within the white matter for any of the hydrogels tested when compared with the control group cultured without any hydrogels, or when groups were compared to each other (Figure 5.8, Control: 3.1 ± 1.2 cells per 0.1 mm^2, DBS-CONHNH2: 2.0 ± 0.5, Alpha 4: 2.2 ± 1.5, Gamma 4: 3.0 ± 0.8, Epsilon 4: 2.6 ± 1.6, Glutamine amide: 1.3 ± 0.6).

There were also no significant differences observed in the number of newly proliferated cells between any of the hydrogel groups and the control group within the grey matter (Control: 3.1 ± 1.1 cells per 0.1 mm^2, DBS-CONHNH2: 1.3 ± 0.3, Alpha 4: 1.4 ± 1.4, Gamma 4: 4.8 ± 1.8, Epsilon 4: 2.5 ± 1.1, Glutamine amide: 1.0 ± 0.5).

However, there was significantly higher proliferation within OSCSCs grown on the Gamma 4 hydrogel (4.8 ± 1.8) when compared with DBS-$CONHNH_2$ (1.3 ± 0.3, p = 0.005), Alpha 4 (1.4 ± 1.4, p = 0.007), and Glutamine-amide hydrogels (1.0 ± 0.5, p = 0.003).

Within the central canal area, the only group displaying a significantly higher degree of proliferation when compared with the control was the Epsilon 4 group (2.5 ± 1.1, p = 0.002 versus control: 5.1 ± 2.3). There was also significantly higher proliferation within the Epsilon 4 group when compared with the DBS-CONHNH2 (0.8 ± 0.7, p = 0.001), Alpha 4 (0.4 ± 0.5, p = 0.001), and Glutamine-amide hydrogel groups (1.2 ± 0.8, p = 0.002). The number of EdU-positive cells within the Gamma 4 group (3.6 ± 0.6) was also significantly higher than that within the Alpha 4 (p = 0.013) and DBS-CONHNH2 groups (p = 0.029).

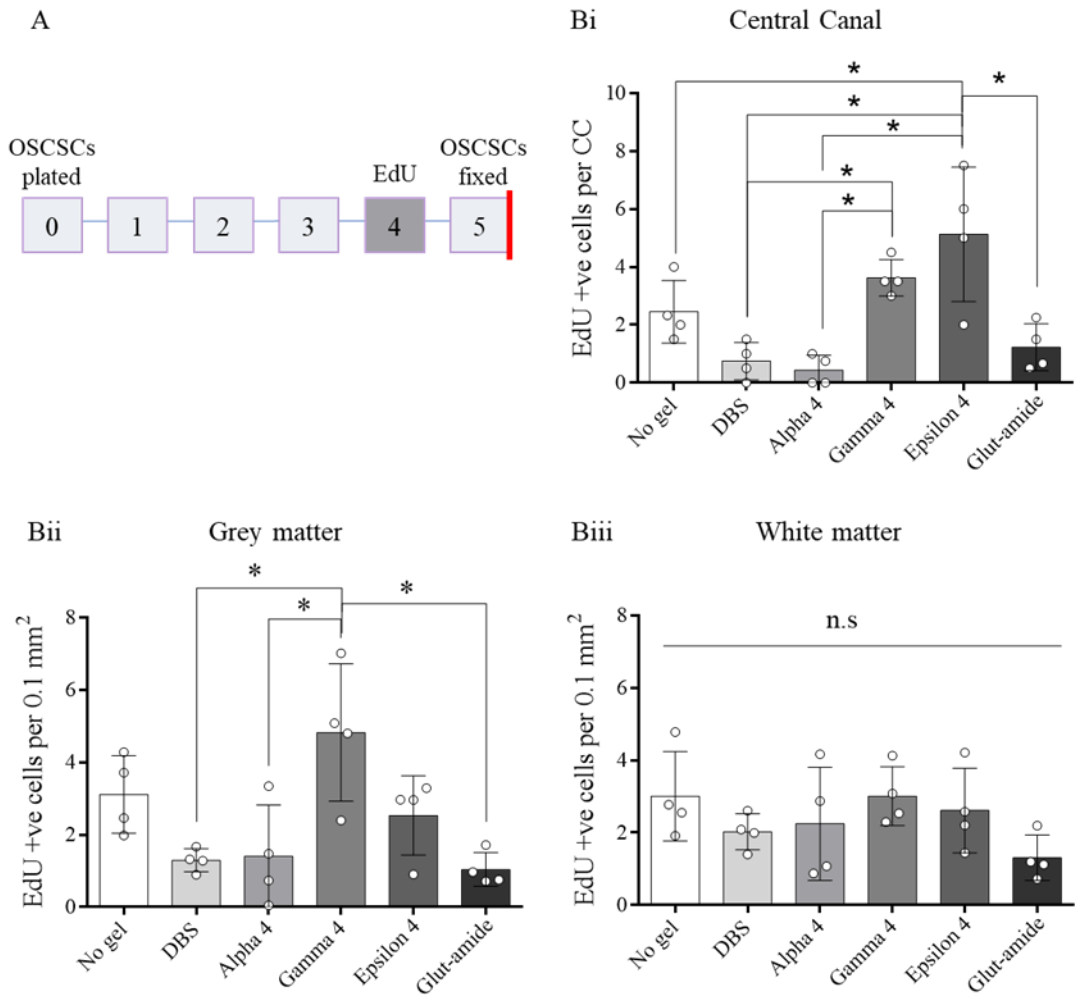

Figure 5.5: The proliferation of cells within the central canal and grey matter is affected by the mechanical stiffness of the substrate.

A. Schematic of the experimental timeline. **B**. Bar graphs of the average number of EdU positive cells in the central canal (**i**), and the average number of EdU positive cells per 0.1 mm^2 in the grey matter (**ii**), and white matter (**iii**) of the spinal cord (N = 4). Abbreviations used: DBS-CONHNH2 (DBS), Glutamine-amide (Glut-Amide). Sections taken from thoracolumbar region. Statistical analysis: One-way ANOVA with Dunnett's multiple comparison test against control condition, significance level $p < 0.05$ (indicated by *).

5.2.3.2 Liraglutide infused hydrogels attenuate proliferation in the central canal, but enhance proliferation in the white matter

The hydrogels were then mixed with liraglutide in order to generate a system of slow release for the liraglutide over a longer period of time than when it is applied acutely. The isoelectric point of liraglutide is 4.9 (Knudsen, 2019), this means that in pH 7.5 neutral culture media this molecule will have an overall slight negative charge and therefore should elute slowly from these positively charged hydrogels. In this experiment the control group consisted of OSCSCs cultured in the presence of liraglutide in the culture media, but without a hydrogel base.

After 5 days in culture, a significant enhancement in the number of newly proliferated cells within the white matter could be seen when OSCSCs were cultured on the DBS-CONHNH2 (11.2 ± 0.5, p = 0.001), Gamma-4 (6.9 ± 0.8, p = 0.001), Epsilon-4 (8.3 ± 1.6, p = 0.005), and glutamine-amide (7.9 ± 1.3, p = 0.001) hydrogels when compared with the control group cultured without any hydrogel (3.4 ± 1.9). No significant differences were observed between the control groups and the Alpha 4 hydrogel group (5.4 ± 1.8, p = 0.207).

Within the grey matter of the spinal cord there was significant higher proliferation only in the DBS-CONHNH2 group (8.7 ± 0.8, p = 0.001) when compared with the control (4.1 ± 1.3). There were no significant differences observed in any of the other hydrogel groups investigated (Alpha 4: 3.2 ± 1.4, p = 0.956; Gamma 4: 5.1 ± 1.4, p = 0.904; Epsilon 4: 6.3 ± 2.4, p = 0.259; Glutamine amide: 4.1 ± 0.3, p > 0.999).

There were also no significant differences in the number of newly proliferated cells in the central canal of DBS-CONHNH2 (7.6 ± 1.4, p = 0.415), Gamma 4 (5.7 ± 2.6, p = 0.091) and Epsilon 4 (10.8 ± 5.1, p = 0.998) hydrogel groups compared with the liraglutide only control (11.5 ± 2.1). However, the Alpha 4 (4.75 ± 2.40, p = 0.015) and glutamine amide (4.8 ± 2.2, p = 0.036) groups displayed significant reductions in the number of EdU positive cells around the central canal when compared with the control group.

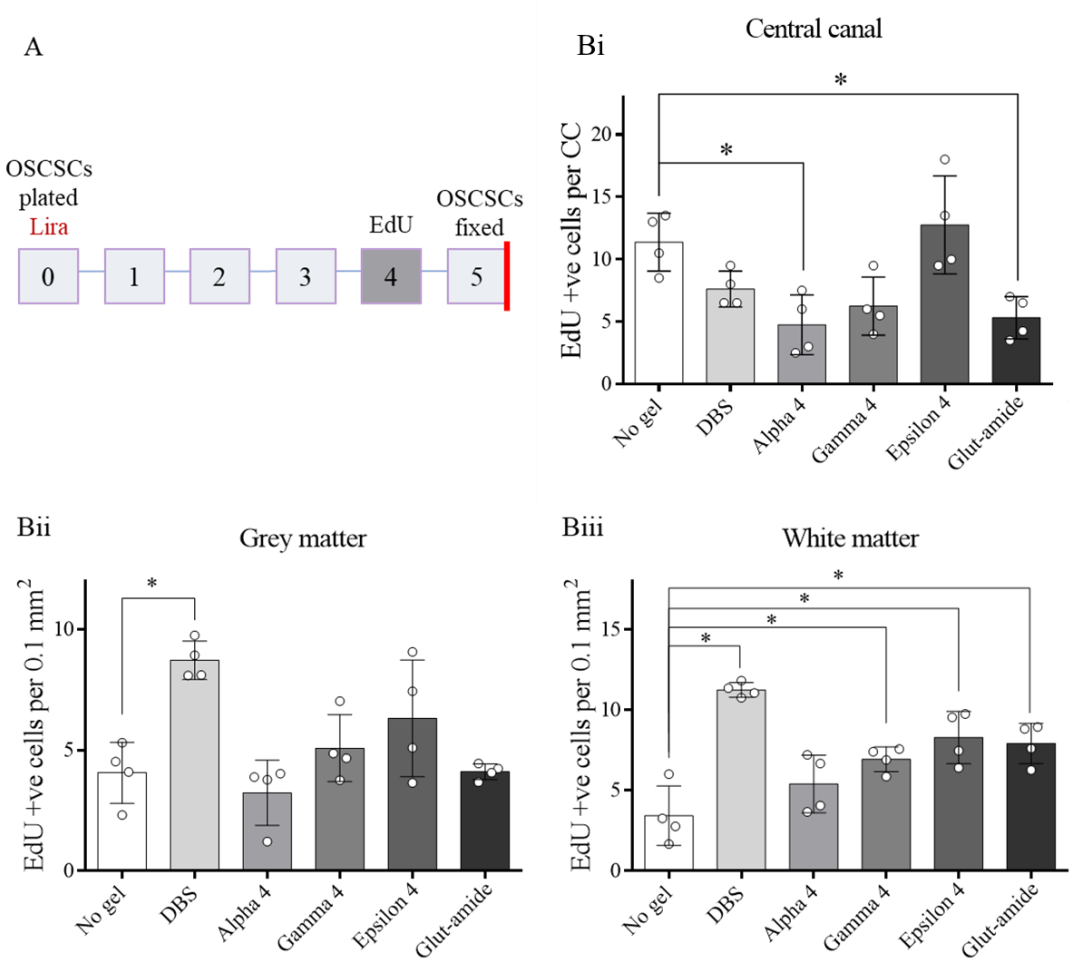

Figure 5.6: Liraglutide infused hydrogels attenuate proliferation in the central canal, but enhance proliferation in the white matter of slice cultures after 5 days.

A. Schematic of the experimental timeline. **B**. Bar graphs of the average number of EdU positive cells in the central canal (**i**), and the average number of EdU positive cells per 0.1 mm^2 in the grey matter (**ii**), and white matter (**iii**) of the spinal cord. Abbreviations used: DBS-CONHNH2 (DBS), Glutamine-amide (Glut-Amide). Sections taken from thoracolumbar region. Statistical analysis: One-way ANOVA with Dunnett's multiple comparison test against control condition, significance level $p < 0.05$ (indicated by *).

5.2.3.3 Hydrogels infused with liraglutide are more effective in enhancing the number of EdU positive cells in the spinal cord than their equivalent non-infused gels.

Lastly, the hydrogel groups infused with liraglutide were directly compared against their respective hydrogel group that did not contain liraglutide in order to determine whether the addition of liraglutide to the hydrogel affected the level of proliferation of cells with the OSCSCs.

There were significantly more EdU positive cells in the entire OSCSCs cultured with a combination of liraglutide and DBS-CONHNH2 (10.1 ± 0.2 versus 1.8 ± 0.2, p = 0.001), Alpha-4 (4.4 ± 2.8 versus 1.5 ± 1.4, p = 0.026,), Epsilon-4 (6.1 ± 0.8 versus 2.8 ± 1.8, p = 0.008), and Glutamine-amide (6.2 ± 0.9 versus 0.9 ± 0.2, p = 0.001) hydrogels when compared with their non-infused hydrogel equivalents.

When only the grey matter was counted, significantly more EdU positive cells were seen in the liraglutide infused hydrogels compared with respective non-infused hydrogels were observed in the DBS-CONHNH2 (8.71 ± 0.79 versus 1.29 ± 0.32, p = 0.001), Epsilon-4 (6.31 ± 2.41 versus 2.53 ± 1.10, p = 0.001), and Glutamine-amide groups (4.11 ± 0.32 versus 0.66 ± 0.13, p = 0.003). No significant differences in proliferation were observed in the Alpha-4 (3.2 ± 1.3 versus 1.4 ± 1.4, p = 0.269), Gamma-4 (5.1 ± 1.4 versus 4.8 ± 1.9, p = 0.998), or non-hydrogel groups (4.1 ± 1.3 versus 3.5 ± 0.9, p = 0.989).

In the white matter there were no significant differences observed only in the non-hydrogel groups, but significantly more newly proliferated cells were observed for all hydrogel groups: DBS-CONHNH2 (11.23 ± 0.45 versus 2.03 ± 0.10, p = 0.001), Alpha-4 (5.40 ± 1.79 versus 1.89 ± 2.03, p = 0.002), Gamma-4 (6.93 ± 0.76 versus 3.01 ± 0.81, p = 0.006), Epsilon-4 (8.28 ± 1.62 versus 2.61 ± 1.17, p = 0.001), and Glutamine-amide (7.91 ± 1.25 versus 1.06 ± 0.23, p = 0.001), when compared with their respective non-infused hydrogels.

Similar results were found when investigating the number of EdU positive cells around the central canal of liraglutide infused vs non-infused hydrogels. With the exception of the Gamma-4 hydrogel group (5.8 ± 2.6 versus 3.6 ± 0.6, p = 0.571), all other conditions displayed a higher number of EdU positive cells when liraglutide was added: DBS-CONHNH2 (7.6 ± 1.4 versus 0.8 ± 0.7, p = 0.001), Alpha-4 (4.5 ± 2.0 versus 0.4 ± 0.5, p = 0.033), Epsilon-4 (12.8 ± 3.9 versus 5.1 ± 2.3, p = 0.001), and Glutamine-amide (5.1 ± 1.7 versus 1.2 ± 0.8, p = 0.049).

As previously observed (Figure 5.3) there were also significantly more EdU positive cells in the non-hydrogel group with liraglutide compared with the non-hydrogel group without liraglutide (11.5 ± 2.1 versus 2.7 ± 1.6, p = 0.001).

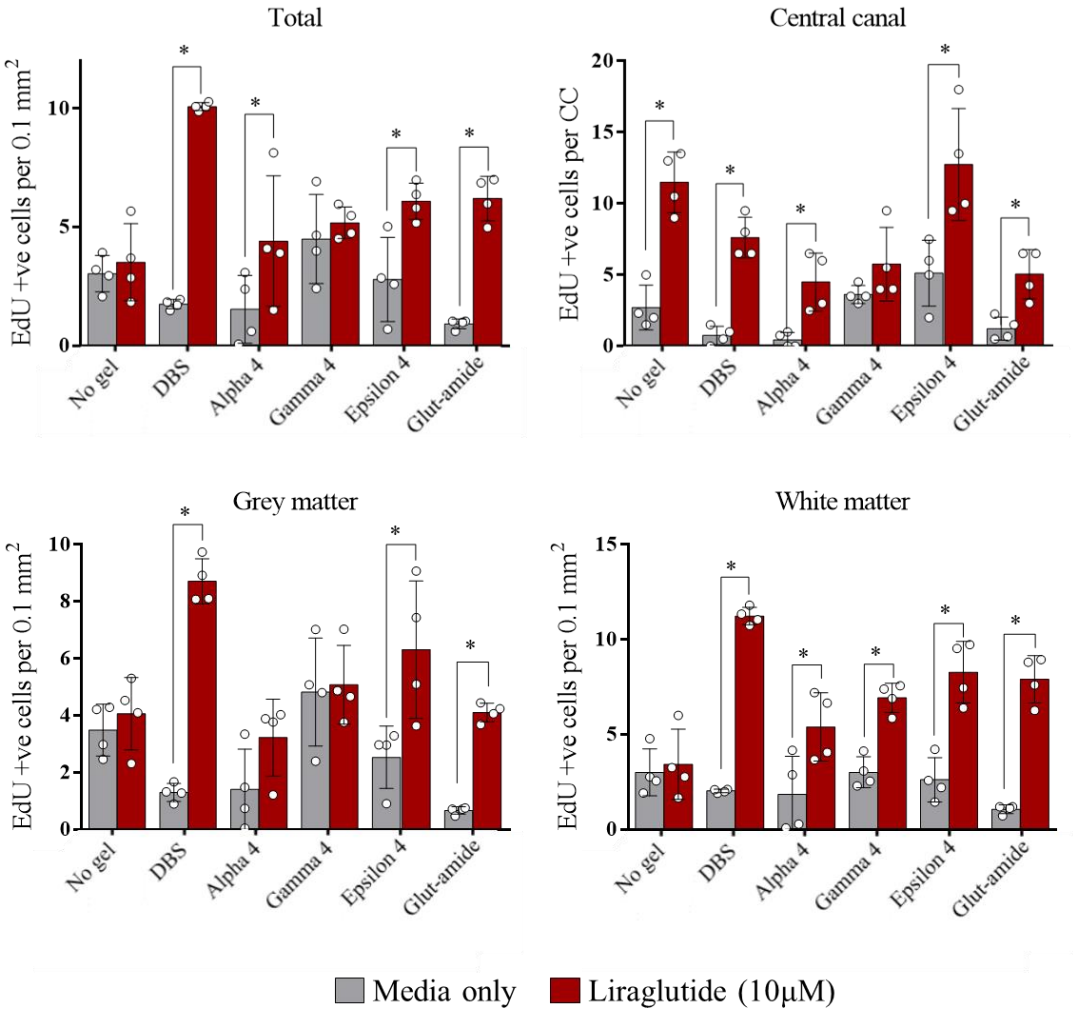

Figure 5.7: Liraglutide infused hydrogels enhances the total number of newly proliferated cells in slice cultures after 5 days compared with hydrogels independently.

Bar graphs showing the average numbers of EdU positive cells per 0.1 mm^2 in the total OSCSC, grey matter, and white matter, and the average number of EdU positive cells in the central canal. Abbreviations used: DBS-CONHNH2 (DBS), Glutamine-amide (Glut-Amide). Sections taken from thoracolumbar region. Statistical analysis: One-way ANOVA with Sidak's multiple comparison test against non-liraglutide condition for each group, significance level $p < 0.05$ (indicated by *).

5.2.4 *In vivo* effects of GLP-1R agonists

5.2.4.1 GLP-1R agonists attenuate proliferation in the central canal and white matter

Having investigated the effects of exendin-4 and liraglutide in various *ex vivo* models which resulted in general enhancement of cell proliferation predominantly around the central canal, a series of experiments were set up to see if the effects were comparable when these drugs were delivered *in vivo.*

Exendin-4

Mice were given daily injections of either exendin-4 (10 μg/Kg) and EdU (10 mM) in sterile saline, or EdU in sterile saline alone to act as the control group for this experiment, over 4 days and the numbers of EdU positive cells were counted (Figure 5.8).

In mice treated with exendin-4, the total number of EdU positive cells was significantly lower (exendin-4 group: 34.1 ± 3.9 versus control: 42.6 ± 6.8, $p = 0.023$). Interestingly, this effect appeared to be mainly due to fewer newly proliferated cells in the white matter (exendin-4 group: 16.3 ± 3.9 versus control: 23.9 ± 4.8, $p = 0.047$).

No significant differences in cell proliferation were observed in the grey matter (exendin-4 group: 16.0 ± 2.7 versus control: 16.5 ± 4.7, $p = 0.997$), or in the central canal of the exendin-4 treated group when compared with the control group (exendin-4 group: 1.9 ± 0.2 versus control: 2.3 ± 0.5, $p = 0.258$).

EdU positive cells within the central canal of both groups were examined for expression of Sox2, a marker of proliferative ability commonly used as an ependymal cell marker (Stenudd et al., 2022), and it was found that 100% of EdU+ cells in vehicle and exendin treated mice were also immunopositive for Sox2 (Figure 5.8). As there were no significant changes in the number of newly proliferated ECs between the two groups the observed proliferation is likely representative of the self-renewal of the ECs common in the physiologically healthy murine spinal cord (X. Li et al., 2016).

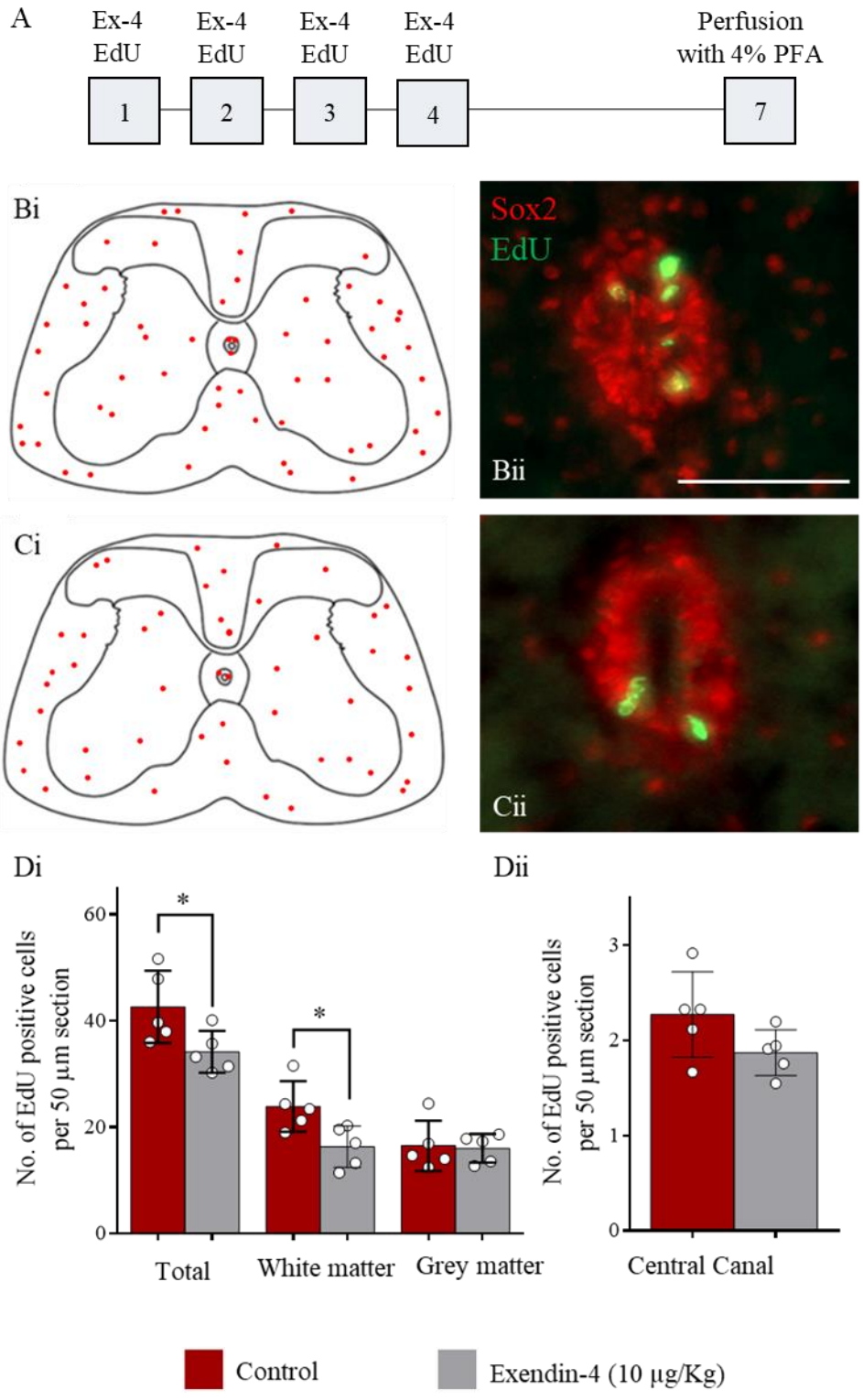
A
Ex-4 EdU
Ex-4 EdU
Ex-4 EdU
Ex-4 EdU
Perfusion with 4% PFA
1
2
3
4
7
Bi
Sox2
EdU
Bii
Ci
Cii
Di
Dii
No. of EdU positive cells per 50 µm section
60
40
20
0
*
*
Total
White matter
Grey matter
3
2
1
0
Central Canal
Control
Exendin-4 (10 µg/Kg)

Figure 5.8: *In vivo* injections of Exendin-4 results in fewer EdU positive cells within the white matter of the lumbar spinal cord.

A. Schematic of the experimental timeline, injections of Exendin-4 and EdU in PBS, or EdU and vehicle (sterile saline) alone were given in the evening every 24 hours for 4 days. **B**. Representative schematic of EdU positive cell distribution within a lumbar spinal cord slice of a control group mouse (**i**), representative image of EdU positive cell distribution with the central canal of a control group mouse co-stained with ependymal cell marker Sox2 (**ii**). Scale bar: 50 μm. **C**. Representative schematic of EdU positive cell distribution within a lumbar spinal cord slice of an exendin-4 treated mouse (**i**), representative image of EdU positive cell distribution with the central canal of an exendin-4 treated mouse co-stained with ependymal cell marker Sox2 (**ii**). **D**. Bar graphs comparing the average numbers of EdU positive cells in the total section, white matter, grey matter (**i**) and central canal (**ii**) areas of a 50 μm thick lumbar spinal cord slice for control and exendin-4 treated mice. Statistical analysis: One-way ANOVA with Sidak's multiple comparison pair-wise test against control condition for each area, significance level $p < 0.05$ (indicated by *).

Liraglutide

Mice were given daily injections of either liraglutide (1 μg/Kg) and EdU (10 mM) in sterile saline, or EdU in sterile saline alone to act as the control group for this experiment, over 4 days and the numbers of EdU positive cells were counted (Figure 5.9).

Similar to the results observed in mice treated with exendin-4, the mice treated with liraglutide had significantly fewer total EdU positive cells when compared with the control group (liraglutide group: 28.9 ± 5.5 versus control: 44.9 ± 9.2, $p = 0.003$). Again, this effect appeared to be mainly due to significantly fewer newly proliferated cells in the white matter (liraglutide group: 16.0 ± 2.8 versus control: 26.5 ± 3.8, $p = 0.016$). No significant differences in cell proliferation were observed in the grey matter of mice treated with liraglutide (liraglutide group: 11.1 ± 2.5 versus control: 15.7 ± 5.8, $p = 0.458$).

In contrast to the results obtained in the exendin-4 *in vivo* experiments (Figure 5.8), the group treated with liraglutide did possess significantly fewer EdU positive cells within the central canal area when compared with the control group (liraglutide group: 1.3 ± 0.5 versus control: 2.6 ± 0.3, $p = 0.001$).

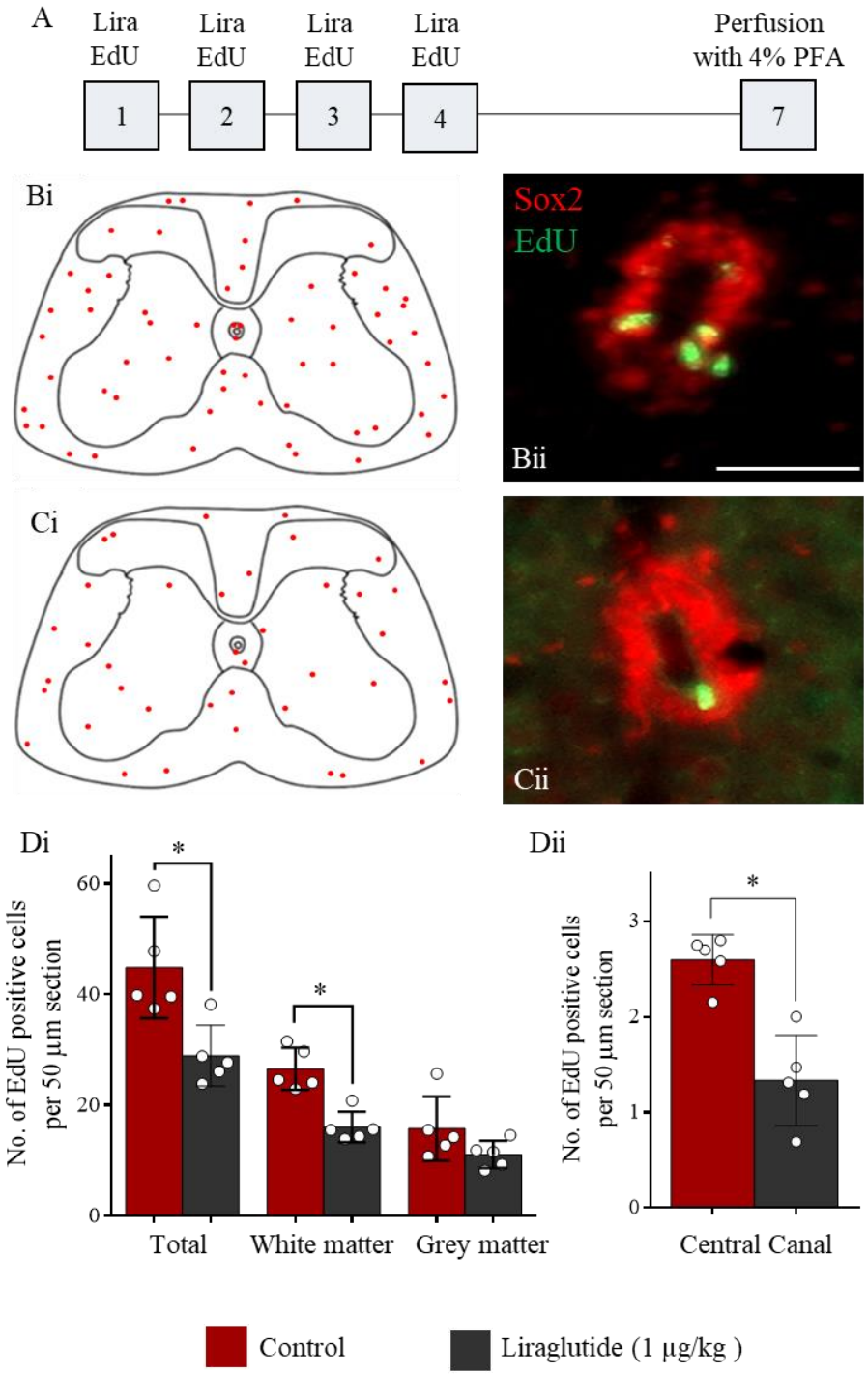

Figure 5.9: *In vivo* injections of Liraglutide attentuates proliferation in the white matter and central canal of the lumbar spinal cord.

A. Schematic of the experimental timeline, injections of liraglutide and EdU in PBS, or EdU and vehicle (sterile saline) alone were given in the evening every 24 hours for 4 days. **B**. Representative schematic of EdU positive cell distribution within a lumbar spinal cord slice of a control group mouse (**i**), representative image of EdU positive cell distribution with the central canal of a control group mouse co-stained with ependymal cell marker Sox2 (**ii**). Scale bar: 50 µm. **C**. Representative

schematic of EdU positive cell distribution within a lumbar spinal cord slice of a liraglutide treated mouse (**i**), representative image of EdU positive cell distribution with the central canal of a liraglutide treated mouse co-stained with ependymal cell marker Sox2 (**ii**). **D**. Bar graphs comparing the average numbers of EdU positive cells in the total section, white matter, grey matter (**i**) and central canal (**ii**) areas of a 50 μm thick lumbar spinal cord slice for control and liraglutide treated mice. Statistical analysis: One-way ANOVA with Sidak's multiple comparison pair-wise test against control condition for each area, significance level $p < 0.05$ (indicated by *).

5.2.4.2 Treatment with GLP-1R agonists results in fewer EdU positive cells expressing Sox2 and PanQKI

To determine the identity of the newly proliferated EdU positive cells in the spinal cord, sections were double labelled and investigated for colocalisation using immunolabelling for neurons (HuC/D), microglia (Iba1), oligodendrocytes (Pan-QKI), and astrocytes (S100β) (Figure5-13).

The number of newly proliferated cells that were also immunopositive for the exclusively neuronal marker HuC/D was not significantly different in either the exendin-4 or liraglutide treated groups when compared with respective control groups (exendin-4: 3.9 ± 2.0 % vs control: 2.9 ± 1.6 %, $p = 0.993$, and liraglutide: 4.4 ± 1.6 % versus control: 2.6 ± 1.6 %, $p = 0.949$). This is consistent with the lack of change in the number of EdU positive cells present in the grey matter of the spinal cord observed previously (Figure 5.8, Figure 5.9).

Neither was the percentage of cells that differentiated into microglia significantly altered (exendin-4: 16.6 ± 4.8 % vs control: 12.0 ± 5.0 %, $p = 0.197$, and liraglutide: 18.1 ± 5.6 % versus control: 12.3 ± 5.2 %, $p = 0.087$). The same was true for the percentage of cells that differentiated down an astrocytic lineage, as identified by colocalisation of EdU with S100 β (exendin-4: 16.32 ± 5.22 % vs control: 11.29 ± 2.30%, $p = 0.124$, and liraglutide: 16.22 ± 4.84 % versus control: 11.58 ± 2.59 %, $p = 0.247$).

Also observed was a significant reduction in the proportion of EdU positive cells that also expressed Pan-QKI in both the exendin-4 and liraglutide groups (exendin-4: 23.83 ± 5.04 % vs control: 16.97 ± 2.14 %, p = 0.015, and liraglutide: 24.59 ± 5.17 % versus control: 15.98 ± 4.03%, p = 0.003), indicating that differentiation along the oligodendrocyte lineage is lower after treatment with GLP-1R agonists. This corresponds with the previously observed reduction in the number of EdU cells within the white matter of the test groups when compared with the control (Figure 5.8, Figure 5.9).

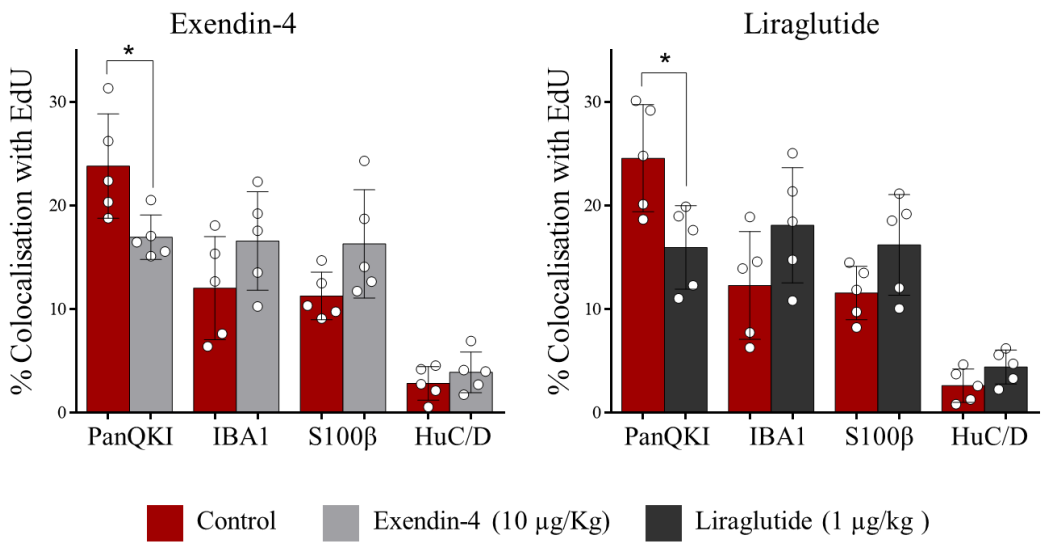

Figure 5.10: Treatment with exendin-4 or liraglutide results in fewer cells that are immunopositive for oligodendrocyte marker PanQKI.

Bar graphs showing the percentage of EdU positive cells that colocalise with immunohistochemical markers for oligodendrocytes (PanQKI), microglia (IBA1), astrocytes (S100β), and neurons (HuC/D) in exendin-4 and liraglutide with their respective controls. Statistical analysis: One-way ANOVA with Sidak's multiple comparison pair-wise test against control condition for each area, significance level $p < 0.05$ (indicated by *).

5.2.4.3 GLP-1R agonists do not alter the number of newly proliferated cells in the hippocampus when given *in vivo*

The dentate gyrus of the hippocampus is an area widely known for its role in adult neurogenesis, and as such was used in this experiment as a positive control when testing the effects of GLP-1R modulation on neurogenesis in a healthy mouse model.

Neither exendin-4 or liraglutide administration resulted in a significant change in the number of EdU positive cells within the dentate gyrus when compared with their respective controls (exendin-4: 55.6 ± 14.1% vs control: 54.0 ± 13.6%, p = 0.859, and liraglutide: 54.4 ± 14.2% versus control: 58.8 ± 11.0%, p = 0.597).

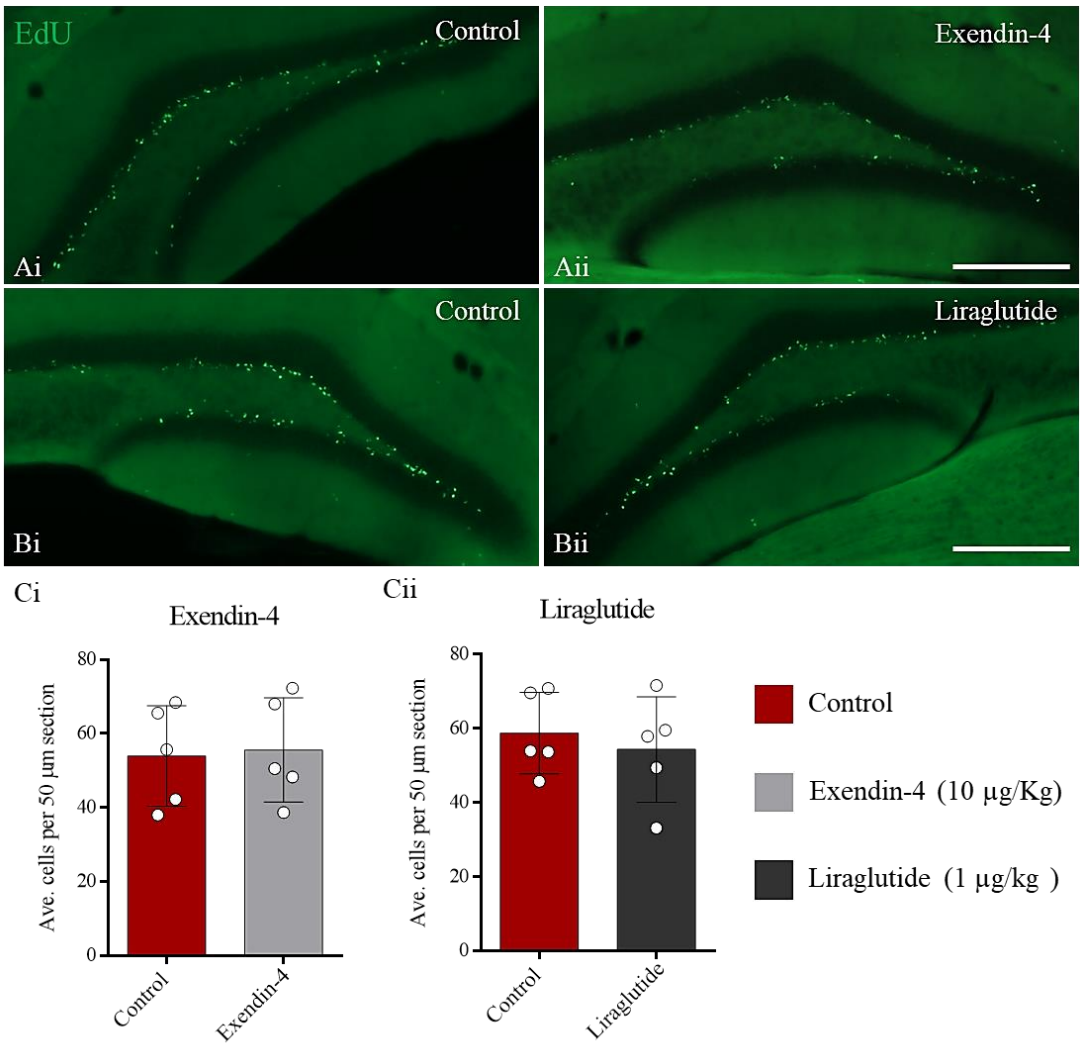

Figure 5.11: *In vivo* injections of exendin-4 or liraglutide does not alter proliferation in the dentate gyrus of the hippocampus.

A. Representative images of the dentate gyrus in a control animal (**i**), and exendin-4 treated animal (**ii**). Scale bar: 500 μm. **B**. Representative images of the dentate gyrus in a control animal (**i**), and liraglutide treated animal (**ii**). Scale bar: 500 μm. **C**. Bar graphs of the average number of EdU positive cells present in a 50 μm thick section of dentate gyrus for exendin-4 (**i**), and liraglutide (**ii**) treated groups with their respective controls. No significant differences can be seen between groups. Statistical analysis: unpaired t-test with Welch's correction.

5.3 DISCUSSION

In this chapter, the effects of GLP-1R agonists on the proliferation of cells within the spinal cord have been investigated using *ex vivo* acute slices, longer term organotypic spinal cord slice cultures, and *in vivo* healthy mouse experiments.

Overall, this research shows that GLP-1R agonists significantly enhance proliferation within the central canal area when applied to all *ex vivo* models over both a short time frame, 5 hours in acute slices, and up to 10 days in culture. This is assumed to be an effect limited to ependymal cells due to their location around the central canal and known proliferative ability following injury (Mothe and Tator, 2005; Meletis et al., 2008). However, as ependymal cells themselves have not been shown to express high levels of GLP-1R mRNA (Russ et al., 2021), nor have been shown to be immunoreactive for the GLP-1R when investigated using transgenic GLP1R-GCaMP3 animals or the GLP-1R antibody (see Chapter 3: section 3.3.2), there is not a straightforward explanation for why ependymal cells are affected in such a way. The implications of this and potential pathways will be discussed in more detail in Chapter 6: General discussion (section 6.2).

Interestingly, the effects of GLP-1R agonists in areas of the spinal cord outside of the central canal appear to vary depending on the mode of delivery. When these drugs were applied directly to the culture media, in the case of both 5- and 10-day OSCSCs, or given in aCSF immediately after slicing, in the case of acute slice experiments, little effect was seen on the number of newly proliferated cells in the grey matter or white matter. When OSCSCs were cultured on a liraglutide loaded hydrogel base, higher numbers of EdU positive cells were observed in most hydrogels examined. This effect was strongest in the white matter area, with an increase in proliferation seen in all hydrogel groups, although enhanced proliferation within the grey matter could also be observed for three out of five hydrogels studied. As this proliferative effect was not observed in OSCSCs cultured on hydrogels without liraglutide it is assumed to be due to a combinatorial effect of liraglutide and hydrogel, perhaps due to the longer exposure of slices to liraglutide over time as it elutes from the hydrogels.

In contrast, when exendin-4 and liraglutide were administered to healthy mice *in vivo* there was a reduction in the total number of newly proliferated cells for both drugs tested. Similar to the hydrogel experiments, this effect appeared to occur predominantly within the white matter for both drugs and a lower proportion of EdU positive cells within these sections were seen to differentiate along an oligodendrocyte lineage. Fewer proliferated cells were also

observed around the central canal, solely in the case of liraglutide. No effects were observed in the dentate gyrus of the hippocampus for either drug.

5.3.1 Acute and slice culture models as simulations of injury response

Organotypic spinal cord slice culture (OSCSC) and acute models allow the study of cellular behaviour in an easily manipulated setting that is more representative of the *in vivo* environment than *in vitro* dissociated cell culture; the overall cytoarchitecture of the spinal cord is conserved, and all endogenous cell types are present. This grants the opportunity to study the cellular response to injury and mechanical insult while minimising the impact on animal use and welfare as multiple conditions can be tested using the same animal.

During preparation, the spinal cord undergoes complete transection both rostral and caudal to the slice resulting in a large mechanical insult and therefore providing access to a representation of the acute phase of spinal cord injury. The slices can then be cultured and maintained *ex vivo* for several weeks, representing the progression from acute injury response to a chronic injury response. While several studies in the literature have maintained OSCSCs *ex vivo* for 7 – 21 days before applying a penetration or contusion injury to the slice to gather information on injury response (Pandamooz et al., 2019; Patar et al., 2019; Lin et al., 2020), this is not strictly necessary in order to study a response to immediate injury.

A study by Pandamooz et al investigated the responses of OSCSC to injury induced solely by the process of acute slice preparation by incubation with propidium iodide on days 1, 3, 5, 7, and 10 after plating. They found that the highest number of dead cells were present on days 1 and 3, with this reducing with time until day 7 where cell death appeared to stabilise (Pandamooz et al., 2019). This is comparable to results obtained in this chapter when control group OSCSCs were treated with propidium iodide to assess the extent of cell death in the slice as the time course progressed; the highest extent of cell death occurred on days 2 and 4, with a peak on day 4 and was then lower for subsequent time points. This loss of cells is very similar temporarily to the progression of cell loss in an *in vivo* model of spinal cord injury, in which most cells are lost in the first 24 – 72 hours post injury (Grossman et al., 2001; Oyinbo, 2011), and therefore may be used as a model of both acute and early stage chronic spinal cord injury.

5.3.2 Treatment with GLP-1R agonists lowers cell death and enhances proliferation within the central canal in *ex vivo* models

In the primary stages of injury, high levels of neuronal and glial apoptosis occur as cells and axonal pathways are directly injured or severed, resulting in a large amount of inflammation, oxidative stress, and necrosis around the site of injury. This is a major obstacle to the recovery from injury and reduces the ability for regeneration within the spinal cord due to the increased presence of inflammatory and inhibitory factors (Oyinbo, 2011).

The research performed within this chapter indicates that the extent of cell death is significantly lower after treatment with liraglutide within the first few days of OSCSC when compared with non-treated controls. Therefore, liraglutide is likely to play a protective role in the acute stages of injury. This is consistent with the neuroprotective role of GLP-1R agonists in the literature, thought to be due to a reduction in cellular apoptosis and correlating increase in autophagy which reduces the extent of secondary damage resulting in a more hospitable microenvironment for cell proliferation and axonal growth (Hölscher, 2014; Chen et al., 2017; Vergès et al., 2022).

Several studies show that GLP-1R agonists are particularly useful for lowering the number of activated astrocytes and microglia that are present after injury, therefore reducing the levels of pro-inflammatory cytokines, such as IL-1α/β and TNF, that are secreted during the secondary injury response (Iwai et al., 2006; Yang et al., 2019; Deng et al., 2022). These cytokines are known to be neurotoxic and therefore reduction in these levels may prevent further neuronal or glia loss, increasing the chances of a more substantial recovery after spinal cord damage (Hölscher, 2014; Poulen et al., 2021; Deng et al., 2022).

GLP-1R agonists have been shown to increase proliferation both *in vitro* (Y. Li et al., 2010), and *in vivo* in several models of neurodegenerative disease and injury (Vergès et al., 2022). Yang et al studied the neuroproliferative effects of the GLP-1R agonist semaglutide in a rat model of ischemic stroke and found higher levels of neurogenesis in the dentate gyrus of animals treated with semaglutide when compared with the injured control group. This higher level of proliferation continued to rise from day 1 post-injury and peak on the 7th day, after which it gradually diminished up until day 28 (Yang et al., 2019). The proliferative response to a GLP-1R agonist in the study by Yang et al is similar to that seen during the investigation of this chapter, although the higher level of proliferation observed over 10 days in experiment 5.2.2.2 appears to be less dependent on time post injury with no significant differences

observed within groups between time points. This could be due to the differences in the extent of injury between the two models, or due to the differences in injury response between an *ex vivo* and *in vivo* model.

In the study by Yang et al they also observed significantly higher levels of nestin, CXCR4, SDF-1 and doublecortin biomarkers in the semaglutide treated group compared with controls which followed this temporal pattern. SDF-1 and its receptor, CXCR4, have multiple functions in the CNS, and have been implicated in neurogenesis as well as having a role in directing progenitor cell migration and axonal guidance (Tysseling et al., 2011; Ling et al., 2022). Interestingly, ependymal cells within the spinal cord express CXCR4 (Tysseling et al., 2011; Russ et al., 2021). Upon injury to the spinal cord, these CXCR4+ ependymal cells migrate towards areas that contain high levels of SDF-1, which is upregulated in injured tissue (Ling et al., 2022). An abundance of CXCR4+ cells were observed to remain in the central canal, indicating that cells within this area may divide in response to injury and one of the progeny migrates towards the injury site in order to not deplete the stem cell niche (Mothe and Tator, 2005; Tysseling et al., 2011). It is possible that this mechanism contributes to the results observed in this chapter, particularly regarding the higher extent of proliferation observed around the central canal area but not in the total slice. However further work to deduce whether these newly proliferated cells are migrated ependymal cells or to discover which lineage they originate from would need to occur before this could be confirmed.

5.3.3 How do OSCSCs interact with hydrogels?

Numerous hydrogels derived from natural and synthetic polymers have been studied in the literature for use as scaffolds providing structural and mechanical support, and also as drug delivery mechanisms transporting pharmacological agents or growth factors directly to the desired area to promote cell survival, proliferation, or migration (Klapka and Müller, 2006; Macaya and Spector, 2012; Assunção-Silva et al., 2015). This research performed in this chapter adds to this body of knowledge, contributing to the understanding of how OSCSCs respond when cultured on different stiffnesses and compositions of hydrogels, as well as the effects of more sustained delivery of liraglutide using a hydrogel delivery system.

5.3.3.1 Mechanical properties of the CNS in health and injury

The spinal cord is thought to have a compressive elastic modulus (also known as the Young's modulus, the most commonly reported measure of compressive material stiffness) of approximately 100 – 2,000 Pa, although there is some debate regarding the validity of this suggested range (Bartlett et al., 2016; Budday et al., 2019).

CNS tissue is highly viscoelastic, meaning that under deformation, it displays a combination of both fluid (viscous) and solid (elastic) behaviours (Ramo et al., 2018b). Because of this, the mechanical properties of the spinal cord cannot be deduced using a standard linear deformation relationship, but instead complex models must be used, frequently utilising finite element analysis or other computational models, to simplify the complexity (Ramo et al., 2018a). One of the main drawbacks of analysing viscoelastic tissue is the inherent stress-strain relationship that exists within this tissue; any modulus value calculated for the tissue is dependent on the particular strain that the tissue is subjected to, and the rate at which this strain is applied. Therefore, instead of one fixed stiffness value being relevant for the entire spinal cord under all conditions, there is a range of values that are dependent heavily on the experimental conditions used during testing (Budday et al., 2019). This can make interpreting results from different sources tricky as not all experimental set ups are the same, nor are they always reported precisely enough to allow direct comparison.

It is important to note that many studies of the mechanical properties of the spinal cord do not include information about the properties of the surrounding pia and dura mater which may contribute largely to the overall spinal cord stiffness and recovery following compression (Ramo et al., 2018b). Many published protocols do not explicitly talk about the removal of the pia or arachnoid mater, usually only focusing on the removal of the dura mater, therefore determining the effects of the meninges on the obtained values is tricky. This, along with the species and age of the animal investigated, and the differing lengths of time taken from extraction of the cord to testing, can partially explain why the proposed mechanical properties of the spinal cord can vary significantly.

Interestingly, the stiffness of the spinal cord also changes after injury. A study by Baumann et al, used atomic force microscopy and determined the stiffness of the uninjured spinal cord to be approximately 450 Pa for the grey matter and approximately 200 Pa for the white matter. Fifteen weeks after a lateral hemisection, the area around the injury site was tested and the Youngs modulus of the grey matter was found to be significantly lower at approximately 180

Pa, representing a 2.6-fold decrease in mechanical stiffness after injury. They hypothesised that the difference in properties was due to a dysregulation of hydrated glycosaminoglycans, including chondroitin sulfate proteoglycans and heparin sulfate proteoglycans, increasing the viscous properties of the spinal cord and therefore decreasing stiffness (Baumann et al., 2020).

The differing mechanical properties of the spinal cord resulted in the choice of a wide range of hydrogel stiffness utilised in this research, with two 'super soft' gels chosen at approximately 100 Pa, two higher stiffness gels at > 1000 Pa, and one middle stiffness gel at 500 Pa. The mechanical stiffness of the PET culture inserts used in this experiment were substantially stiffer at approximately 2 - 3 GPa, far above the proposed highest spinal cord stiffness of 2 kPa.

5.3.3.2 The number of newly proliferating cells in different areas of the OSCSCs varied with the mechanical properties of the hydrogels.

As these hydrogels are proposed for use as a scaffold for OSCSC, the first experiment was to test whether the hydrogels alone had any effect on the number of newly proliferated cells. In the central canal of the spinal cord the highest extent of proliferation was observed in one of the softest gels (Epsilon 4; 100 Pa), but not in the other softest gel (glutamine amide; 85 Pa). This was unexpected as it was assumed that hydrogels with similar mechanical stiffnesses would have a similar effect on proliferation. Therefore, it is assumed that the difference is likely a result of the chemical composition of the hydrogels as they were composed of two different peptides, or due to variances in microstructural architecture (such as porosity and fibre diameter) upon gel formation.

Operating under the assumption that ependymal cells are the cells that proliferate within the central canal area after injury and have neural stem cell (NSC) like properties (Mothe and Tator, 2005), it could be assumed that they would favour similar conditions to those favoured by NSCs harvested from the other known neurogenic niches when grown in culture. A study by Banerjee et al isolated NSCs from the hippocampus of 6-week-old rats and grew these on an array of alginate hydrogels spanning 180 – 19,700 Pa. After 7 days in culture, they found a 14-fold higher number of cells within the softest hydrogel and a two-fold higher number for

the stiffest hydrogel, when compared with the number of originally plated cells (Banerjee et al., 2009). This indicates that NSC proliferation was significantly higher with lower hydrogel stiffness, similar to that observed in the experiment within this chapter.

Within the grey matter of the spinal cord, the highest level of proliferation was observed in the mid-range hydrogel (Gamma 4; 500 Pa). This was significantly higher than that in the two stiffer hydrogels (> 1000 Pa) and the lowest (100 Pa), but was not significantly different than the control OSCSCs cultured directly onto the PET insert. Neuronal differentiation occurs most favourably on hydrogels of lower stiffnesses: Banerjee et al (as mentioned above) found a 20-fold higher level of β-tubulin III expression in NSCs grown on soft substrates compared with stiffer substrates. This is corroborated by studies by Saha et al who found that NSCs cultured on hydrogels with a stiffness of 500 Pa had a 6-fold higher level of β-tubulin III expression compared with 1000 Pa hydrogels (Saha et al., 2008), similar to the changes in extent of proliferation observed in the experiment within this chapter. It could be possible that the enhanced proliferation observed is due to a higher number of neural progenitor cells existing either within the grey matter or migrating to the grey matter.

It is also likely that the proliferation within the grey matter is not due to neural progenitors, but a different cell type such as astrocytes or microglia. Microglia isolated from neonatal rat cortices were found to proliferate much more rapidly on a 600 Pa silicone rubber-based substrate than on a 1 kPa substrate (Blaschke et al., 2020), lending credence to this hypothesis. However, as the phenotypes of the EdU-positive cells in our investigation were not tested this remains as speculation.

No differences in the levels of proliferation were observed in the white matter of any of the hydrogel groups tested, which was a little surprising. Jagielska et al cultured oligodendrocyte progenitor cells (OPC) on a range of polyacrylamide hydrogels between 0.1 – 70 kPa and found a significantly higher level of OPC survival and proliferation within hydrogels of 0.7 kPa and above, and a lower level of proliferation for those below 400 Pa (Jagielska et al., 2012). This difference in proliferation was not observed in the data within this chapter.

5.3.3.3 Liraglutide infused hydrogels enhance proliferation within OSCSCs

It is likely that the higher levels of proliferation observed in OSCSCs cultured on liraglutide-infused hydrogels follows the same principles as discussed above in section 5.3.2.

Unfortunately, propidium iodide experiments to determine the extent of cell death could not be easily reproduced due to the fluctuations in autofluorescence seen with the hydrogel bases. Future experiments could investigate the use of alternative markers of cell death or apoptosis, such as caspase-3, to determine whether the use of liraglutide-infused hydrogels could aid in the reduction of cell death after injury over liraglutide or hydrogels on their own.

In all OSCSCs cultured on liraglutide-infused hydrogels, there were higher levels of proliferation observed within the white matter, which was not seen in OSCSCs cultured on hydrogels alone (Figure 5.8). Neither was this effect seen when OSCSCs were cultured on the standard PET culture insert (as can be seen in Figure 5.1, Figure 5.2, and Figure 5.7) without any hydrogels, but with the addition of liraglutide to the culture media. This indicates that the effect of liraglutide on cells within the white matter is likely due to sustained modulation of the GLP-1R over a more prolonged period of time.

Injury to the spinal cord results in a widespread loss of oligodendrocytes and myelin within the white matter, the degradation of which releases inflammatory compounds and results in further damage to oligodendrocytes and nearby cells (Crowe et al., 1997; Huntemer-Silveira et al., 2021). Several studies have shown that in mouse models of experimental autoimmune encephalitis (EAE), a model that mimics the demyelinating lesions common in multiple sclerosis, treatment with GLP-1R agonists delayed disease onset and progression, reduced inflammation, reduced astrocytic and microglial activation, and ameliorated demyelination (C.-H. Lee et al., 2018; Qian et al., 2022; Song et al., 2022). It could be possible that prolonged treatment with liraglutide encapsulated within hydrogels also ameliorates the loss of myelin, inflammation, and subsequent apoptotic cell death within the white matter of OSCSCs, resulting in greater cell survival and therefore a higher ability to proliferate. It is unclear why this effect is not seen in cultures without liraglutide-infused hydrogels, so further work is needed to elucidate the precise mechanisms behind these results.

5.3.4 GLP-1R agonists *in vivo* result in lower spinal cord cell proliferation

This series of experiments was set up to determine the effects of exendin-4 and liraglutide on cell proliferation and differentiation *in vivo*. Exendin-4 is a short acting GLP-1R agonist with a half-life of approximately 2-5 hours when administered intraperitoneally, whereas liraglutide has a longer half-life of approximately 9 – 12 hours under the same conditions

(Knudsen et al., 2000). Both drugs were given once per day over 4 days, at a dose of 10 μg/kg and 1 μg/kg respectively.

Interestingly and somewhat unexpectedly, both drugs resulted in similar outcomes with an overall lower total number of EdU positive cells present within the spinal cord slices, an effect predominantly caused by a lower number of newly proliferated cells within the white matter. The main point of difference between the two drugs was that cell proliferation around the central canal was lower in the group treated with liraglutide, but not exendin-4. As liraglutide has a longer half-life than exendin-4, it was hypothesised that this drug would display more of an effect, this was only found to be true in this area.

When the colocalisation of the cells positive for EdU was considered, both drugs showed significantly lower proportions of cells that also expressed an oligodendrocyte marker. This was expected, given the lower number of EdU positive cells present within the white matter. As described above (section 5.3.3.3), GLP-1R agonists play a protective role in the white matter in models of EAE, it is possible that the lower number of newly proliferated cells observed in this experiment is due to a preference towards cell survival rather than increased renewal or proliferation.

5.3.4.1 A result of GABAergic signalling?

It is possible that the lower levels of proliferation observed throughout the spinal cord, and around the central canal of the spinal cord in particular due to the presence of CSFcNs, is due to the exocytosis stimulating effects of GLP-1R agonists on GABAergic cells within the spinal cord.

A large proportion of GLP-1R positive cells within the CNS are GABAergic neurons (Chapter 3: section 3.2.2.2, Rebosio et al., 2018; Zheng et al., 2019), and application of GLP-1R agonists has been found to exert a multiplicity of excitatory and inhibitory effects on these neurons, depending on the concentration, duration, and location of the drug given and neurons studied (S. J. Lee et al., 2018; Rebosio et al., 2018; Povysheva et al., 2021). Importantly, Rebosio et al show that in purified synaptosomal preparations of hippocampal boutons, exendin-4 promotes the release of GABA which is abolished by application of the antagonist (Rebosio et al., 2018).

No studies within the literature have focused on the effects of GLP-1R stimulation on GABAergic neurons within the spinal cord, but it could be proposed that if GLP-1R agonists increased the levels of GABA then the result would be fewer newly proliferated cells. New et al show that healthy mice treated with GABA transaminase inhibitor Vigabatrin, which increases endogenous GABA levels, resulted in significantly lower proliferation within all areas of the spinal cord. This result is similar to that observed through the experiments detailed here, although further work would need to be undertaken to identify whether this mechanism is responsible and why particularly oligodendrocytes appear to be affected.

5.3.4.2 A result of peripheral effects?

A study by Andersen et al used a GLP-1R tdTomato transgenic mouse line to identify the presence of the GLP-1R within cells of the stomach, heart, smooth muscle of arteries, liver, lungs, and thyroid, which indicates a possibility for several unexpected effects when administered peripherally (Andersen et al., 2021). Indeed, GLP-1R agonists are widely known for their pleiotropic effects, which can include stimulating insulin release, increasing heart rate and blood pressure, and reducing blood glucose levels (Yamagishi and Matsui, 2011; Rowlands et al., 2018). Many of these effects may induce as of yet unknown effects on proliferation within the CNS, and therefore the influence of peripheral effects cannot be ruled out.

5.3.4.3 GLP-1R agonists showed no change in proliferation within the hippocampus

Perhaps the most surprising result from this study was the lack of difference in proliferation observed within the dentate gyrus of the hippocampus. Previous studies have shown that GLP-1R agonists enhance proliferation within this area, when administered both directly to the CNS or peripherally. Bertilsson et al gave intraperitoneal injections of 1 μg/kg of exendin-4 twice daily for 7 days and saw significantly higher numbers of BrdU positive cells and Dcx positive cells within the dentate gyrus. A similar result was seen when 1 μg/kg was administered twice daily for 21 days (H. Li et al., 2010). However, Isacson et al found that intraperitoneal administration of the same dose of exendin-4, but over 3 days, did not result in significantly higher levels of hippocampal proliferation (Isacson et al., 2011). It is possible that the lack of observed significance in the results of our experiments are due to differences

in dosage schedule, due to the twice daily administration in the literature studies and once daily in these experiments, or the duration of the experiment not being long enough. It would be interesting to study whether twice daily dosing over a longer time period would lead to different results in spinal cord cell proliferation than those observed here.

Alternatively, the method of proliferation detection may play a role in the lack of significance of our results. Parthsarathy and Hölscher gave mice once daily liraglutide (10 μg/kg) intraperitoneally for 7 days and did not observe any significant differences in the number of BrdU positive cells within the hippocampus. However, upon staining for Ki67, a marker of active cell proliferation which is absent from quiescent cells, they observed significantly higher numbers of positive cells within the dentate gyrus indicating a move from quiescence to proliferation. However, in mice treated with the same dose of liraglutide daily for 37 days, an enhancement in both BrdU and Ki67 staining could be observed (Parthsarathy and Hölscher, 2013). It could be possible that these cells were primed for active proliferation, but had not reached the stage in the cell cycle in which BrdU is incorporated into the DNA. As Ki67 staining was not utilised in our experiments it is impossible to say whether the same results would be observed in this case.

5.3.5 Conclusion

Research within this chapter found that GLP-1R agonists significantly enhanced proliferation within the central canal area in all *ex vivo* models, whereas the effects of GLP-1R agonists on other spinal cord areas varied depending on the mode of delivery, with hydrogel-based delivery showing enhanced proliferation in white and grey matter in some cases. Somewhat surprisingly, *in vivo* administration of exendin-4 and liraglutide in healthy mice led to a reduction in the total number of newly proliferated cells, predominantly in the white matter, with fewer cells differentiating into oligodendrocytes.

This research contributes novel information regarding the impact of GLP-1R agonists on proliferation within the spinal cord, yet raises further questions regarding the mechanisms behind this effects which will require further investigation. Ideas for future research are outlined in chapter 6: general discussion (section 6.6).

Chapter 6 – General Discussion

6.1 SUMMARY

The GLP-1 system has been implicated in various aspects of CNS function, with activation of GLP-1Rs being shown to promote neurogenesis, enhance neuronal survival and attenuate neuroinflammation in various animal models of neuronal injury and disease (Erbil et al., 2019; Nizari et al., 2021; Monti et al., 2022). Within the spinal cord, most adult neurogenesis takes place inside the ependymal layer that surrounds the central canal so this research sought to determine if the GLP-1 system was also implicated in spinal neurogenesis.

Ependymal cells (ECs) within this layer possess NSC like properties, self-renewing for population maintenance and proliferating rapidly in response to injury (Meletis et al., 2008; Moreno-Manzano, 2020). While mRNA for the GLP-1R has been found within many neuronal and glial cells throughout the spinal cord (Merchenthaler et al., 1999; Russ et al., 2021), little is known about the cell specific expression of this receptor within the ependymal cell layer area. Of particular interest are the CSFcNs, enigmatic cells, which neighbour ECs and express GLP-1R mRNA (Russ et al, 2021). The research presented within this thesis is the first to explore the relationship between the GLP-1R and CSFcNs, with a focus on the role of these two components in influencing spinal cord neurogenesis.

In the first chapter, immunohistochemistry revealed that approximately 80% of CSFcNs express the GLP-1R, the distribution of which is the same throughout the spinal cord. A substantial number of CSFcNs in the thoracic region received direct appositions from axons of GLP-1 producing neurons, indicating a possibility that these cells are integrated into the wider GLP-1 network.

To test for potential functional effects of GLP-1R activation on CSFcN activity, the second chapter describes the effects of GLP-1R agonists on CSFcN intracellular Ca^{2+} levels through calcium imaging studies. These cells displayed a concentration-dependent response to liraglutide, largely responding by increasing the frequency and decreasing the amplitude of Ca^{2+} spiking events in response to immediate liraglutide application. Prolonged exposure to liraglutide resulted in complete silencing of Ca^{2+} spiking activity in a number of CSFcNs, which was reversible after extended washing with aCSF.

The final results chapter investigated the effects of GLP-1R agonists on the proliferation of cells within the spinal cord using *ex vivo* acute slices, longer term OSCSCs, and *in vivo* healthy mouse experiments. In acute and cultured spinal cord slices, application of GLP-1R agonists resulted in more proliferating cells in the ependymal cell layer compared to control

experiments, but effects on cell proliferation outside of this area were only observed when OSCSCs were cultured on hydrogels infused with liraglutide. *In vivo* studies found that both exendin-4 and liraglutide applications resulted in fewer labelled proliferating cells, specifically within the ependymal cell layer and the white matter.

In summary, research presented within this thesis demonstrates that CSFcNs express the GLP-1R, respond to bath application of GLP-1 agonists through changes in their intracellular Ca^{2+} concentrations, and that GLP-1 agonists influence neurogenesis within the central canal area of the spinal cord.

6.2 THE EFFECTS OF GLP-1R AGONISTS ON CELL PROLIFERATION

Throughout this thesis, the relationship between GLP-1 signalling and spinal neurogenesis has been explored, with CSFcNs being implicated in this process. Here, a potential mechanism underlying this process will be proposed.

In chapter 3, immunohistochemistry was used to identify cells within the ependymal layer that showed immunoreactivity for GLP-1R. While ECs may contain limited mRNA for GLP-1R (as shown in Chapter 3, Figure 3.1), they do not express this receptor at a detectable level, and such expression is unlikely to hold functional significance. In contrast, CSFcNs not only display substantial mRNA expression of GLP-1R but also exhibit detectable levels of this receptor protein on both their cell bodies and CSF-contacting end bulbs.

Activation of these receptors was shown to modulate the calcium activity of CSFcNs, resulting in an increased frequency of Ca^{2+} spiking in the short term, and silencing of CSFcN calcium activity in approximately half of CSFcNs, when applied over a prolonged period of time. This is particularly intriguing as previous studies have linked GLP-1R activation to exocytotic pathways (Drucker et al., 1987; Rebosio et al., 2018; Graham et al., 2020; González-Santana et al., 2021). This change in Ca^{2+} spiking may signify an initial increase in exocytosis of compounds from CSFcNs, which is followed by a substantial reduction upon continuous exposure.

While the notion of CSFcNs releasing compounds into the cerebrospinal fluid has been a long-standing hypothesis, it has remained relatively unproven as of yet. However, the presence of synaptic proteins known to be involved in calcium-triggered vesicle release, such as SV2 and synaptophysin (Chapter 3, Figure 3.8; Conte et al., 2008; Wu et al., 2021), on the end bulbs of CSFcNs, coupled with their possession of the necessary machinery for the synthesis and release of GABA, including VGAT and GAD65/67 (Orts-Del'immagine et al., 2012; Corns et al., 2013; Johnson et al., 2023), strongly implies that this is one of the possible functions.

Should GLP-1R activation lead to an enhanced release of GABA from CSFcNs, it's plausible that GABA receptors on neighbouring ECs might become engaged. An investigation by Corns et al., employing whole cell patch clamp electrophysiology in rat spinal cord, illustrates that ECs respond to GABA application by undergoing depolarisation. This effect is partly mediated through the $GABA_A$ receptor (Corns et al., 2013). While the specific consequences of this depolarisation were not explored in that study, it's established that

elevating ambient GABA levels within the central nervous system (CNS) inhibits proliferation and restricts progression through the cell cycle in various types of progenitor cells, including the ECs (Liu et al., 2005; Tozuka et al., 2005; New et al., 2023).

Hypothetically, if prolonged GLP-1R activation results in the silencing of CSFcNs, it could entail a reduction in GABA exocytosis and subsequently lead to decreased ambient GABA levels in the CSF and the immediate vicinity of ependymal cells. This reduction in GABA concentration could potentially trigger an increase in ependymal cell proliferation, similar to that observed in the *ex vivo* experiments conducted within this thesis.

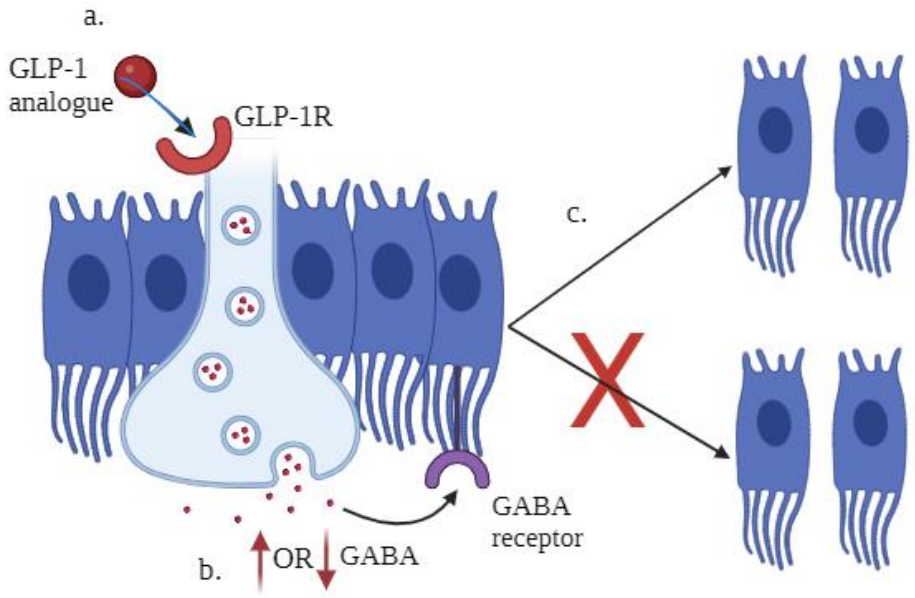

Figure 6.1: Proposed mechanism behind CSFcN mediated proliferation of ependymal cells.
GLP-1R agonists bind to the GLP-1R on CSFcNs (**a**), resulting in an immediate increase in calcium activity, which leads to exocytosis of GABA which interacts with the GABA receptors on neighbouring ECs (**b**). After prolonged activation of the GLP-1R, the calcium mediated exocytosis is reduced, and GABA transmission is halted. If the ambient GABA levels are increased, then EC proliferation is inhibited, and the cell remains quiescent. If GABA levels are decreased, then ECs are no longer inhibited, and some proliferation may occur (**c**).

6.3 How do CSFcNs fit into the wider GLP-1 network?

The research presented within this thesis delves into the involvement of CSFcNs in the GLP-1 pathway, network, and signalling within the murine spinal cord. It provides valuable insights into the localisation of GLP-1R in CSFcNs and their connections with PPG neurons, shedding light on their potential role in the broader GLP-1 system.

Moreover, this study underscores regional variations in PPG neuron appositions onto CSFcNs, which may suggest distinct functions for GLP-1R-positive CSFcNs in different spinal cord regions. In particular, CSFcNs in the thoracic region may play a more prominent role in spinal circuitry, potentially responding to GLP-1 release in their vicinity. This could be linked to the increased heart rate mediated by spinal GLP-1 innervation of sympathetic preganglionic neurons (SPNs) (Llewellyn-Smith et al., 2015; Trapp and Cork, 2015; Holt et al., 2020), and may suggest a complex feedback loop that encompasses CSFcNs, SPNs, and PPG neurons, all contributing to the spinal GLP-1 network (Discussed further in Chapter 3: section 3.4.2).

Furthermore, the presence of GLP-1R positive cells not receiving direct PPG neuron appositions implies their potential response to non-synaptic GLP-1 transmission, likely through their proximity to the CSF. This raises intriguing questions about how, and why, CSFcNs might sense and modulate CSF composition in the context of the GLP-1 signalling pathway.

In summary, this research provides valuable insights into the involvement of CSFcNs in the GLP-1 pathway, network, and signalling, with potential implications for autonomic functions and the regulation of homeostasis. However, substantial further exploration is needed to fully understand the intricate roles these cells play in the broader GLP-1 system.

6.4 APPLICABILITY TO HUMAN STUDIES

There is great debate over the cellular composition, cytoarchitecture, and proliferative capacity of the human adult spinal cord. Studies have revealed inconsistencies in the patency of the central canal in the adult human spinal cord compared to commonly studied rat and mouse spinal cords (Milhorat et al., 1994; Saker et al., 2016; Torrillas de la Cal et al., 2021). Autopsy investigations and MRI scans have shown that the central canal tends to close partially or completely with age, with most individuals experiencing at least partial closure by adolescence (Milhorat et al., 1994; Torrillas de la Cal et al., 2021). This closure is associated with a dense accumulation of cells in the ependymal region, including glial cells expressing GFAP, vimentin-positive ECs, and CD15-expressing cells (Saker et al., 2016). Notably, ECs were observed around pseudo-canals and perivascular pseudo-rosettes, a feature also found in ependymomas (Saker et al., 2016; Torrillas de la Cal et al., 2021).

However, recent RNA profiling of ECs has revealed the conservation of numerous transcription factors and genes between adult humans and rodents indicating the potential for similarly conserved functionality between mammalian species (Rosenberg et al., 2018; Ghazale et al., 2019). *In vitro* studies have further demonstrated the multipotent potential of human stem cells. One such study conducted by Dromard et al, discovered heterogenous expression of sox2, CD15, Nkx6.1, and PSA-NCAM in cells within the ependymal layer of the central canal of the human spinal cord, indicating proliferative potential. Upon dissociation and culturing of these cells in a medium containing supplemental epidermal growth factor (EGF) and basic fibroblast growth factor (bFGF), they found consistent formation of neurospheres which contained proliferative precursors which could generate glial and neuronal cells (Dromard et al., 2008). A similar study by Mothe et al also found multipotent and self-renewing NSCs within the adult human spinal cord (Mothe et al., 2011). The question of whether these cells respond in a manner analogous to animal models remains unknown and requires further investigation.

While it is possible that the research provided within this thesis may not be therapeutically applicable to human EC proliferation, it is important to note the potential usefulness of this research in other degenerative conditions. Several GLP-1R agonists have gained FDA approval and are currently being explored for human therapeutic use for a variety of neurodegenerative conditions (detailed in chapter 1: general introduction, section 1.3.4, Zhang et al., 2021; Kopp et al., 2022). As of yet, there have been no human studies regarding

the therapeutic benefits of GLP-1 modulation within SCI, but the promising results from animal studies and human neurodegenerative studies indicate that this may be an avenue worth further exploration.

Although all care was taken to ensure experiments conducted in this research were designed and carried out with the utmost care there are some limitations and technical considerations.

6.5.1 The use of spinal cord slices in both acute and culture conditions

Spinal cord slices are commonly used in electrophysiological and calcium imaging studies, as well as in OSCSCs, to study properties and functions of cells and their networks. Slice models offer distinct advantages over isolated cell cultures because they maintain the structural integrity and local neural circuits within the tissue slice (Lin et al., 2020). The cells of interest are easily accessible, allowing direct access for electrophysiological studies, or allowing for the imaging of many neurons simultaneously in calcium imaging experiments. Experimental conditions are also easier to control, with less unknown variables than in *in vivo* conditions.

However, there are associated disadvantages. Preparation of slices may sever some descending/ascending axons, leading to the deterioration and death of affected cells, as well as a loss of synaptic inputs onto the cells of interest. In an attempt to counteract this, ice-cold sucrose-based aCSF solution was used during spinal cord extraction, and the spinal cord was consistently kept chilled throughout the preparation process to minimize cell death from excitotoxicity. Balancing efficiency of spinal cord extraction with the preservation of spinal cord integrity was a top priority in the preparation process, hence the method of spinal cord extrusion was chosen over more traditional dissection methods (discussed in chapter 2: general methods, section 2.4).

While CSFcNs have fewer processes compared to many neurons or astrocytes, making them perhaps more resilient to the slicing procedure, they may still experience interruptions in their synaptic inputs, such as descending input from GLP-1 neurons. Even if the cells of interest remain unharmed, local environmental changes could induce alterations within these cells. The absence of synaptic inputs, and indeed of any native CSF, could result in varying levels of neurotransmitters released from tonically active neurons or glial cells around ECs and CSFcNs, altering base levels of excitability/inhibition during recordings and changing CSFcN responses to stimulation.

6.5.1.1 OSCSCs

Control over the extracellular environment in the culture model was maintained by manipulating the culture medium for the slices. In this study, the medium was transitioned to a serum-free formulation after 24 hours in culture. This change not only slowed the growth of astrocytes but also allowed for precise determination of the culture medium's composition, as serum may contain undefined components that affect cell activity (Stoppini et al., 1991; Daniel et al., 2016).

One significant practical and ethical advantage of the organotypic culture model over *in vivo* studies is the possibility to conduct numerous experiments using spinal cord tissue obtained from a single animal, thereby reducing the number of animals required. Each set of experiments included both control and drug-treated slices from the same animal, accounting for any potential inter-animal variability. Additionally, this model allows for the assessment of adverse effects on cell viability caused by drugs without subjecting animals to potential suffering. These factors contribute to the growing popularity of organotypic spinal cord and brain cultures as *ex vivo* tissue models for studying neurological diseases (Croft et al., 2019), injuries (Krassioukov et al., 2002; Pandamooz et al., 2019; Lin et al., 2020), and the neurogenic potential of transplanted stem cells (Kim et al., 2010; Xiao et al., 2019). However, OSCSCs cannot fully replicate all *in vivo* properties, such as a drug's ability to penetrate the blood-brain barrier or its toxic effects on other tissues. Therefore, follow-up *in vivo* studies are necessary.

6.5.2 The use of EdU as a marker of proliferation

Central to these investigations was the need for a reliable marker to identify and quantify cell proliferation in both *ex vivo* and *in vivo* investigations. To address this, the thymidine analogue known as EdU was employed to detect newly synthesized DNA during the S-phase of mitosis enabling visualisation of cells using a fluorescent azide (see chapter 2: general methods, section 2.3.2, for a detailed protocol).

EdU was chosen as an alternative to the more conventional BrdU for several reasons. Firstly, the EdU labelling process was quicker and gentler on the delicate organotypic slices (Zeng et al., 2010). Secondly, BrdU processing involves denaturing DNA through heat or acid

treatment, which can potentially harm other antigens, leading to disruption of tissue structure and reduced antigen detection (Rakic, 2002; Chehrehasa et al., 2009).

While EdU offers the advantage of highly sensitive detection of proliferating cells, it's important to note that prolonged exposure to EdU *in vitro* may affect cell viability (Diermeier-Daucher et al., 2009; Colquhoun, 2019). However, since the studies in this research involved only short-term EdU exposure of up to 5 days *in vivo* and 24 hours in culture, it is unlikely to have been a significant concern. Nonetheless, it's advisable to assess cellular viability when considering longer-term studies, a point to bear in mind for any future research involving extended time frames.

6.5.3 The use of animals in research

Although the use of animals in this research was unavoidable, every effort was taken to uphold the three R's of refinement, replacement, and reduction. Where possible, experiments were performed using OSCSCs and acute slices so many conditions could be tested using the same animals, reducing the overall number required. Tissue was also shared between researchers within the group as much as possible.

Research within this thesis has focused on the link between CSFcNs and the GLP-1 system in the spinal cord, indicating that CSFcNs possess functional GLP-1Rs that can modulate the calcium activity of these cells. The neuroprotective and proliferative effects of GLP-1R agonists were also confirmed using *ex vivo* models. While this is interesting, potentially leading the way for new therapeutic approaches to spinal cord injury and neurodegenerative conditions, further research is needed to fully understand the mechanisms and factors behind the results obtained in this research. Some ideas for future investigations are outlined in this section.

6.6.1 What are the mechanisms and network effects behind the response of CSFcNs to liraglutide?

6.6.1.1 Presynaptic effects

In chapter 4, the direct effects of GLP-1R stimulation on the frequency and amplitude of calcium events in CSFcNs were investigated. It was found that bath application of liraglutide resulted in a concentration-dependent modulation of CSFcN activity, and prolonged application over 3 minutes caused the loss of spontaneous activity in many of these neurons. It would be interesting to further investigate whether this effect was solely due to the activation of the GLP-1R on CSFcNs, or whether this is due to regulatory feedback from other cells that synapse onto CSFcNs. It could also be possible that this is a form of autoregulation by CSFcNs, as they are known to form synapses with other CSFcNs in the network (Nakamura et al., 2023). Perhaps CSFcNs release GABA when stimulated, an abundance of which has inhibitory actions onto other CSFcNs or indeed results in autoregulation of the originating CSFcN? Co-application of a synaptic blockade cocktail and liraglutide could be performed in order to further determine any indirect or autoregulatory effects. Furthermore, the specific receptors and neurotransmitters could be narrowed down using individual selective receptor antagonists, such as gabazine to block GABAergic receptor activation, allowing for the precise elucidation of the mechanisms involved.

6.6.1.2 Influence of calcium channels

In the paper by Johnson et al, different types of calcium channel influenced the Ca^{2+} spiking of CSFcNs in response to stimulation by different neurotransmitters. They found that larger amplitude spikes were generated under control of high voltage-activated (HVA) Cd^{2+} sensitive Ca^{2+} calcium channels, whereas smaller amplitude spikes were generated by T-type calcium channels (Johnson et al., 2023). Given the apparent decrease in amplitude of Ca^{2+} spikes seen during application of liraglutide in chapter 4 (section 4.3.2), it would be interesting to investigate the roles of the various calcium channels in this response. This could be done through the co-application of liraglutide and various calcium channel blockers such as Cd^{2+}, to block HVA channels, and ML218 to block T-type Ca^{2+} channels. This investigation would yield further investigation regarding the cellular mechanisms behind the CSFcN response to liraglutide, as well as potentially furthering the knowledge regarding the expression of different calcium channels on CSFcNs and their activity in general.

6.6.1.3 Electrophysiological investigations

Another important further experiment, that was not performed in this thesis due to time constraints, would be the electrophysiological investigation of liraglutide on CSFcNs. Through the use of patch-clamp electrophysiology, the hyperpolarizing vs depolarising effects of GLP-1R stimulation could be deduced, further contributing critical information about the integration of CSFcNs into the GLP-1 network and further information regarding CSFcNs and their subtypes in general.

6.6.2 Do CSFcNs release compounds in response to stimulation of GLP-1Rs?

The central question of whether CSFcNs are capable of releasing compounds into the CSF, and if so, what the nature of these compounds is, remains unanswered as of yet. This could be answered experimentally using a few different methods.

Firstly, samples of CSF could be taken before and after stimulation of CSFcNs, and measured using microdialysis and HPLC techniques. To ensure only CSFcNs are influenced, chemogenetic activation of designer receptor exclusively activated by designer drugs (DREADD) expressed exclusively in CSFcNs could be used. This could be performed

through the crossing of PKD2L1-Cre mice with a flexed-DREADD mouse line to selectively activate (hM3Dq-DREADD) or inhibit (hM4Di-DREADD) CSFcNs, and use of the DREADD specific ligand clozapine N-oxide (Zhu and Roth, 2015; Zhang et al., 2022). This method is well established in the literature, the high sensitivity and selectivity of this method would allow for the quantification of changes in concentrations of several different neurotransmitters simultaneously (Zapata et al., 2009; Cifuentes Castro et al., 2014; Pencheva et al., 2022). However, this method can be time consuming, due to the collection of CSF and sample preparation required, and has poor temporal resolution.

A second method, that would allow for more specific detection of neurotransmitter release from CSFcNs is the use of Cre-inducible viral vectors. One example would be the use of a PKD2L1-cre mouse line and the iGABASnFR virus, which is composed of a genetically encoded GABA sensor bound to a circularly permuted fluorescent protein which fluoresces in response to the synaptic release of GABA (Marvin et al., 2019). Changes in fluorescence intensity could then be visualised using acute slices under a high-powered fluorescence microscope. Preliminary research in the Deuchars lab has tested this approach and found that limited transfection of CSFcNs is possible (Figure 6.2, A). When these cells were stimulated by ACh there was a distinct increase in fluorescence within the endbulb (Figure 6.2, B), but not the soma or dendrite-like process, indicating that GABA is released from the endbulb. Unfortunately, due to time constraints and technical difficulties, this could not be fully explored, but would be interesting to investigate further.

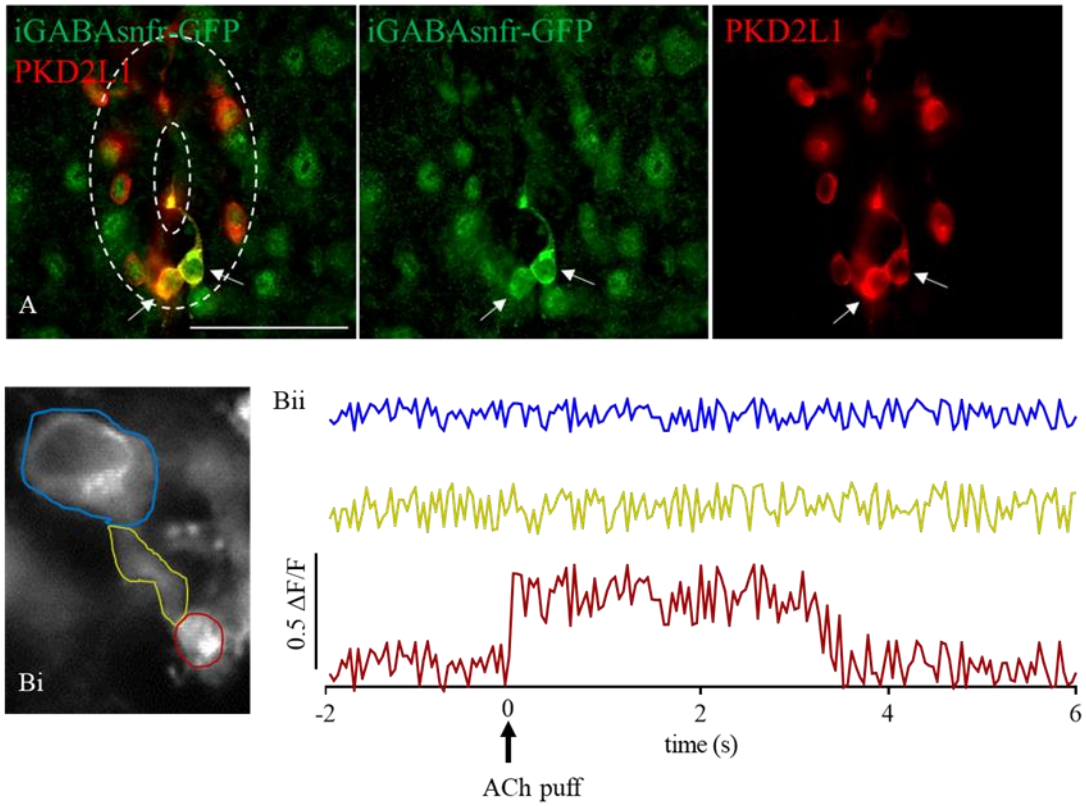

Figure 6.2: Expression of iGABASnFR virus in CSFcNs.

A. Image of merged, iGABASnFR (enhanced with GFP), and PKD2L1-IR in a PKD2L1-cre lumbar spinal cord section. iGABASnFR can be seen expressed only in a small number of ventral CSFcNs.

B. Image of a single CSFcN (N=1) expressing the iGABASnFR under a two-photon microscope (i), with corresponding traces from the somata, process, and endbulb showing GABA release in response to ACh (ii).

6.6.3 Does activation/inhibition of CSFcNs alter proliferation in the spinal cord?

An effective approach for investigating the impact of activation of CSFcNs on spinal cell proliferation could involve employing chemo- or opto-genetic techniques to either activate or inhibit these neurons. For instance, channelrhodopsins (ChRs) represent a widely used tool for probing neuronal function as they can respond to specific light wavelengths, inducing neuronal activation through the transport of cations across the plasma membrane (Möglich and Hegemann, 2011). By generating a mouse strain with ChRs exclusively expressed in CSFcNs, these cells can be activated in acute slices using light. By adding EdU to the aCSF, a methodology similar to the one described in Chapter 5 (section link) can be implemented to

assess proliferation within acute spinal cord slices. This approach offers the advantage of evaluating the influence of CSFcNs directly while bypassing potential off-target effects associated with GLP-1R agonists on other cell types.

Alternatively, the PKD2L1-DREADD mouse model could also be used in this instance, as described above. This setup enables the direct stimulation or inhibition of CSFcNs through treatment with the DREADD agonist clozapine n-oxide (Zhu and Roth, 2015; Zhang et al., 2022). Subsequently, the effects on proliferation can be assessed using EdU. This experimentation can be conducted either *ex vivo* using cultured slices or *in vivo*, facilitating the assessment over an extended time frame.

6.6.4 Does treatment with liraglutide affect proliferation of cells within an *in vivo* SCI model?

In Chapter 5, the study observed that GLP-1R agonists had a positive impact on proliferation in *ex vivo* models. Notably, this effect was even more pronounced when OSCSCs were cultured on hydrogels infused with liraglutide. Given the growing interest in the utilization of biomaterials as scaffolds for spinal cord repair (Haggerty et al., 2018; Koffler, 2019), a prospective experiment could entail investigating whether hydrogels infused with GLP-1R agonists lead to increased proliferation within an *in vivo* spinal cord injury (SCI) model, as opposed to using injections of either GLP-1R agonists or hydrogels alone. Moreover, exploring the specific cell types that proliferate in response to this treatment, through co-labelling or lineage tracing experiments, could provide valuable insights into the therapeutic potential of GLP-1R agonists for central nervous system injuries.

6.7 CONCLUSION

The research presented in this thesis provides the first evidence of GLP-1R expression within CSFcNs. These enigmatic cells within the ependymal cell layer of the spinal cord respond to bath application of GLP-1R agonists through changes in their intracellular Ca^{2+} concentrations, although further research is required to determine whether these effects are fully due to direct stimulation of the GLP-1R. Furthermore, CSFcNs receive direct appositions from PPG neurons onto their somata and processes, predominantly within the thoracic region, indicates potential integration into the wider GLP-1 network. Application of GLP-1R agonists in *ex vivo* spinal cord models resulted in a significant enhancement of proliferation around the central canal area, a response attributed to ECs present within this area that exhibit characteristics resembling neural stem cells. However, as ECs themselves lack GLP-1R expression, this is proposed to be a result of signalling through neighbouring CSFcNs, although further work is needed to explore this link.

Overall, this thesis proposes a link between CSFcNs and the GLP-1 system within the spinal cord, contributing to a wider understanding of the potential therapeutic applications of GLP-1 analogues in traumatic injury and neurodegenerative conditions.

References

Abbott, L.C., Nigussie, F., 2020. Adult neurogenesis in the mammalian dentate gyrus. Anat Histol Embryol 49, 3–16. https://doi.org/10.1111/ahe.12496

Acuna-Goycolea, C., van den Pol, A., 2004. Glucagon-Like Peptide 1 Excites Hypocretin/Orexin Neurons by Direct and Indirect Mechanisms: Implications for Viscera-Mediated Arousal. J Neurosci 24, 8141–8152. https://doi.org/10.1523/JNEUROSCI.1607-04.2004

Agduhr, E., 1922. Über ein zentrales Sinnesorgan (?) bei den Vertebraten. Z. Anat. Entwickl. Gesch. 66, 223–360. https://doi.org/10.1007/BF02593586

Agnati, L.F., Fuxe, K., Zoli, M., Ozini, I., Toffano, G., Ferraguti, F., 1986. A correlation analysis of the regional distribution of central enkephalin and β-endorphin immunoreactive terminals and of opiate receptors in adult and old male rats. Evidence for the existence of two main types of communication in the central nervous system: the volume transmission and the wiring transmission. Acta Physiologica Scandinavica 128, 201–207. https://doi.org/10.1111/j.1748-1716.1986.tb07967.x

Alcántara, A.I., Morales, M., Delgado, E., López-Delgado, M.I., Clemente, F., Luque, M.A., Malaisse, W.J., Valverde, I., Villanueva-Peñacarrillo, M.L., 1997. Exendin-4 agonist and exendin(9-39)amide antagonist of the GLP-1(7-36)amide effects in liver and muscle. Arch Biochem Biophys 341, 1–7. https://doi.org/10.1006/abbi.1997.9951

Alfaro-Cervello, C., Soriano-Navarro, M., Mirzadeh, Z., Alvarez-Buylla, A., Garcia-Verdugo, J.M., 2012. Biciliated ependymal cell proliferation contributes to spinal cord growth. J. Comp. Neurol. 520, 3528–3552. https://doi.org/10.1002/cne.23104

Alhadeff, A.L., Grill, H.J., 2014. Hindbrain nucleus tractus solitarius glucagon-like peptide-1 receptor signaling reduces appetitive and motivational aspects of feeding. Am J Physiol Regul Integr Comp Physiol 307, R465-470. https://doi.org/10.1152/ajpregu.00179.2014

Alizadeh, A., Dyck, S.M., Karimi-Abdolrezaee, S., 2019. Traumatic Spinal Cord Injury: An Overview of Pathophysiology, Models and Acute Injury Mechanisms. Front Neurol 10, 282. https://doi.org/10.3389/fneur.2019.00282

Alvarez, E., Roncero, I., Chowen, J.A., Thorens, B., Blázquez, E., 1996. Expression of the glucagon-like peptide-1 receptor gene in rat brain. Journal of Neurochemistry 66, 920–927. https://doi.org/10.1046/j.1471-4159.1996.66030920.x

Alvarez-Buylla, A., García-Verdugo, J.M., 2002. Neurogenesis in Adult Subventricular Zone. J. Neurosci. 22, 629–634. https://doi.org/10.1523/JNEUROSCI.22-03-00629.2002

An, F.-M., Chen, S., Xu, Z., Yin, L., Wang, Y., Liu, A.-R., Yao, W.-B., Gao, X.-D., 2015. Glucagon-like peptide-1 regulates mitochondrial biogenesis and tau phosphorylation against advanced glycation end product-induced neuronal insult: Studies in vivo and in vitro. Neuroscience 300, 75–84. https://doi.org/10.1016/j.neuroscience.2015.05.023

Andersen, D.B., Grunddal, K.V., Pedersen, J., Kuhre, R.E., Lund, M.L., Holst, J.J., Ørskov, C., 2021. Using a Reporter Mouse to Map Known and Novel Sites of GLP-1 Receptor Expression in Peripheral Tissues of Male Mice. Endocrinology 162, bqaa246. https://doi.org/10.1210/endocr/bqaa246

Andersen, O., Fahrenkrug, J., Wikkelsø, C., Johansson, B.B., 1984. VIP in cerebrospinal fluid of patients with multiple sclerosis. Peptides 5, 435–437. https://doi.org/10.1016/0196-9781(84)90249-3

Assunção-Silva, R.C., Gomes, E.D., Sousa, N., Silva, N.A., Salgado, A.J., 2015. Hydrogels and Cell Based Therapies in Spinal Cord Injury Regeneration. Stem Cells Int 2015, 948040. https://doi.org/10.1155/2015/948040

Athauda, D., Maclagan, K., Skene, S.S., Bajwa-Joseph, M., Letchford, D., Chowdhury, K., Hibbert, S., Budnik, N., Zampedri, L., Dickson, J., Li, Y., Aviles-Olmos, I., Warner, T.T., Limousin, P., Lees, A.J., Greig, N.H., Tebbs, S., Foltynie, T., 2017. Exenatide once weekly versus placebo in Parkinson's disease: a randomised, double-blind, placebo-controlled trial. Lancet 390, 1664–1675. https://doi.org/10.1016/S0140-6736(17)31585-4

Attar, A., Kaptanoglu, E., Aydın, Z., Ayten, M., Sargon, M.F., 2005. Electron microscopic study of the progeny of ependymal stem cells in the normal and injured spinal cord. Surgical Neurology 64, S28–S32. https://doi.org/10.1016/j.surneu.2005.07.057

Bachleda, A.R., Pevny, L.H., Weiss, E.R., 2016. Sox2-Deficient Müller Glia Disrupt the Structural and Functional Maturation of the Mammalian Retina. Invest Ophthalmol Vis Sci 57, 1488–1499. https://doi.org/10.1167/iovs.15-17994

Baggio, L.L., Drucker, D.J., 2007. Biology of Incretins: GLP-1 and GIP. Gastroenterology 132, 2131–2157. https://doi.org/10.1053/j.gastro.2007.03.054

Banerjee, A., Arha, M., Choudhary, S., Ashton, R.S., Bhatia, S.R., Schaffer, D.V., Kane, R.S., 2009. The Influence of Hydrogel Modulus on the Proliferation and Differentiation of Encapsulated Neural Stem Cells. Biomaterials 30, 4695–4699. https://doi.org/10.1016/j.biomaterials.2009.05.050

Bao, Y., Jiang, L., Chen, H., Zou, J., Liu, Z., Shi, Y., 2015. The Neuroprotective Effect of Liraglutide is Mediated by Glucagon-Like Peptide 1 Receptor-Mediated Activation of cAMP/PKA/CREB Pathway. Cell Physiol Biochem 36, 2366–2378. https://doi.org/10.1159/000430199

Barber, R.P., Vaughn, J.E., Roberts, E., 1982. The cytoarchitecture of GABAergic neurons in rat spinal cord. Brain Res 238, 305–328. https://doi.org/10.1016/0006-8993(82)90107-x

Barnabé-Heider, F., Frisén, J., 2008. Stem Cells for Spinal Cord Repair. Cell Stem Cell 3, 16–24. https://doi.org/10.1016/j.stem.2008.06.011

Barnabé-Heider, F., Göritz, C., Sabelström, H., Takebayashi, H., Pfrieger, F.W., Meletis, K., Frisén, J., 2010. Origin of New Glial Cells in Intact and Injured Adult Spinal Cord. Cell Stem Cell 7, 470–482. https://doi.org/10.1016/j.stem.2010.07.014

Bartlett, R.D., Choi, D., Phillips, J.B., 2016. Biomechanical properties of the spinal cord: implications for tissue engineering and clinical translation. Regen Med 11, 659–673. https://doi.org/10.2217/rme-2016-0065

Bassil, F., Canron, M.-H., Vital, A., Bezard, E., Li, Y., Greig, N.H., Gulyani, S., Kapogiannis, D., Fernagut, P.-O., Meissner, W.G., 2017. Insulin resistance and exendin-4 treatment for multiple system atrophy. Brain 140, 1420–1436. https://doi.org/10.1093/brain/awx044

Batista, A.F., Bodart-Santos, V., De Felice, F.G., Ferreira, S.T., 2019. Neuroprotective Actions of Glucagon-Like Peptide-1 (GLP-1) Analogues in Alzheimer's and Parkinson's Diseases. CNS Drugs 33, 209–223. https://doi.org/10.1007/s40263-018-0593-6

Bauer, S., Hay, M., Amilhon, B., Jean, A., Moyse, E., 2005. In vivo neurogenesis in the dorsal vagal complex of the adult rat brainstem. Neuroscience 130, 75–90. https://doi.org/10.1016/j.neuroscience.2004.08.047

Baumann, H.J., Mahajan, G., Ham, T.R., Betonio, P., Kothapalli, C.R., Shriver, L.P., Leipzig, N.D., 2020. Softening of the chronic hemi-section spinal cord injury scar parallels dysregulation of cellular and extracellular matrix content. Journal of the Mechanical Behavior of Biomedical Materials 110, 103953. https://doi.org/10.1016/j.jmbbm.2020.103953

Bech, E.M., Pedersen, S.L., Jensen, K.J., 2018. Chemical Strategies for Half-Life Extension of Biopharmaceuticals: Lipidation and Its Alternatives. ACS Med Chem Lett 9, 577–580. https://doi.org/10.1021/acsmedchemlett.8b00226

Beiroa, D., Imbernon, M., Gallego, R., Senra, A., Herranz, D., Villarroya, F., Serrano, M., Fernø, J., Salvador, J., Escalada, J., Dieguez, C., Lopez, M., Frühbeck, G., Nogueiras, R., 2014. GLP-1 agonism stimulates brown adipose tissue thermogenesis and browning through hypothalamic AMPK. Diabetes 63, 3346–3358. https://doi.org/10.2337/db14-0302

Bernal, A., Arranz, L., 2018. Nestin-expressing progenitor cells: function, identity and therapeutic implications. Cell Mol Life Sci 75, 2177–2195. https://doi.org/10.1007/s00018-018-2794-z

Bertilsson, G., Patrone, C., Zachrisson, O., Andersson, A., Dannaeus, K., Heidrich, J., Kortesmaa, J., Mercer, A., Nielsen, E., Rönnholm, H., Wikström, L., 2008. Peptide hormone exendin-4 stimulates subventricular zone neurogenesis in the adult rodent brain and induces recovery in an animal model of parkinson's disease. Journal of Neuroscience Research 86, 326–338. https://doi.org/10.1002/jnr.21483

Bettler, B., Kaupmann, K., Mosbacher, J., Gassmann, M., 2004. Molecular Structure and Physiological Functions of GABAB Receptors. Physiological Reviews 84, 835–867. https://doi.org/10.1152/physrev.00036.2003

Binor, E., Heathcote, R.D., 2001. Development of GABA-immunoreactive neuron patterning in the spinal cord. Journal of Comparative Neurology 438, 1–11. https://doi.org/10.1002/cne.1298

Bjorefeldt, A., Andreasson, U., Daborg, J., Riebe, I., Wasling, P., Zetterberg, H., Hanse, E., 2015. Human cerebrospinal fluid increases the excitability of pyramidal neurons in the in vitro brain slice. The Journal of Physiology 593, 231–243. https://doi.org/10.1113/jphysiol.2014.284711

Bjorefeldt, A., Illes, S., Zetterberg, H., Hanse, E., 2018. Neuromodulation via the Cerebrospinal Fluid: Insights from Recent in Vitro Studies. Front Neural Circuits 12, 5. https://doi.org/10.3389/fncir.2018.00005

Bjorefeldt, A., Wasling, P., Zetterberg, H., Hanse, E., 2016. Neuromodulation of fast-spiking and non-fast-spiking hippocampal CA1 interneurons by human cerebrospinal fluid. The Journal of Physiology 594, 937–952. https://doi.org/10.1113/JP271553

Bjornsson, C.S., Apostolopoulou, M., Tian, Y., Temple, S., 2015. It Takes a Village: Constructing the Neurogenic Niche. Dev Cell 32, 435–446. https://doi.org/10.1016/j.devcel.2015.01.010

Blaschke, S.J., Demir, S., König, A., Abraham, J.-A., Vay, S.U., Rabenstein, M., Olschewski, D.N., Hoffmann, C., Hoffmann, M., Hersch, N., Merkel, R., Hoffmann, B., Schroeter, M., Fink, G.R., Rueger, M.A., 2020. Substrate Elasticity Exerts Functional Effects on Primary Microglia. Frontiers in Cellular Neuroscience 14. https://doi.org/10.3389/fncel.2020.590500

Bolteus, A.J., Bordey, A., 2004. GABA Release and Uptake Regulate Neuronal Precursor Migration in the Postnatal Subventricular Zone. J. Neurosci. 24, 7623–7631. https://doi.org/10.1523/JNEUROSCI.1999-04.2004

Boonacker, E., Van Noorden, C.J.F., 2003. The multifunctional or moonlighting protein CD26/DPPIV. Eur J Cell Biol 82, 53–73. https://doi.org/10.1078/0171-9335-00302

Bradaïa, A., Trouslard, J., 2002. Nicotinic receptors regulate the release of glycine onto lamina X neurones of the rat spinal cord. Neuropharmacology 43, 1044–1054. https://doi.org/10.1016/S0028-3908(02)00121-1

Brezina, V., 2010. Beyond the wiring diagram: signalling through complex neuromodulator networks. Philos Trans R Soc Lond B Biol Sci 365, 2363–2374. https://doi.org/10.1098/rstb.2010.0105

Brierley, D.I., Holt, M.K., Singh, A., de Araujo, A., McDougle, M., Vergara, M., Afaghani, M.H., Lee, S.J., Scott, K., Maske, C., Langhans, W., Krause, E., de Kloet, A., Gribble, F.M., Reimann, F., Rinaman, L., de Lartigue, G., Trapp, S., 2021. Central and peripheral GLP-1 systems independently suppress eating. Nat Metab 3, 258–273. https://doi.org/10.1038/s42255-021-00344-4

Brown, P.D., Davies, S.L., Speake, T., Millar, I.D., 2004. Molecular mechanisms of cerebrospinal fluid production. Neuroscience 129, 957–970. https://doi.org/10.1016/j.neuroscience.2004.07.003

Bruni, J.E., 1998. Ependymal development, proliferation, and functions: A review. Microscopy Research and Technique 41, 2–13. https://doi.org/10.1002/(SICI)1097-0029(19980401)41:1<2::AID-JEMT2>3.0.CO;2-Z

Bruni, J.E., Reddy, K., 1987. Ependyma of the central canal of the rat spinal cord: a light and transmission electron microscopic study. J Anat 152, 55–70.

Budday, S., Holzapfel, G.A., Steinmann, P., Kuhl, E., 2019. Challenges and perspectives in brain tissue testing and modeling. PAMM 19, e201900269. https://doi.org/10.1002/pamm.201900269

Bullock, B.P., Heller, R.S., Habener, J.F., 1996. Tissue distribution of messenger ribonucleic acid encoding the rat glucagon-like peptide-1 receptor. Endocrinology 137, 2968–2978. https://doi.org/10.1210/endo.137.7.8770921

Buteau, J., Roduit, R., Susini, S., Prentki, M., 1999. Glucagon-like peptide-1 promotes DNA synthesis, activates phosphatidylinositol 3-kinase and increases transcription factor pancreatic and duodenal homeobox gene 1 (PDX-1) DNA binding activity in beta (INS-1)-cells. Diabetologia 42, 856–864. https://doi.org/10.1007/s001250051238

Cai, H.-Y., Wang, Z.-J., Hölscher, C., Yuan, L., Zhang, J., Sun, P., Li, J., Yang, W., Wu, M.-N., Qi, J.-S., 2017. Lixisenatide attenuates the detrimental effects of amyloid β protein on spatial working memory and hippocampal neurons in rats. Behav Brain Res 318, 28–35. https://doi.org/10.1016/j.bbr.2016.10.033

Cerrato, V., Mercurio, S., Leto, K., Fucà, E., Hoxha, E., Bottes, S., Pagin, M., Milanese, M., Ngan, C.-Y., Concina, G., Ottolenghi, S., Wei, C.-L., Bonanno, G., Pavesi, G., Tempia, F., Buffo, A., Nicolis, S.K., 2018. Sox2 conditional mutation in mouse causes ataxic symptoms, cerebellar vermis hypoplasia, and postnatal defects of Bergmann glia. Glia 66, 1929–1946. https://doi.org/10.1002/glia.23448

Chang, W.-P., Südhof, T.C., 2009. SV2 renders primed synaptic vesicles competent for Ca2+ -induced exocytosis. J Neurosci 29, 883–897. https://doi.org/10.1523/JNEUROSCI.4521-08.2009

Chehrehasa, F., Meedeniya, A.C.B., Dwyer, P., Abrahamsen, G., Mackay-Sim, A., 2009. EdU, a new thymidine analogue for labelling proliferating cells in the nervous system. J Neurosci Methods 177, 122–130. https://doi.org/10.1016/j.jneumeth.2008.10.006

Chen, J., Wang, Z., Mao, Y., Zheng, Z., Chen, Y., Khor, S., Shi, K., He, Z., Li, J., Gong, F., Liu, Y., Hu, A., Xiao, J., Wang, X., 2017. Liraglutide activates autophagy via GLP-1R to improve functional recovery after spinal cord injury. Oncotarget 8, 85949–85968. https://doi.org/10.18632/oncotarget.20791

Chen, T.-W., Wardill, T.J., Sun, Y., Pulver, S.R., Renninger, S.L., Baohan, A., Schreiter, E.R., Kerr, R.A., Orger, M.B., Jayaraman, V., Looger, L.L., Svoboda, K., Kim, D.S., 2013. Ultra-sensitive fluorescent proteins for imaging neuronal activity. Nature 499, 295–300. https://doi.org/10.1038/nature12354

Chen, X.-Y., Chen, L., Yang, W., Xie, A.-M., 2021. GLP-1 Suppresses Feeding Behaviors and Modulates Neuronal Electrophysiological Properties in Multiple Brain Regions. Front Mol Neurosci 14, 793004. https://doi.org/10.3389/fnmol.2021.793004

Cheng, J., Wang, F., Yu, D.-F., Wu, P.-F., Chen, J.-G., 2011. The cytotoxic mechanism of malondialdehyde and protective effect of carnosine via protein cross-linking/mitochondrial dysfunction/reactive oxygen species/MAPK pathway in neurons. Eur J Pharmacol 650, 184–194. https://doi.org/10.1016/j.ejphar.2010.09.033

Chiazza, F., Tammen, H., Pintana, H., Lietzau, G., Collino, M., Nyström, T., Klein, T., Darsalia, V., Patrone, C., 2018. The effect of DPP-4 inhibition to improve functional outcome after stroke is mediated by the SDF-1α/CXCR4 pathway. Cardiovascular Diabetology 17, 60. https://doi.org/10.1186/s12933-018-0702-3

Chien, C.-T., Jou, M.-J., Cheng, T.-Y., Yang, C.-H., Yu, T.-Y., Li, P.-C., 2015. Exendin-4-loaded PLGA microspheres relieve cerebral ischemia/reperfusion injury and neurologic deficits through long-lasting bioactivity-mediated phosphorylated Akt/eNOS signaling in rats. J Cereb Blood Flow Metab 35, 1790–1803. https://doi.org/10.1038/jcbfm.2015.126

Christensen, M., Sparre-Ulrich, A.H., Hartmann, B., Grevstad, U., Rosenkilde, M.M., Holst, J.J., Vilsbøll, T., Knop, F.K., 2015. Transfer of liraglutide from blood to cerebrospinal fluid is minimal in patients with type 2 diabetes. Int J Obes 39, 1651–1654. https://doi.org/10.1038/ijo.2015.136

Cifuentes Castro, V.H., López Valenzuela, C.L., Salazar Sánchez, J.C., Peña, K.P., López Pérez, S.J., Ibarra, J.O., Villagrán, A.M., 2014. An Update of the Classical and Novel Methods Used for Measuring Fast Neurotransmitters During Normal and Brain Altered Function. Curr Neuropharmacol 12, 490–508. https://doi.org/10.2174/1570159X13666141223223657

Circu, M.L., Yee Aw, T., 2008. Glutathione and apoptosis. Free Radic Res 42, 689–706. https://doi.org/10.1080/10715760802317663

Ciruelas, K., Marcotulli, D., Bajjalieh, S.M., 2019. Synaptic Vesicle Protein 2: a multi-faceted regulator of secretion. Semin Cell Dev Biol 95, 130–141. https://doi.org/10.1016/j.semcdb.2019.02.003

Clapham, D.E., 2007. Calcium Signaling. Cell 131, 1047–1058. https://doi.org/10.1016/j.cell.2007.11.028

Clements, J.D., Westbrook, G.L., 1991. Activation kinetics reveal the number of glutamate and glycine binding sites on the N-methyl-D-aspartate receptor. Neuron 7, 605–613. https://doi.org/10.1016/0896-6273(91)90373-8

Collins, L., Costello, R.A., 2022. Glucagon-like Peptide-1 Receptor Agonists, in: StatPearls. StatPearls Publishing, Treasure Island (FL).

Colquhoun, C.S., 2019. Manipulating the Properties of Hydrogels to Promote Ependymal Cell Behaviour for Spinal Cord Repair (phd). University of Leeds.

Conte, D., Lall, V.K., Dobson, G., Deuchars, S.A., Deuchars, J., 2008. Cerebrospinal fluid contacting neurones in the spinal cord of the mouse and rat: small cells with a big purpose?, in: The Physiological Society. Presented at the Cardiovascular, Respiratory and Autonomic Control, University of Leeds, p. PC45.

Cork, S.C., Richards, J.E., Holt, M.K., Gribble, F.M., Reimann, F., Trapp, S., 2015. Distribution and characterisation of Glucagon-like peptide-1 receptor expressing cells in the mouse brain. Mol Metab 4, 718–731. https://doi.org/10.1016/j.molmet.2015.07.008

Corns, L.F., 2012. Characterisation of cells in the postnatal neurogenic niche of the murine spinal cord (phd). University of Leeds.

Corns, L.F., Atkinson, L., Daniel, J., Edwards, I.J., New, L., Deuchars, J., Deuchars, S.A., 2015. Cholinergic Enhancement of Cell Proliferation in the Postnatal Neurogenic Niche of the Mammalian Spinal Cord. Stem Cells 33, 2864–2876. https://doi.org/10.1002/stem.2077

Corns, L.F., Deuchars, J., Deuchars, S.A., 2013. GABAergic responses of mammalian ependymal cells in the central canal neurogenic niche of the postnatal spinal cord. Neurosci Lett 553, 57–62. https://doi.org/10.1016/j.neulet.2013.07.007

Coskun, V., Wu, H., Blanchi, B., Tsao, S., Kim, K., Zhao, J., Biancotti, J.C., Hutnick, L., Krueger, R.C., Fan, G., de Vellis, J., Sun, Y.E., 2008. CD133+ neural stem cells in the ependyma of mammalian postnatal forebrain. Proc Natl Acad Sci U S A 105, 1026–1031. https://doi.org/10.1073/pnas.0710000105

Courtine, G., 2019. Spinal cord repair: advances in biology and technology. Nature Medicine 25, 11.

Crane, J., McGowan, B., 2016. The GLP-1 agonist, liraglutide, as a pharmacotherapy for obesity. Therapeutic Advances in Chronic Disease 7, 92–107. https://doi.org/10.1177/2040622315620180

Croft, C.L., Futch, H.S., Moore, B.D., Golde, T.E., 2019. Organotypic brain slice cultures to model neurodegenerative proteinopathies. Molecular Neurodegeneration 14, 45. https://doi.org/10.1186/s13024-019-0346-0

Crowe, M.J., Bresnahan, J.C., Shuman, S.L., Masters, J.N., Beattie, M.S., 1997. Apoptosis and delayed degeneration after spinal cord injury in rats and monkeys. Nat Med 3, 73–76. https://doi.org/10.1038/nm0197-73

Currie, K.P., 2010. G protein inhibition of CaV2 calcium channels. Channels (Austin) 4, 497–509. https://doi.org/10.4161/chan.4.6.12871

Cusimano, M., Brambilla, E., Capotondo, A., De Feo, D., Tomasso, A., Comi, G., D'Adamo, P., Muzio, L., Martino, G., 2018. Selective killing of spinal cord neural stem cells impairs locomotor recovery in a mouse model of spinal cord injury. Journal of Neuroinflammation 15, 58. https://doi.org/10.1186/s12974-018-1085-9

Custer, K.L., Austin, N.S., Sullivan, J.M., Bajjalieh, S.M., 2006. Synaptic vesicle protein 2 enhances release probability at quiescent synapses. J Neurosci 26, 1303–1313. https://doi.org/10.1523/JNEUROSCI.2699-05.2006

Daniel, J., 2015. Characterising properties and responses of cells in the post natal neurogenic niche of the spinal cord (PhD). University of Leeds.

Daniel, J., Deuchars, J., Deuchars, S., 2016. Organotypic Spinal Cord Slice Cultures and a Method to Detect Cell Proliferation in These Slices. BIO-PROTOCOL 6. https://doi.org/10.21769/BioProtoc.1951

Daynac, M., Chicheportiche, A., Pineda, J.R., Gauthier, L.R., Boussin, F.D., Mouthon, M.-A., 2013. Quiescent neural stem cells exit dormancy upon alteration of GABAAR signaling following radiation damage. Stem Cell Res 11, 516–528. https://doi.org/10.1016/j.scr.2013.02.008

Deganutti, G., Liang, Y.-L., Zhang, X., Khoshouei, M., Clydesdale, L., Belousoff, M.J., Venugopal, H., Truong, T.T., Glukhova, A., Keller, A.N., Gregory, K.J., Leach, K., Christopoulos, A., Danev, R., Reynolds, C.A., Zhao, P., Sexton, P.M., Wootten, D., 2022. Dynamics of GLP-1R peptide agonist engagement are correlated with kinetics of G protein activation. Nat Commun 13, 92. https://doi.org/10.1038/s41467-021-27760-0

Demartini, B., Invernizzi, R.W., Campiglio, L., Bocci, T., D'Arrigo, A., Arighi, A., Sciacca, F., Galimberti, D., Scarpini, E., Gambini, O., Priori, A., 2020. Cerebrospinal fluid glutamate changes in functional movement disorders. npj Parkinsons Dis. 6, 1–4. https://doi.org/10.1038/s41531-020-00140-z

Deng, J., Meng, F., Zhang, K., Gao, J., Liu, Z., Li, M., Liu, X., Li, J., Wang, Y., Zhang, L., Tang, P., 2022. Emerging Roles of Microglia Depletion in the Treatment of Spinal Cord Injury. Cells 11, 1871. https://doi.org/10.3390/cells11121871

Di Bella, D.J., Carcagno, A.L., Bartolomeu, M.L., Pardi, M.B., Löhr, H., Siegel, N., Hammerschmidt, M., Marín-Burgin, A., Lanuza, G.M., 2019. Ascl1 Balances Neuronal versus Ependymal Fate in the Spinal Cord Central Canal. Cell Reports 28, 2264-2274.e3. https://doi.org/10.1016/j.celrep.2019.07.087

Diermeier-Daucher, S., Clarke, S.T., Hill, D., Vollmann-Zwerenz, A., Bradford, J.A., Brockhoff, G., 2009. Cell type specific applicability of 5-ethynyl-2'-deoxyuridine (EdU) for dynamic proliferation assessment in flow cytometry. Cytometry A 75, 535–546. https://doi.org/10.1002/cyto.a.20712

Djenoune, L., Desban, L., Gomez, J., Sternberg, J.R., Prendergast, A., Langui, D., Quan, F.B., Marnas, H., Auer, T.O., Rio, J.-P., Bene, F.D., Bardet, P.-L., Wyart, C., 2017. The dual developmental origin of spinal cerebrospinal fluid-contacting neurons gives rise to distinct functional subtypes. Sci Rep 7, 1–14. https://doi.org/10.1038/s41598-017-00350-1

Djenoune, L., Khabou, H., Joubert, F., Quan, F.B., Nunes Figueiredo, S., Bodineau, L., Del Bene, F., Burcklé, C., Tostivint, H., Wyart, C., 2014. Investigation of spinal cerebrospinal fluid-contacting neurons expressing PKD2L1: evidence for a conserved system from fish to primates. Frontiers in Neuroanatomy 8, 26. https://doi.org/10.3389/fnana.2014.00026

Doetsch, F., García-Verdugo, J.M., Alvarez-Buylla, A., 1999. Regeneration of a germinal layer in the adult mammalian brain. Proc Natl Acad Sci U S A 96, 11619–11624.

Dolma, S., Kumar, H., 2021. Neutrophil, Extracellular Matrix Components, and Their Interlinked Action in Promoting Secondary Pathogenesis After Spinal Cord Injury. Mol Neurobiol 58, 4652–4665. https://doi.org/10.1007/s12035-021-02443-5

Dolphin, A.C., 1998. Mechanisms of modulation of voltage-dependent calcium channels by G proteins. J Physiol 506, 3–11. https://doi.org/10.1111/j.1469-7793.1998.003bx.x

Donnelly, D., 2012a. The structure and function of the glucagon-like peptide-1 receptor and its ligands. Br J Pharmacol 166, 27–41. https://doi.org/10.1111/j.1476-5381.2011.01687.x

Donnelly, D., 2012b. The structure and function of the glucagon-like peptide-1 receptor and its ligands. British Journal of Pharmacology 166, 27. https://doi.org/10.1111/j.1476-5381.2011.01687.x

Dromard, C., Guillon, H., Rigau, V., Ripoll, C., Sabourin, J. c., Perrin, F. e., Scamps, F., Bozza, S., Sabatier, P., Lonjon, N., Duffau, H., Vachiery-Lahaye, F., Prieto, M., Tran Van Ba, C., Deleyrolle, L., Boularan, A., Langley, K., Gaviria, M., Privat, A., Hugnot, J. p., Bauchet, L., 2008. Adult human spinal cord harbors neural precursor cells that generate neurons and glial cells in vitro. Journal of Neuroscience Research 86, 1916–1926. https://doi.org/10.1002/jnr.21646

Drucker, D.J., 1998. Glucagon-like peptides. Diabetes 47, 159–169. https://doi.org/10.2337/diab.47.2.159

Drucker, D.J., Philippe, J., Mojsov, S., Chick, W.L., Habener, J.F., 1987. Glucagon-like peptide I stimulates insulin gene expression and increases cyclic AMP levels in a rat islet cell line. PNAS 84, 3434–3438. https://doi.org/10.1073/pnas.84.10.3434

du Boulay, G.H., 1966. Pulsatile Movements in the CSF Pathways. BJR 39, 255–262. https://doi.org/10.1259/0007-1285-39-460-255

During, M.J., Cao, L., Zuzga, D.S., Francis, J.S., Fitzsimons, H.L., Jiao, X., Bland, R.J., Klugmann, M., Banks, W.A., Drucker, D.J., Haile, C.N., 2003. Glucagon-like peptide-1 receptor is involved in learning and neuroprotection. Nat Med 9, 1173–1179. https://doi.org/10.1038/nm919

Eccles, J.C., 1964. The physiology of synapses, The physiology of synapses. Academic Press, Oxford, England. https://doi.org/10.1007/978-3-642-64950-9

Edelstein, A., Amodaj, N., Hoover, K., Vale, R., Stuurman, N., 2010. Computer control of microscopes using μManager. Curr Protoc Mol Biol Chapter 14, Unit14.20. https://doi.org/10.1002/0471142727.mb1420s92

Ellis, P., Fagan, B.M., Magness, S.T., Hutton, S., Taranova, O., Hayashi, S., McMahon, A., Rao, M., Pevny, L., 2004. SOX2, a persistent marker for multipotential neural stem cells derived from embryonic stem cells, the embryo or the adult. Dev Neurosci 26, 148–165. https://doi.org/10.1159/000082134

Erbil, D., Eren, C.Y., Demirel, C., Küçüker, M.U., Solaroğlu, I., Eser, H.Y., 2019. GLP-1's role in neuroprotection: a systematic review. Brain Injury 33, 734–819. https://doi.org/10.1080/02699052.2019.1587000

Falcão, A.M., Marques, F., Novais, A., Sousa, N., Palha, J.A., Sousa, J.C., 2012. The path from the choroid plexus to the subventricular zone: go with the flow! Front Cell Neurosci 6, 34. https://doi.org/10.3389/fncel.2012.00034

Fan, Y.-J., Zong, W.-X., 2013. The cellular decision between apoptosis and autophagy. Chin J Cancer 32, 121–129. https://doi.org/10.5732/cjc.012.10106

Farkas, E., Szilvásy-Szabó, A., Ruska, Y., Sinkó, R., Rasch, M.G., Egebjerg, T., Pyke, C., Gereben, B., Knudsen, L.B., Fekete, C., 2021. Distribution and ultrastructural localization of the glucagon-like peptide-1 receptor (GLP-1R) in the rat brain. Brain Struct Funct 226, 225–245. https://doi.org/10.1007/s00429-020-02189-1

Fidelin, K., Djenoune, L., Stokes, C., Prendergast, A., Gomez, J., Baradel, A., Del Bene, F., Wyart, C., 2015. State-Dependent Modulation of Locomotion by GABAergic Spinal Sensory Neurons. Current Biology 25, 3035–3047. https://doi.org/10.1016/j.cub.2015.09.070

Frangaj, A., Fan, Q.R., 2018. Structural biology of GABAB receptor. Neuropharmacology 136, 68–79. https://doi.org/10.1016/j.neuropharm.2017.10.011

Franze, K., Janmey, P.A., Guck, J., 2013. Mechanics in Neuronal Development and Repair. Annual Review of Biomedical Engineering 15, 227–251. https://doi.org/10.1146/annurev-bioeng-071811-150045

Frederico, B., Martins, I., Chapela, D., Gasparrini, F., Chakravarty, P., Ackels, T., Piot, C., Almeida, B., Carvalho, J., Ciccarelli, A., Peddie, C.J., Rogers, N., Briscoe, J., Guillemot, F., Schaefer, A.T., Saúde, L., Reis e Sousa, C., 2022. DNGR-1-tracing marks an ependymal cell subset with damage-

responsive neural stem cell potential. Dev Cell 57, 1957-1975.e9. https://doi.org/10.1016/j.devcel.2022.07.012
Frisén, J., Johansson, C.B., Török, C., Risling, M., Lendahl, U., 1995. Rapid, widespread, and longlasting induction of nestin contributes to the generation of glial scar tissue after CNS injury. J Cell Biol 131, 453–464. https://doi.org/10.1083/jcb.131.2.453
Fu, H., Qi, Y., Tan, M., Cai, J., Hu, X., Liu, Z., Jensen, J., Qiu, M., 2003. Molecular mapping of the origin of postnatal spinal cord ependymal cells: Evidence that adult ependymal cells are derived from Nkx6.1+ ventral neural progenitor cells. Journal of Comparative Neurology 456, 237–244. https://doi.org/10.1002/cne.10481
Fuxe, K., Borroto-Escuela, D.O., Romero-Fernandez, W., Zhang, W., Agnati, L.F., 2013. Volume transmission and its different forms in the central nervous system. Chin. J. Integr. Med. 19, 323–329. https://doi.org/10.1007/s11655-013-1455-1
Fuxe, K., Dahlström, A.B., Jonsson, G., Marcellino, D., Guescini, M., Dam, M., Manger, P., Agnati, L., 2010. The discovery of central monoamine neurons gave volume transmission to the wired brain. Prog Neurobiol 90, 82–100. https://doi.org/10.1016/j.pneurobio.2009.10.012
Gao, X.B., van den Pol, A.N., 2001. Melanin concentrating hormone depresses synaptic activity of glutamate and GABA neurons from rat lateral hypothalamus. J Physiol 533, 237–252. https://doi.org/10.1111/j.1469-7793.2001.0237b.x
Gasbjerg, L.S., Bari, E.J., Christensen, M., Knop, F.K., 2021. Exendin(9-39)NH2: Recommendations for clinical use based on a systematic literature review. Diabetes, Obesity and Metabolism 23, 2419–2436. https://doi.org/10.1111/dom.14507
Gejl, M., Brock, B., Egefjord, L., Vang, K., Rungby, J., Gjedde, A., 2017. Blood-Brain Glucose Transfer in Alzheimer's disease: Effect of GLP-1 Analog Treatment. Sci Rep 7, 17490. https://doi.org/10.1038/s41598-017-17718-y
Gerstmann, K., Jurčić, N., Blasco, E., Kunz, S., Sassi, F. de A., Wanaverbecq, N., Zampieri, N., 2022. The role of intraspinal sensory neurons in the control of quadrupedal locomotion. Current Biology 32, 2442-2453.e4. https://doi.org/10.1016/j.cub.2022.04.019
Ghazale, H., Ripoll, C., Leventoux, N., Jacob, L., Azar, S., Mamaeva, D., Glasson, Y., Calvo, C.-F., Thomas, J.-L., Meneceur, S., Lallemand, Y., Rigau, V., Perrin, F.E., Noristani, H.N., Rocamonde, B., Huillard, E., Bauchet, L., Hugnot, J.-P., 2019. RNA Profiling of the Human and Mouse Spinal Cord Stem Cell Niches Reveals an Embryonic-like Regionalization with MSX1+ Roof-Plate-Derived Cells. Stem Cell Reports 12, 1159–1177. https://doi.org/10.1016/j.stemcr.2019.04.001
Gibson, S.J., Polak, J.M., Bloom, S.R., Wall, P.D., 1981. The distribution of nine peptides in rat spinal cord with special emphasis on the substantia gelatinosa and on the area around the central canal (lamina X). J Comp Neurol 201, 65–79. https://doi.org/10.1002/cne.902010106
Göke, R., Fehmann, H.C., Linn, T., Schmidt, H., Krause, M., Eng, J., Göke, B., 1993. Exendin-4 is a high potency agonist and truncated exendin-(9-39)-amide an antagonist at the glucagon-like peptide 1-(7-36)-amide receptor of insulin-secreting beta-cells. J Biol Chem 268, 19650–19655.
Göke, R., Larsen, P.J., Mikkelsen, J.D., Sheikh, S.P., 1995. Distribution of GLP-1 binding sites in the rat brain: evidence that exendin-4 is a ligand of brain GLP-1 binding sites. Eur J Neurosci 7, 2294–2300. https://doi.org/10.1111/j.1460-9568.1995.tb00650.x
Goldstein, D.S., Holmes, C., Sharabi, Y., 2012. Cerebrospinal fluid biomarkers of central catecholamine deficiency in Parkinson's disease and other synucleinopathies. Brain 135, 1900–1913. https://doi.org/10.1093/brain/aws055
Gong, N., Xiao, Q., Zhu, B., Zhang, C.-Y., Wang, Y.-C., Fan, H., Ma, A.-N., Wang, Y.-X., 2014. Activation of Spinal Glucagon-Like Peptide-1 Receptors Specifically Suppresses Pain Hypersensitivity. J Neurosci 34, 5322–5334. https://doi.org/10.1523/JNEUROSCI.4703-13.2014
González-García, I., Milbank, E., Diéguez, C., López, M., Contreras, C., 2019. Glucagon, GLP-1 and Thermogenesis. Int J Mol Sci 20, 3445. https://doi.org/10.3390/ijms20143445
González-Santana, A., Estévez-Herrera, J., Seward, E.P., Borges, R., Machado, J.D., 2021. Glucagon-like peptide-1 receptor controls exocytosis in chromaffin cells by increasing full-fusion events. Cell Rep 36, 109609. https://doi.org/10.1016/j.celrep.2021.109609
Gotts, J., Atkinson, L., Yanagawa, Y., Deuchars, J., Deuchars, S.A., 2016. Co-expression of GAD67 and choline acetyltransferase in neurons in the mouse spinal cord: A focus on lamina X. Brain Research 1646, 570–579. https://doi.org/10.1016/j.brainres.2016.07.001
Graham, G.V., McCloskey, A., Abdel-Wahab, Y.H., Conlon, J.M., Flatt, P.R., 2020. A long-acting, dual-agonist analogue of lamprey GLP-1 shows potent insulinotropic, β-cell protective, and anorexic

activities and improves glucose homeostasis in high fat-fed mice. Mol Cell Endocrinol 499, 110584. https://doi.org/10.1016/j.mce.2019.110584
Gray, E.G., 1959. Electron microscopy of synaptic contacts on dendrite spines of the cerebral cortex. Nature 183, 1592–1593. https://doi.org/10.1038/1831592a0
Green, B.D., Gault, V.A., Flatt, P.R., Harriott, P., Greer, B., O'Harte, F.P.M., 2004. Comparative effects of GLP-1 and GIP on cAMP production, insulin secretion, and in vivo antidiabetic actions following substitution of Ala8/Ala2 with 2-aminobutyric acid. Archives of Biochemistry and Biophysics 428, 136–143. https://doi.org/10.1016/j.abb.2004.05.005
Griffioen, K.J., Wan, R., Okun, E., Wang, X., Lovett-Barr, M.R., Li, Y., Mughal, M.R., Mendelowitz, D., Mattson, M.P., 2011. GLP-1 receptor stimulation depresses heart rate variability and inhibits neurotransmission to cardiac vagal neurons. Cardiovasc Res 89, 72–78. https://doi.org/10.1093/cvr/cvq271
Grossman, S.D., Rosenberg, L.J., Wrathall, J.R., 2001. Temporal–Spatial Pattern of Acute Neuronal and Glial Loss after Spinal Cord Contusion. Experimental Neurology 168, 273–282. https://doi.org/10.1006/exnr.2001.7628
Gullo, F., Ceriani, M., D'Aloia, A., Wanke, E., Constanti, A., Costa, B., Lecchi, M., 2017. Plant Polyphenols and Exendin-4 Prevent Hyperactivity and TNF-α Release in LPS-Treated In vitro Neuron/Astrocyte/Microglial Networks. Front Neurosci 11, 500. https://doi.org/10.3389/fnins.2017.00500
Haggerty, A.E., Maldonado-Lasunción, I., Oudega, M., 2018. Biomaterials for revascularization and immunomodulation after spinal cord injury. Biomed. Mater. 13, 044105. https://doi.org/10.1088/1748-605X/aaa9d8
Hällbrink, M., Holmqvist, T., Olsson, M., Ostenson, C.G., Efendic, S., Langel, U., 2001. Different domains in the third intracellular loop of the GLP-1 receptor are responsible for Galpha(s) and Galpha(i)/Galpha(o) activation. Biochim Biophys Acta 1546, 79–86. https://doi.org/10.1016/s0167-4838(00)00270-3
Hamilton, A., Patterson, S., Porter, D., Gault, V.A., Holscher, C., 2011. Novel GLP-1 mimetics developed to treat type 2 diabetes promote progenitor cell proliferation in the brain. J. Neurosci. Res. 89, 481–489. https://doi.org/10.1002/jnr.22565
Hamilton, L.K., Truong, M., Bednarcyk, M., Aumont, A., Fernandes, K.J., 2009. Cellular organization of the central canal ependymal zone, a niche of latent neural stem cells in the adult mammalian spinal cord. Neuroscience 164, 1044–1056. https://doi.org/10.1016/j.neuroscience.2009.09.006
Han, W., Li, Y., Cheng, J., Zhang, J., Chen, D., Fang, M., Xiang, G., Wu, Y., Zhang, H., Xu, K., Wang, H., Xie, L., Xiao, J., 2020. Sitagliptin improves functional recovery via GLP-1R-induced anti-apoptosis and facilitation of axonal regeneration after spinal cord injury. J Cell Mol Med 24, 8687–8702. https://doi.org/10.1111/jcmm.15501
Hansen, H.H., Fabricius, K., Barkholt, P., Niehoff, M.L., Morley, J.E., Jelsing, J., Pyke, C., Knudsen, L.B., Farr, S.A., Vrang, N., 2015. The GLP-1 Receptor Agonist Liraglutide Improves Memory Function and Increases Hippocampal CA1 Neuronal Numbers in a Senescence-Accelerated Mouse Model of Alzheimer's Disease. J Alzheimers Dis 46, 877–888. https://doi.org/10.3233/JAD-143090
Harada, A., Teng, J., Takei, Y., Oguchi, K., Hirokawa, N., 2002. MAP2 is required for dendrite elongation, PKA anchoring in dendrites, and proper PKA signal transduction. J Cell Biol 158, 541–549. https://doi.org/10.1083/jcb.200110134
Hawkins, K., Patterson, A.K., Clarke, P.A., Smith, D.K., 2020. Catalytic Gels for a Prebiotically Relevant Asymmetric Aldol Reaction in Water: From Organocatalyst Design to Hydrogel Discovery and Back Again. J Am Chem Soc 142, 4379–4389. https://doi.org/10.1021/jacs.9b13156
He, Y., Shi, X., Chen, L., Zhao, W., Shan, J., Lin, Z.-L., Yang, L., Li, Q., 2021. Cerebrospinal fluid-contacting neurons affect the expression of endogenous neural progenitor cells and the recovery of neural function after spinal cord injury. International Journal of Neuroscience 131, 615–624. https://doi.org/10.1080/00207454.2020.1750396
He, Z., Gao, Y., Lieu, L., Afrin, S., Cao, J., Michael, N.J., Dong, Y., Sun, J., Guo, H., Williams, K.W., 2019. Direct and indirect effects of liraglutide on hypothalamic POMC and NPY/AgRP neurons - Implications for energy balance and glucose control. Mol Metab 28, 120–134. https://doi.org/10.1016/j.molmet.2019.07.008
Heile, A.M.B., Wallrapp, C., Klinge, P.M., Samii, A., Kassem, M., Silverberg, G., Brinker, T., 2009. Cerebral transplantation of encapsulated mesenchymal stem cells improves cellular pathology

after experimental traumatic brain injury. Neuroscience Letters 463, 176–181. https://doi.org/10.1016/j.neulet.2009.07.071
Heppner, K.M., Baquero, A.F., Bennett, C.M., Lindsley, S.R., Kirigiti, M.A., Bennett, B., Bosch, M.A., Mercer, A.J., Rønnekleiv, O.K., True, C., Grove, K.L., Smith, M.S., 2017. GLP-1R Signaling Directly Activates Arcuate Nucleus Kisspeptin Action in Brain Slices but Does not Rescue Luteinizing Hormone Inhibition in Ovariectomized Mice During Negative Energy Balance. eNeuro 4, ENEURO.0198-16.2016. https://doi.org/10.1523/ENEURO.0198-16.2016
Heppner, K.M., Kirigiti, M., Secher, A., Paulsen, S.J., Buckingham, R., Pyke, C., Knudsen, L.B., Vrang, N., Grove, K.L., 2015. Expression and Distribution of Glucagon-Like Peptide-1 Receptor mRNA, Protein and Binding in the Male Nonhuman Primate (Macaca mulatta) Brain. Endocrinology 156, 255–267. https://doi.org/10.1210/en.2014-1675
Herlitze, S., Garcia, D.E., Mackie, K., Hille, B., Scheuer, T., Catterall, W.A., 1996. Modulation of Ca2+ channels by G-protein beta gamma subunits. Nature 380, 258–262. https://doi.org/10.1038/380258a0
Hilfiker, S., Augustine, G.J., 1999. Regulation of synaptic vesicle fusion by protein kinase C. J Physiol 515, 1. https://doi.org/10.1111/j.1469-7793.1999.001ad.x
Hiramatsu, K., 2020. Chicken Intestinal L Cells and Glucagon-like Peptide-1 Secretion. J Poult Sci 57, 1–6. https://doi.org/10.2141/jpsa.0190003
Hisadome, K., Reimann, F., Gribble, F.M., Trapp, S., 2010. Leptin directly depolarizes preproglucagon neurons in the nucleus tractus solitarius: electrical properties of glucagon-like Peptide 1 neurons. Diabetes 59, 1890–1898. https://doi.org/10.2337/db10-0128
Hökfelt, T., Elde, R., Johansson, O., Terenius, L., Stein, L., 1977. The distribution of enkephalin-immunoreactive cell bodies in the rat central nervous system. Neurosci Lett 5, 25–31. https://doi.org/10.1016/0304-3940(77)90160-4
Hölscher, C., 2022. Protective properties of GLP-1 and associated peptide hormones in neurodegenerative disorders. Br J Pharmacol 179, 695–714. https://doi.org/10.1111/bph.15508
Hölscher, C., 2014. Central effects of GLP-1: new opportunities for treatments of neurodegenerative diseases. Journal of Endocrinology 221, T31–T41. https://doi.org/10.1530/JOE-13-0221
Holst, J.J., 2007. The Physiology of Glucagon-like Peptide 1. Physiological Reviews 87, 1409–1439. https://doi.org/10.1152/physrev.00034.2006
Holt, M.K., Cook, D.R., Brierley, D.I., Richards, J.E., Reimann, F., Gourine, A.V., Marina, N., Trapp, S., 2020. PPG neurons in the nucleus of the solitary tract modulate heart rate but do not mediate GLP-1 receptor agonist-induced tachycardia in mice. Mol Metab 39, 101024. https://doi.org/10.1016/j.molmet.2020.101024
Holt, M.K., Richards, J.E., Cook, D.R., Brierley, D.I., Williams, D.L., Reimann, F., Gribble, F.M., Trapp, S., 2019. Preproglucagon Neurons in the Nucleus of the Solitary Tract Are the Main Source of Brain GLP-1, Mediate Stress-Induced Hypophagia, and Limit Unusually Large Intakes of Food. Diabetes 68, 21–33. https://doi.org/10.2337/db18-0729
Holt, M.K., Rinaman, L., 2022. The role of nucleus of the solitary tract glucagon-like peptide-1 and prolactin-releasing peptide neurons in stress: anatomy, physiology and cellular interactions. Br J Pharmacol 179, 642–658. https://doi.org/10.1111/bph.15576
Holt, M.K., Trapp, S., 2016. The physiological role of the brain GLP-1 system in stress. Cogent Biol 2, 1229086. https://doi.org/10.1080/23312025.2016.1229086
Horner, P.J., Power, A.E., Kempermann, G., Kuhn, H.G., Palmer, T.D., Winkler, J., Thal, L.J., Gage, F.H., 2000. Proliferation and differentiation of progenitor cells throughout the intact adult rat spinal cord. J. Neurosci. 20, 2218–2228.
Hornung, J.-P., 2012. Chapter 11 - Raphe Nuclei, in: Mai, J.K., Paxinos, G. (Eds.), The Human Nervous System (Third Edition). Academic Press, San Diego, pp. 401–424. https://doi.org/10.1016/B978-0-12-374236-0.10011-2
Hsu, T.M., Hahn, J.D., Konanur, V.R., Lam, A., Kanoski, S.E., 2015. Hippocampal GLP-1 Receptors Influence Food Intake, Meal Size, and Effort-Based Responding for Food through Volume Transmission. Neuropsychopharmacol 40, 327–337. https://doi.org/10.1038/npp.2014.175
Huang, A.L., Chen, X., Hoon, M.A., Chandrashekar, J., Guo, W., Tränkner, D., Ryba, N.J.P., Zuker, C.S., 2006. The cells and logic for mammalian sour taste detection. Nature 442, 934–938. https://doi.org/10.1038/nature05084
Hugnot, J.P., Franzen, R., 2011. The spinal cord ependymal region: a stem cell niche in the caudal central nervous system. Front Biosci (Landmark Ed) 16, 1044–1059. https://doi.org/10.2741/3734

Huntemer-Silveira, A., Patil, N., Brickner, M.A., Parr, A.M., 2021. Strategies for Oligodendrocyte and Myelin Repair in Traumatic CNS Injury. Frontiers in Cellular Neuroscience 14.
Ikeda, S.R., 1996. Voltage-dependent modulation of N-type calcium channels by G-protein β γsubunits. Nature 380, 255–258. https://doi.org/10.1038/380255a0
Inoue, M., 2021. Genetically encoded calcium indicators to probe complex brain circuit dynamics in vivo. Neuroscience Research 169, 2–8. https://doi.org/10.1016/j.neures.2020.05.013
Irwin, D.M., Huner, O., Youson, J.H., 1999. Lamprey proglucagon and the origin of glucagon-like peptides. Mol Biol Evol 16, 1548–1557. https://doi.org/10.1093/oxfordjournals.molbev.a026067
Isacson, R., Nielsen, E., Dannaeus, K., Bertilsson, G., Patrone, C., Zachrisson, O., Wikström, L., 2011. The glucagon-like peptide 1 receptor agonist exendin-4 improves reference memory performance and decreases immobility in the forced swim test. European Journal of Pharmacology 650, 249–255. https://doi.org/10.1016/j.ejphar.2010.10.008
Iwai, T., Ito, S., Tanimitsu, K., Udagawa, S., Oka, J.-I., 2006. Glucagon-like peptide-1 inhibits LPS-induced IL-1β production in cultured rat astrocytes. Neuroscience Research 55, 352–360. https://doi.org/10.1016/j.neures.2006.04.008
Jagielska, A., Norman, A.L., Whyte, G., Van Vliet, K.J., Guck, J., Franklin, R.J.M., 2012. Mechanical Environment Modulates Biological Properties of Oligodendrocyte Progenitor Cells. Stem Cells Dev 21, 2905–2914. https://doi.org/10.1089/scd.2012.0189
Jaiswal, M., Martin, C.L., Brown, M.B., Callaghan, B., Albers, J.W., Feldman, E.L., Pop-Busui, R., 2015. Effects of exenatide on measures of diabetic neuropathy in subjects with type 2 diabetes: results from an 18-month proof-of-concept open-label randomized study. J Diabetes Complications 29, 1287–1294. https://doi.org/10.1016/j.jdiacomp.2015.07.013
Jalalvand, E., Robertson, B., Tostivint, H., Löw, P., Wallén, P., Grillner, S., 2018. Cerebrospinal Fluid-Contacting Neurons Sense pH Changes and Motion in the Hypothalamus. J Neurosci 38, 7713–7724. https://doi.org/10.1523/JNEUROSCI.3359-17.2018
Jalalvand, E., Robertson, B., Wallén, P., Grillner, S., 2016. Ciliated neurons lining the central canal sense both fluid movement and pH through ASIC3. Nat Commun 7, 10002. https://doi.org/10.1038/ncomms10002
Janz, R., Südhof, T.C., Hammer, R.E., Unni, V., Siegelbaum, S.A., Bolshakov, V.Y., 1999. Essential roles in synaptic plasticity for synaptogyrin I and synaptophysin I. Neuron 24, 687–700. https://doi.org/10.1016/s0896-6273(00)81122-8
Jay, M., McDearmid, J.R., 2015. Motor Control: The Curious Case of Cerebrospinal-Fluid-Contacting Neurons. Current Biology 25, R1138–R1140. https://doi.org/10.1016/j.cub.2015.10.034
Jensen, C.B., Pyke, C., Rasch, M.G., Dahl, A.B., Knudsen, L.B., Secher, A., 2018. Characterization of the Glucagonlike Peptide-1 Receptor in Male Mouse Brain Using a Novel Antibody and In Situ Hybridization. Endocrinology 159, 665–675. https://doi.org/10.1210/en.2017-00812
Jessen, L., Smith, E.P., Ulrich-Lai, Y., Herman, J.P., Seeley, R.J., Sandoval, D., D'Alessio, D., 2017. Central Nervous System GLP-1 Receptors Regulate Islet Hormone Secretion and Glucose Homeostasis in Male Rats. Endocrinology 158, 2124–2133. https://doi.org/10.1210/en.2016-1826
Jiménez, A.J., Domínguez-Pinos, M.-D., Guerra, M.M., Fernández-Llebrez, P., Pérez-Fígares, J.-M., 2014. Structure and function of the ependymal barrier and diseases associated with ependyma disruption. Tissue Barriers 2, e28426. https://doi.org/10.4161/tisb.28426
Jin, S.L., Han, V.K., Simmons, J.G., Towle, A.C., Lauder, J.M., Lund, P.K., 1988. Distribution of glucagonlike peptide I (GLP-I), glucagon, and glicentin in the rat brain: an immunocytochemical study. J Comp Neurol 271, 519–532. https://doi.org/10.1002/cne.902710405
Jin, Y., Song, Y., Lin, J., Liu, T., Li, G., Lai, B., Gu, Y., Chen, G., Xing, L., 2023. Role of inflammation in neurological damage and regeneration following spinal cord injury and its therapeutic implications. Burns Trauma 11, tkac054. https://doi.org/10.1093/burnst/tkac054
Johansson, C.B., Momma, S., Clarke, D.L., Risling, M., Lendahl, U., Frisén, J., 1999. Identification of a Neural Stem Cell in the Adult Mammalian Central Nervous System. Cell 96, 25–34. https://doi.org/10.1016/S0092-8674(00)80956-3
Johnson, E., Clark, M., Oncul, M., Pantiru, A., MacLean, C., Deuchars, J., Deuchars, S.A., Johnston, J., 2023. Graded spikes differentially signal neurotransmitter input in cerebrospinal fluid contacting neurons of the mouse spinal cord. iScience 26, 105914. https://doi.org/10.1016/j.isci.2022.105914
Jonas, P., Sakmann, B., 1992. Glutamate receptor channels in isolated patches from CA1 and CA3 pyramidal cells of rat hippocampal slices. J Physiol 455, 143–171. https://doi.org/10.1113/jphysiol.1992.sp019294

Jurčić, N., Er-Raoui, G., Airault, C., Trouslard, J., Wanaverbecq, N., Seddik, R., 2019. GABAB receptors modulate Ca2+ but not G protein-gated inwardly rectifying K+ channels in cerebrospinal-fluid contacting neurones of mouse brainstem. J Physiol 597, 631–651. https://doi.org/10.1113/JP277172

Jurčić, N., Michelle, C., Trouslard, J., Wanaverbecq, N., Kastner, A., 2021. Evidence for PKD2L1-positive neurons distant from the central canal in the ventromedial spinal cord and medulla of the adult mouse. European Journal of Neuroscience 54, 4781–4803. https://doi.org/10.1111/ejn.15342

Kaneko, T., Fujiyama, F., Hioki, H., 2002. Immunohistochemical localization of candidates for vesicular glutamate transporters in the rat brain. J Comp Neurol 444, 39–62. https://doi.org/10.1002/cne.10129

Kennedy, H.S., Jones, C., Caplazi, P., 2013. Comparison of standard laminectomy with an optimized ejection method for the removal of spinal cords from rats and mice. Journal of Histotechnology 36, 86–91. https://doi.org/10.1179/014788813X13756994210382

Khasawneh, A.H., Garling, R.J., Harris, C.A., 2018. Cerebrospinal fluid circulation: What do we know and how do we know it? Brain Circ 4, 14–18. https://doi.org/10.4103/bc.bc_3_18

Kim, H., Kim, M., Im, S.-K., Fang, S., 2018. Mouse Cre-LoxP system: general principles to determine tissue-specific roles of target genes. Lab Anim Res 34, 147–159. https://doi.org/10.5625/lar.2018.34.4.147

Kim, H.M., Lee, H.J., Lee, M.Y., Kim, S.U., Kim, B.G., 2010. Organotypic Spinal Cord Slice Culture to Study Neural Stem/Progenitor Cell Microenvironment in the Injured Spinal Cord. Exp Neurobiol 19, 106–113. https://doi.org/10.5607/en.2010.19.2.106

Király, K., Kozsurek, M., Lukácsi, E., Barta, B., Alpár, A., Balázsa, T., Fekete, C., Szabon, J., Helyes, Z., Bölcskei, K., Tékus, V., Tóth, Z.E., Pap, K., Gerber, G., Puskár, Z., 2018. Glial cell type-specific changes in spinal dipeptidyl peptidase 4 expression and effects of its inhibitors in inflammatory and neuropatic pain. Sci Rep 8, 3490. https://doi.org/10.1038/s41598-018-21799-8

Klapka, N., Müller, H.W., 2006. Collagen matrix in spinal cord injury. J. Neurotrauma 23, 422–435. https://doi.org/10.1089/neu.2006.23.422

Knudsen, L.B., 2019. Inventing Liraglutide, a Glucagon-Like Peptide-1 Analogue, for the Treatment of Diabetes and Obesity. ACS Pharmacol. Transl. Sci. 2, 468–484. https://doi.org/10.1021/acsptsci.9b00048

Knudsen, L.B., Nielsen, P.F., Huusfeldt, P.O., Johansen, N.L., Madsen, K., Pedersen, F.Z., Thøgersen, H., Wilken, M., Agersø, H., 2000. Potent derivatives of glucagon-like peptide-1 with pharmacokinetic properties suitable for once daily administration. J Med Chem 43, 1664–1669. https://doi.org/10.1021/jm9909645

Koffler, J., 2019. Biomimetic 3D-printed scaffolds for spinal cord injury repair. Nature Medicine 25, 12.

Kolmer, W., 1931. Über das Sagittalorgan, ein zentrales Sinnesorgan der Wirbeltiere, insbesondere beim Affen. Z.Zellforsch 13, 236–248. https://doi.org/10.1007/BF00406356

Kolmer, W., 1921. Das „Sagittalorgan“ der Wirbeltiere. Zeitschrift für Anatomie und Entwicklungsgeschichte 60, 652–717.

Kolodziejski, P.A., Sassek, M., Chalupka, D., Leciejewska, N., Nogowski, L., Mackowiak, P., Jozefiak, D., Stadnicka, K., Siwek, M., Bednarczyk, M., Szwaczkowski, T., Pruszynska-Oszmalek, E., 2018. GLP1 and GIP are involved in the action of synbiotics in broiler chickens. Journal of Animal Science and Biotechnology 9, 13. https://doi.org/10.1186/s40104-017-0227-8

Kopp, K.O., Glotfelty, E.J., Li, Y., Greig, N.H., 2022. Glucagon-like peptide-1 (GLP-1) receptor agonists and neuroinflammation: Implications for neurodegenerative disease treatment. Pharmacological Research 186, 106550. https://doi.org/10.1016/j.phrs.2022.106550

K. Patterson, A., K. Smith, D., 2020. Two-component supramolecular hydrogel for controlled drug release. Chemical Communications 56, 11046–11049. https://doi.org/10.1039/D0CC03962D

Krassioukov, A.V., Ackery, A., Schwartz, G., Adamchik, Y., Liu, Y., Fehlings, M.G., 2002. An in vitro model of neurotrauma in organotypic spinal cord cultures from adult mice. Brain Research Protocols 10, 60–68. https://doi.org/10.1016/S1385-299X(02)00180-0

Kuhn, H.G., Eisch, A.J., Spalding, K., Peterson, D.A., 2016. Detection and Phenotypic Characterization of Adult Neurogenesis. Cold Spring Harb Perspect Biol 8, a025981. https://doi.org/10.1101/cshperspect.a025981

Kullmann, D.M., Ruiz, A., Rusakov, D.M., Scott, R., Semyanov, A., Walker, M.C., 2005. Presynaptic, extrasynaptic and axonal GABAA receptors in the CNS: where and why? Progress in Biophysics

and Molecular Biology, Biophysics of Excitable Tissues 87, 33–46. https://doi.org/10.1016/j.pbiomolbio.2004.06.003
Kumar, V., Umair, Z., Kumar, S., Goutam, R.S., Park, S., Kim, J., 2021. The regulatory roles of motile cilia in CSF circulation and hydrocephalus. Fluids and Barriers of the CNS 18, 31. https://doi.org/10.1186/s12987-021-00265-0
Kútna, V., Ševc, J., Gombalová, Z., Matiašová, A., Daxnerová, Z., 2014. Enigmatic cerebrospinal fluid-contacting neurons arise even after the termination of neurogenesis in the rat spinal cord during embryonic development and retain their immature-like characteristics until adulthood. Acta Histochemica 116, 278–285. https://doi.org/10.1016/j.acthis.2013.08.004
Kwon, S.E., Chapman, E.R., 2011. Synaptophysin regulates the kinetics of synaptic vesicle endocytosis in central neurons. Neuron 70, 847–854. https://doi.org/10.1016/j.neuron.2011.04.001
Lacroix, S., Hamilton, L.K., Vaugeois, A., Beaudoin, S., Breault-Dugas, C., Pineau, I., Lévesque, S.A., Grégoire, C.-A., Fernandes, K.J.L., 2014. Central canal ependymal cells proliferate extensively in response to traumatic spinal cord injury but not demyelinating lesions. PLoS ONE 9, e85916. https://doi.org/10.1371/journal.pone.0085916
Lamotte, C.C., 1987. Vasoactive intestinal polypeptide cerebrospinal fluid-contacting neurons of the monkey and cat spinal central canal. Journal of Comparative Neurology 258, 527–541. https://doi.org/10.1002/cne.902580405
Larsen, P.J., Tang-Christensen, M., Holst, J.J., Ørskov, C., 1997. Distribution of glucagon-like peptide-1 and other preproglucagon-derived peptides in the rat hypothalamus and brainstem. Neuroscience 77, 257–270. https://doi.org/10.1016/S0306-4522(96)00434-4
Laterra, J., Keep, R., Betz, L.A., Goldstein, G.W., 1999. Blood—Cerebrospinal Fluid Barrier. Basic Neurochemistry: Molecular, Cellular and Medical Aspects. 6th edition.
Lau, J., Bloch, P., Schäffer, L., Pettersson, I., Spetzler, J., Kofoed, J., Madsen, K., Knudsen, L.B., McGuire, J., Steensgaard, D.B., Strauss, H.M., Gram, D.X., Knudsen, S.M., Nielsen, F.S., Thygesen, P., Reedtz-Runge, S., Kruse, T., 2015. Discovery of the Once-Weekly Glucagon-Like Peptide-1 (GLP-1) Analogue Semaglutide. J. Med. Chem. 58, 7370–7380. https://doi.org/10.1021/acs.jmedchem.5b00726
Leal-Filho, M.B., 2011. Spinal cord injury: From inflammation to glial scar. Surg Neurol Int 2, 112. https://doi.org/10.4103/2152-7806.83732
Lee, C.-H., Jeon, S.J., Cho, K.S., Moon, E., Sapkota, A., Jun, H.S., Ryu, J.H., Choi, J.W., 2018. Activation of Glucagon-Like Peptide-1 Receptor Promotes Neuroprotection in Experimental Autoimmune Encephalomyelitis by Reducing Neuroinflammatory Responses. Mol Neurobiol 55, 3007–3020. https://doi.org/10.1007/s12035-017-0550-2
Lee, S.J., Sanchez-Watts, G., Krieger, J.-P., Pignalosa, A., Norell, P.N., Cortella, A., Pettersen, K.G., Vrdoljak, D., Hayes, M.R., Kanoski, S.E., Langhans, W., Watts, A.G., 2018. Loss of dorsomedial hypothalamic GLP-1 signaling reduces BAT thermogenesis and increases adiposity. Molecular Metabolism 11, 33–46. https://doi.org/10.1016/j.molmet.2018.03.008
Lehtinen, M.K., Walsh, C.A., 2011. Neurogenesis at the brain-cerebrospinal fluid interface. Annu. Rev. Cell Dev. Biol. 27, 653–679. https://doi.org/10.1146/annurev-cellbio-092910-154026
Lehtinen, M.K., Zappaterra, M.W., Chen, X., Yang, Y.J., Hill, A.D., Lun, M., Maynard, T., Gonzalez, D., Kim, S., Ye, P., D'Ercole, A.J., Wong, E.T., LaMantia, A.S., Walsh, C.A., 2011. The cerebrospinal fluid provides a proliferative niche for neural progenitor cells. Neuron 69, 893–905. https://doi.org/10.1016/j.neuron.2011.01.023
Lein, E.S., Hawrylycz, M.J., Ao, N., Ayres, M., Bensinger, A., Bernard, A., Boe, A.F., Boguski, M.S., Brockway, K.S., Byrnes, E.J., Chen, Lin, Chen, Li, Chen, T.-M., Chin, M.C., Chong, J., Crook, B.E., Czaplinska, A., Dang, C.N., Datta, S., Dee, N.R., Desaki, A.L., Desta, T., Diep, E., Dolbeare, T.A., Donelan, M.J., Dong, H.-W., Dougherty, J.G., Duncan, B.J., Ebbert, A.J., Eichele, G., Estin, L.K., Faber, C., Facer, B.A., Fields, R., Fischer, S.R., Fliss, T.P., Frensley, C., Gates, S.N., Glattfelder, K.J., Halverson, K.R., Hart, M.R., Hohmann, J.G., Howell, M.P., Jeung, D.P., Johnson, R.A., Karr, P.T., Kawal, R., Kidney, J.M., Knapik, R.H., Kuan, C.L., Lake, J.H., Laramee, A.R., Larsen, K.D., Lau, C., Lemon, T.A., Liang, A.J., Liu, Y., Luong, L.T., Michaels, J., Morgan, J.J., Morgan, R.J., Mortrud, M.T., Mosqueda, N.F., Ng, L.L., Ng, R., Orta, G.J., Overly, C.C., Pak, T.H., Parry, S.E., Pathak, S.D., Pearson, O.C., Puchalski, R.B., Riley, Z.L., Rockett, H.R., Rowland, S.A., Royall, J.J., Ruiz, M.J., Sarno, N.R., Schaffnit, K., Shapovalova, N.V., Sivisay, T., Slaughterbeck, C.R., Smith, S.C., Smith, K.A., Smith, B.I., Sodt, A.J., Stewart, N.N., Stumpf, K.-R., Sunkin, S.M., Sutram, M., Tam, A., Teemer, C.D., Thaller, C., Thompson,

C.L., Varnam, L.R., Visel, A., Whitlock, R.M., Wohnoutka, P.E., Wolkey, C.K., Wong, V.Y., Wood, M., Yaylaoglu, M.B., Young, R.C., Youngstrom, B.L., Yuan, X.F., Zhang, B., Zwingman, T.A., Jones, A.R., 2007. Genome-wide atlas of gene expression in the adult mouse brain. Nature 445, 168–176. https://doi.org/10.1038/nature05453

Leonhardt, H., 1976. [The cerebrospinal fluid contact processes in the central canal of the spinal cord. A scanning and transmission electron microscopic study of the rabbit]. Z Mikrosk Anat Forsch 90, 1–15.

Li, H., Jia, Z., Li, G., Zhao, X., Sun, P., Wang, J., Fan, Z., Lv, G., 2015. Neuroprotective effects of exendin-4 in rat model of spinal cord injury via inhibiting mitochondrial apoptotic pathway. Int J Clin Exp Pathol 8, 4837–4843.

Li, H., Lee, C.H., Yoo, K.-Y., Choi, J.H., Park, O.K., Yan, B.C., Byun, K., Lee, B., Hwang, I.K., Won, M.-H., 2010. Chronic treatment of exendin-4 affects cell proliferation and neuroblast differentiation in the adult mouse hippocampal dentate gyrus. Neurosci Lett 486, 38–42. https://doi.org/10.1016/j.neulet.2010.09.040

Li, H.-T., Zhao, X.-Z., Zhang, X.-R., Li, G., Jia, Z.-Q., Sun, P., Wang, J.-Q., Fan, Z.-K., Lv, G., 2016. Exendin-4 Enhances Motor Function Recovery via Promotion of Autophagy and Inhibition of Neuronal Apoptosis After Spinal Cord Injury in Rats. Mol Neurobiol 53, 4073–4082. https://doi.org/10.1007/s12035-015-9327-7

Li, X., Floriddia, E.M., Toskas, K., Fernandes, K.J.L., Guérout, N., Barnabé-Heider, F., 2016. Regenerative Potential of Ependymal Cells for Spinal Cord Injuries Over Time. EBioMedicine 13, 55–65. https://doi.org/10.1016/j.ebiom.2016.10.035

Li, Y., Chigurupati, S., Holloway, H.W., Mughal, M., Tweedie, D., Bruestle, D.A., Mattson, M.P., Wang, Y., Harvey, B.K., Ray, B., Lahiri, D.K., Greig, N.H., 2012. Exendin-4 Ameliorates Motor Neuron Degeneration in Cellular and Animal Models of Amyotrophic Lateral Sclerosis. PLOS ONE 7, e32008. https://doi.org/10.1371/journal.pone.0032008

Li, Y., Gao, X.B., Sakurai, T., van den Pol, A.N., 2002. Hypocretin/Orexin excites hypocretin neurons via a local glutamate neuron-A potential mechanism for orchestrating the hypothalamic arousal system. Neuron 36, 1169–1181. https://doi.org/10.1016/s0896-6273(02)01132-7

Li, Y., Perry, T., Kindy, M.S., Harvey, B.K., Tweedie, D., Holloway, H.W., Powers, K., Shen, H., Egan, J.M., Sambamurti, K., Brossi, A., Lahiri, D.K., Mattson, M.P., Hoffer, B.J., Wang, Y., Greig, N.H., 2009. GLP-1 receptor stimulation preserves primary cortical and dopaminergic neurons in cellular and rodent models of stroke and Parkinsonism. Proc Natl Acad Sci U S A 106, 1285–1290. https://doi.org/10.1073/pnas.0806720106

Li, Y., Tweedie, D., Mattson, M.P., Holloway, H.W., Greig, N.H., 2010. Enhancing the GLP-1 receptor signaling pathway leads to proliferation and neuroprotection in human neuroblastoma cells. J Neurochem 113, 1621–1631. https://doi.org/10.1111/j.1471-4159.2010.06731.x

Li, Z., 2013. CD133: a stem cell biomarker and beyond. Exp Hematol Oncol 2, 17. https://doi.org/10.1186/2162-3619-2-17

Liao, C.-C., Hou, T.-H., Yu, H.-P., Li, A., Liu, F.-C., 2021. Cerebrospinal fluid electrolytes and acid-base in diabetic patients. Transl Neurosci 12, 448–455. https://doi.org/10.1515/tnsci-2020-0196

Lin, C., Calzarossa, C., Fernandez-Zafra, T., Liu, J., Li, X., Ekblad-Nordberg, Å., Vazquez-Juarez, E., Codeluppi, S., Holmberg, L., Lindskog, M., Uhlén, P., Åkesson, E., 2020. Human ex vivo spinal cord slice culture as a useful model of neural development, lesion, and allogeneic neural cell therapy. Stem Cell Research & Therapy 11, 320. https://doi.org/10.1186/s13287-020-01771-y

Ling, L., Hou, J., Liu, D., Tang, D., Zhang, Y., Zeng, Q., Pan, H., Fan, L., 2022. Important role of the SDF-1/CXCR4 axis in the homing of systemically transplanted human amnion-derived mesenchymal stem cells (hAD-MSCs) to ovaries in rats with chemotherapy-induced premature ovarian insufficiency (POI). Stem Cell Research & Therapy 13, 79. https://doi.org/10.1186/s13287-022-02759-6

Liu, X., Wang, Q., Haydar, T.F., Bordey, A., 2005. Nonsynaptic GABA signaling in postnatal subventricular zone controls GFAP-expressing progenitor proliferation. Nat Neurosci 8, 1179–1187. https://doi.org/10.1038/nn1522

Liu, Y., Schweitzer, E., Nirenberg, M.J., Pickel, V.M., Evans, C.J., Edwards, R.H., 1994. Preferential localization of a vesicular monoamine transporter to dense core vesicles in PC12 cells. J Cell Biol 127, 1419–1433.

Llewellyn-Smith, I.J., Gnanamanickam, G.J.E., Reimann, F., Gribble, F.M., Trapp, S., 2013. Preproglucagon (PPG) neurons innervate neurochemically identified autonomic neurons in the mouse brainstem. Neuroscience 229, 130–143. https://doi.org/10.1016/j.neuroscience.2012.09.071

Llewellyn-Smith, I.J., Marina, N., Manton, R.N., Reimann, F., Gribble, F.M., Trapp, S., 2015. Spinally projecting preproglucagon axons preferentially innervate sympathetic preganglionic neurons. Neuroscience 284, 872–887. https://doi.org/10.1016/j.neuroscience.2014.10.043

Llewellyn-Smith, I.J., Reimann, F., Gribble, F.M., Trapp, S., 2011. Preproglucagon neurons project widely to autonomic control areas in the mouse brain. Neuroscience 180, 111–121. https://doi.org/10.1016/j.neuroscience.2011.02.023

Llorens-Bobadilla, E., Chell, J.M., Le Merre, P., Wu, Y., Zamboni, M., Bergenstråhle, J., Stenudd, M., Sopova, E., Lundeberg, J., Shupliakov, O., Carlén, M., Frisén, J., 2020. A latent lineage potential in resident neural stem cells enables spinal cord repair. Science 370, eabb8795. https://doi.org/10.1126/science.abb8795

Loetscher, P.D., Rossaint, J., Rossaint, R., Weis, J., Fries, M., Fahlenkamp, A., Ryang, Y.-M., Grottke, O., Coburn, M., 2009. Argon: Neuroprotection in in vitro models of cerebral ischemia and traumatic brain injury. Crit Care 13, R206. https://doi.org/10.1186/cc8214

Lorenz, M., Lawson, F., Owens, D., Raccah, D., Roy-Duval, C., Lehmann, A., Perfetti, R., Blonde, L., 2017. Differential effects of glucagon-like peptide-1 receptor agonists on heart rate. Cardiovasc Diabetol 16, 6. https://doi.org/10.1186/s12933-016-0490-6

Lu, R.-M., Hwang, Y.-C., Liu, I.-J., Lee, C.-C., Tsai, H.-Z., Li, H.-J., Wu, H.-C., 2020. Development of therapeutic antibodies for the treatment of diseases. Journal of Biomedical Science 27, 1. https://doi.org/10.1186/s12929-019-0592-z

Lu, X., Geng, X., Zhang, L., Zeng, Y., 2008. The methodology for labeling the distal cerebrospinal fluid-contacting neurons in rats. Journal of Neuroscience Methods 168, 98–103. https://doi.org/10.1016/j.jneumeth.2007.09.033

Ludwig, M.Q., Cheng, W., Gordian, D., Lee, J., Paulsen, S.J., Hansen, S.N., Egerod, K.L., Barkholt, P., Rhodes, C.J., Secher, A., Knudsen, L.B., Pyke, C., Myers, M.G., Pers, T.H., 2021. A genetic map of the mouse dorsal vagal complex and its role in obesity. Nat Metab 3, 530–545. https://doi.org/10.1038/s42255-021-00363-1

Luque, M.A., González, N., Márquez, L., Acitores, A., Redondo, A., Morales, M., Valverde, I., Villanueva-Peñacarrillo, M.L., 2002. Glucagon-like peptide-1 (GLP-1) and glucose metabolism in human myocytes. J Endocrinol 173, 465–473. https://doi.org/10.1677/joe.0.1730465

Ma, D.-L., Chen, F.-Q., Xu, W.-J., Yue, W.-Z., Yuan, G., Yang, Y., 2015. Early intervention with glucagon-like peptide 1 analog liraglutide prevents tau hyperphosphorylation in diabetic db/db mice. J Neurochem 135, 301–308. https://doi.org/10.1111/jnc.13248

Macaya, D., Spector, M., 2012. Injectable hydrogel materials for spinal cord regeneration: a review. Biomed Mater 7, 012001. https://doi.org/10.1088/1748-6041/7/1/012001

MacLean, C.C., 2016. ATP elicits electrophysiological and migratory responses in cells of the spinal cord stem cell niche. University of Leeds.

Madisen, L., Garner, A.R., Shimaoka, D., Chuong, A.S., Klapoetke, N.C., Li, L., van der Bourg, A., Niino, Y., Egolf, L., Monetti, C., Gu, H., Mills, M., Cheng, A., Tasic, B., Nguyen, T.N., Sunkin, S.M., Benucci, A., Nagy, A., Miyawaki, A., Helmchen, F., Empson, R.M., Knöpfel, T., Boyden, E.S., Reid, R.C., Carandini, M., Zeng, H., 2015. Transgenic mice for intersectional targeting of neural sensors and effectors with high specificity and performance. Neuron 85, 942–958. https://doi.org/10.1016/j.neuron.2015.02.022

Maniscalco, J.W., Zheng, H., Gordon, P.J., Rinaman, L., 2015. Negative Energy Balance Blocks Neural and Behavioral Responses to Acute Stress by "Silencing" Central Glucagon-Like Peptide 1 Signaling in Rats. J Neurosci 35, 10701–10714. https://doi.org/10.1523/JNEUROSCI.3464-14.2015

Margeta-Mitrovic, M., Mitrovic, I., Riley, R.C., Jan, L.Y., Basbaum, A.I., 1999. Immunohistochemical localization of GABA(B) receptors in the rat central nervous system. J Comp Neurol 405, 299–321. https://doi.org/10.1002/(sici)1096-9861(19990315)405:3<299::aid-cne2>3.0.co;2-6

Marichal, N., García, G., Radmilovich, M., Trujillo-Cenóz, O., Russo, R.E., 2012. Spatial Domains of Progenitor-Like Cells and Functional Complexity of a Stem Cell Niche in the Neonatal Rat Spinal Cord. STEM CELLS 30, 2020–2031. https://doi.org/10.1002/stem.1175

Marichal, N., García, G., Radmilovich, M., Trujillo-Cenóz, O., Russo, R.E., 2009. Enigmatic Central Canal Contacting Cells: Immature Neurons in "Standby Mode"? J. Neurosci. 29, 10010–10024. https://doi.org/10.1523/JNEUROSCI.6183-08.2009

Marvin, J.S., Shimoda, Y., Magloire, V., Leite, M., Kawashima, T., Jensen, T.P., Kolb, I., Knott, E.L., Novak, O., Podgorski, K., Leidenheimer, N.J., Rusakov, D.A., Ahrens, M.B., Kullmann, D.M., Looger, L.L., 2019. A genetically encoded fluorescent sensor for in vivo imaging of GABA. Nat Methods 16, 763–770. https://doi.org/10.1038/s41592-019-0471-2

Marzvanyan, A., Alhawaj, A.F., 2023. Physiology, Sensory Receptors, in: StatPearls. StatPearls Publishing, Treasure Island (FL).

Massirer, K.B., Carromeu, C., Griesi-Oliveira, K., Muotri, A.R., 2011. Maintenance and differentiation of neural stem cells. WIREs Systems Biology and Medicine 3, 107–114. https://doi.org/10.1002/wsbm.100

McGovern, S.F.J., Hunter, K., Hölscher, C., 2012. Effects of the glucagon-like polypeptide-1 analogue (Val8)GLP-1 on learning, progenitor cell proliferation and neurogenesis in the C57B/16 mouse brain. Brain Res. 1473, 204–213. https://doi.org/10.1016/j.brainres.2012.07.029

Mcintyre, N., Holdsworth, C.D., Turner, D.S., 1964. NEW INTERPRETATION OF ORAL GLUCOSE TOLERANCE. The Lancet, Originally published as Volume 2, Issue 7349 284, 20–21. https://doi.org/10.1016/S0140-6736(64)90011-X

McKerracher, L., Winton, M.J., 2002. Nogo on the go. Neuron 36, 345–348. https://doi.org/10.1016/s0896-6273(02)01018-8

McLaughlin, B.J., Barber, R., Saito, K., Roberts, E., Wu, J.Y., 1975. Immunocytochemical localization of glutamate decarboxylase in rat spinal cord. Journal of Comparative Neurology 164, 305–321. https://doi.org/10.1002/cne.901640304

McLean, B.A., Wong, C.K., Campbell, J.E., Hodson, D.J., Trapp, S., Drucker, D.J., 2020. Revisiting the Complexity of GLP-1 Action from Sites of Synthesis to Receptor Activation. Endocr Rev 42, 101–132. https://doi.org/10.1210/endrev/bnaa032

Meletis, K., Barnabé-Heider, F., Carlén, M., Evergren, E., Tomilin, N., Shupliakov, O., Frisén, J., 2008. Spinal Cord Injury Reveals Multilineage Differentiation of Ependymal Cells. PLOS Biology 6, e182. https://doi.org/10.1371/journal.pbio.0060182

Merchenthaler, I., Lane, M., Shughrue, P., 1999. Distribution of pre-pro-glucagon and glucagon-like peptide-1 receptor messenger RNAs in the rat central nervous system. Journal of Comparative Neurology 403, 261–280. https://doi.org/10.1002/(SICI)1096-9861(19990111)403:2<261::AID-CNE8>3.0.CO;2-5

Mercurio, S., Serra, L., Motta, A., Gesuita, L., Sanchez-Arrones, L., Inverardi, F., Foglio, B., Barone, C., Kaimakis, P., Martynoga, B., Ottolenghi, S., Studer, M., Guillemot, F., Frassoni, C., Bovolenta, P., Nicolis, S.K., 2019a. Sox2 Acts in Thalamic Neurons to Control the Development of Retina-Thalamus-Cortex Connectivity. iScience 15, 257–273. https://doi.org/10.1016/j.isci.2019.04.030

Mercurio, S., Serra, L., Nicolis, S.K., 2019b. More than just Stem Cells: Functional Roles of the Transcription Factor Sox2 in Differentiated Glia and Neurons. Int J Mol Sci 20, 4540. https://doi.org/10.3390/ijms20184540

Mietlicki-Baase, E.G., Ortinski, P.I., Reiner, D.J., Sinon, C.G., McCutcheon, J.E., Pierce, R.C., Roitman, M.F., Hayes, M.R., 2014. Glucagon-like peptide-1 receptor activation in the nucleus accumbens core suppresses feeding by increasing glutamatergic AMPA/kainate signaling. J Neurosci 34, 6985–6992. https://doi.org/10.1523/JNEUROSCI.0115-14.2014

Mietlicki-Baase, E.G., Ortinski, P.I., Rupprecht, L.E., Olivos, D.R., Alhadeff, A.L., Pierce, R.C., Hayes, M.R., 2013. The food intake-suppressive effects of glucagon-like peptide-1 receptor signaling in the ventral tegmental area are mediated by AMPA/kainate receptors. Am J Physiol Endocrinol Metab 305, E1367–E1374. https://doi.org/10.1152/ajpendo.00413.2013

Milhorat, T.H., Kotzen, R.M., Anzil, A.P., 1994. Stenosis of central canal of spinal cord in man: incidence and pathological findings in 232 autopsy cases. J Neurosurg 80, 716–722. https://doi.org/10.3171/jns.1994.80.4.0716

Mineo, I., Matsumura, T., Shingu, R., Namba, M., Kuwajima, M., Matsuzawa, Y., 1995. The Role of Prohormone Convertases Pc1 (PC3) and PC2 in the Cell-Specific Processing of Proglucagon. Biochemical and Biophysical Research Communications 207, 646–651. https://doi.org/10.1006/bbrc.1995.1236

Ming, G., Song, H., 2011. Adult Neurogenesis in the Mammalian Brain: Significant Answers and Significant Questions. Neuron 70, 687–702. https://doi.org/10.1016/j.neuron.2011.05.001

Mojsov, S., Heinrich, G., Wilson, I.B., Ravazzola, M., Orci, L., Habener, J.F., 1986. Preproglucagon gene expression in pancreas and intestine diversifies at the level of post-translational processing. J Biol Chem 261, 11880–11889.

Monti, G., Gomes Moreira, D., Richner, M., Mutsaers, H.A.M., Ferreira, N., Jan, A., 2022. GLP-1 Receptor Agonists in Neurodegeneration: Neurovascular Unit in the Spotlight. Cells 11, 2023. https://doi.org/10.3390/cells11132023

Montrose-Rafizadeh, C., Avdonin, P., Garant, M.J., Rodgers, B.D., Kole, S., Yang, H., Levine, M.A., Schwindinger, W., Bernier, M., 1999. Pancreatic glucagon-like peptide-1 receptor couples to multiple G proteins and activates mitogen-activated protein kinase pathways in Chinese hamster ovary cells. Endocrinology 140, 1132–1140. https://doi.org/10.1210/endo.140.3.6550

Montrose-Rafizadeh, C., Yang, H., Rodgers, B.D., Beday, A., Pritchette, L.A., Eng, J., 1997. High potency antagonists of the pancreatic glucagon-like peptide-1 receptor. J Biol Chem 272, 21201–21206. https://doi.org/10.1074/jbc.272.34.21201

Moore, S.A., 2016. The Spinal Ependymal Layer in Health and Disease. Vet Pathol 53, 746–753. https://doi.org/10.1177/0300985815618438

Moreno-Manzano, V., 2020. Ependymal cells in the spinal cord as neuronal progenitors. Current Opinion in Pharmacology, Neurosciences: Neurogenesis 50, 82–87. https://doi.org/10.1016/j.coph.2019.11.008

Moreno-Manzano, V., Rodríguez-Jiménez, F.J., García-Roselló, M., Laínez, S., Erceg, S., Calvo, M.T., Ronaghi, M., Lloret, M., Planells-Cases, R., Sánchez-Puelles, J.M., Stojkovic, M., 2009. Activated spinal cord ependymal stem cells rescue neurological function. Stem Cells 27, 733–743. https://doi.org/10.1002/stem.24

Morris, A.J., Malbon, C.C., 1999. Physiological regulation of G protein-linked signaling. Physiol Rev 79, 1373–1430. https://doi.org/10.1152/physrev.1999.79.4.1373

Mothe, A.J., Tator, C.H., 2005. Proliferation, migration, and differentiation of endogenous ependymal region stem/progenitor cells following minimal spinal cord injury in the adult rat. Neuroscience 131, 177–187. https://doi.org/10.1016/j.neuroscience.2004.10.011

Mothe, A.J., Zahir, T., Santaguida, C., Cook, D., Tator, C.H., 2011. Neural stem/progenitor cells from the adult human spinal cord are multipotent and self-renewing and differentiate after transplantation. PLoS One 6, e27079. https://doi.org/10.1371/journal.pone.0027079

Müller, T.D., Finan, B., Bloom, S.R., D'Alessio, D., Drucker, D.J., Flatt, P.R., Fritsche, A., Gribble, F., Grill, H.J., Habener, J.F., Holst, J.J., Langhans, W., Meier, J.J., Nauck, M.A., Perez-Tilve, D., Pocai, A., Reimann, F., Sandoval, D.A., Schwartz, T.W., Seeley, R.J., Stemmer, K., Tang-Christensen, M., Woods, S.C., DiMarchi, R.D., Tschöp, M.H., 2019. Glucagon-like peptide 1 (GLP-1). Mol Metab 30, 72–130. https://doi.org/10.1016/j.molmet.2019.09.010

Muñoz, R.I., Kähne, T., Herrera, H., Rodríguez, S., Guerra, Ma.M., Vío, K., Hennig, R., Rapp, E., Rodríguez, E., 2019. The subcommissural organ and the Reissner fiber: old friends revisited. Cell Tissue Res 375, 507–529. https://doi.org/10.1007/s00441-018-2917-8

Muthusamy, N., Vijayakumar, A., Cheng, G., Ghashghaei, H.T., 2014. A knock-in Foxj1(CreERT2::GFP) mouse for recombination in epithelial cells with motile cilia. Genesis 52, 350–358. https://doi.org/10.1002/dvg.22753

Nakamura, Y., Kurabe, M., Matsumoto, M., Sato, T., Miyashita, S., Hoshina, K., Kamiya, Y., Tainaka, K., Matsuzawa, H., Ohno, N., Ueno, M., 2022. Cerebrospinal fluid-contacting neuron tracing reveals structural and functional connectivity for locomotion in the mouse spinal cord. https://doi.org/10.1101/2022.08.15.501844

Nakamura, Y., Kurabe, M., Matsumoto, M., Sato, T., Miytashita, S., Hoshina, K., Kamiya, Y., Tainaka, K., Matsuzawa, H., Ohno, N., Ueno, M., 2023. Cerebrospinal fluid-contacting neuron tracing reveals structural and functional connectivity for locomotion in the mouse spinal cord. eLife 12, e83108. https://doi.org/10.7554/eLife.83108

Nakayama, Y., 1976. The openings of the central canal in the filum terminale internum of some mammals. J Neurocytol 5, 531–544. https://doi.org/10.1007/BF01175567

New, L.E., 2019. GABAergic regulation of proliferation in the postnatal spinal cord. The University of Leeds PhD thesis.

New, L.E., Yanagawa, Y., McConkey, G.A., Deuchars, J., Deuchars, S.A., 2023. GABAergic regulation of cell proliferation within the adult mouse spinal cord. Neuropharmacology 223, 109326. https://doi.org/10.1016/j.neuropharm.2022.109326

Nizari, S., Basalay, M., Chapman, P., Korte, N., Korsak, A., Christie, I.N., Theparambil, S.M., Davidson, S.M., Reimann, F., Trapp, S., Yellon, D.M., Gourine, A.V., 2021. Glucagon-like peptide-1 (GLP-1) receptor activation dilates cerebral arterioles, increases cerebral blood flow, and mediates remote (pre)conditioning neuroprotection against ischaemic stroke. Basic Res Cardiol 116, 32. https://doi.org/10.1007/s00395-021-00873-9

Oka, J.-I., Goto, N., Kameyama, T., 1999. Glucagon-like peptide-1 modulates neuronal activity in the rat's hippocampus. NeuroReport 10, 1643.

Okesola, B.O., Smith, D.K., 2013. Versatile supramolecular pH-tolerant hydrogels which demonstrate pH-dependent selective adsorption of dyes from aqueous solution. Chem. Commun. 49, 11164–11166. https://doi.org/10.1039/C3CC45969A

Olsen, R.W., DeLorey, T.M., 1999. GABA Receptor Physiology and Pharmacology. Basic Neurochemistry: Molecular, Cellular and Medical Aspects. 6th edition.

Olsen, R.W., Sieghart, W., 2008. International Union of Pharmacology. LXX. Subtypes of γ-Aminobutyric AcidA Receptors: Classification on the Basis of Subunit Composition, Pharmacology, and Function. Update. Pharmacol Rev 60, 243–260. https://doi.org/10.1124/pr.108.00505

Ong, Z.Y., Liu, J.-J., Pang, Z.P., Grill, H.J., 2017. Paraventricular Thalamic Control of Food Intake and Reward: Role of Glucagon-Like Peptide-1 Receptor Signaling. Neuropsychopharmacology 42, 2387–2397. https://doi.org/10.1038/npp.2017.150

Orešković, D., Klarica, M., 2010. The formation of cerebrospinal fluid: Nearly a hundred years of interpretations and misinterpretations. Brain Research Reviews 64, 241–262. https://doi.org/10.1016/j.brainresrev.2010.04.006

Orskov, C., Holst, J.J., Nielsen, O.V., 1988. Effect of truncated glucagon-like peptide-1 [proglucagon-(78-107) amide] on endocrine secretion from pig pancreas, antrum, and nonantral stomach. Endocrinology 123, 2009–2013. https://doi.org/10.1210/endo-123-4-2009

Orts-Del'Immagine, A., Cantaut-Belarif, Y., Thouvenin, O., Roussel, J., Baskaran, A., Langui, D., Koëth, F., Bivas, P., Lejeune, F.-X., Bardet, P.-L., Wyart, C., 2020. Sensory Neurons Contacting the Cerebrospinal Fluid Require the Reissner Fiber to Detect Spinal Curvature In Vivo. Current Biology 30, 827-839.e4. https://doi.org/10.1016/j.cub.2019.12.071

Orts-Del'Immagine, A., Kastner, A., Tillement, V., Tardivel, C., Trouslard, J., Wanaverbecq, N., 2014. Morphology, Distribution and Phenotype of Polycystin Kidney Disease 2-like 1-Positive Cerebrospinal Fluid Contacting Neurons in The Brainstem of Adult Mice. PLOS ONE 9, e87748. https://doi.org/10.1371/journal.pone.0087748

Orts-Del'Immagine, A., Seddik, R., Tell, F., Airault, C., Er-Raoui, G., Najimi, M., Trouslard, J., Wanaverbecq, N., 2016. A single polycystic kidney disease 2-like 1 channel opening acts as a spike generator in cerebrospinal fluid-contacting neurons of adult mouse brainstem. Neuropharmacology 101, 549–565. https://doi.org/10.1016/j.neuropharm.2015.07.030

Orts-Del'Immagine, A., Trouslard, J., Airault, C., Hugnot, J.-P., Cordier, B., Doan, T., Kastner, A., Wanaverbecq, N., 2017. Postnatal maturation of mouse medullo-spinal cerebrospinal fluid-contacting neurons. Neuroscience 343, 39–54. https://doi.org/10.1016/j.neuroscience.2016.11.028

Orts-Del'immagine, A., Wanaverbecq, N., Tardivel, C., Tillement, V., Dallaporta, M., Trouslard, J., 2012. Properties of subependymal cerebrospinal fluid contacting neurones in the dorsal vagal complex of the mouse brainstem. J Physiol 590, 3719–3741. https://doi.org/10.1113/jphysiol.2012.227959

O'Shea, T.M., Burda, J.E., Sofroniew, M.V., 2017. Cell biology of spinal cord injury and repair. Journal of Clinical Investigation 127, 3259–3270. https://doi.org/10.1172/JCI90608

Oyinbo, C.A., 2011. Secondary injury mechanisms in traumatic spinal cord injury: a nugget of this multiply cascade. Acta Neurobiol Exp (Wars) 71, 281–299.

Pachitariu, M., Stringer, C., Dipoppa, M., Schröder, S., Rossi, L.F., Dalgleish, H., Carandini, M., Harris, K.D., 2017. Suite2p: beyond 10,000 neurons with standard two-photon microscopy. https://doi.org/10.1101/061507

Palmer, A.M., Marion, D.W., Botscheller, M.L., Bowen, D.M., DeKosky, S.T., 1994. Increased transmitter amino acid concentration in human ventricular CSF after brain trauma. NeuroReport 6, 153.

Pandamooz, S., Salehi, M.S., Zibaii, M.I., Safari, A., Nabiuni, M., Ahmadiani, A., Dargahi, L., 2019. Modeling traumatic injury in organotypic spinal cord slice culture obtained from adult rat. Tissue and Cell 56, 90–97. https://doi.org/10.1016/j.tice.2019.01.002

Paravati, S., Rosani, A., Warrington, S.J., 2023. Physiology, Catecholamines, in: StatPearls. StatPearls Publishing, Treasure Island (FL).

Parkes, D., Jodka, C., Smith, P., Nayak, S., Rinehart, L., Gingerich, R., Chen, K., Young, A., 2001. Pharmacokinetic actions of exendin-4 in the rat: Comparison with glucagon-like peptide-1. Drug Development Research 53, 260–267. https://doi.org/10.1002/ddr.1195

Parthsarathy, V., Hölscher, C., 2013. Chronic treatment with the GLP1 analogue liraglutide increases cell proliferation and differentiation into neurons in an AD mouse model. PLoS One 8, e58784. https://doi.org/10.1371/journal.pone.0058784

Patar, A., Dockery, P., Howard, L., McMahon, S.S., 2019. Cell viability in three ex vivo rat models of spinal cord injury. Journal of Anatomy 234, 244–251. https://doi.org/10.1111/joa.12909

Patel, Y., Rao, K., Reichlin, S., 1977. Somatostatin in human cerebrospinal fluid. N Engl J Med 296, 529–533. https://doi.org/10.1056/NEJM197703102961002

Pencheva, D., Teneva, D., Denev, P., 2022. Validation of HPLC Method for Analysis of Gamma-Aminobutyric and Glutamic Acids in Plant Foods and Medicinal Plants. Molecules 28, 84. https://doi.org/10.3390/molecules28010084

Perry, T., Haughey, N.J., Mattson, M.P., Egan, J.M., Greig, N.H., 2002. Protection and Reversal of Excitotoxic Neuronal Damage by Glucagon-Like Peptide-1 and Exendin-4. J Pharmacol Exp Ther 302, 881–888. https://doi.org/10.1124/jpet.102.037481

Perry, T.L., Hansen, S., Wall, R.A., Gauthier, S.G., 1982. Human CSF GABA concentrations: revised downward for controls, but not decreased in Huntington's chorea. J Neurochem 38, 766–773. https://doi.org/10.1111/j.1471-4159.1982.tb08697.x

Petracca, Y.L., Sartoretti, M.M., Di Bella, D.J., Marin-Burgin, A., Carcagno, A.L., Schinder, A.F., Lanuza, G.M., 2016. The late and dual origin of cerebrospinal fluid-contacting neurons in the mouse spinal cord. Development 143, 880–891. https://doi.org/10.1242/dev.129254

Pfenninger, C.V., Steinhoff, C., Hertwig, F., Nuber, U.A., 2011. Prospectively isolated CD133/CD24-positive ependymal cells from the adult spinal cord and lateral ventricle wall differ in their long-term in vitro self-renewal and in vivo gene expression. Glia 59, 68–81. https://doi.org/10.1002/glia.21077

Poulen, G., Aloy, E., Bringuier, C.M., Mestre-Francés, N., Artus, E.V.F., Cardoso, M., Perez, J.-C., Goze-Bac, C., Boukhaddaoui, H., Lonjon, N., Gerber, Y.N., Perrin, F.E., 2021. Inhibiting microglia proliferation after spinal cord injury improves recovery in mice and nonhuman primates. Theranostics 11, 8640–8659. https://doi.org/10.7150/thno.61833

Povysheva, N., Zheng, H., Rinaman, L., 2021. Glucagon-like peptide 1 receptor-mediated stimulation of a GABAergic projection from the bed nucleus of the stria terminalis to the hypothalamic paraventricular nucleus. Neurobiology of Stress 15, 100363. https://doi.org/10.1016/j.ynstr.2021.100363

Prasad-Reddy, L., Isaacs, D., 2015. A clinical review of GLP-1 receptor agonists: efficacy and safety in diabetes and beyond. Drugs Context 4, 212283. https://doi.org/10.7573/dic.212283

Pyke, C., Knudsen, L.B., 2013. The Glucagon-Like Peptide-1 Receptor—or Not? Endocrinology 154, 4–8. https://doi.org/10.1210/en.2012-2124

Qian, Z., Chen, H., Xia, M., Chang, J., Li, X., Ye, S., Wu, S., Jiang, S., Bao, J., Wang, B., Kong, R., Zhang, S., Zheng, S., Cao, X., Hong, X., 2022. Activation of glucagon-like peptide-1 receptor in microglia attenuates neuroinflammation-induced glial scarring via rescuing Arf and Rho GAP adapter protein 3 expressions after nerve injury. Int J Biol Sci 18, 1328–1346. https://doi.org/10.7150/ijbs.68974

Rakic, P., 2002. Neurogenesis in adult primate neocortex: an evaluation of the evidence. Nat Rev Neurosci 3, 65–71. https://doi.org/10.1038/nrn700

Ramo, N.L., Shetye, S.S., Streijger, F., Lee, J.H.T., Troyer, K.L., Kwon, B.K., Cripton, P., Puttlitz, C.M., 2018a. Comparison of In-Vivo and Ex-Vivo Viscoelastic Behavior of the Spinal Cord. Acta Biomater 68, 78–89. https://doi.org/10.1016/j.actbio.2017.12.024

Ramo, N.L., Troyer, K.L., Puttlitz, C.M., 2018b. Viscoelasticity of spinal cord and meningeal tissues. Acta Biomaterialia 75, 253–262. https://doi.org/10.1016/j.actbio.2018.05.045

Rebosio, C., Balbi, M., Passalacqua, M., Ricciarelli, R., Fedele, E., 2018. Presynaptic GLP-1 receptors enhance the depolarization-evoked release of glutamate and GABA in the mouse cortex and hippocampus. BioFactors 44, 148–157. https://doi.org/10.1002/biof.1406

Reimann, F., Habib, A.M., Tolhurst, G., Parker, H.E., Rogers, G.J., Gribble, F.M., 2008. Glucose sensing in L cells: a primary cell study. Cell Metab 8, 532–539. https://doi.org/10.1016/j.cmet.2008.11.002

Reiner, D.J., Mietlicki-Baase, E.G., McGrath, L.E., Zimmer, D.J., Bence, K.K., Sousa, G.L., Konanur, V.R., Krawczyk, J., Burk, D.H., Kanoski, S.E., Hermann, G.E., Rogers, R.C., Hayes, M.R., 2016. Astrocytes Regulate GLP-1 Receptor-Mediated Effects on Energy Balance. J Neurosci 36, 3531–3540. https://doi.org/10.1523/JNEUROSCI.3579-15.2016

Ren, Y., Ao, Y., O'Shea, T.M., Burda, J.E., Bernstein, A.M., Brumm, A.J., Muthusamy, N., Ghashghaei, H.T., Carmichael, S.T., Cheng, L., Sofroniew, M.V., 2017. Ependymal cell contribution to scar formation after spinal cord injury is minimal, local and dependent on direct ependymal injury. Sci Rep 7, 41122. https://doi.org/10.1038/srep41122

Richard, J.E., Farkas, I., Anesten, F., Anderberg, R.H., Dickson, S.L., Gribble, F.M., Reimann, F., Jansson, J.-O., Liposits, Z., Skibicka, K.P., 2014. GLP-1 Receptor Stimulation of the Lateral Parabrachial Nucleus Reduces Food Intake: Neuroanatomical, Electrophysiological, and Behavioral Evidence. Endocrinology 155, 4356–4367. https://doi.org/10.1210/en.2014-1248

Richards, P., Parker, H.E., Adriaenssens, A.E., Hodgson, J.M., Cork, S.C., Trapp, S., Gribble, F.M., Reimann, F., 2014. Identification and characterisation of glucagon-like peptide-1 receptor expressing cells using a new transgenic mouse model. Diabetes 63, 1224–1233. https://doi.org/10.2337/db13-1440

Richner, M., Jager, S.B., Siupka, P., Vaegter, C.B., 2017. Hydraulic Extrusion of the Spinal Cord and Isolation of Dorsal Root Ganglia in Rodents. J Vis Exp 55226. https://doi.org/10.3791/55226

Rinaman, L., 1999a. Interoceptive stress activates glucagon-like peptide-1 neurons that project to the hypothalamus. Am J Physiol 277, R582-590. https://doi.org/10.1152/ajpregu.1999.277.2.R582

Rinaman, L., 1999b. A functional role for central glucagon-like peptide-1 receptors in lithium chloride-induced anorexia. Am J Physiol 277, R1537-1540. https://doi.org/10.1152/ajpregu.1999.277.5.R1537

Riondel, P., Jurčić, N., Trouslard, J., Wanaverbecq, N., Seddik, R., 2022. GABA excitatory actions in cerebrospinal-fluid contacting neurones of adult mouse spinal cord. https://doi.org/10.1101/2022.12.14.520067

Robinson, L.E., Holt, T.A., Rees, K., Randeva, H.S., O'Hare, J.P., 2013. Effects of exenatide and liraglutide on heart rate, blood pressure and body weight: systematic review and meta-analysis. BMJ Open 3, e001986. https://doi.org/10.1136/bmjopen-2012-001986

Rodríguez, S., Hein, S., Yulis, R., Delannoy, L., Siegmund, I., Rodríguez, E., 1985. Reissner's fiber and the wall of the central canal in the lumbo-sacral region of the bovine spinal cord. Cell Tissue Res. 240, 649–662. https://doi.org/10.1007/BF00216353

Rosenberg, A.B., Roco, C.M., Muscat, R.A., Kuchina, A., Sample, P., Yao, Z., Graybuck, L.T., Peeler, D.J., Mukherjee, S., Chen, W., Pun, S.H., Sellers, D.L., Tasic, B., Seelig, G., 2018. Single-cell profiling of the developing mouse brain and spinal cord with split-pool barcoding. Science 360, 176–182. https://doi.org/10.1126/science.aam8999

Rowlands, J., Heng, J., Newsholme, P., Carlessi, R., 2018. Pleiotropic Effects of GLP-1 and Analogs on Cell Signaling, Metabolism, and Function. Frontiers in Endocrinology 9.

Russ, D.E., Cross, R.B.P., Li, L., Koch, S.C., Matson, K.J.E., Yadav, A., Alkaslasi, M.R., Lee, D.I., Le Pichon, C.E., Menon, V., Levine, A.J., 2021. A harmonized atlas of mouse spinal cord cell types and their spatial organization. Nat Commun 12, 5722. https://doi.org/10.1038/s41467-021-25125-1

Sabelström, H., Stenudd, M., Réu, P., Dias, D.O., Elfineh, M., Zdunek, S., Damberg, P., Göritz, C., Frisén, J., 2013. Resident neural stem cells restrict tissue damage and neuronal loss after spinal cord injury in mice. Science 342, 637–640. https://doi.org/10.1126/science.1242576

Sabourin, J.-C., Ackema, K.B., Ohayon, D., Guichet, P.-O., Perrin, F.E., Garces, A., Ripoll, C., Charité, J., Simonneau, L., Kettenmann, H., Zine, A., Privat, A., Valmier, J., Pattyn, A., Hugnot, J.-P., 2009. A Mesenchymal-Like ZEB1+ Niche Harbors Dorsal Radial Glial Fibrillary Acidic Protein-Positive Stem Cells in the Spinal Cord. STEM CELLS 27, 2722–2733. https://doi.org/10.1002/stem.226

Saha, K., Keung, A.J., Irwin, E.F., Li, Y., Little, L., Schaffer, D.V., Healy, K.E., 2008. Substrate Modulus Directs Neural Stem Cell Behavior. Biophys J 95, 4426–4438. https://doi.org/10.1529/biophysj.108.132217

Saker, E., Henry, B.M., Tomaszewski, K.A., Loukas, M., Iwanaga, J., Oskouian, R.J., Tubbs, R.S., 2016. The Human Central Canal of the Spinal Cord: A Comprehensive Review of its Anatomy, Embryology, Molecular Development, Variants, and Pathology. Cureus 8, e927. https://doi.org/10.7759/cureus.927

Sakka, L., Coll, G., Chazal, J., 2011. Anatomy and physiology of cerebrospinal fluid. Eur Ann Otorhinolaryngol Head Neck Dis 128, 309–316. https://doi.org/10.1016/j.anorl.2011.03.002

Salcedo, I., Tweedie, D., Li, Y., Greig, N.H., 2012. Neuroprotective and neurotrophic actions of glucagon-like peptide-1: an emerging opportunity to treat neurodegenerative and cerebrovascular disorders. Br J Pharmacol 166, 1586–1599. https://doi.org/10.1111/j.1476-5381.2012.01971.x

Salic, A., Mitchison, T.J., 2008. A chemical method for fast and sensitive detection of DNA synthesis in vivo. Proc Natl Acad Sci U S A 105, 2415–2420. https://doi.org/10.1073/pnas.0712168105

Sang, L., Dick, I.E., Yue, D.T., 2016. Protein kinase A modulation of CaV1.4 calcium channels. Nat Commun 7, 12239. https://doi.org/10.1038/ncomms12239

Schirra, J., Sturm, K., Leicht, P., Arnold, R., Göke, B., Katschinski, M., 1998. Exendin(9-39)amide is an antagonist of glucagon-like peptide-1(7-36)amide in humans. J Clin Invest 101, 1421–1430.

Schivell, A.E., Batchelor, R.H., Bajjalieh, S.M., 1996. Isoform-specific, Calcium-regulated Interaction of the Synaptic Vesicle Proteins SV2 and Synaptotagmin *. Journal of Biological Chemistry 271, 27770–27775. https://doi.org/10.1074/jbc.271.44.27770

Schoeler, M., Loetscher, P.D., Rossaint, R., Fahlenkamp, A.V., Eberhardt, G., Rex, S., Weis, J., Coburn, M., 2012. Dexmedetomidine is neuroprotective in an in vitro model for traumatic brain injury. BMC Neurol 12, 20. https://doi.org/10.1186/1471-2377-12-20

Schwartz, A.B., Kapur, A., Huang, Z., Anangi, R., Spear, J.M., Stagg, S., Fardone, E., Dekan, Z., Rosenberg, J.T., Grant, S.C., King, G.F., Mattoussi, H., Fadool, D.A., 2021. Olfactory bulb targeted QD bioconjugate and Kv1.3 blocking peptide improve metabolic health in obese male mice. J Neurochem 157, 1876–1896. https://doi.org/10.1111/jnc.15200

Scimemi, A., Beato, M., 2009. Determining the Neurotransmitter Concentration Profile at Active Synapses. Mol Neurobiol 40, 289–306. https://doi.org/10.1007/s12035-009-8087-7

Secher, A., Jelsing, J., Baquero, A.F., Hecksher-Sørensen, J., Cowley, M.A., Dalbøge, L.S., Hansen, G., Grove, K.L., Pyke, C., Raun, K., Schäffer, L., Tang-Christensen, M., Verma, S., Witgen, B.M., Vrang, N., Bjerre Knudsen, L., 2014. The arcuate nucleus mediates GLP-1 receptor agonist liraglutide-dependent weight loss. J Clin Invest 124, 4473–4488. https://doi.org/10.1172/JCI75276

Sewards, T.V., Sewards, M.A., 2003. Fear and power-dominance motivation: proposed contributions of peptide hormones present in cerebrospinal fluid and plasma. Neurosci Biobehav Rev 27, 247–267. https://doi.org/10.1016/s0149-7634(03)00034-4

Shimosegawa, T., Koizumi, M., Toyota, T., Goto, Y., Yanaihara, C., Yanaihara, N., 1986. An immunohistochemical study of methionine-enkephalin-Arg6-Gly7-Leu8-like immunoreactivity-containing liquor-contacting neurons (LCNs) in the rat spinal cord. Brain Research 379, 1–9. https://doi.org/10.1016/0006-8993(86)90249-0

Shin, J., Poling, J., Park, H.-C., Appel, B., 2007. Notch signaling regulates neural precursor allocation and binary neuronal fate decisions in zebrafish. Development 134, 1911–1920. https://doi.org/10.1242/dev.001602

Siesjö, B.K., 1972. The regulation of cerebrospinal fluid pH. Kidney International 1, 360–374. https://doi.org/10.1038/ki.1972.47

Siesjö, B.K., von Hanwehr, R., Nergelius, G., Nevander, G., Ingvar, M., 1985. Extra- and intracellular pH in the brain during seizures and in the recovery period following the arrest of seizure activity. J Cereb Blood Flow Metab 5, 47–57. https://doi.org/10.1038/jcbfm.1985.7

Silva, M., Tran, V., Marty, A., 2021. Calcium-dependent docking of synaptic vesicles. Trends Neurosci 44, 579–592. https://doi.org/10.1016/j.tins.2021.04.003

Smits, M.M., Tonneijck, L., Muskiet, M.H.A., Hoekstra, T., Kramer, M.H.H., Diamant, M., Raalte, D.H. van, 2017. Heart rate acceleration with GLP-1 receptor agonists in type 2 diabetes patients: an acute and 12-week randomised, double-blind, placebo-controlled trial. European Journal of Endocrinology 176, 77–86. https://doi.org/10.1530/EJE-16-0507

Soleimani, L., Oquendo, M.A., Sullivan, G.M., Mathé, A.A., Mann, J.J., 2014. Cerebrospinal Fluid Neuropeptide Y Levels in Major Depression and Reported Childhood Trauma. Int J Neuropsychopharmacol 18, pyu023. https://doi.org/10.1093/ijnp/pyu023

Song, S., Guo, R., Mehmood, A., Zhang, L., Yin, B., Yuan, C., Zhang, H., Guo, L., Li, B., 2022. Liraglutide attenuate central nervous inflammation and demyelination through AMPK and pyroptosis-related NLRP3 pathway. CNS Neuroscience & Therapeutics 28, 422–434. https://doi.org/10.1111/cns.13791

Spassky, N., Merkle, F.T., Flames, N., Tramontin, A.D., García-Verdugo, J.M., Alvarez-Buylla, A., 2005. Adult Ependymal Cells Are Postmitotic and Are Derived from Radial Glial Cells during Embryogenesis. J. Neurosci. 25, 10–18. https://doi.org/10.1523/JNEUROSCI.1108-04.2005

Spike, R.C., Todd, A.J., Johnston, H.M., 1993. Coexistence of NADPH diaphorase with GABA, glycine, and acetylcholine in rat spinal cord. Journal of Comparative Neurology 335, 320–333. https://doi.org/10.1002/cne.903350303

Stenudd, M., Sabelström, H., Frisén, J., 2015. Role of Endogenous Neural Stem Cells in Spinal Cord Injury and Repair. JAMA Neurol 72, 235–237. https://doi.org/10.1001/jamaneurol.2014.2927

Stenudd, M., Sabelström, H., Llorens-Bobadilla, E., Zamboni, M., Blom, H., Brismar, H., Zhang, S., Basak, O., Clevers, H., Göritz, C., Barnabé-Heider, F., Frisén, J., 2022. Identification of a discrete subpopulation of spinal cord ependymal cells with neural stem cell properties. Cell Reports 38, 110440. https://doi.org/10.1016/j.celrep.2022.110440

Sternberg, J.R., Prendergast, A.E., Brosse, L., Cantaut-Belarif, Y., Thouvenin, O., Orts-Del'Immagine, A., Castillo, L., Djenoune, L., Kurisu, S., McDearmid, J.R., Bardet, P.-L., Boccara, C., Okamoto, H., Delmas, P., Wyart, C., 2018. Pkd2l1 is required for mechanoception in cerebrospinal fluid-contacting neurons and maintenance of spine curvature. Nat Commun 9. https://doi.org/10.1038/s41467-018-06225-x

Stoeckel, M.-E., Uhl-Bronner, S., Hugel, S., Veinante, P., Klein, M.-J., Mutterer, J., Freund-Mercier, M.-J., Schlichter, R., 2003. Cerebrospinal fluid-contacting neurons in the rat spinal cord, a gamma-aminobutyric acidergic system expressing the P2X2 subunit of purinergic receptors, PSA-NCAM, and GAP-43 immunoreactivities: light and electron microscopic study. J Comp Neurol 457, 159–174. https://doi.org/10.1002/cne.10565

Stolp, H.B., Molnár, Z., 2015. Neurogenic niches in the brain: help and hindrance of the barrier systems. Frontiers in Neuroscience 9. https://doi.org/10.3389/fnins.2015.00020

Stoppini, L., Buchs, P.A., Muller, D., 1991. A simple method for organotypic cultures of nervous tissue. J Neurosci Methods 37, 173–182. https://doi.org/10.1016/0165-0270(91)90128-m

Sudhof, T.C., 2004. The synaptic vesicle cycle. Annu Rev Neurosci 27, 509–547. https://doi.org/10.1146/annurev.neuro.26.041002.131412

Svensson, E., Apergis-Schoute, J., Burnstock, G., Nusbaum, M.P., Parker, D., Schiöth, H.B., 2019. General Principles of Neuronal Co-transmission: Insights From Multiple Model Systems. Frontiers in Neural Circuits 12.

Swanson, L.W., McKellar, S., 1979. The distribution of oxytocin- and neurophysin-stained fibers in the spinal cord of the rat and monkey. Journal of Comparative Neurology 188, 87–106. https://doi.org/10.1002/cne.901880108

Taber, K.H., Hurley, R.A., 2014. Volume Transmission in the Brain: Beyond the Synapse. JNP 26, iv–4. https://doi.org/10.1176/appi.neuropsych.13110351

Tarsa, L., Goda, Y., 2002. Synaptophysin regulates activity-dependent synapse formation in cultured hippocampal neurons. Proc Natl Acad Sci U S A 99, 1012–1016. https://doi.org/10.1073/pnas.022575999

Telano, L.N., Baker, S., 2022. Physiology, Cerebral Spinal Fluid, in: StatPearls. StatPearls Publishing, Treasure Island (FL).

Terrill, S.J., Holt, M.K., Maske, C.B., Abrams, N., Reimann, F., Trapp, S., Williams, D.L., 2019. Endogenous GLP-1 in lateral septum promotes satiety and suppresses motivation for food in mice. Physiol Behav 206, 191–199. https://doi.org/10.1016/j.physbeh.2019.04.008

Thiebaud, N., Llewellyn-Smith, I.J., Gribble, F., Reimann, F., Trapp, S., Fadool, D.A., 2016. The incretin hormone glucagon-like peptide 1 increases mitral cell excitability by decreasing conductance of a voltage-dependent potassium channel. J Physiol 594, 2607–2628. https://doi.org/10.1113/JP272322

Thorens, B., Porret, A., Bühler, L., Deng, S.-P., Morel, P., Widmann, C., 1993. Cloning and Functional Expression of the Human Islet GLP-1 Receptor: Demonstration That Exendin-4 Is an Agonist and Exendin-(9–39) an Antagonist of the Receptor. Diabetes 42, 1678–1682. https://doi.org/10.2337/diab.42.11.1678

Thureson-Klein, A., 1983. Exocytosis from large and small dense cored vesicles in noradrenergic nerve terminals. Neuroscience 10, 245–259. https://doi.org/10.1016/0306-4522(83)90132-x

Tomas, A., Jones, B., Leech, C., 2020. New Insights into Beta-Cell GLP-1 Receptor and cAMP Signaling. Journal of Molecular Biology, Islet Biology in Type 2 diabetes 432, 1347–1366. https://doi.org/10.1016/j.jmb.2019.08.009

Tonelli Gombalová, Z., Košuth, J., Alexovič Matiašová, A., Zrubáková, J., Žežula, I., Giallongo, T., Di Giulio, A.M., Carelli, S., Tomašková, L., Daxnerová, Z., Ševc, J., 2020. Majority of cerebrospinal fluid-contacting neurons in the spinal cord of C57Bl/6N mice is present in ectopic position unlike in other studied experimental mice strains and mammalian species. Journal of Comparative Neurology 528, 2523–2550. https://doi.org/10.1002/cne.24909

Toonen, R.F.G., Verhage, M., 2007. Munc18-1 in secretion: lonely Munc joins SNARE team and takes control. Trends Neurosci 30, 564–572. https://doi.org/10.1016/j.tins.2007.08.008

Torrillas de la Cal, A., Paniagua-Torija, B., Arevalo-Martin, A., Faulkes, C.G., Jiménez, A.J., Ferrer, I., Molina-Holgado, E., Garcia-Ovejero, D., 2021. The Structure of the Spinal Cord Ependymal Region in Adult Humans Is a Distinctive Trait among Mammals. Cells 10, 2235. https://doi.org/10.3390/cells10092235

Tozuka, Y., Fukuda, S., Namba, T., Seki, T., Hisatsune, T., 2005. GABAergic excitation promotes neuronal differentiation in adult hippocampal progenitor cells. Neuron 47, 803–815. https://doi.org/10.1016/j.neuron.2005.08.023

Trapp, S., Brierley, D.I., 2022. Brain GLP-1 and the regulation of food intake: GLP-1 action in the brain and its implications for GLP-1 receptor agonists in obesity treatment. Br J Pharmacol 179, 557–570. https://doi.org/10.1111/bph.15638

Trapp, S., Cork, S.C., 2015. PPG neurons of the lower brain stem and their role in brain GLP-1 receptor activation. Am J Physiol Regul Integr Comp Physiol 309, R795–R804. https://doi.org/10.1152/ajpregu.00333.2015

Trueta, C., De-Miguel, F., 2012. Extrasynaptic exocytosis and its mechanisms: a source of molecules mediating volume transmission in the nervous system. Frontiers in Physiology 3.

Trujillo, J.M., Nuffer, W., Smith, B.A., 2021. GLP-1 receptor agonists: an updated review of head-to-head clinical studies. Therapeutic Advances in Endocrinology 12, 2042018821997320. https://doi.org/10.1177/2042018821997320

Tysseling, V.M., Mithal, D., Sahni, V., Birch, D., Jung, H., Miller, R.J., Kessler, J.A., 2011. SDF1 in the dorsal corticospinal tract promotes CXCR4+ cell migration after spinal cord injury. Journal of Neuroinflammation 8, 16. https://doi.org/10.1186/1742-2094-8-16

Veening, J.G., Barendregt, H.P., 2010. The regulation of brain states by neuroactive substances distributed via the cerebrospinal fluid; a review. Cerebrospinal Fluid Research 7, 1. https://doi.org/10.1186/1743-8454-7-1

Veening, J.G., Gerrits, P.O., Barendregt, H.P., 2012. Volume transmission of beta-endorphin via the cerebrospinal fluid; a review. Fluids Barriers CNS 9, 16. https://doi.org/10.1186/2045-8118-9-16

Venkatachalam, K., Montell, C., 2007. TRP Channels. Annual Review of Biochemistry 76, 387–417. https://doi.org/10.1146/annurev.biochem.75.103004.142819

Vergès, B., Aboyans, V., Angoulvant, D., Boutouyrie, P., Cariou, B., Hyafil, F., Mohammedi, K., Amarenco, P., 2022. Protection against stroke with glucagon-like peptide-1 receptor agonists: a comprehensive review of potential mechanisms. Cardiovascular Diabetology 21, 242. https://doi.org/10.1186/s12933-022-01686-3

Vígh, B., Manzano e Silva, M.J., Frank, C.L., Vincze, C., Czirok, S.J., Szabó, A., Lukáts, A., Szél, A., 2004. The system of cerebrospinal fluid-contacting neurons. Its supposed role in the nonsynaptic signal transmission of the brain. Histol Histopathol 19, 607–628. https://doi.org/10.14670/HH-19.607

Vigh, B., Vigh-Teichmann, I., 1998. Actual problems of the cerebrospinal fluid-contacting neurons. Microsc Res Tech 41, 57–83. https://doi.org/10.1002/(SICI)1097-0029(19980401)41:1<57::AID-JEMT6>3.0.CO;2-R

Vigh, B., Vigh-Teichmann, I., Aros, B., 1977. Special dendritic and axonal endings formed by the cerebrospinal fluid contacting neurons of the spinal cord. Cell Tissue Res 183, 541–552. https://doi.org/10.1007/BF00225666

Vigh, B., Vigh-Teichmann, I., Manzano e Silva, M.J., van den Pol, A.N., 1983. Cerebrospinal fluid-contacting neurons of the central canal and terminal ventricle in various vertebrates. Cell Tissue Res. 231, 615–621. https://doi.org/10.1007/BF00218119

Vigh-Teichmann, I., Vigh, B., 1989. The cerebrospinal fluid-contacting neuron: a peculiar cell type of the central nervous system. Immunocytochemical aspects. Arch Histol Cytol 52 Suppl, 195–207. https://doi.org/10.1679/aohc.52.suppl_195

Vilsbøll, T., Holst, J.J., 2004. Incretins, insulin secretion and Type 2 diabetes mellitus. Diabetologia 47, 357–366. https://doi.org/10.1007/s00125-004-1342-6

Vizi, E., Fekete, A., Karoly, R., Mike, A., 2010. Non-synaptic receptors and transporters involved in brain functions and targets of drug treatment. British Journal of Pharmacology 160, 785–809. https://doi.org/10.1111/j.1476-5381.2009.00624.x

Vrang, N., Grove, K., 2011. The brainstem preproglucagon system in a non-human primate (Macaca mulatta). Brain Res 1397, 28–37. https://doi.org/10.1016/j.brainres.2011.05.002

Vrang, N., Larsen, P.J., 2010. Preproglucagon derived peptides GLP-1, GLP-2 and oxyntomodulin in the CNS: Role of peripherally secreted and centrally produced peptides. Progress in Neurobiology 92, 442–462. https://doi.org/10.1016/j.pneurobio.2010.07.003

Wang, J.T., Rodrigo, A.C., Patterson, A.K., Hawkins, K., Aly, M.M.S., Sun, J., Al Jamal, K.T., Smith, D.K., 2021. Enhanced Delivery of Neuroactive Drugs via Nasal Delivery with a Self-Healing Supramolecular Gel. Adv Sci (Weinh) 8, 2101058. https://doi.org/10.1002/advs.202101058

Wang, S., He, Y., Zhang, H., Chen, L., Cao, L., Yang, L., Wang, C., Pan, Y., Tang, Q., Tan, W., Dou, X., Li, Q., 2021. The Neural Stem Cell Properties of PKD2L1+ Cerebrospinal Fluid-Contacting Neurons in vitro. Frontiers in Cellular Neuroscience 15.

Wang, X.-F., Liu, J.-J., Xia, J., Liu, J., Mirabella, V., Pang, Z.P., 2015. Endogenous Glucagon-like Peptide-1 Suppresses High-Fat Food Intake by Reducing Synaptic Drive onto Mesolimbic Dopamine Neurons. Cell Rep 12, 726–733. https://doi.org/10.1016/j.celrep.2015.06.062

Wanner, I.B., Anderson, M.A., Song, B., Levine, J., Fernandez, A., Gray-Thompson, Z., Ao, Y., Sofroniew, M.V., 2013. Glial scar borders are formed by newly proliferated, elongated astrocytes that interact to corral inflammatory and fibrotic cells via STAT3-dependent mechanisms after spinal cord injury. J. Neurosci. 33, 12870–12886. https://doi.org/10.1523/JNEUROSCI.2121-13.2013

Webster, M.A., 2012. Evolving concepts of sensory adaptation. F1000 Biol Rep 4, 21. https://doi.org/10.3410/B4-21

Wei, Y., Mojsov, S., 1995. Tissue-specific expression of the human receptor for glucagon-like peptide-I: brain, heart and pancreatic forms have the same deduced amino acid sequences. FEBS Lett. 358, 219–224. https://doi.org/10.1016/0014-5793(94)01430-9

Weina, H., Yuhu, N., Christian, H., Birong, L., Feiyu, S., Le, W., 2018. Liraglutide attenuates the depressive- and anxiety-like behaviour in the corticosterone induced depression model via improving hippocampal neural plasticity. Brain Research 1694, 55–62. https://doi.org/10.1016/j.brainres.2018.04.031

Welch, M.J., Markham, C.H., Jenden, D.J., 1976. Acetylcholine and choline in cerebrospinal fluid of patients with Parkinson's disease and Huntington's chorea. J Neurol Neurosurg Psychiatry 39, 367–374. https://doi.org/10.1136/jnnp.39.4.367

Weston, C., Poyner, D., Patel, V., Dowell, S., Ladds, G., 2014. Investigating G protein signalling bias at the glucagon-like peptide-1 receptor in yeast. British Journal of Pharmacology 171, 3651–3665. https://doi.org/10.1111/bph.12716

White, D.N., Stowell, M.H.B., 2021. Room for Two: The Synaptophysin/Synaptobrevin Complex. Frontiers in Synaptic Neuroscience 13.

Whitmire, C.J., Stanley, G.B., 2016. Rapid sensory adaptation redux: A circuit perspective. Neuron 92, 298–315. https://doi.org/10.1016/j.neuron.2016.09.046

Williams, D.L., Lilly, N.A., Edwards, I.J., Yao, P., Richards, J.E., Trapp, S., 2018. GLP-1 action in the mouse bed nucleus of the stria terminalis. Neuropharmacology 131, 83–95. https://doi.org/10.1016/j.neuropharm.2017.12.007

Wu, J., Lipinski, M.M., 2019. Autophagy in Neurotrauma: Good, Bad, or Dysregulated. Cells 8, 693. https://doi.org/10.3390/cells8070693

Wu, M.-Y., Carbo-Tano, M., Mirat, O., Lejeune, F.-X., Roussel, J., Quan, F.B., Fidelin, K., Wyart, C., 2021. Spinal sensory neurons project onto the hindbrain to stabilize posture and enhance locomotor speed. Current Biology 31, 3315-3329.e5. https://doi.org/10.1016/j.cub.2021.05.042

Xiao, L., Saiki, C., Okamura, H., 2019. Oxidative Stress-Tolerant Stem Cells from Human Exfoliated Deciduous Teeth Decrease Hydrogen Peroxide-Induced Damage in Organotypic Brain Slice Cultures from Adult Mice. Int. J. Mol. Sci. 13.

Xie, Z., Long, J., Liu, J., Chai, Z., Kang, X., Wang, C., 2017. Molecular Mechanisms for the Coupling of Endocytosis to Exocytosis in Neurons. Front Mol Neurosci 10, 47. https://doi.org/10.3389/fnmol.2017.00047

Yamagishi, S., Matsui, T., 2011. Pleiotropic effects of glucagon-like peptide-1 (GLP-1)-based therapies on vascular complications in diabetes. Curr Pharm Des 17, 4379–4385. https://doi.org/10.2174/138161211798999456

Yamamoto, H., Lee, C.E., Marcus, J.N., Williams, T.D., Overton, J.M., Lopez, M.E., Hollenberg, A.N., Baggio, L., Saper, C.B., Drucker, D.J., Elmquist, J.K., 2002. Glucagon-like peptide-1 receptor stimulation increases blood pressure and heart rate and activates autonomic regulatory neurons. J Clin Invest 110, 43–52. https://doi.org/10.1172/JCI15595

Yamamoto, S., Nagao, M., Sugimori, M., Kosako, H., Nakatomi, H., Yamamoto, N., Takebayashi, H., Nabeshima, Y., Kitamura, T., Weinmaster, G., Nakamura, K., Nakafuku, M., 2001. Transcription Factor Expression and Notch-Dependent Regulation of Neural Progenitors in the Adult Rat Spinal Cord. J. Neurosci. 21, 9814–9823. https://doi.org/10.1523/JNEUROSCI.21-24-09814.2001

Yang, X., Feng, P., Zhang, X., Li, D., Wang, R., Ji, C., Li, G., Hölscher, C., 2019. The diabetes drug semaglutide reduces infarct size, inflammation, and apoptosis, and normalizes neurogenesis in a rat model of stroke. Neuropharmacology 158, 107748. https://doi.org/10.1016/j.neuropharm.2019.107748

Ye, W., Chang, R.B., Bushman, J.D., Tu, Y.-H., Mulhall, E.M., Wilson, C.E., Cooper, A.J., Chick, W.S., Hill-Eubanks, D.C., Nelson, M.T., Kinnamon, S.C., Liman, E.R., 2016. The K+ channel KIR2.1 functions in tandem with proton influx to mediate sour taste transduction. Proceedings of the National Academy of Sciences 113, E229–E238. https://doi.org/10.1073/pnas.1514282112

Yu, S., Liewald, J.F., Shao, J., Steuer Costa, W., Gottschalk, A., 2021. Synapsin Is Required for Dense Core Vesicle Capture and cAMP-Dependent Neuropeptide Release. J Neurosci 41, 4187–4201. https://doi.org/10.1523/JNEUROSCI.2631-20.2021

Zapata, A., Chefer, V.I., Shippenberg, T.S., Denoroy, L., 2009. Detection and Quantification of Neurotransmitters in Dialysates. Curr Protoc Neurosci CHAPTER, Unit-7.430. https://doi.org/10.1002/0471142301.ns0704s48

Zeng, C., Pan, F., Jones, L.A., Lim, M.M., Griffin, E.A., Sheline, Y.I., Mintun, M.A., Holtzman, D.M., Mach, R.H., 2010. Evaluation of 5-ethynyl-2′-deoxyuridine staining as a sensitive and reliable method for studying cell proliferation in the adult nervous system. Brain Res 1319C, 21–32. https://doi.org/10.1016/j.brainres.2009.12.092

Zeng, S., Bai, J., Jiang, H., Zhu, Jin-jin, Fu, C., He, M., Zhu, Jiang-hu, Chen, S., Li, P., Fu, X., Lin, Z., 2020. Treatment With Liraglutide Exerts Neuroprotection After Hypoxic–Ischemic Brain Injury in Neonatal Rats via the PI3K/AKT/GSK3β Pathway. Front Cell Neurosci 13, 585. https://doi.org/10.3389/fncel.2019.00585

Zhang, D., Lv, G., 2018. Therapeutic potential of spinal GLP-1 receptor signaling. Peptides 101, 89–94. https://doi.org/10.1016/j.peptides.2018.01.003

Zhang, L., Zeng, Y.-M., Ting, J., Cao, J., Wang, M., 2003. The distributions and signaling directions of the cerebrospinal fluid contacting neurons in the parenchyma of a rat brain. Brain Res 989, 1–8. https://doi.org/10.1016/s0006-8993(03)03123-8

Zhang, L., Zhang, W., Tian, X., 2021. The pleiotropic of GLP-1/GLP-1R axis in central nervous system diseases. International Journal of Neuroscience 0, 1–38. https://doi.org/10.1080/00207454.2021.1924707

Zhang, S., Gumpper, R.H., Huang, X.-P., Liu, Y., Krumm, B.E., Cao, C., Fay, J.F., Roth, B.L., 2022. Molecular basis for selective activation of DREADD-based chemogenetics. Nature 612, 354–362. https://doi.org/10.1038/s41586-022-05489-0

Zheng, H., Cai, L., Rinaman, L., 2015. Distribution of glucagon-like peptide 1-immunopositive neurons in human caudal medulla. Brain Struct Funct 220, 1213–1219. https://doi.org/10.1007/s00429-014-0714-z

Zheng, H., Reiner, D.J., Hayes, M.R., Rinaman, L., 2019. Chronic Suppression of Glucagon-Like Peptide-1 Receptor (GLP1R) mRNA Translation in the Rat Bed Nucleus of the Stria Terminalis Reduces Anxiety-Like Behavior and Stress-Induced Hypophagia, But Prolongs Stress-Induced Elevation of Plasma Corticosterone. J. Neurosci. 39, 2649–2663. https://doi.org/10.1523/JNEUROSCI.2180-18.2019

Zhu, H., Roth, B.L., 2015. DREADD: A Chemogenetic GPCR Signaling Platform. International Journal of Neuropsychopharmacology 18, pyu007. https://doi.org/10.1093/ijnp/pyu007

Zhu, H., Zhang, Y., Shi, Z., Lu, D., Li, T., Ding, Y., Ruan, Y., Xu, A., 2016. The Neuroprotection of Liraglutide Against Ischaemia-induced Apoptosis through the Activation of the PI3K/AKT and MAPK Pathways. Sci Rep 6, 26859. https://doi.org/10.1038/srep26859